DEEP CRUSTAL SEISMIC REFLECTION PROFILES ACROSS THE LITTLE CARPATHIANS AND ADJACENT MARGINS OF VIENNA BASIN AND WEST DANUBE BASIN IN CZECHOSLOVAKIA

ESTELLE BLAIS

DEEP CRUSTAL SEISMIC REFLECTION PROFILES ACROSS THE LITTLE CARPATHIANS AND ADJACENT MARGINS OF VIENNA BASIN AND WEST DANUBE BASIN IN CZECHOSLOVAKIA

BY

© ESTELLE BLAIS

A thesis submitted to the School of Graduate
Studies in partial fulfilment of the
requirements for the degree of
Master of Science

Department of Earth Sciences
Memorial University of Newfoundland
1992

St. John's Newfoundland

National Library of Canada
Acquisitions and Bibliographic Services Branch
395 Wellington Street
Ottawa, Ontario
K1A 0N4

Bibliothèque nationale du Canada
Direction des acquisitions et des services bibliographiques
395, rue Wellington
Ottawa (Ontario)
K1A 0N4

Your file Votre référence

Our file Notre référence

ISBN 0-315-96088-4

ABSTRACT

Within the accretionary wedge forming the Carpathians of Central Europe, several 'basement' horsts occur within the usual sequence of thrust wedges, or nappes. This thesis is concerned with one such anomaly - the Little Carpathian horst in the Western Carpathians in Czechoslovakia. The horst is located between two deep post-nappe basins: the Vienna and West Danube basins, so that the structural relations with the underlying nappe sequences is unclear from surface geology.

The main objective of this study is to define the structure of the Little Carpathian portion of the accretionary prism and the basin margins. To address this tectonic problem, three seismic reflection lines from Geofyzika Brno were reprocessed. The objective of the reprocessing was to improve the signal-to-noise ratio and velocity analysis to enhance reflectors buried in cultural noise (12.5 Hz and 16.7 Hz) in many places. Deconvolution, bandpass filtering, frequency filtering and velocity analysis were the main steps of reprocessing. Only common-mid-point (CMP) gathers without binning information were available, thereby limiting re-processing to post gather processes. Reprocessing greatly attenuated diffractions at the margins of the Vienna basin and West Danube basin and improved signal-to-noise ratio in some zones of the seismic sections. The main objectives of reprocessing were met though the extent of improvement is modest.

The interpretation of the reprocessed seismic sections yielded interesting results. Late Cretaceous thrust related structures within the Little Carpathian horst were identified, such as the base of the Bratislava massif, thrust onto the Modra massif. A trailing imbricate fan structure within the Envelope nappe was also imaged. Reflections at the margin of the Vienna basin and West Danube basin were correlated with borehole data, and their dips are in agreement with no or very little thermal subsidence in the Vienna basin as the reflections are close to horizontal and faulting is intensive.

ACKNOWLEDGEMENTS

I would like to thank my supervisors, Drs Jeremy Hall and James A. Wright, for their support, Dr Čestmír Tomek from Geofyzika Brno who provided the seismic and borehole data as well as invaluable information, Mr Brian Roberts who wrote the program to translate the data into SEGY format, Mr Tony Kocurko for help with software, Mr Jiri Husa from Memorial University of Newfoundland Computing Services for translation of documents from Czech to English, Dr František Hrouda for permission to use map of nappes as a background for borehole location map, Dr Leigh H. Royden and the permission editor of the AAPG for permission to use Pannonian area geologic map as a general location map, Dr Otto Fusán for permission to reprint part of Geologic map of Czechoslovakia and all others who helped and supported me.

This research was financially supported by Memorial University of Newfoundland through a graduate fellowship and through NSERC operating grants to Drs Jeremy Hall and James A. Wright.

CONTENT

LIST OF TABLES

LIST OF FIGURES

LIST OF PLATES

Pocket C:

Plate 8: Line drawing from line 671/87 with interpretation.

Plate 9: Line drawing from line 671A/87 with interpretation.

Plate 10: Line drawing from line 689/87 with interpretation.

Plate 11: Dynamite source seismic line 3T.

Plate 12: Dynamite source seismic line 8HR.

LIST OF ABBREVIATIONS

AGC: Automatic gain control

amsl: Above mean sea level

C.C.W.: Counter-clockwise

CMP: Common mid-point

CVS: Common velocity stack

K_3: Late Cretaceous

N.: nappe

NMO: Normal moveout

P.A.L.: Peri-Adriatic lineament

Pg: Paleogene

Sed.: Sediments

S.E.A.: Shortening in Eastern Alps

rms: Root mean square

T: Triassic

T.E.: Tectonic escape

T_2: Middle Triassic

T_3: Late Triassic

1. INTRODUCTION AND BACKGROUND

1.1 THE PROBLEM

Accretionary prisms are formed from the successive thrusted, compressed, tilted, slices of rocks, usually deep-water sediments, scraped off the top of a lower oceanic plate during subduction. The prism usually contains a regular age sequence, with younger formations farther away from the ocean within each slice (this is caused by tilting and erosion) but with the overall youngest rocks occurring towards the ocean (due to their sedimentation on younger crust). This simple picture is sometimes disturbed by anomalies, especially in prisms brought to the surface during or after orogenesis. This thesis examines one such anomaly: the Little Carpathian horst in Czechoslovakia.

The objective of this work is to determine the mode of emplacement of the basement of the Little Carpathian horst into the accretionary complex of the Carpathian belt. Why are continental basement rocks of Precambrian to Hercynian age in the horst emplaced into superficial nappe sequences of Cretaceous age and why are those nappes preserved at the surface between deep basins regarded as formed by strike-slip movement during terminal stages of accretion? The Little Carpathian horst is an example of a large basement uplift juxtaposed against strike-slip basins. Unlike crystalline nappes in high mountain belts, where regional metamorphism and granite emplacement are always found in deeper levels of an orogenic belt and is coeval with the orogenic episode, such basement highs commonly carry slighlty older or significantly older thrust sheets or nappes, some of which containing granitoid formations. In the Little Carpathians, the granitoids and metamorphic rocks from an older orogen, the Carboniferous Hercynian orogen, were exposed by nappe movement during the more recent, Late Cretaceous to Late Tertiary, Alpine-Carpathian orogeny.

The three main factors that controlled the creation, extension and subsidence of deep basins on both sides of the Little Carpathians are: 1) their distance from the Early Miocene nappe front, 2) their distance from partial melting under the Pannonian basin and 3) paleostress direction changes in Miocene corresponding to the rotation of the Little Carpathians. Though the seismic lines used in this thesis are too short to give information on the first two factors, this thesis will look at the third factor above: relations between Cretaceous thrusts and Miocene faulting caused by paleostress changes.

The main objective is to better image fault zones and their relations with structures interpreted from previous geologic studies. Numerous faults cut the horst, transversely slicing it into blocks forming second order horst and graben structures. Do these faults show important normal offset? Normal faulting followed by strike-slip movement is suggested as due to a stress field change during the Miocene (Nemčok et al., 1989), superimposed on the results of a Cretaceous to Miocene formation of a larger horst between two deep basins (Vienna basin and West Danube basin). The changes in stress orientation are linked to the successive closure of the Pieniny Ocean, the Magura Ocean, the Silesian Ocean and the Krosno Sea, and subsequent thrusting of the Eastern

Alps and Carpathians (Fig. 1.1). There are several extensional horst blocks in the western part of the Inner West Carpathians. The study area contains the oldest and westernmost horst block, the Little Carpathians, and adjacent margins of a purely strike-slip basin, the Vienna basin, on the NW and, on the SE, the Danube basin which began as a strike-slip basin before back-arc-style extension.

To address the tectonic problem cited above, three Vibroseis seismic reflection lines were recorded in 1987 by Geofyzika Brno and first processed by them. The total length of the seismic lines is 50.9 km (Plate 1, simplified sketch on Fig. A.1 in appendix A). Line 689/87 crosses the Little Carpathians mountain range lengthwise. Lines 671 and 671a/87, when tied, run from the Vienna basin, through the Little Carpathians to the western margin of the West Danube basin, also called Galanta basin, intersecting line 689/87. Line 3T crosses the Vienna Basin, the Little Carpathians and the Danube Basin. This last line, shot with dynamite, was not reprocessed but, because of its very good quality was used for comparison with the reprocessed lines. Line 8HR, also shot with dynamite was also used for comparison with the reprocessed lines.

The objective of the reprocessing is to improve both the signal-to-noise ratio and the velocity analyses to enhance reflectors concealed by cultural noise in many places. Deconvolution, bandpass filtering, frequency filtering and velocity analysis were the main steps of reprocessing. The signal-to-noise ratio from lines 671/87, 671a/87 and 689/87 was originally quite low because of monofrequency noise and inadequate choice of the velocity field in the first second of reflection time. Only CMP gathers without binning information were available, thereby limiting reprocessing to post gather processes. Specifically, no residual statics could be performed as the centroid of the bin northing and easting required were not written in the trace header. To help interpretation of seismic lines, borehole data was provided by Dr Čestmír Tomek of Geofyzika Brno (Appendix A).

1.2 REGIONAL GEOLOGY

The Western Carpathians were formed by the Cretaceous to Miocene accretion of far travelled terranes containing formations of Proterozoic through the Late Miocene in age. The Western Carpathians formations were deposited in ocean basins near the Tatric-Austroalpine margin (all formations south of the Pieniny Klippen belt) and ocean basins near the European margin (the Outer Carpathians and Pieniny Klippen belt of Fig. 1.1) of the Pieniny (Penninic) ocean, one of several subparallel but not synchronous Jurassic-late Late Cretaceous narrow oceans (Hamilton, 1991). The ocean basins closed from south to north, and no oceanic crust was completely subducted. The paleoposition of Austroalpine and Carpathian terranes is impossible to determine as they were faulted and thrust as the narrow oceans between them closed, and the terranes were reworked in successive episodes of oceanic closure and thrusting (Tomek, 1992, personal communication). The southern ocean closed in Turonian (Early late Cretaceous). Upper plate nappes (Choč and Križna nappes) and lower plate nappes (Austroalpine and Tatric

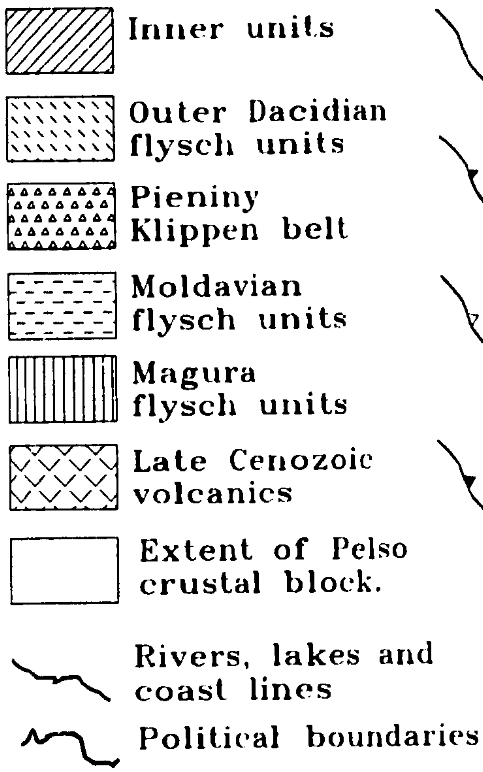

Fig. 1.1: Geologic map of the Carpathian-Pannonian area. The study area is the rectangle to the upper left. Abbreviations. A.M.: Apuseni Mountains, D.B.: Danube basin, I.E.C.: Inner East Carpathians, I.W.C.: Inner West Carpathians, L.C.: Little Carpathians, P.A.L.: Periadriatic lineament (strike-slip movement), T.D.R.: Transdanubian range, T.S.B.: Transylvanian basin, V.B.: Vienna basin. Modified from Royden and Sandulescu (1988) with permission, with additional information from Kókai and Pogácsás (1991) and Royden (1988).

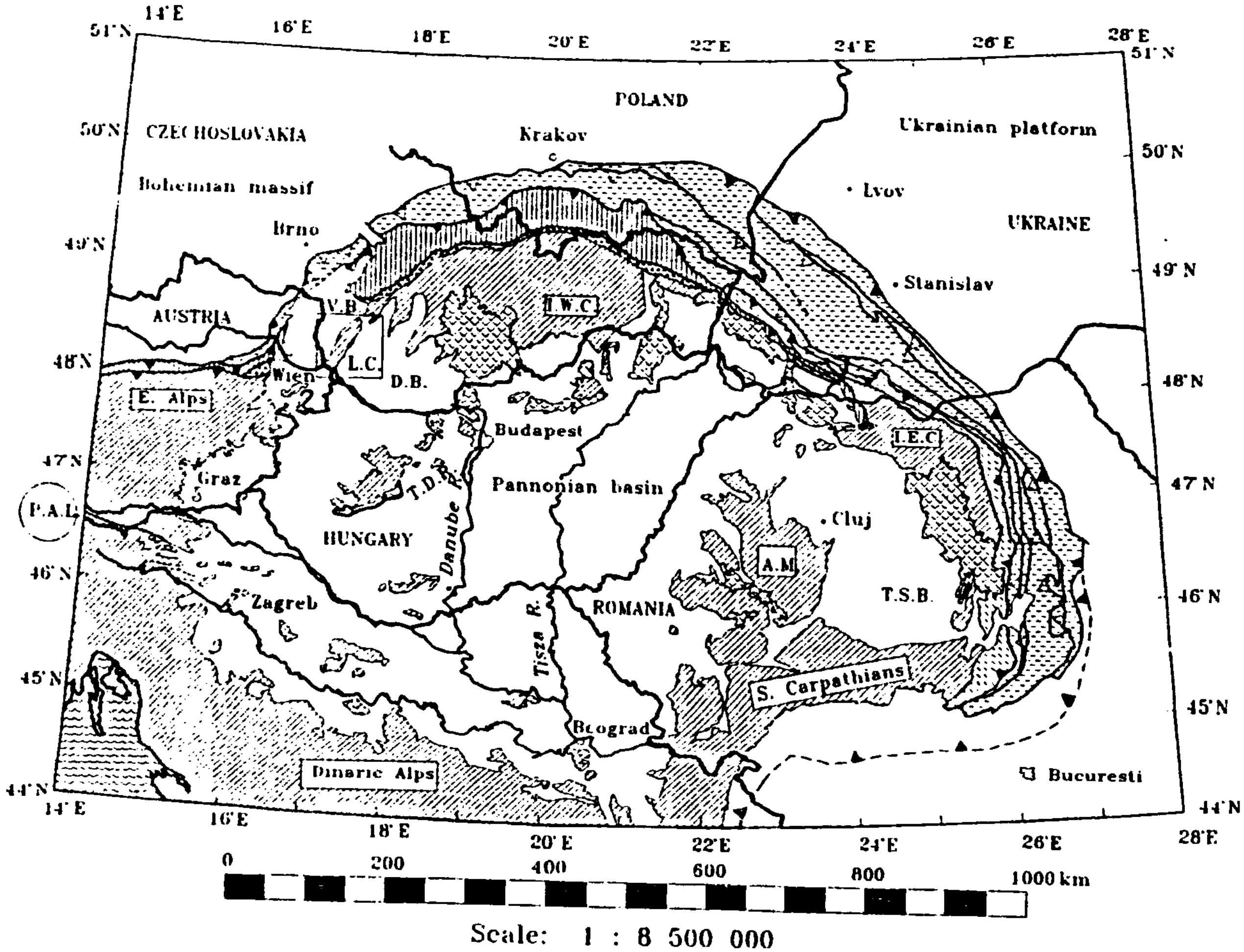
14°E
16°E
18°E
20°E
22°E
24°E
26°E
28°E
51°N
50°N
49°N
48°N
47°N
46°N
45°N
44°N
POLAND
CZECHOSLOVAKIA
Bohemian massif
Krakov
Ukrainian platform
Lvov
UKRAINE
Brno
Stanislav
AUSTRIA
V.B.
I.W.C.
L.C.
Wien
D.B.
E. Alps
Budapest
I.E.C.
Graz
T.D.R.
Pannonian basin
P.A.L.
HUNGARY
Cluj
Danube R.
A.M.
T.S.B.
Zagreb
ROMANIA
Tisza R.
S. Carpathians
Beograd
Dinaric Alps
Bucuresti
0
200
400
600
800
1000 km
Scale: 1 : 8 500 000

crystalline nappes such as the Envelope nappe of the Little Carpathians) were formed. These nappes became the southern subduction boundary for the Pieniny ocean, which closed in Late Cretaceous to Palaeogene (Tomek, 1992, personal communication). As the Pieniny Ocean closed, oceanic basins successively widened in the north (Magura basin, Silesian basin and Krosno Sea), separated by island arcs (Pieniny Cordillera, Czorsztyn ridge, Silesian cordillera) (Fig. 1.2). In Oligocene and Miocene, the former northern margin of the Pieniny Ocean became the southern boundary of Magura oceanic basin, and so on until the Krosno Sea (also called Subsilesian oceanic basin) was subducted in Middle Miocene. As subduction progressed from west to east, a basin could be completely closed on its western end while still widening at its eastern end (Hamilton, 1991). During the Neogene, transtensional basins opened to compensate for the shortening. Two of them, the Vienna basin and the West Danube basin, lie on each side of the Little Carpathians. Appendix B contains a schematic version of the tectono-stratigraphic history of the Carpatho-Pannonian area.

1.2.1 Continental margins and Pieniny ocean

The oldest rocks known in the Eastern Alpine-Carpathian-Pannonian area are found in the Bruno-Vistulicum of the Bohemian massif (top left corner of fig. 1.1). The Bruno-Vistulicum is a complex of Proterozoic rocks from accreted terranes (Bližkovský et al., 1986; Suk, 1987). The oldest K/Ar, Rb-Sr and U-Pb ages range from 1065 to 1410 Ma (Chaloupský, 1989; Rudakov, 1985). The block was folded around 800 Ma and

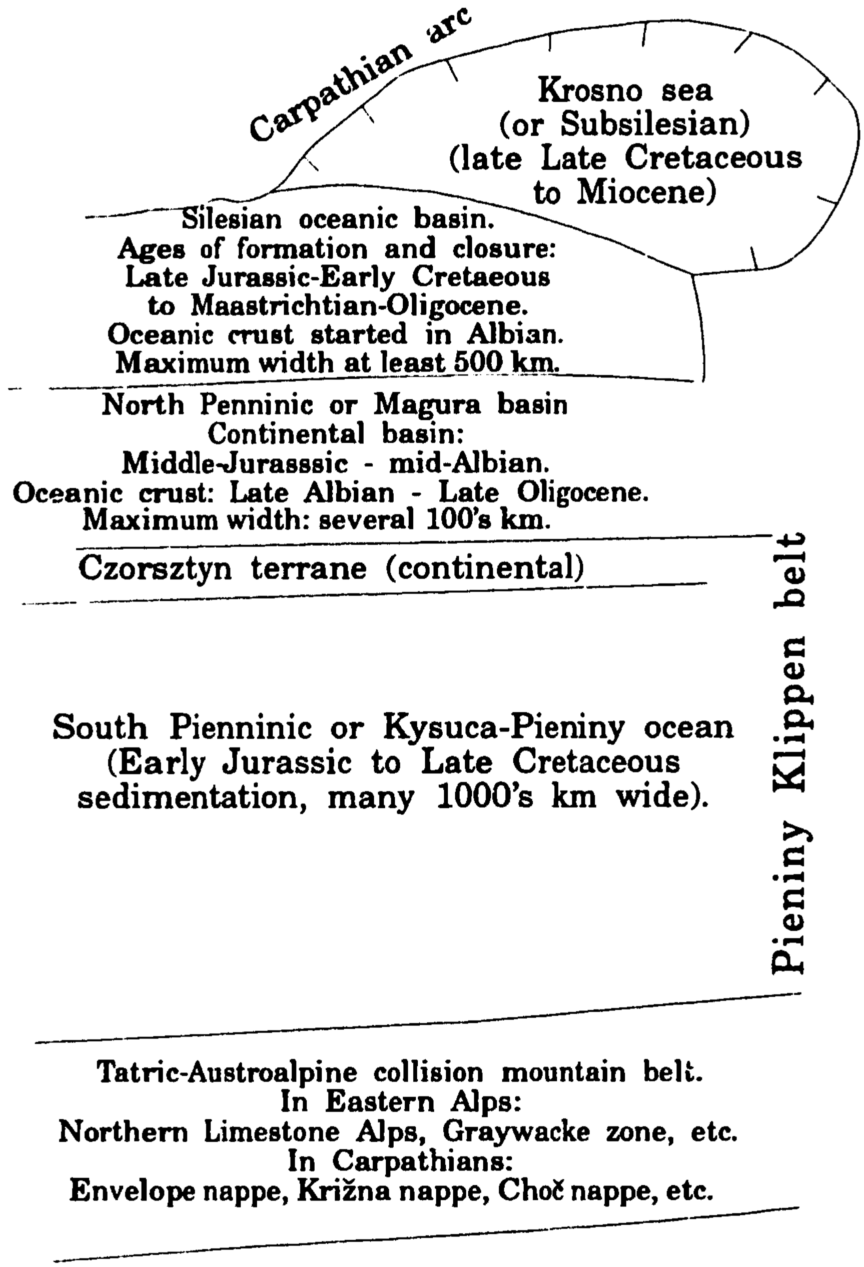

Fig. 1.2: Succession of oceanic basins between Europe and the Tatric-Austroalpine block with ages. The basins were not opened simultaneously so this figure is not a palinspatic reconstruction (Tomek, 1992, personal communication).

metamorphosed between 550 to 620 Ma (Blížkovský et al, 1986; Suk, 1987).

The basement of the southern margin of the Pieniny Ocean was also formed by Late Proterozoic accreted terranes. The Pezinok-Pernek and Harmonia Series found in the Little Carpathians (Plate 1) are exposed examples of such formations. The primary sediments deposited in the Late Proterozoic or earlier were folded (with a now NW-SE axis, see Plate 1 over Modra massif) in a tectonic episode coeval with folding of the Bruno-Vistulicum. They were buried from Cambrian to Late Carboniferous to sufficient depth to be metamorphosed into gneiss-schist during the Cambrian or into phyllites up to the Devonian (Fig. B.2) (Burchart et al., 1987; Földvary, 1988; Rudakov, 1985).

During the Palaeozoic (Fig. B.3), while the whole Bohemian massif was folded, faulted aud intruded by the Hercynian Orogeny, a coeval but possibly independant orogen caused many intrusions in the basement of the Tatric-Austroalpine margin, such as the Bratislava and Modra massif of the Little Carpathians at around 302±40 Ma (Burchart et al., 1987). The metasediments of the Pezinok-Pernek and Harmonia Series were metamorphosed, sometimes retrogressively, by contact with the intrusives. They were exposed again at the surface and were eroded during the Permian (Mahel' et al., 1972).

During the Late Triassic (Fig. B.4), a transform zone was initiated between Laurasia, the European margin, and Gondwana, the Tatric-Austroalpine margin (Rakús, 1988). A series of oceanic or paraoceanic basins formed on both sides of the transform zone, which became the Pieniny Ocean after the opening of the Central Atlantic around 165 Ma (Artyushkov and Baer, 1986).

From SSW to NNE, the nappes forming the Little Carpathians are the Envelope nappe, the Križna nappe, the Choč nappe and a small parcel of the Havran nappe at the northern edge of the Little Carpathians. On the Tatric-Austroalpine margin, the Tatric ridge which included the root zone of the Envelope nappe, was the northernmost terrane, the closest to the Pieniny Ocean. The Envelope nappe contains the Bratislava and Modra massifs, the Proterozoic-Palaeozoic cover they intruded through and their Permian to late Early Cretaceous cover, the Little Carpathian group (Mahel' et al., 1961, 1972; Rakús and the IGCP National Working Groups, 1988). Behind was the Zliechov Basin (at least a hundred kilometres wide) and the deposition area of the Vysoká unit, both now forming the Križna nappe (Fig. 1.2). The Križna nappe is composed of Early Triassic to late Early Cretaceous sedimentary rocks, which are mostly limestone, marlstone and similar rocks. Further behind, probably behind another ocean basin, were the root zones of the Choč nappe and Havran nappe (Hovorka and Spišiak, 1988; Michalík and Soták, 1991; Mišík and Marschalko, 1988; Tomek, 1992, personal communication). The Choč nappe contains a Carboniferous (?) to Permian volcanoclastic series, the melaphyre formation (Plate 1). Besides this formation, most units are made up of carbonate rocks.

The southernmost deposits of the Pieniny Klippen belt are from the Pieniny Ocean which was many thousands of kilometres wide (deposits contain radiolarites in the

Kysuca formation which require open sea). The Pieniny ocean was bordered to the north by a moderately submerged terrane (the Czorsztyn ridge). Behind was the Magura oceanic basin, several hundreds of kilometres wide, where the formations of the Magura nappe (Figs. 1.1, 1.2) were deposited. Closer to the European continent were the Silesian oceanic basin, at least 500 km wide, and the Krosno sea as well as smaller basins, where the sediments found in the Outer West Carpathians were deposited. The Bruno-Vistulicum of the Bohemian massif formed the boundary of the passive margin of the Krosno Sea. The Outer Western Carpathians indeed follow its edge.

1.2.2 Oceanic closure

In the Tatric-Austroalpine domain, nappe formation occurred from the hinterland to its foreland: the Havran nappe was thrust onto the Choč nappe in Aptian or earlier while thrusting of the Envelope nappe started in Coniacian or earlier from dating of basalts containing carbonate xenoliths (Hovorka et al., 1982). The apparent reversal of position is explained by overthrusting of the Choč nappe onto the root zone of the Križna nappe and this pile onto the root zone of the Envelope nappe. The Little Carpathians are close to the nappe front where the thrusting plane was going downward. Erosion removed the nappes between the nappe front and the root zone (Fig. 1.5). The nappe transport stopped after the Turonian, in Late Cretaceous, in the Inner West Carpathians (Tomek, 1992, personal communication). Besides the Envelope nappe and other Tatric nappes, which were from an area that was already in a ridge position during the subduction of the Pieniny Ocean, West Carpathian nappes do not contain crystalline basement fragments - they are rootless nappes.

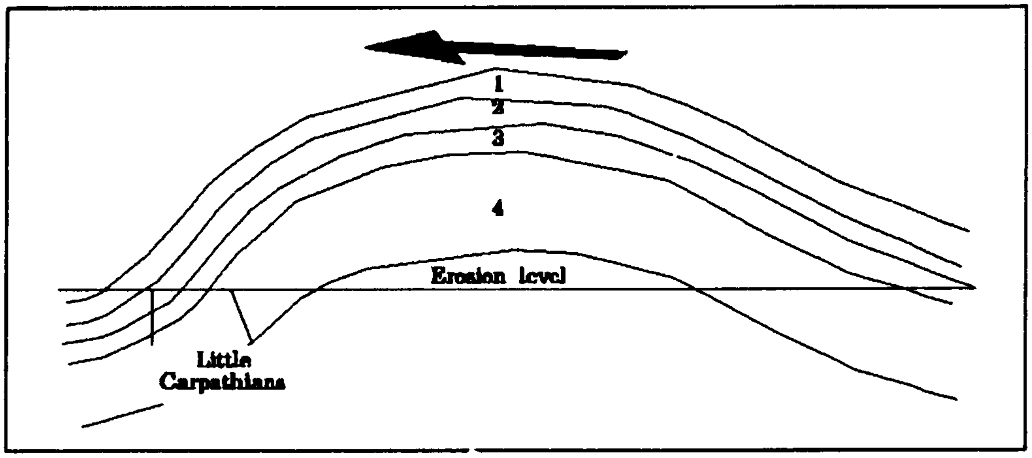

Fig. 1.3: Schematic explanation of nappe structure of the Little Carpathians. Nappes: 1) Silica nappe, 2) Choč nappe, 3) Križna nappe, 4) Envelope nappe. Subvertical lines indicate the present margins of the Little Carpathian horst block. The arrow indicates the nappe transport direction.

Subduction of the Pieniny ocean started at the end of the Early Cretaceous. The oceanic crust subducted under the northward moving Tatric-Austroalpine terrane. Ocean spreading did not end before the end of the Aptian, the first stage of the late Early Cretaceous (Rakús, 1988). Meanwhile, deep basinal conditions where continuing on the European Margin (Magura, Silesian and Krosno oceanic basins) up to the Oligocene and Early Miocene (Fig. B.7 to B.9). From occurrence of thin radiolarian deposits, oceanic crust in the Magura and Silesian oceanic basins likely formed at the closure of the Pieniny ocean (Rakús and the IGCP National working groups, 1988). In the Oligocene and early Miocene, deposits from the relict basins in the Pieniny realm (Magura) were thrust together with Jurassic and younger deposits of the Kysuca-Pieniny basin and of the Czorsztyn ridge to form the Pieniny Klippen Belt and the Magura flysch belt (Tomek, 1992, personal communication). The southern boundary of this Kysuca-Pieniny terrane seems to be of strike-slip nature and runs along the southern limit of the Pieniny Klippen belt, 20 to 25 km NNW of the Little Carpathian horst block.

1.2.3 Little Carpathian horst block

After the end of the nappe thrusting and strike-slip faulting, localized sedimentation occurred in a deep trough over the nappes in the eroding Inner West Carpathians. This depositional area includes the basement of the Vienna Basin south of the Pieniny Klippen belt, the Little Carpathians and the basement of the Danube basin. From the late Eocene to the end of the Oligocene, the deposition area widened south of the Carpathians to form the forebear of the Pannonian basin, the Palaeogene Hungarian basin (Royden and Baldí, 1988). This occurred while the tectonic blocks forming the basement of the Pannonian basin moved NNE along strike-slip faults from a zone between the Eastern Alps and the Southern Alps to their present position (Ratschbacher et al., 1991, 1990; Royden, 1988; Royden et al., 1982).

The Oligocene to Early Miocene (26 to 18 Ma) movement of crustal blocks in the Pannonian basin during the Krosno sea subduction pushed the Little Carpathians and other West Carpathian ranges against the Bohemian massif (Lalla, 1984; Ratschbacher et al., 1991, 1990) and caused the progressive west to east folding and thrusting of the Outer West Carpathians. The Little Carpathians are dissected by a tight array of Neogene normal and strike-slip faults (Fodor et al., 1990; Kováč et al., 1989; Nemčok et al., 1989) that accommodated the rotation of the stress field (Fig. 1.4). At the transition between Oligocene and Miocene (Egerian stage), the Vienna basin opened between the Little Carpathians and the nappe front as a piggy-back basin as the nappes of its pre-Neogene basement were still moving (Royden, 1985; Wessely, 1988). The horst and graben structures thus formed explain some of the irregular topography of the pre-Neogene basement of the Vienna basin as seen from borehole data (Table A.1). In Lower Miocene, the rotation was accommodated in the Little Carpathians by N-S left-slip faulting that moved the Modra Massif northward relative to the Bratislava massif. Related normal faults perpendicular to the Little Carpathians horst dissected it into a horst and graben structure. The West Danube basin also opened at the beginning of the Miocene as a series of parallel transtensional half-grabens such as the narrow trough on Fig. 1.5, to accommodate the movement of crustal blocks in the Pannonian basin (Bergerat, 1989; Tomek and Thon, 1988).

Thrusting along this segment of the Eastern Alps and Outer West Carpathians ended in early Middle Miocene (Karpatian stage). The former normal faults crossing the Little Carpathians became right-slip faults and the left-slip faults became normal faults. The Vienna basin then became a transtensional basin. Up to 80 km of strike-slip

Fault orientation across the Little Carpathians, Vienna basin and immediate margin of the West Danube basin (18.27):

(1) Early Miocene (Eggenburgian to Carpathian or Early Badenian) phase. Paleostress related to formation of Outer Carpathian nappes.

- WNW-ESE
- N-S , plus NNE-SSW in Vienna basin and West Danube basin
- NNW-SSE
- NE-SW in Vienna basin, related to strike-slip.

(2) Lower to Middle Miocene (Karpatian to Early Badenian phase. Paleostress related to progressive eastward stop of Outer Carpathians nappe movement.

- NNW-SSE
- N-S
- ca E-W + N30-N60 in Vienna basin and West Danube basin.
- small W-E with 60^0-70^0 dip, related to strike-slip movement.

(3) Middle Miocene (Middle to Late Badenian) phase, main period of Vienna Basin transtensional extension.

- N-S
- ca E-W
- NE-SW, in Vienna basin and West Danube basin.

(4) Late Miocene-Pliocene (Sarmatian-Pliocene) phase. Widening of Vienna and West Danube basin by normal faulting along the Little Carpathians.

- ca NE-SW difining of margins of the Little Carpathians.
- NE-SW in the Vienna basin at the beginning of this period on dip-slip faults.
- NE-SW at the end of the Sarmatian (12-11.5 Ma) near Rohožník. Short reversal of slip orientation on dip-slip faults.

Fig. 1.3: Paleostress changes across the Little Carpathians, the Vienna basin and the Danube basin during the Neogene (Fodor et al., 1990; Kováč et al., 1989; Nemčok et al., 1989).

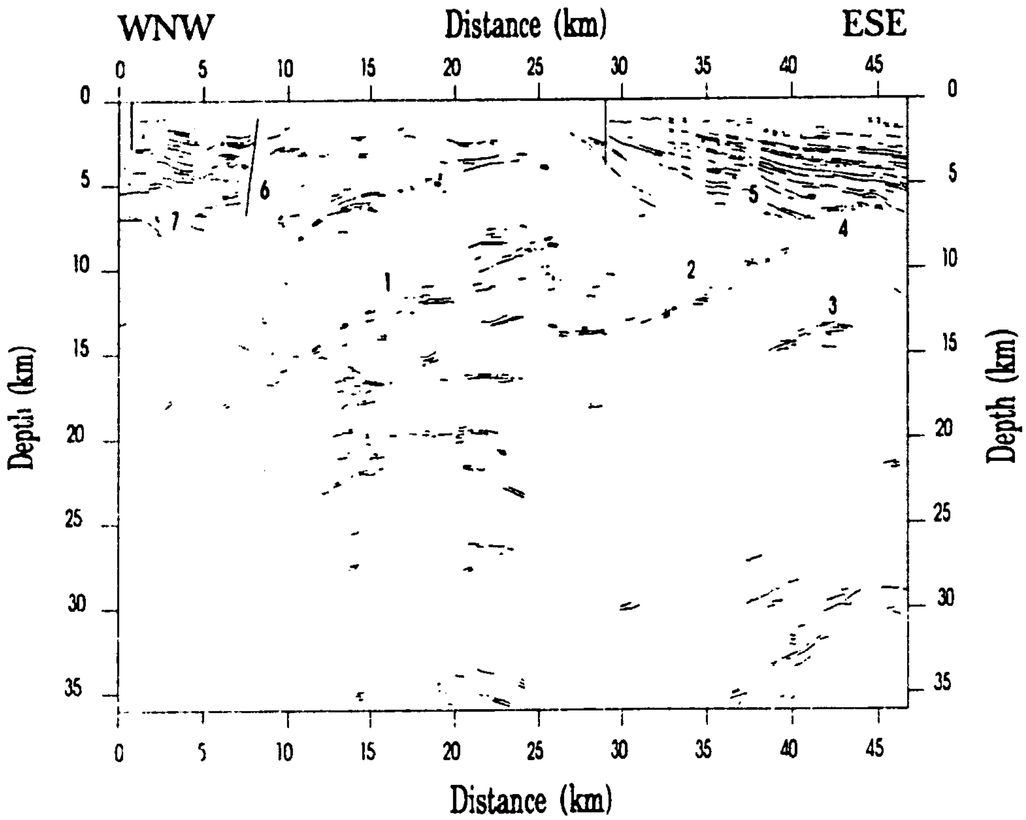

Fig. 1.4: Line Drawing from line 3T. 1) and 2) detachment surfaces of Badenian-Pannonian low-angle normal faults related to the formation of the horst and graben structure. 3) Thrust fault within Tatric nappes. 4) pre-Neogene basement of the West Danube basin. 5) horst. 6) Litava faults which are a segment of the Peripieninian lineament. 7) base of the Zohor-Plavecky graben of the Vienna basin. The vertical lines are an average of the boreholes around Láb in the Vienna basin and borehole G-1 in the West Danube basin. The depth scale is the equivalent depth for a 6 km/s stacking velocity (Modified from Tomek et al., 1987).

movement brought nappes of the Little Carpathians parallel to nappes of the Austroalpine domain (Northern Limestone Alps, Graywacke zone).

Middle Miocene partial melting and crustal thinning under the Pannonian basin caused thermal subsidence and extension of the West Danube basin, inclining the sedimentary layers toward the Pannonian basin as seen on Fig. 1.5, and the incorporation of the SE edge of the Little Carpathians into the basin margin (Beránek and Zátopek, 1981b; Čermák, 1981; Horvath, 1984; Sclater et al., 1980; Tomek and Thon, 1988). Subsidence of the Vienna basin at the Little Carpathians margin likely did not begin until the Badenian (16.5-13.5 Ma, Middle Miocene, Table 1.1), the main extension stage of the Vienna basin. Normal faulting of the West Danube basin and Vienna basin margins further narrowed the Little Carpathian horst, while small blocks within the Little Carpathians were displaced along N-S right-slip faults.

The resulting array of faults makes correlation of units a complex task in the Little Carpathians. The presence of the Little Carpathians as a horst between these two basins may be partly explained by the fact that it was too far from the Outer Carpathians nappe front for piggy-back extension and too far from the Pannonian basin to subside completely, though its West Danube margin subsided dramatically during the Late Miocene. This is similar to the Basin and Range subsidence in Western United States (Wernicke, 1985). The Little Carpathian horst thus stayed as a SSW-NNE oriented horst within a series of horsts and grabens.

Table 1.1: Sediment thicknesses at the northwestern margin of the Vienna basin (Jiřiček and Tomek, 1981)				
Epoch	Age	Time (Ma)	Sediment thickness	Type of sediments
Pleistocene		1.8 - 0	Up to 30 m	Varied
Pliocene	Romanian	4.0 - 1.8	50 to 60 m	Freshwater marls and gravels
	Dacian	5.6 - 4.0	100 to 150 m	Varied
Late Miocene	Pontian	8.5 - 5.6	Up to 100 to 180 m	Variegated clays, gravels and sands
	Pannonian	11.5 - 8.5	400 to 600 m	Halfbrackish with decreasing salinity, from calcareous clay to gravel
Middle Miocene	Sarmatian	13.6 - 11.5	300 to 600 m	Brackish to freshwater
	Middle and Upper Badenian	~ 15.5 - 13.6	800 to 1300 m	Frequent shallow and freshwater beds in marine sediments
	Lower Badenian	16.5 - ~ 15.5	500 to 800 m	Marine

1.3 GEOLOGICAL MODEL

1.3.1 Simplified geological model

A simplified geological model for the horst block would thus be: 1) a Late Proterozoic zone of sedimentation, folded and metamorphosed, intruded by granitoid intrusives at the end of the Hercynian orogen (Burchart et al., 1987). 2) In the Late Cretaceous, as the oceans were closing, the Proterozoic formations of the Little Carpathians and overlying rocks were broken off their basement to form the Envelope nappe. This nappe was thrust onto parauthochthonous near-ocean calcareous formations (Hovorka et al., 1982). The Choč and Križna nappes were thrust onto the Envelope nappe, the compressive forces bringing the intrusives in the lower nappe to a higher level relative to the other nappes. 3) In the Tertiary, this nappe pile was rotated altogether anticlockwise against the edge of the Bohemian massif as terranes escaping from the Eastern Alps pushed the Carpathian blocks northward. 4) Meanwhile, the strike-slip movement associated with tectonic escape initiated tectonic subsidence of a portion of the nappe pile to form the West Danube basin. This early subsidence included what are now the Little Carpathians so that formations from the Little Carpathians can be correlated with formations of the basement of the West Danube basin. 5) NNE slip of blocks from the Northern Limestone Alps nappe system brought them parallel to the Little Carpathian horst block and started the subsidence of the Vienna Basin. These nappes form the basement of the Vienna basin west of the main strike-slip fault on the NW edge of the Little Carpathians horst block. This implies that formations from the basement of the Vienna basin cannot be correlated with formations from the Little Carpathians. 6) Because of the change of paleostress during the Neogene that induced intensive strike-slip and normal faulting in changing directions, the nappe structures of the Little Carpathians were themselves broken into smaller blocks.

1.3.2 Testing the model

If the above model is correct, the seismic lines could show:

1) A deep detachment horizon between the basement and the rotated block above it.

2) Detachment horizons of faults active during the formation of the NNE trending horst and graben structure. 1) and 2) could be the same.

3) Large offset on dip-slip faults on both sides of the horst to form the margin of the Vienna basin and West Danube basin. The faults on the West Danube margin would probably not be as steep as on the Vienna basin side because the subsidence of the West Danube side was influenced by crustal thinning of the Pannonian basin.

4) Normal faults on line 689 bounding the NNW trending horst and graben structure. These faults would be unlikely to appear on lines 671/87 and 671A/87 as the strike of these two lines is close to the strike of these faults. This should be seen on line 689 as the other lines are roughly parallel to these.

5) Many diffractions indicative of a rough basement topography caused by the horst and graben structure.

Because of the intensive Neogene strike-slip and dip-slip movement in the Vienna basin, in the West Danube basin and in the Little Carpathians, correlation of sedimentary units must be controlled by borehole data from boreholes quite close to seismic lines to avoid misties due to faults between boreholes and seismic lines.

1.4 GEOPHYSICAL BACKGROUND

1.4.1 Gravity field

The Bouguer gravity anomaly is 25 mGal higher above the West Danube basin (-15 mGal) than above the Vienna basin (-40 mGal) though the maximum thickness of sediments is 5 to 6 km in both basins. The higher Bouguer gravity and higher heat flow above the West Danube Basin is attributed to crustal thinning under the Danube basin coeval with partial melting and crustal thinning under the Pannonian basin in Middle to Late Miocene (Čermák, 1984). The alternating negative and positive anomalies in the West Danube basin are partly produced by the horst and graben created during the initial strike-slip phase of extension and also by high density Neogene volcanic rocks, outcropping east of this map (Fig. 1.1).

The abrupt decrease in Bouguer anomaly at the Vienna basin margin indicates large offset dip-slip faults at the NE margin of the Vienna basin, as observed at the NW end of seismic reflection line 3T (Fig. 1.4) as opposed to back-arc type extension after strike-slip in the West Danube basin as suggested by the gently dipping horizon observed on the SE end of the same line (Tomek and Thon, 1988; Tomek, 1988; Tomek, personal communication, 1990). Results of the integrated modelling of seismic refraction velocity and Bouguer anomaly through the northern end of the Little Carpathians yielded results of Table 1.4 and showed that the Modra massif granodiorite intrusive is not vertical but dipping through the Proterozoic-Palaeozoic metasediments of the Pezinok-Pernek and Harmonia Series (Blížkovský, 1989). The dip of the Modra massif is likely to originate at least in part from rotation during the nappe emplacement. The metasediments and intrusive were modelled as resting on rocks from Inner West Carpathian nappes as suggested by the presence of carbonate xenoliths in basalt dikes of the Modra massif (Hovorka et al., 1982). However, because of the low density and velocity contrast within the Little Carpathians (Table 1.3), this model should be taken with caution, and the asymmetry of the Bouguer gravity is then probably not caused by the inclination of the Modra intrusive but by the difference between the margin of the Vienna basin which shows a large vertical offset and the smaller offsets of the faults at the West Danube margin.

Fig. 1.6 also indicates that the Neogene depression between the northern margin of the Little Carpathian horst and the next range of the Western Carpathians is shallow as suspected from the geological map (Plate 1). Gravity modelling of the Carpatho-Pannonian area is complicated by the similar density of all the rocks within the nappes, as seen in Tables 1.2 and 1.3. Besides the flysch nappes, which have a density of 2.45

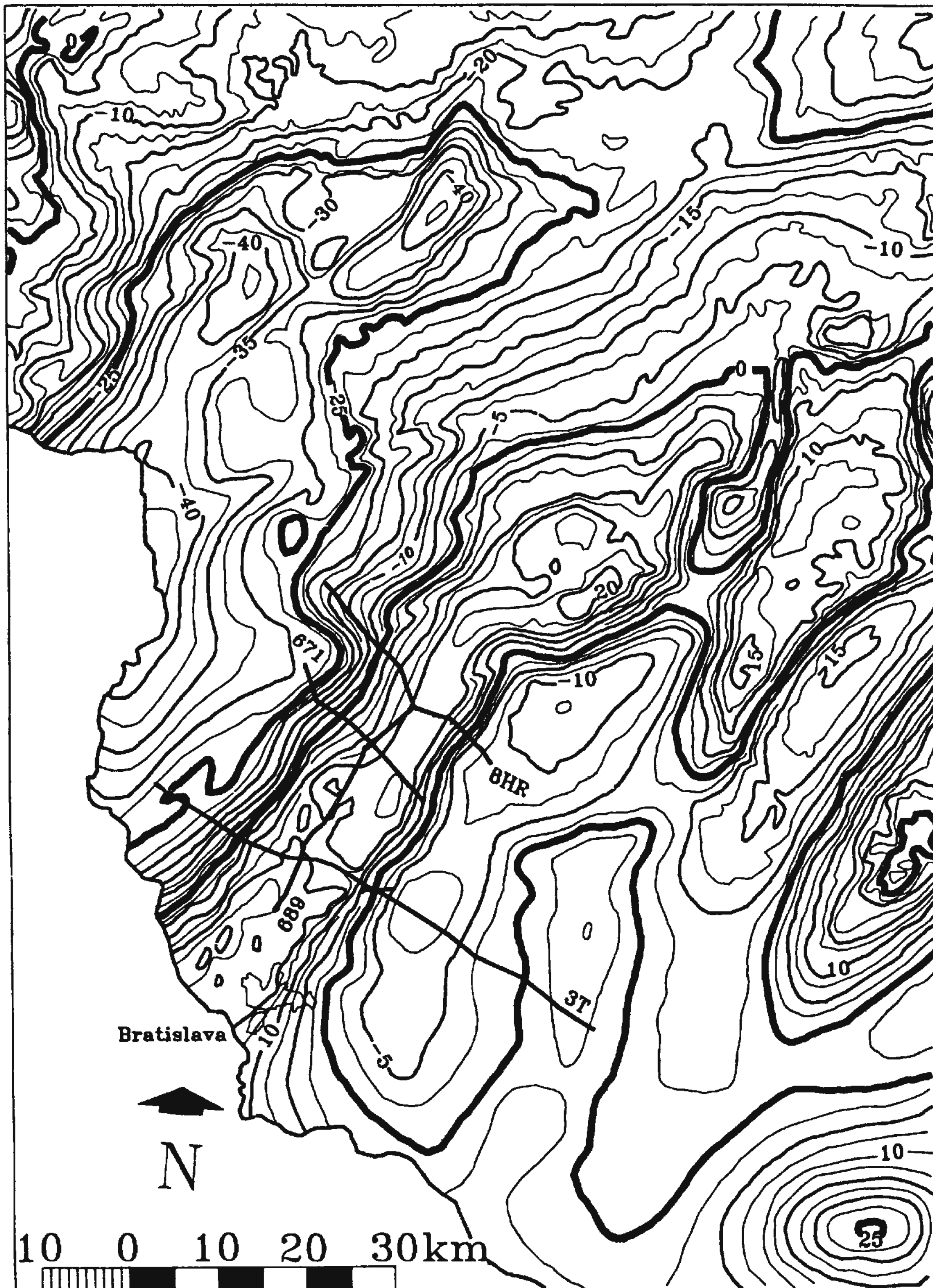

Fig. 1.5: Bouguer gravity map of central Czechoslovakia (Tomek, 1992, personal communication. Isonomal interval is 2.5 mGals. Location of seismic reflection lines is shown over the gravity map.

g cm^{-3} and higher, and the basin fill, with a low density of 2.1 g cm^{-3} close to the surface and a gradient due to compaction, all formations have a density close to 2.7 g cm^{-3}.

Table 1.2: Average densities of formations.

Formation	Average density (g/cm^3)	Reference
Bohemian massif	2.70, samples collected throughout the massif.	Granser, Meurers and Steinhauser, 1989)
Flysch nappes	2.45	Jiřiček and Tomek, 1981
Amphibolites of Pezinok-Pernek series	2.936	Dvořaková, 1987
Hercynian Bratislava massif (intensely mylonitised white-grey granodiorite, borehole MKM-2)	2.602, more than 70 samples over a depth range of 500 m.	Dvořaková, 1987
Hercynian Bratislava massif (migmatite with 0.5% porosity, borehole MKM-2)	2.732, a few samples interspaced with above samples.	Dvořaková, 1987
Hercynian Bratislava massif (granitoids, borehole MKM-6)	2.675, more than 40 samples over a depth range of 600 m.	Dvořaková, 1987
Mesozoic tectonic breccia	2.722 1 sample, z = 0.2795 km	Dvořaková, 1987
Middle to Late Jurassic limestone	2.711 1 sample, z = 0.2987 km	Dvořaková, 1987
Early Triassic quartzite	2.588 1 sample, z = 0.2919 km	Dvořaková, 1987
Northern Limestone Alps	2.70	Granser, Meurers and Steinhauser, 1989

Table 1.3: Densities inferred from interval velocities calculated from stacking velocities.		
Formation	Velocity (km/s)	Average density (g/cm^3)
Basin fill	2.2 to 2.4	2.1
Triassic to Cretaceous sedimentary rocks from Križna and Choč nappes	5.3 to 5.7	2.6
Hercynian Modra massif	5.8 to 6.2	2.68

Table 1.4: Approximate lower depth of major groups of rocks at the northern end of the Little Carpathians from integrated modelling of refraction and Bouguer gravity data (Blížkovský, 1989)	
Group of units	Depth of lower boundary
Higher Inner West Carpathian nappes (Choč nappe and Križna nappe and maybe Silica or Havran nappe)	2.7 to 3.3 km
Proterozoic to Palaeozoic metasediments (Pezinok-Pernek and/or Harmonia Series in Plate 1)	6.4 to 7 km
Inner West Carpathians para-autochthonous nappes containing carbonate rocks (Hovorka et al., 1982)	8.7 to 9.1 km
Autochthonous granitoids	17.5 to 18 km
Upper part of lower crust	around 21 km
Lower part of lower crust	around 28 to 30 km

1.4.2 Palaeomagnetism and rock magnetism

Comparative study of the magnetisation of sedimentary rocks from the Little

Carpathian group, the Križna nappe and the Choč nappes indicates that the crystalline core complex rotated together with the nappes (Hrouda, 1986) and is thus also allochthonous. Thrusting of the nappes thus occurred before the rotation of the massif. Palaeodirections in Lower Miocene sediments indeed indicate a counter-clockwise rotation of the West Carpathians: 43° since the mid-Early Miocene (Eggenburgian, 19-22 Ma), 37° since the early Middle Miocene (Karpatian, 16.5-17 Ma) (Kováč et al., 1989). The rotation of the Little Carpathians may have been larger than this Inner West Carpathian average as suggested by the change in orientation of the faults north of the Little Carpathians (Plate 1).

Palaeomagnetic orientation from Permian melaphyre rocks (Plate 1) in the Choč nappe of the Little Carpathians show close to 90° rotation since the Permian (Krs et al., 1981) as the paleo-north is now pointing westward. Around 45° of rotation thus occurred between the Permian and the Early Miocene.

1.4.3 Earthquake seismology and subsidence

Some seismic activity along the axis of the Little Carpathians and the NE margin of the Vienna basin and levelling surveys indicate that tectonic processes are still occurring. Fault plane solutions of earthquakes in the southern part of the Vienna basin (in Austria) suggest N-S compression and E-W extension, resulting in left-slip along a NE-SW trending fault, the same mechanism that created the Vienna basin. These earthquakes are part of a belt running from Eastern Austria to the Pieniny Klippen belt, the Peri-Pieninian lineament (Gutdeutsch and Aric, 1988; Karnic et al., 1984). Many faults on the Little Carpathian margin of the Vienna basin are related to this lineament. Statistical analysis of Mercalli intensities show that the earthquakes in the Little Carpathians have smaller source zones, cause lower stress drops and occur in more homogeneous material than in neighbouring areas (Gutdeutsh and Aric, 1988). Their foci usually have a depth of 10 km or less (Zátopek, 1979), that this is the depth of the transition from brittle to ductile deformation. A model where extrusion of blocks from the Eastern Alps into the Carpatho-Pannonian area occurs by slip between these two blocks would explain the following recent movements.

1) Quaternary terraces of the Danube River are broken by the fault bounding the Little Carpathians near Bratislava are 100 m above the river on the horst side and buried below about 300 m of river and lake sediments on the other side (Kvítovič and Plančar, 1979).

2) Transpression is indicated by recent folding in the northern part of the Little Carpathians coincident with transtension in the pull-apart grabens of southwestern Slovakia (Tomek, 1988).

This model would also explain the disparity in the subsidence of the tectonic blocks in the area (Table 1.5).

Table 1.5: Quaternary subsidence. (Kvitkovič, 1979)	
Area	Average subsidence (mm/year)
Malé Karpaty block	0.0 to 0.5
Plain part of Danube basin	1.0 to 3.0
Northern West Danube basin	0.0 to 1.0
Vienna Basin	0.5 to 1.5
White Carpathians	0.0 to -0.5

1.4.4 Explosion seismics

1.4.4.1 **Refraction profiling**

A few tens of kilometres north of the Little Carpathians, refraction modelling shows a 10 km jump in the Moho depth across the Peripieninian lineament (Beránek and Zátopek, 1981) indicating a major tectonic discontinuity coincident with the oceanic suture, the crust being thinner on the Apulian (Little Carpathian) side, which is compatible with earthquake data outlined above: slip movement between both sides may still be occurring, and be partly accommodated through the many faults on the Little Carpathians' NW edge, such as the one crossed by line 671/87, and by transpression on the northern end of the horst.

1.4.4.2 Reflection profiling and borehole data

A thrust fault cutting Pliocene deposits with almost 500 m of thrust separation was found by seismic reflection tied to boreholes in the West Danube basin (Tomek and Thon 1988). It is identified on line 3T beneath kms 34 to 35 (Fig. 1.4 and Plate C). It is the first indication of compressive structures that far north in the West Danube basin. There are also low-angle normal faults related to the formation of the horst and graben structure during the main phase of subsidence of the Vienna basin (Badenian time, 13.5-16.5 Ma) and West Danube basin (Pannonian time, 8.5-11.5 Ma) at about 10-15 km depth which may correspond to the lower depth of earthquake foci in this area. Line 3T does not show many reflectors close to the surface across the Little Carpathians. This seismic line tied to borehole data shows block rotation and faulting in the sediments and basement of the Vienna basin.

2. PROCESSING

Re-processing of lines 689/87, 671/87 and 671A/87, as suggested by Dr Čestmír Tomek from Geofysika Brno, should enhance the reflectors in the data. On all three lines, many short segments of reflectors appear in the first two seconds of *data, and if reprocessing could bring out more signal to link them together, the interpretation would become easier. The original line 689/87 (Plate 4) was already well processed, though contaminated with 12.5 Hz noise (Fig. 2.12). European railroads often use a frequency of 12.5 Hz and a railroad passes 5 to 8 km away from line 689/87, over thin Pliocene to Quaternary sediments deposited on the Bratislava granitoid intrusive (Mahel', 1972; Mahel' et al., 1961). The geophones have likely picked up inductively the EM railroad signal, especially strongly along the line 689/87. Lines 671/87 and 671A/87 were extremely noisy with very few reflectors visible on the original stacked sections (Plates 2 and 3). Line 671/87 shows incoherent noise and some ringing under the margin of the Vienna basin (Plate 2). The lack of reflectors corresponding to the margin of the West Danube basin on line 671A/87 seems to have two causes: ground roll and inappropriate stacking velocity (Plate 2). The original stacking velocity caused the reflectors of the Danube basin to be buried under diffractions and ground roll. The quality of the original data can be assessed from the CMP gathers (see Figs 2.1 and 2.2). The quality of the stack would be improved by the removal of 12.5 Hz noise and by improved velocity analysis.

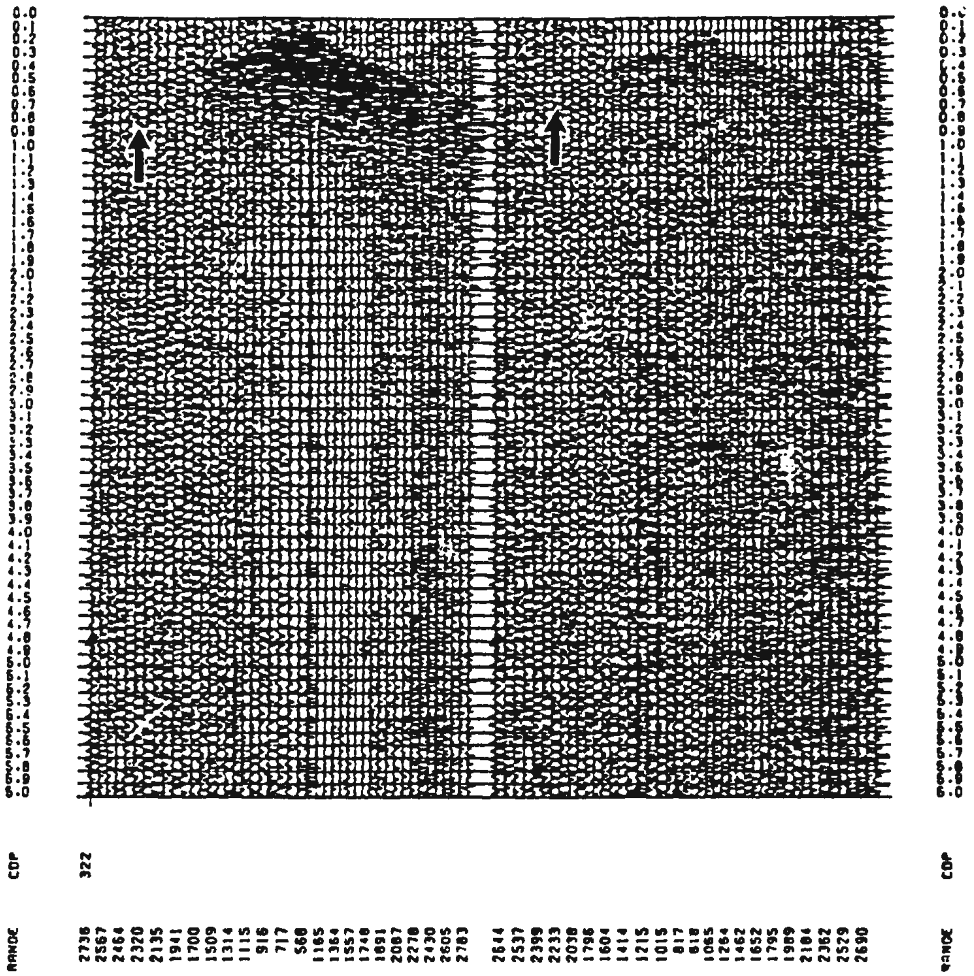

Fig. 2.1: CMP 322 from line 671/87 after statics corrections with (right) and without (left) pre-plot AGC. Note how the 12 to 17 Hz noise masks the direct wave on its left side. Comparison of gained and ungained panel show that this noise is already serious before AGC is applied. The range scale is the number of meters between the geophone point and the shot point corresponding to this trace. Vertical scale is the two-way time. Before we received the data, some kind of scaling by trace energy was likely done, since short offset traces have higher early, and lower later signal levels than large offset traces (on left panel).

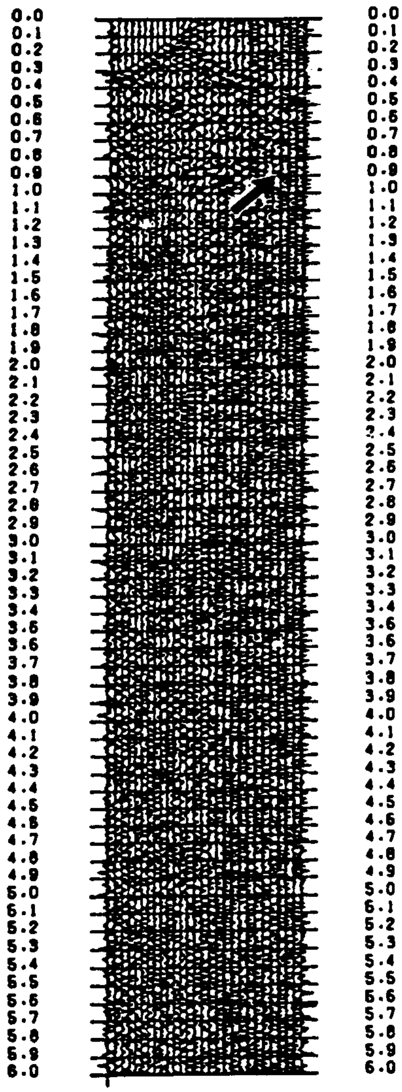

Fig. 2.2: CMP 335 from line 671A/87 after statics corrections. Pre-plot AGC has been applied. Note the dominant 38 to 40 Hz noise on the right side. Vertical scale is the two-way time.

The processing system used at MUN consists of a CONVEX C1-XL linked to an IKON-10085 hardcopy controller serving a Versatec 7000 series 36" wide electrostatic plotter (Fig. 2.3). This system runs the TEXACO's STARPAK™ seismic processing software under UNIX. The STARPAK package originated as Merlin Geophysics SKS package and is a set of Fortran routines linked by mgl language (Merlin Geophysical Language). Most processors work in trace-in/trace-out mode. In the remainder of this chapter, processor names that appear in parentheses preceded by a colon are STARPAK processor names. On the STARPAK produced figures, the maximum amplitude of each trace is adjusted to be 1.5 times the width of the trace unless otherwise indicated. The pre-processed, CMP gathered, data were originally in CGG-BGN format which cannot be read by the STARPAK™ software. So the data were first translated to SEGY format. The processing stream used in reprocessing appears on Fig. 2.4.

2.1 DESCRIPTION OF DATA

The three lines were recorded in 1987 by Geofyzika Brno. Their location appears on Plate 1. Line 671/87 is 9.7 km long, line 671A/87 is 12.7 km long and line 689/87 is 28.5 km long. The seismic source was Vibroseis with a 14 s sweep over 10-40 Hz or 12-48 Hz. Other details of the acquisition are given in Table 2.1, while the layout of vibrator stations appears on Fig. 2.5. The sweep was not available

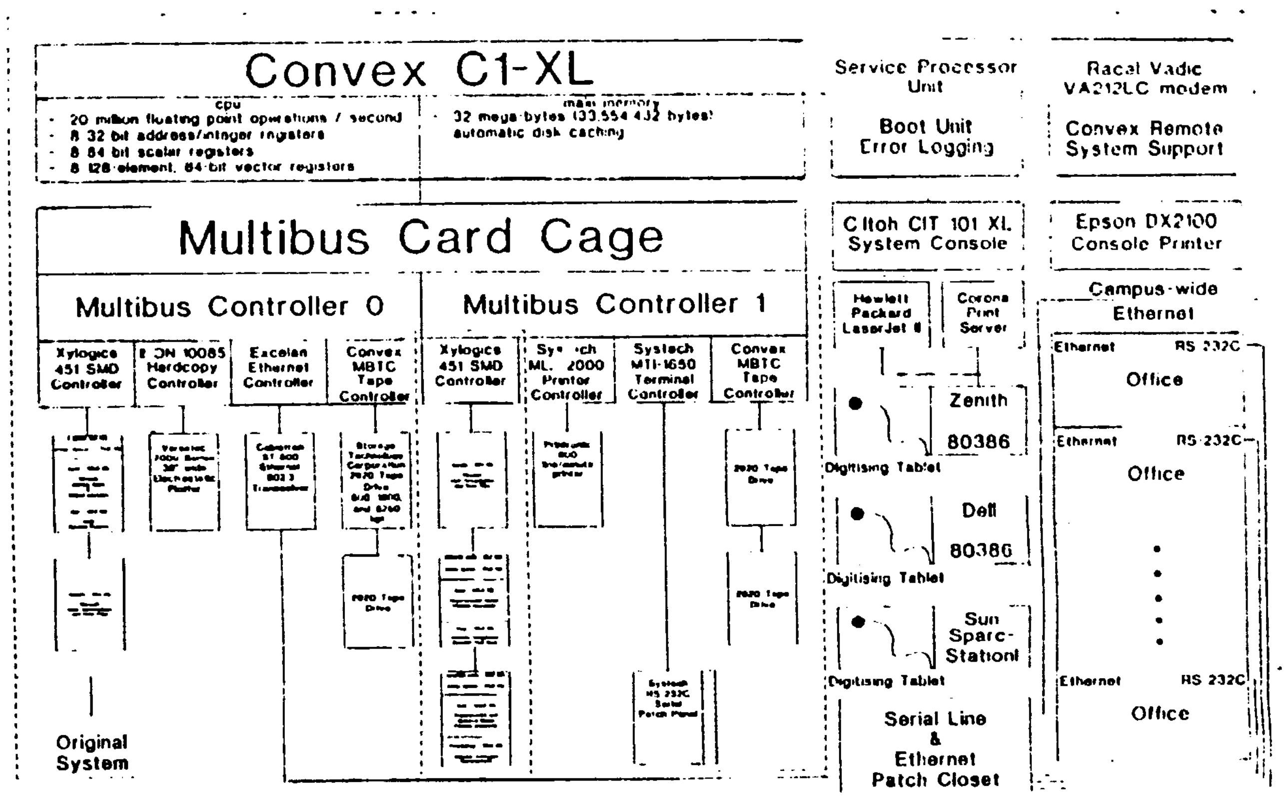

Fig. 2.3: Hardware schematic (Hall and Kocurko, 1992, personal communication).

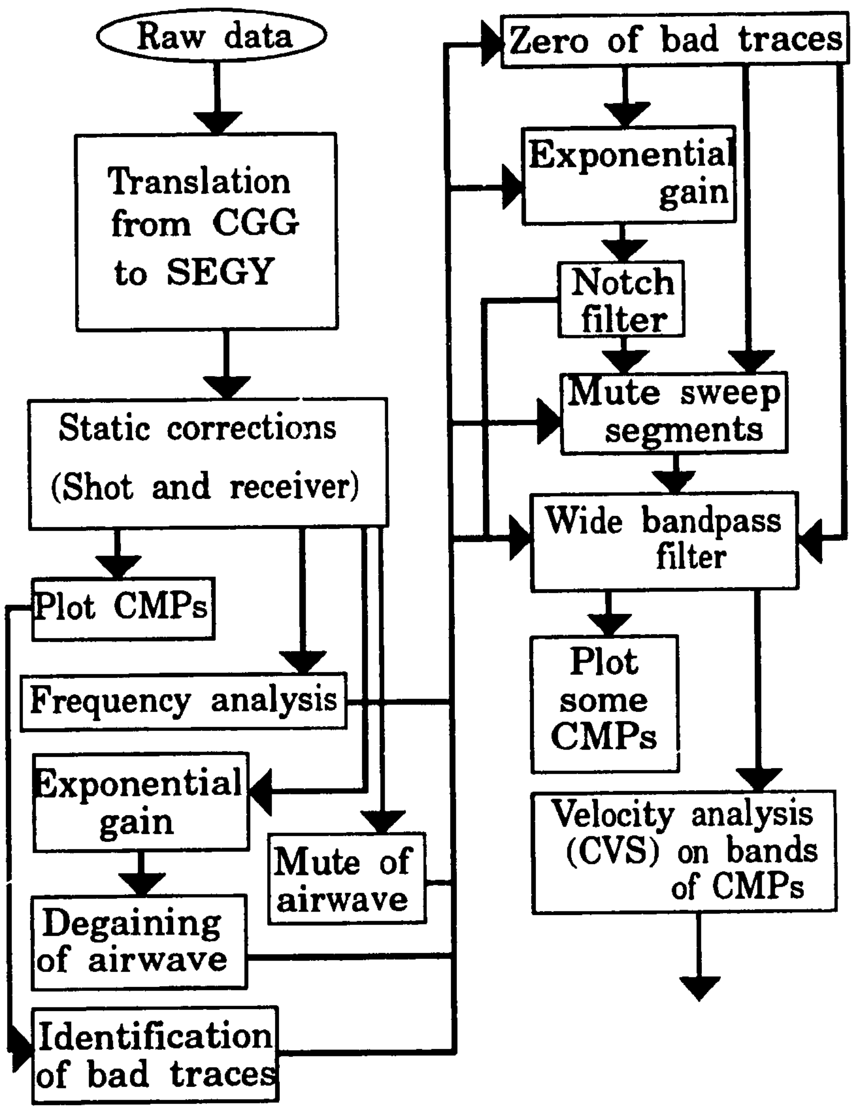

Fig. 2.4: Processing flow chart.

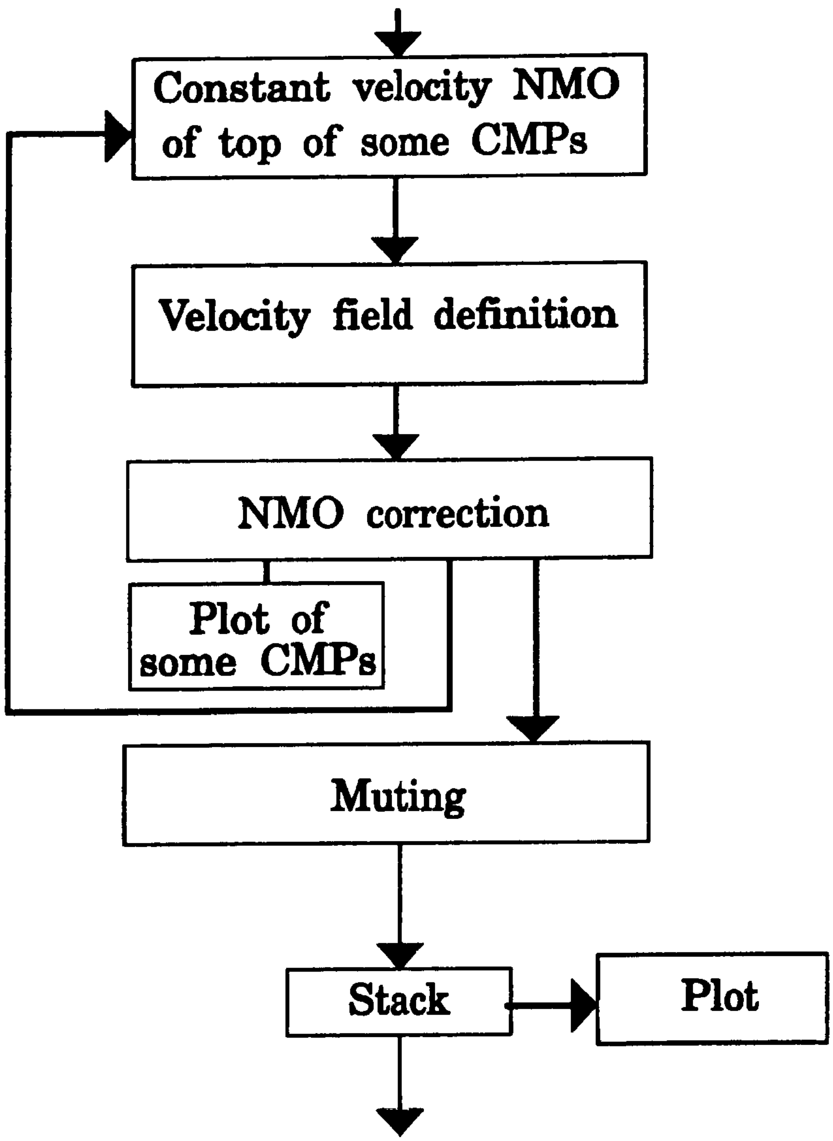

Fig. 2.4: Processing flow chart (continued).

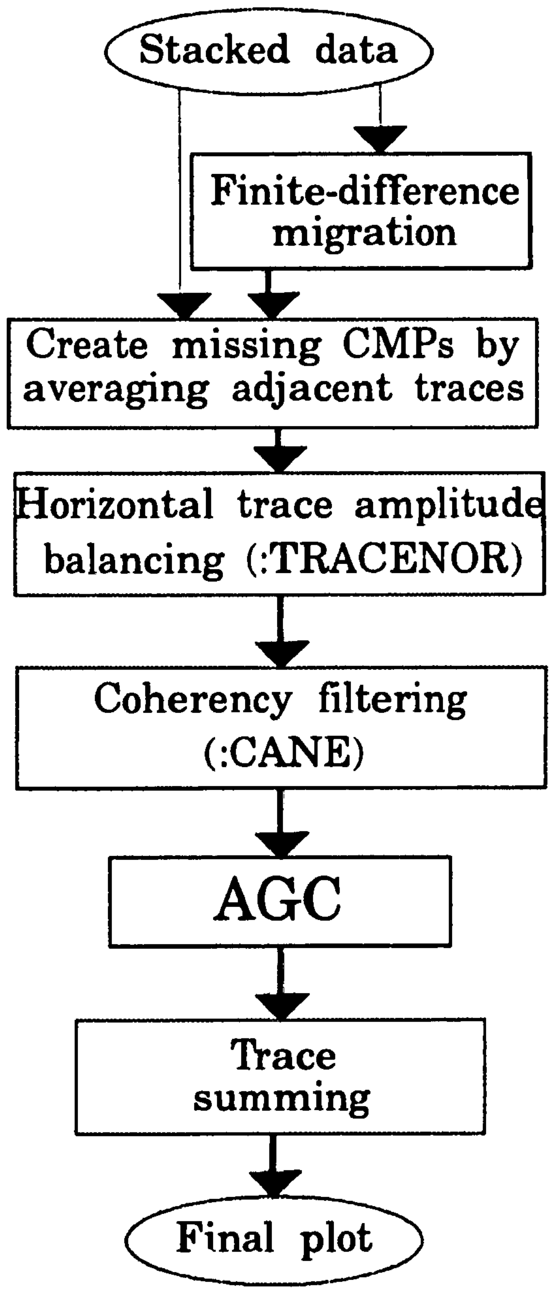

Fig. 2.4: Processing flow chart (continued), post-stack processing.

Parameter	689/87	671/87, 671A/87
Vibration point (v.p.) interval	50 m	50 m
Number of vibrators	5	5
Number of stands of vibrators/v.p.	8	8
Number of sweeps per stand	2	2
Distance between vibrators	12.5 m	12.5 m
Length of v.p. source pattern	100 m	100 m
Stand of vibrators interval	≈ 7.9 m	≈ 7.9 m
Length of sweep	14 s	14 s
Length of uncorrelated record	20 s	20 s
Length of correlated record	6 s	6 s
Length after extended correlation	12 s	12 s
Sweep frequency range	10 - 40 Hz	12 - 48 Hz
Sampling rate	4 ms	4 ms
Geophone frequency	10 ± 0.5 Hz	10 ± 0.5 Hz
Bandpass filter	8 - 62 Hz	8 - 62 Hz
Group interval	50 m	50 m
Number of geophones per group	24	24
Number of channels recorded	96	96
Maximum number of traces/CMP	48	48
First CMP number	89	73
Last CMP number	1229	460,580
Length of line (km)	28.5	9.7,12.7
Datum level (m amsl)	300	200

Table 2.1: Field parameters for lines 689/87, 671/87 and 671A/87

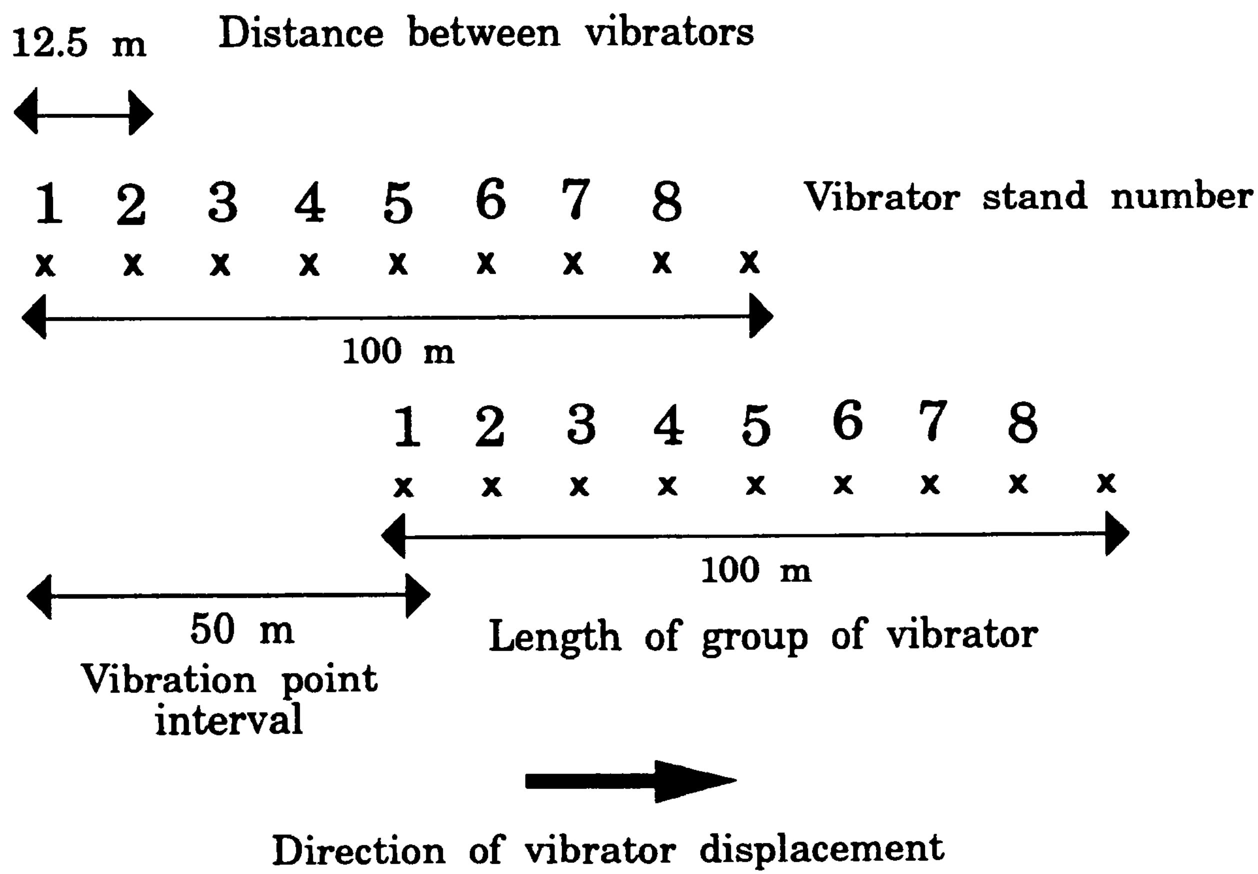

Fig. 2.5: Layout of vibrator stations.

with data as an auxiliary trace: it is linear but the tapers are not known.

Twenty seconds of data were recorded to provide a conventional 6 second record. Extended correlation was used to provide a 12 second record. Extended correlation (correlation with the sweep as it runs off the end of the data) means that after 6s the effective frequency spectrum of the source reduces (to 0 at 20 s). The bandwidth and signal to noise ratio thus decrease linearly with two-way time past 6s two-way time.

One shot is composed of a summation of 16 separately recorded sweeps divided into 8 pairs with a move up of about 5 m between successive pairs. Though 96 receiver groups were used the gathers rarely reach the full-fold of 48 traces, because of crooked lines and vibration points missed for cultural reasons. The actual fold ranges from 5 to 40. Some gathers do not have traces with ranges of less than 1000 m from the shot, like CMPs 130 to 142 from line 671A/87 and many shots on line 689/87. This limits resolution on the shallow part of the section. We do not have any information on the binning parameters used by Geofyzika Brno for the pre-processing of the lines.

The data available were already demultiplexed and correlated. According to processing information provided by Geofyzika Brno, deconvolution was not carried out on the CMP gathers we received.

The seismic lines were shot along roads but since the central part of the Little

Carpathians is not as densely populated as the basin margins, line 689/87 and the massif ends of lines 671/87 and 671A/87 might be expected to have a higher signal to noise ratio, but this is not the case.

2.2 PRE-STACK PROCESSING

2.2.1 Statics corrections

The first step in re-processing the data was to re-apply the static corrections calculated by Geofyzika Brno for elevation and weathering to a datum level of 300 m above mean sea level (amsl) for line 689/87 and 200 m for the other lines. The time delays at shot and receiver stations were computed by Geofyzika Brno from a shallow refraction survey.

Most shot stations and receiver stations sharing the same number were 25 m apart but there are a few side shots up to 60 m from the corresponding receiver station (Tomek, personal communication, 1992). The datum level was chosen close to the lower end of the range of elevation, so the statics corrections were almost always negative, with some positive but close to zero at the basin margins (Table 2.2). However the source shifts do not seem to correlate consistently with elevations and are quite large. This may indicate that weathering corrections make up an important portion of the statics corrections. There are areas of thick Quaternary sediment cover in valleys, but the pre-Neogene formations outcrop in many areas (Mahel' et al., 1972). If Quaternary sediments were the main cause of the weathering corrections, the zones of large corrections would correspond to the valleys where they were deposited, which is not always the case.

Table 2.2: Minimum and maximum time shift in static corrections with range of elevations along the lines (Tomek, personal communication, 1990 and 1992)

Line	Minimum source time shift (ms)	Maximum source time shift (ms)	Minimum receiver time shift (ms)	Maximum receiver time shift (ms)
Line 671/87	-95	0	-95	0
Line 671A/87	-97	1	-94	1
Line 689/87	-95	-5	-94	-6
Line	**Datum level (m amsl)**		**Minimum elevation (m amsl)**	**Maximum elevation (m amsl)**
Line 671/87	200		189	550
Line 671A/87	200		223	533
Line 689/87	300		318	634

A deep weathered layer is the most likely explanation of the negative statics corrections. Indeed, a significant portion of the Bratislava granitoid massif and overlying metamorphic rocks crossed by the SSW half of line 689/87 has undergone erosion almost continuously for the last 23 Ma or so, removing a few kilometres thickness of rock. The intensive reverse faulting, horst and graben formation, strike-slip movement and differential uplift across the Little Carpathians in the Miocene to Holocene has also created a closely spaced network of faults (Kvitkovič and Plancar, 1979; Nemčok et al., 1990) that are most likely associated with small scale fractures. Fractures deepen the weathered layer, increasing the weathering correction.

2.2.2 Air wave removal

The air wave is a highly variable noise source in these data and was removed in our processing by narrow window muting. The air wave does not always start at time 0 at the source because it is sometimes reflected from cliffs, so that the start time of the noise train increases with distance from the cliff. Moreover, this causes the air wave pattern on the two sides of a given gather to be slightly asymmetrical. Because of this, the muting windows used have to be about 100 to 150 ms larger than the air wave pattern for the interpolation to be satisfactory on both sides. Because of the high amplitude of the air wave it is difficult to recover any signal coincident with the air wave, thus justifying the muting (Yilmaz, 1988). This method is however not suitable for low fold CMP gathers because it causes windows of zeroed data on the stacked trace.

As an alternative to window muting, gaining down the air wave with 2-D interpolation (:HAIRCUT) was tried but without success: as the air wave is reflected from a cliff, starting time on CMPs increases with their distance from the cliff, but :HAIRCUT is designed for primary air waves and requires a constant starting time.

For CMP gathers of less than 12 traces at the ends of the lines, where muting is not suitable, variation of air wave starting time is not important. On these CMP gathers, degaining of the air wave with zero starting time (using :HAIRCUT) is carried in a 250 ms long window whose position in each trace is calculated using the distance of the trace from the midpoint of the gather and the air wave velocity of 335.3 m/s (Fig. 2.6). After the air wave degaining, any remaining segments of air waves were muted (Fig. 2.7).

2.2.3 Deconvolution

Zero-phase spiking deconvolution with a 200 ms operator length and 0.01% prewhitening removed a significant amount of the ringing (Fig. 2.8 and 2.9). The operator length was chosen to minimize degradation of data. It also decreased the signal to noise ratio but not enough to significantly degrade the data: indeed the noise generated by the ringing was less on the stacked section. Because deconvolution whitens the frequency-amplitude spectra and tends to enhance high frequencies, deconvolution may, if desired, can be followed by bandpass filtering.

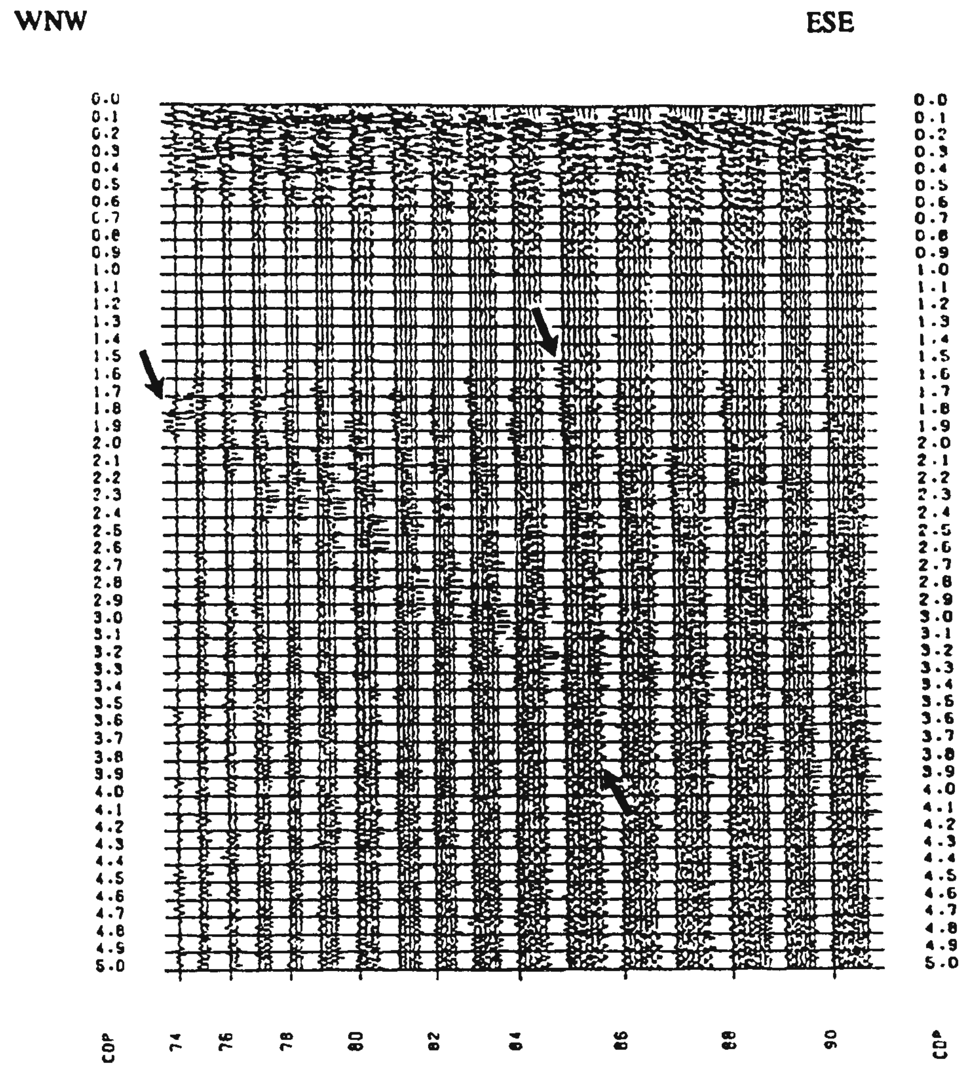

Fig. 2.6: CMPs 77 to 88 from line 671A/87 before air wave removal. Vertical scale is two-way time in seconds. Horizontal scale is CMP number. This subset of data was taken at the beginning of the line so the fold starts at 1 and increases. The airwave starting time increases with distance from the cliff on which the air wave is reflected. Down arrows indicate the start of the air wave while up arrows indicate its end.

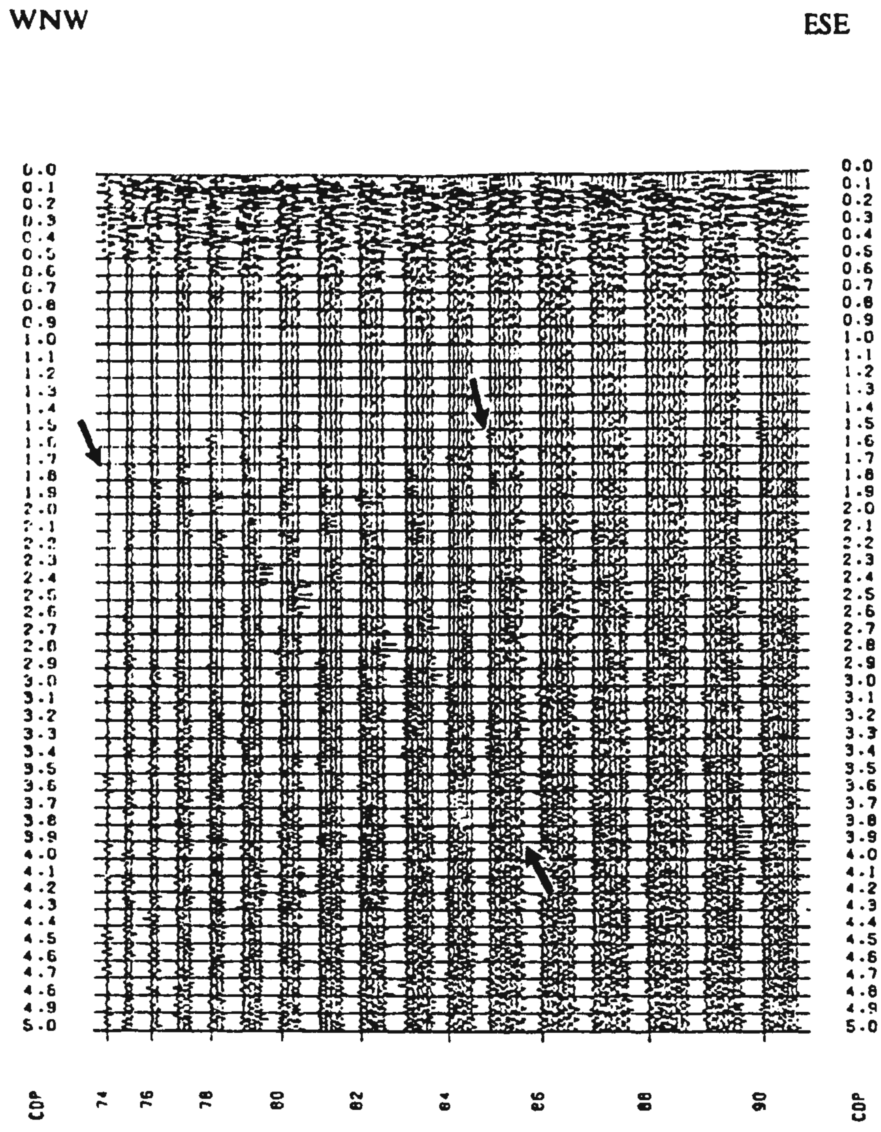

Fig. 2.7: CMPs 77 to 88 from line 671A/87 after air wave degaining. The high amplitude air wave of Fig. 2.6 was attenuated though there are some high amplitude remnants of the air wave. They were muted when it was possible to do so without creating windows of zeroed data on the stacked trace. Vertical scale is two-way time in seconds. Horizontal scale is CMP number.

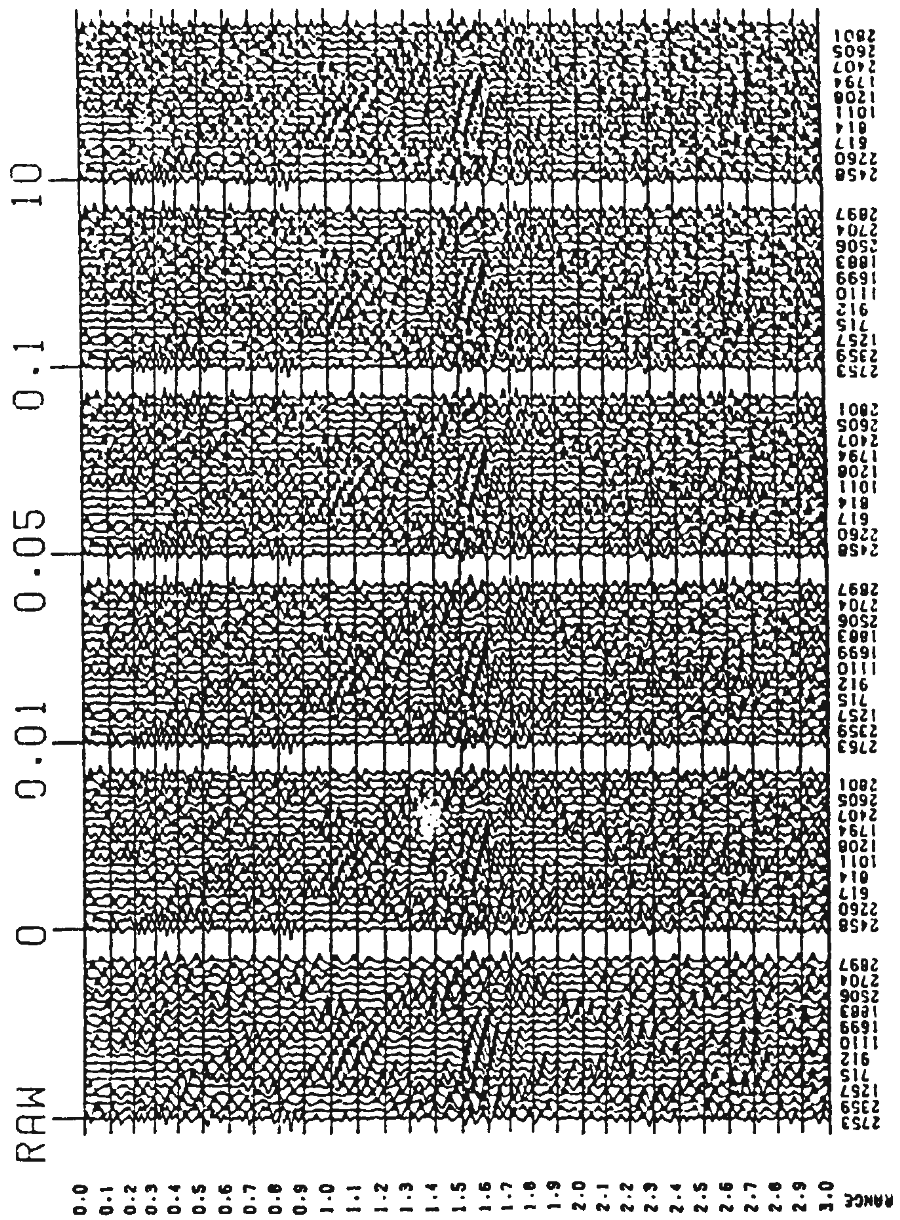

Fig. 2.8: Prewhitening test for spiking deconvolution, comparison of a CMP gather. CMP 155 from line 671/87 in the Vienna basin had deconvolution applied with different percentages of prewhitening: a) no deconvolution, b to f) 0, 0.01, 0.05, 0.1 and 10% prewhitening. Vertical scale two-way-time in seconds.

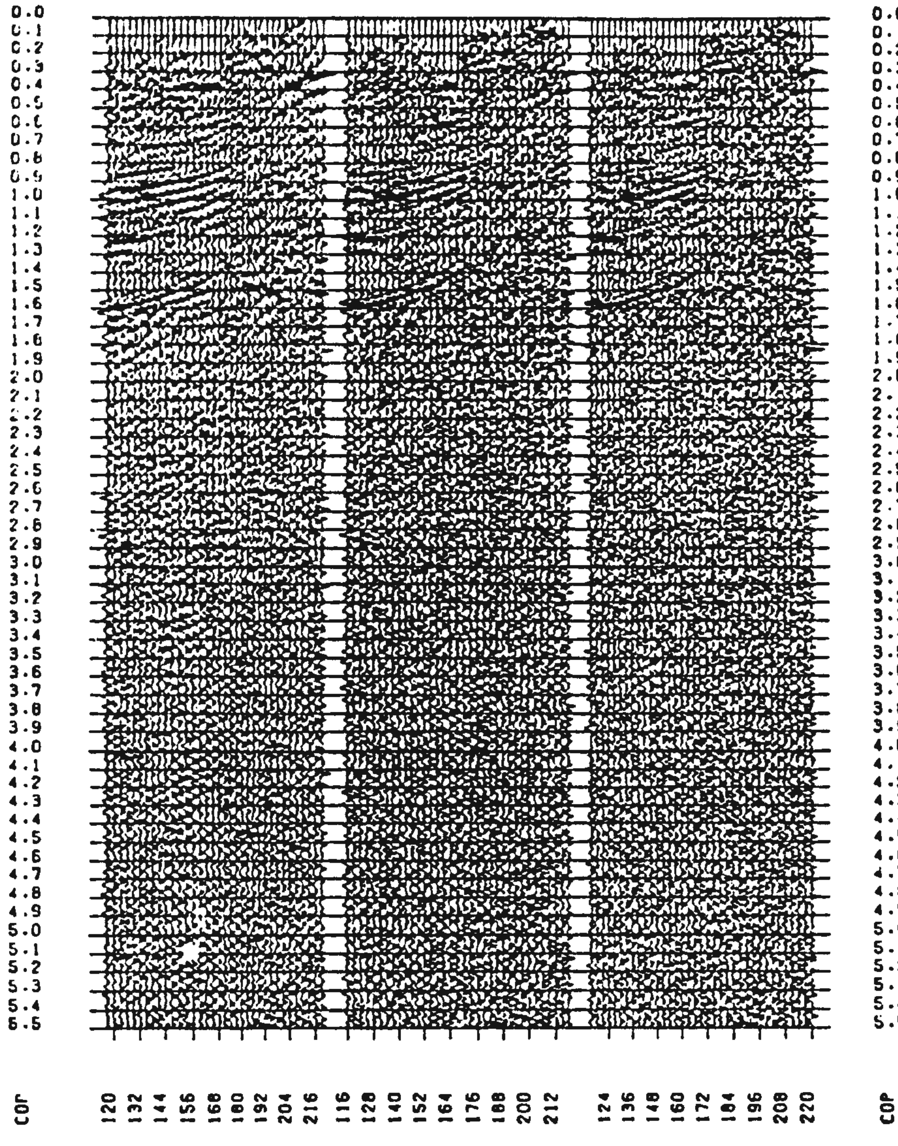

Fig. 2.9: Prewhitening test for spiking deconvolution, comparison of stacked data. a) no deconvolution, b) deconvolution with 0.01% prewhitening, c) deconvolution with 0.1% prewhitening. Since there is no significant difference between b) and c), 0.01% prewhitening was used as it adds less noise and attenuates a bit more of the coherent noise under the lower reflector at the margin of the Vienna basin. Horizontal scale: 80.8 m/cm. Vertical scale: 1 km/cm for a velocity of 6 km/s.

2.2.4 Gain

Exponential gain applies to each trace a user defined sum of exponential functions to compensate for the attenuation of the seismic signal with depth. Exponential gain was applied before deconvolution as it eases correlation (the steady state signal assumption), and is required before frequency filtering (see 2.2.5). A 4 dB/sec increase was used starting at 750 ms to avoid boosting up the direct wave.

Just before plotting, AGC is applied. AGC adjusts the gain factor to have an average amplitude for each window equal to that of the design window. AGC destroys relative amplitudes and degrades the signal to noise ratio a little (Hatton et al., 1986). The lowering of signal-to-noise ratio comes from the fact that AGC brings to about the same final amplitude both noisy low amplitude zones and reflectors of higher amplitude. The noise amplification is the main concern for this work: signal to noise ratio cannot be reduced much on these three lines as it is already very low. For all these reasons AGC is not applied in the main processing stream except just before plotting. Given the major noise problem caused by uniform amplitude traces like those on Fig. 2.1, the amplitude information of the stacked trace was not mainly indicative of geology but rather of noise. Long AGC windows are used below the high amplitude portion of the raw data to avoid distorting the signal as much as possible, while short AGC windows are used on top of the section to bring out the reflectors as clearly as possible. The first sample gained in pre-stack data was at 152 ms TWT to avoid gaining over the direct wave. The window length varied from 800 ms at 1300 ms TWT to 2000 ms at 3000 ms TWT. To make comparisons easier, the same gain function was used for all plots.

2.2.5 Filtering

The original frequency spectra of CMP 518 from line 689/87 appear in Fig. 2.10. The peak at 12.5 Hz, which dominates the signal by 10 dB, is caused by electrical noise, probably railroad noise which operates at 1/4 of domestic power frequency, as discussed in the introduction to this chapter. The CMPs 500 to 530 are especially badly affected by this noise. A similar signal is seen in short segments throughout the lines, though line 671/87 is less affected. The frequency spectra from line 671A/87 are similar to the spectra from line 689/87 though the 12.5 Hz peak extends up to 13 Hz, and has a slightly lower amplitude than on line 689/87 since less traces are affected in each CMP. On line 671/87, this noise spans from 12.5 to 16.7 Hz, as seen on Fig. 2.11. Railroads lie close to the Vienna basin end of line 671/87. Since European railroads sometimes operate at 1/3 rather than 1/4 of the domestic electric current frequency of 50 Hz, it may also explain the presence of 16.7 Hz noise there.

A standard short notch filter was tried first. This filter also removes the harmonics of the troublesome frequency. This is theoretically good but since the bandwidth of our signal is already quite narrow, the filtered signal looked too monochromatic.

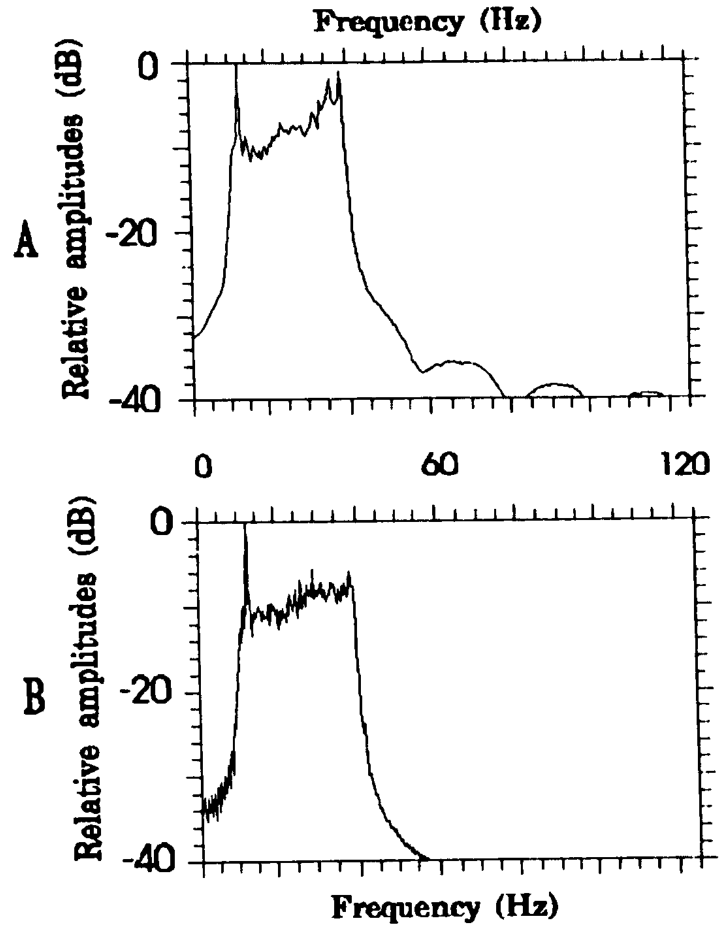

Fig. 2.10: Frequency spectra of CMP 518 from line 689/87 before notch filtering. a) between 2 and 4 seconds, b) between 4 and 7 seconds.

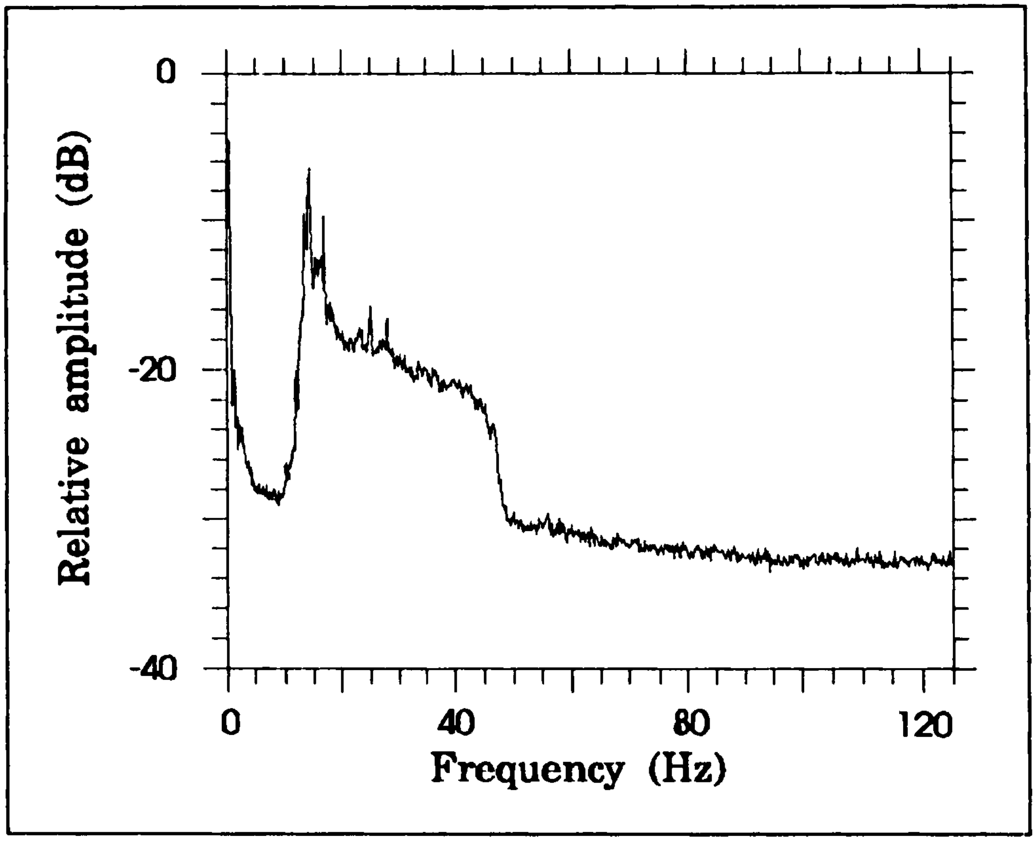

Fig. 2.11: Frequency spectra of CMP 305 to 311 from line 671/87 before deconvolution. Note the 12.5 and 16.7 Hz peaks. The high amplitude peak at very low frequency is caused by ringing which appears inside low frequency half-sines. This peak disappeared after bandpass filtering following deconvolution.

Next, to remove the 12.5 Hz peak, a notch filter was designed on ISAN software by adding a lowpass and a high-pass filter together. ISAN is an interactive signature analysis software for test processing, from Merlin Profilers Research Ltd. The cutoffs and slopes of both are chosen so as to:

1) Remove as much as possible of the 12.5 Hz noise, which means that the amplitude at 12.5 Hz of the filter frequency spectrum will be as low as possible.
2) Minimize the loss of seismic signal, this means that the cutoff frequencies should be as close as possible to 12.5 Hz.
3) Minimize Gibbs effect which is a damped oscillation decreasing away from the cut-off point (Ramirez, 1985). The effect increases with the slope of the filter.

Some oscillation on the filter spectra is unavoidable so there is a trade-off between distorting the spectra because of Gibbs effects as the slopes are increased to preserve more signal and losing signal by filtering it out as the slopes are lowered to reduce Gibbs effect. The best trade off was found to be a filter with cutoff points at 10.6 and 14.9 Hz with slopes of 94 and 92 dB/octave respectively (Fig. 2.12). The notch filter is very effective but removes some low frequency signal from the reflectors. The addition of a lowpass and a highpass filter is not a very elegant way to design a filter nor does it produces a notch as narrow as desired. This method of notch filtering was not chosen.

The solution finally adopted was to use a long filter (:FREQFILT) defined by a series of (amplitude,frequency) points which, when applied to the data traces is translated into long operators, i.e. with more polynomial terms than in other filters. Because of the large number of terms, the slopes of the filter can be very steep and the cutoff frequencies can be close to 12.5 Hz (Table 2.3, Fig. 2.13). However these frequency filters require the amplitude of the signal to be balanced along the trace. Again, a gentle exponential gain was applied to the traces to be filtered and proved effective in test panels. The balanced amplitude is required because the long filter operator repeats unwanted high amplitude portions of the traces far down along it, which would lower even more the signal to noise ratio of the data. To limit this, the impulse responses of the filters were plotted to make sure they were decaying fast away from impulse time. The amplitude of the second peaks were 40 dB and 50 dB down from the impulse time peak for the filters applied on lines 671A/87 and 689/87 respectively. These filters being defined in the frequency domain, they do not have Gibb's effect in the frequency domain but ringing in the time domain which carries noise down the trace as seen earlier. On line 671/87, the deconvolution was sufficient to control the problem to an acceptable level and the wide frequency range of noise precluded use of a notch filter.

Some 12.5 Hz noise remains below 8 to 10 sec TWT but since there are no reflectors seen at that depth and since frequencies become lower as depth increases, this is not a serious problem. To check the efficiency of the filter, a few CMPs were stacked and compared to the stack of non-filtered traces. Before application of the long filter, a standard bandpass filter was applied to the data.

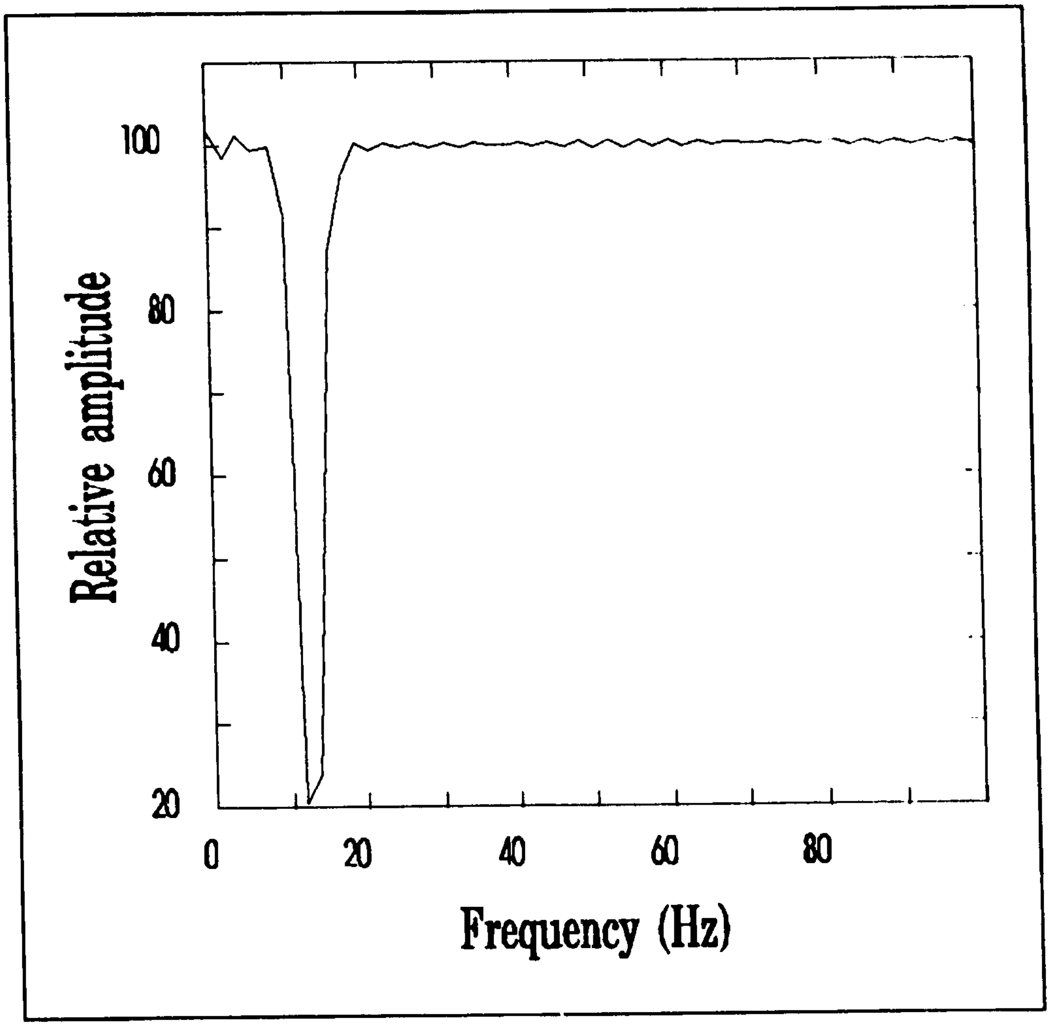

Fig. 2.12: Frequency spectra of filter designed in ISAN by addition of a low-pass and a high-pass filter. Cutoff points are 10.6 and 14.9 Hz with slopes of 94 and 92 dB/octave respectively.

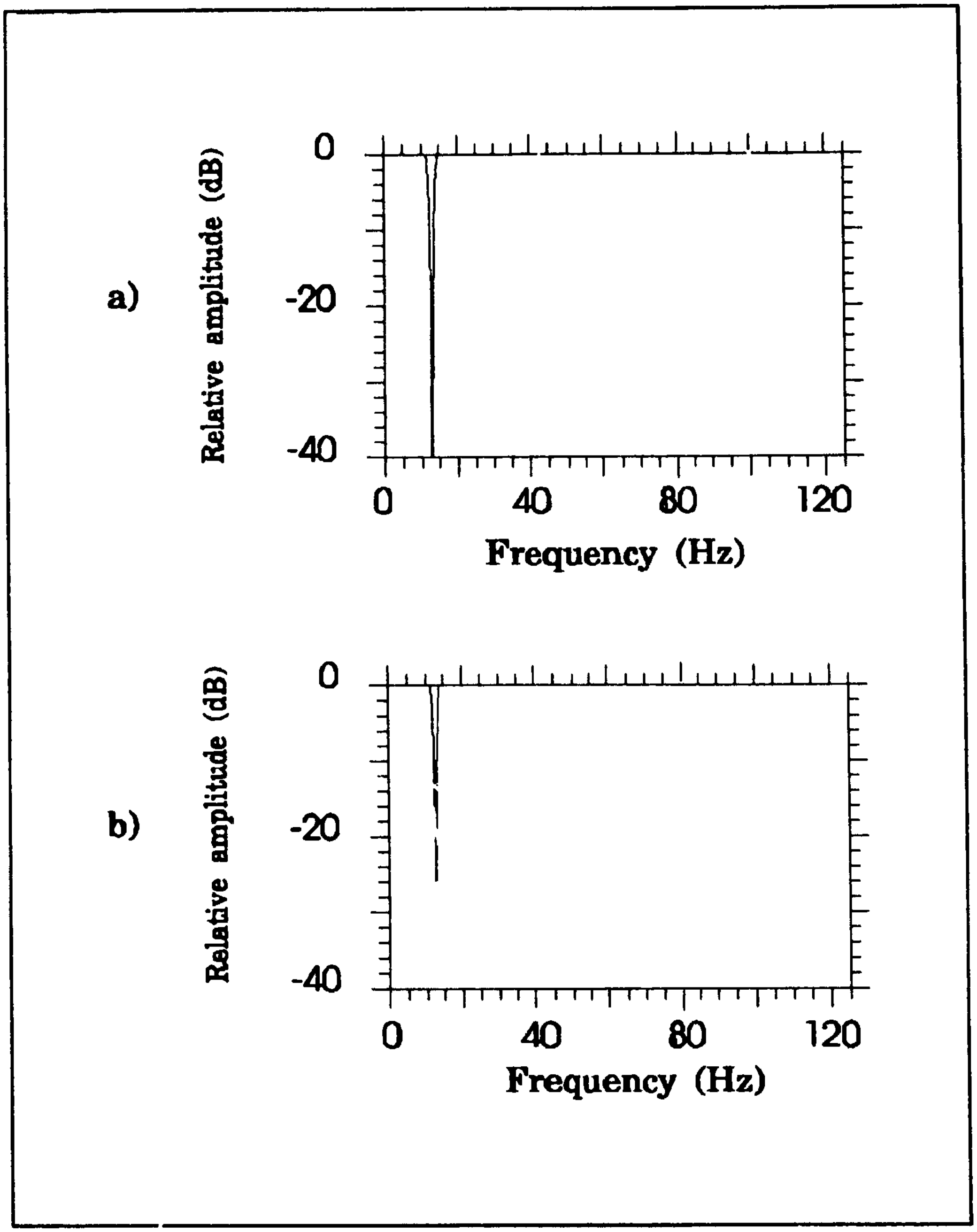

Fig. 2.13: Frequency spectra of notch filter for a) line 671A/87 b) line 689/187.

Table 2.3: Frequency notch filter parameter			
Line	Points (Hz)	Amplitude	Slopes (dB/octave)
671/87	No notch filter applied		
671A/87	11.4 12.5 13.0 14.2	1 0 0 1	-85.2 -89.0
689/87	11.4 12.5 13.75	1 0 1	-85.2 -85.3

Since the filter applied in the field kept frequencies from 8 to 62 Hz, the cutoff frequency on the high-pass side of the filter was set to 3 Hz with a slope of 15 dB/octave, just to remove a group of very low frequencies that remained after the field filter. To preserve as much as possible of the bandwidth, the notch filter was applied only to the affected traces of each CMP. Comparison of CMP 518 before and after the application of the notch filter appears on Fig. 2.14.

Bandpass filtering was carried out before velocity analysis (Figs. 2.15 and 2.16). The highpass slope cutoff frequency of the filter was 7 Hz with a 15 dB/octave slope. This cutoff point is 1 Hz lower than the filter applied by Geofyzika Brno before gathering (Table 2.1) so as to not remove more signal around 10 Hz. To remove the high frequency noise, the low-pass side of the bandpass filter was set to 40 Hz with a slope of 50 dB/octave. This cut off is only a little less than the sweep highest frequency

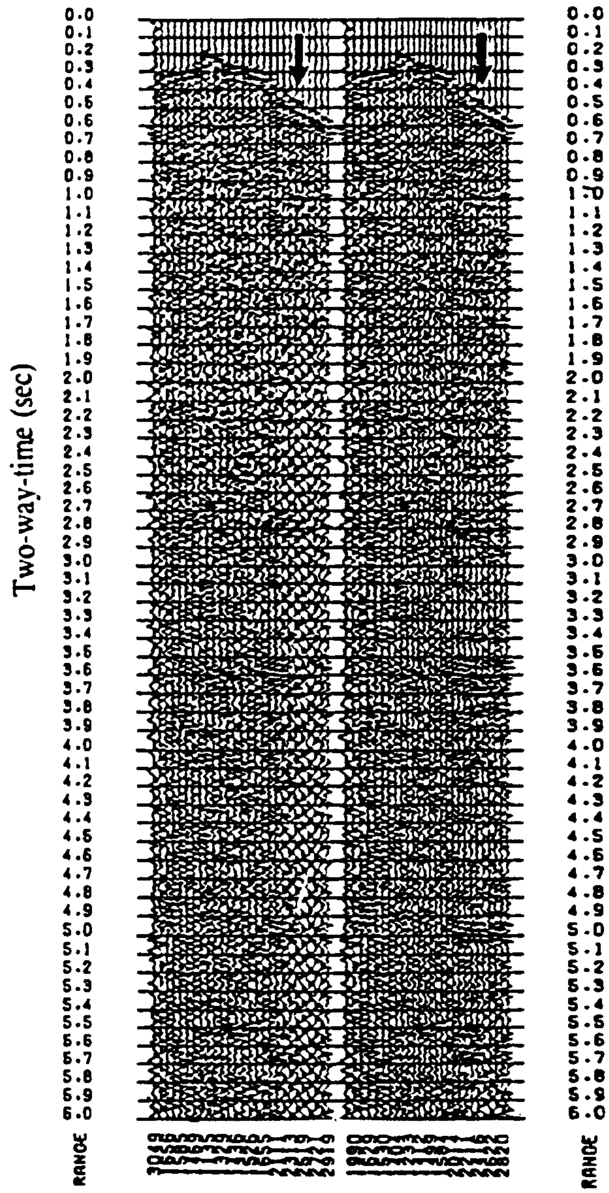

Fig. 2.14: CMP 518 from line 689/87 before and after notch filtering. On the left panel, the traces under and right of the arrow are overwhelmed by 12.5 Hz noise. Strong events were recovered once the 12.5 Hz was filtered out in the right panel.The range scale is the number of meters between the CMP point and the shot point corresponding to this trace. Vertical scale is the two-way time.

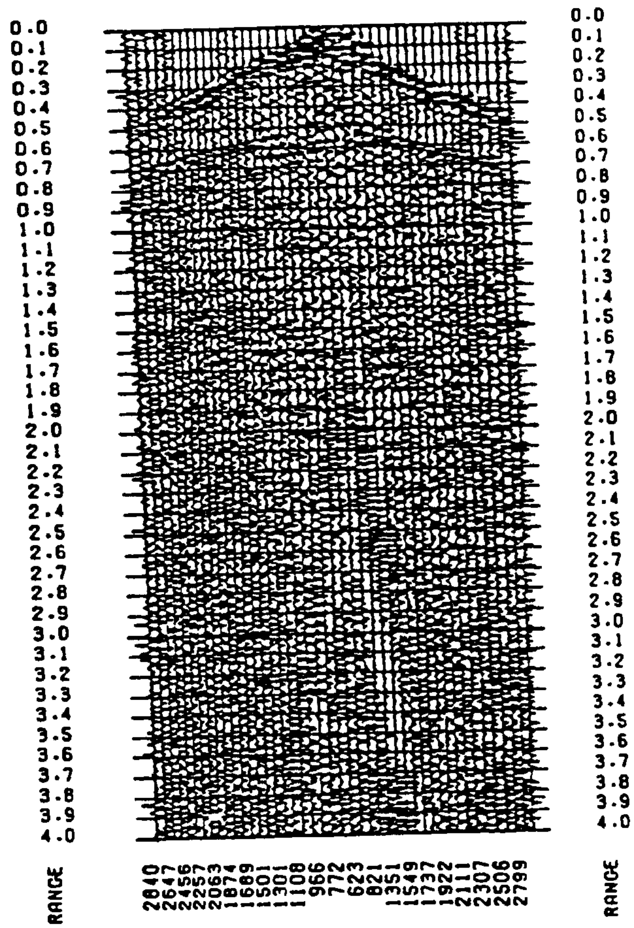

Fig. 2.15: CMP 205 from line 671A/87 before bandpass filtering. Vertical scale is two-way-time in seconds.

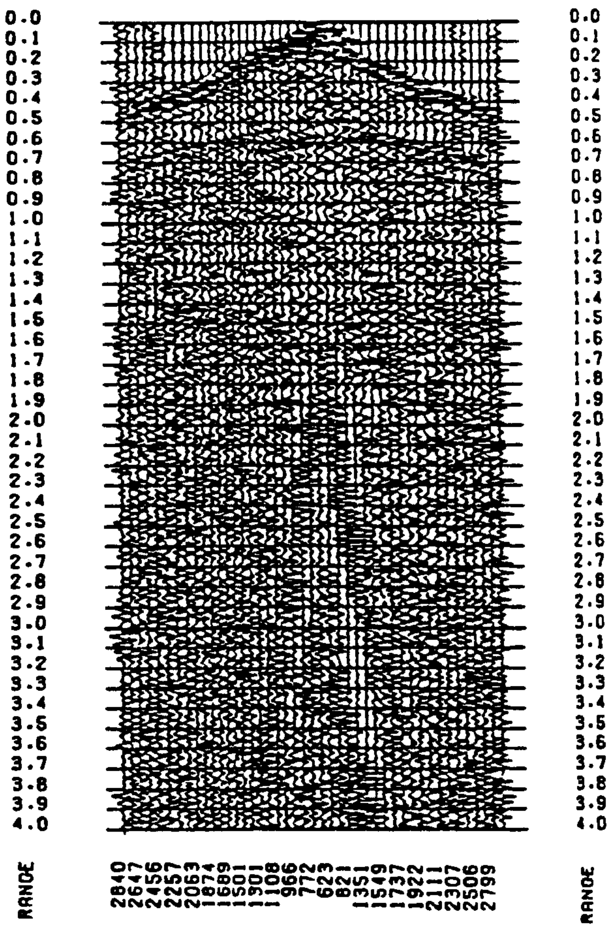

Fig. 2.16: CMP 205 from line 671A/87 after bandpass filtering. Bandpass filtering reduced the noise only on some segments of the data. When compared to Fig. 2.15, there is less high frequency noise near the top reflection and in the lower left corner of the figure. Vertical scale is two-way-time in seconds.

of 48 Hz (line 671/87 and 671A/87) or 40 Hz (line 689/87), and could not have been set lower because much of the useful signal lies in the 25 to 36 Hz range on the first second of the data and 2 to 2.5 octaves of frequencies should be kept as a general rule, i.e. from 8 to between 32 and 48 Hz. A lowpass filter with cutoff frequency of 32 Hz and 70 dB/octave slope was applied to some traces with significant noise in the 30 to 40 Hz range such as pointed out on Fig. 2.2.

2.2.6 Removal of inverted Vibroseis sweep segments

A major source of systematic noise in the data is produced by segments of inverted Vibroseis sweeps. These appear as a result of the Vibroseis correlation with noise spikes. Such segments have high amplitude, degrading the signal to noise ratio of the data, especially when they cut events. Examples are shown in Fig. 2.17. Long segments were muted.

2.2.7 Velocity analysis, NMO and stacking

The method chosen for velocity analysis is constant velocity stack (CVS). Velocity spectrum analysis is not usually successful in deep crustal data because the reflectors do not have high enough amplitude relative to the noise, and are also often shorter than the spread length. But in this case, the major problem with the velocity spectrum method is that it is very sensitive to noise (Yilmaz, 1988). Below 4 seconds

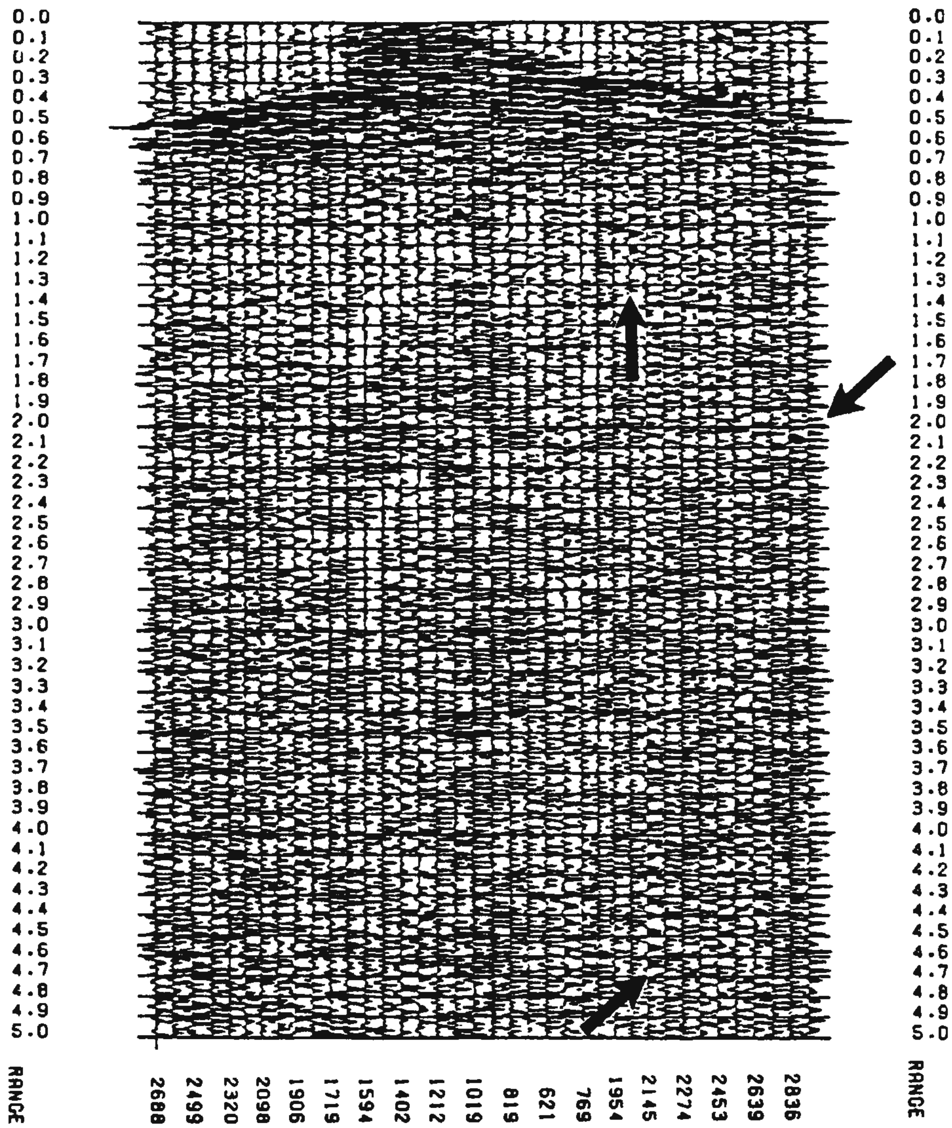

Fig. 2.17: Segment of Vibroseis sweep on CMP 289 from line 671/87. Arrows indicate segments of inverted Vibroseis sweep. The range scale is the number of meters between the CMP point and the shot point corresponding to this trace. Vertical scale is the two-way time in seconds.

or so, the reflectors have low move-out and any reasonable velocity will stack them properly. There was one event at 4.6 sec TWT that stacked slightly better around 6400 m/s (± 400 m/s), so this velocity was chosen for this TWT value throughout the lines. The error incated corresponds to the stacking velo..'y interval between CVS panels. The CVS method of velocity analysis requires that 100 CMP wide or so subset of the data be stacked with constant stacking velocities using different velocities over a likely range. The velocity for which a given reflector shows the best focus and for which the amount of scattering is minimum is chosen as the stacking velocity at that TWT. The velocity at zero time is the velocity at which the NMO corrected gather has its direct wave 'horizontal'. Since short offset traces are not often present in the CMP gathers, the first refracted wave was often used as a maximum value instead (Fig. 2.18). NMO corrected gather displays were also compared to the CVS to help in defining the stacking velocity field. The process is repeated in many places along the line, especially when the type of rock changes across a fault. For an example of CVS see Fig. 2.19. In this figure, event D fits the calculated curve for diffraction (section 3.1). The final stacking velocity field chosen appears on Figs. 2.20 to 2.22. Since there are large rapid lateral velocity changes, the velocity gradient is not uniform and reflector dip varies significantly, it is difficult to get reasonable interval velocity fields from the staacking velocity field using Dix' equation (flat parallel layer approximation).

The velocity field was chosen so that the interval velocity at the bottom of the section is 6.8 to 7 km/s, slightly lower than the lower crustal velocities of 7 to 7.1 km/s

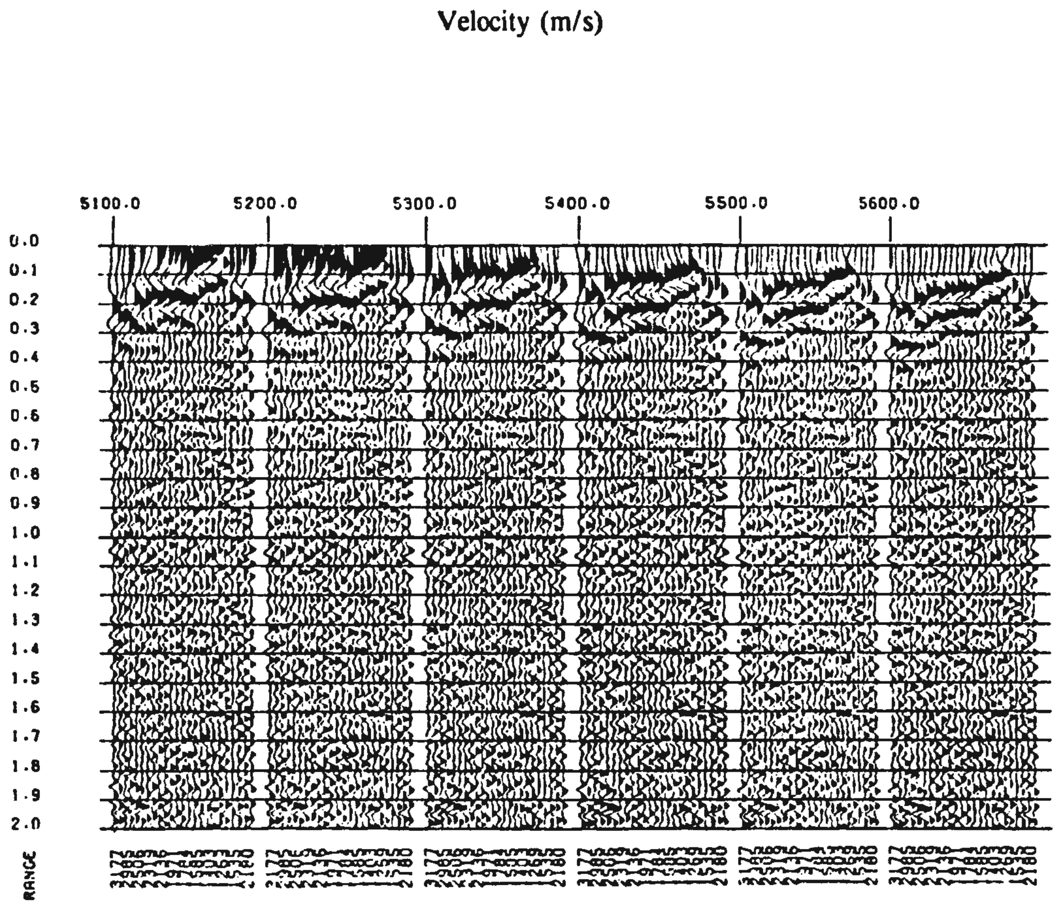

Fig. 2.18: Example of velocity tests on NMO corrected split-CMP gather. Correct velocity for 0 sec TWT is the velocity at which the direct wave is horizontal. As there are few traces showing the direct wave, the refracted wave was used to provide a maximum value. Note the change in the refracted wave as it passes from upward curve at low to downward slope at high velocity. Deviation from horizontal at near-range and far-range are caused by inhomogeneities in the overburden that were not corrected successfully by the static corrections. Vertical scale is two-way-time in seconds. Horizontal scale is the range, or distance in meters.

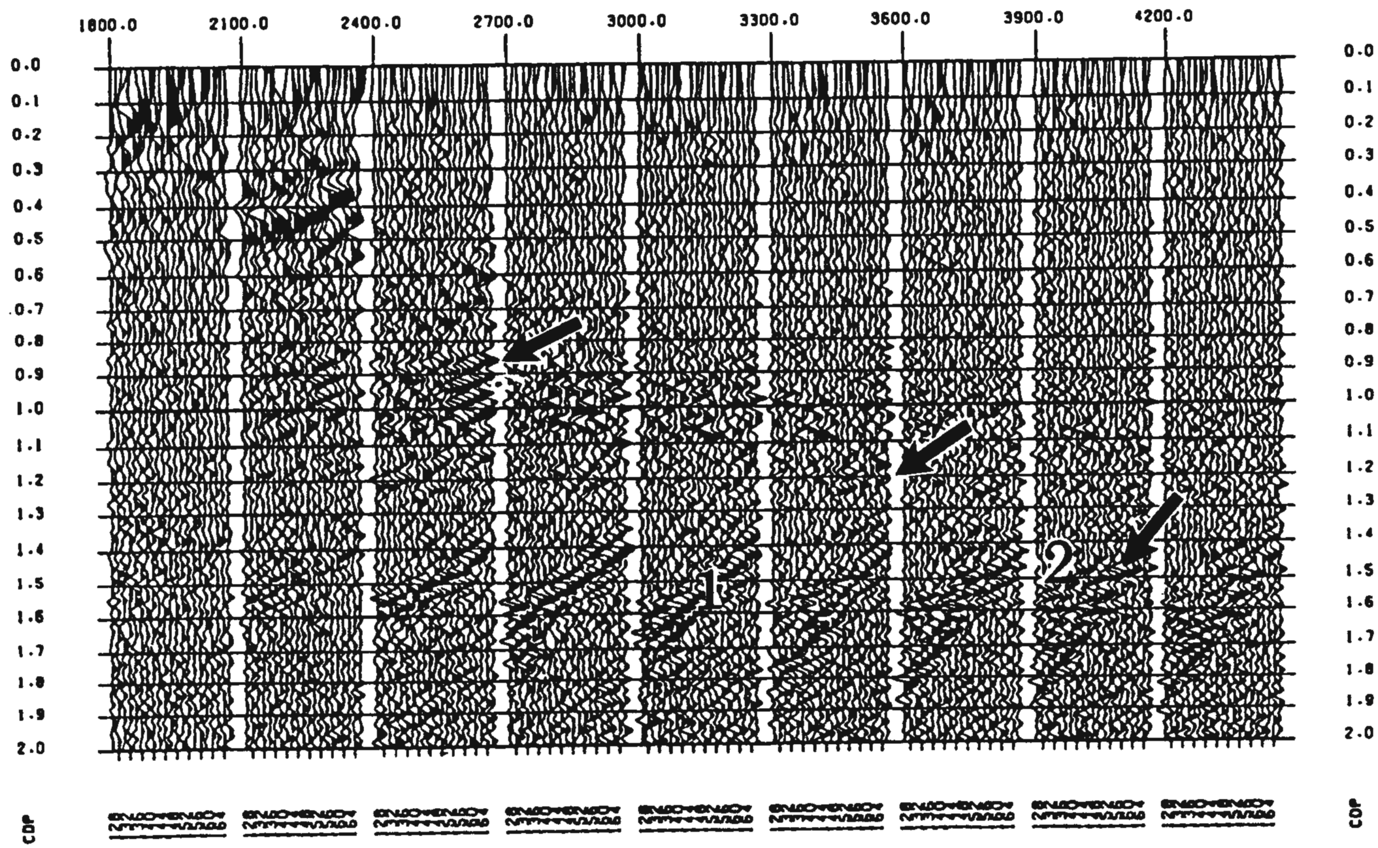

Fig. 2.19: Example of CVS display with CMPs 130 to 166 from line 671/87. Note the change in the reflectors focus as it passes from too low to too high velocity, and the passage from diffraction (1) to reflection (2) coming though diffraction at higher velocities. Velocity picks are indicated by arrows. Vertical scale is two-way-time in seconds.

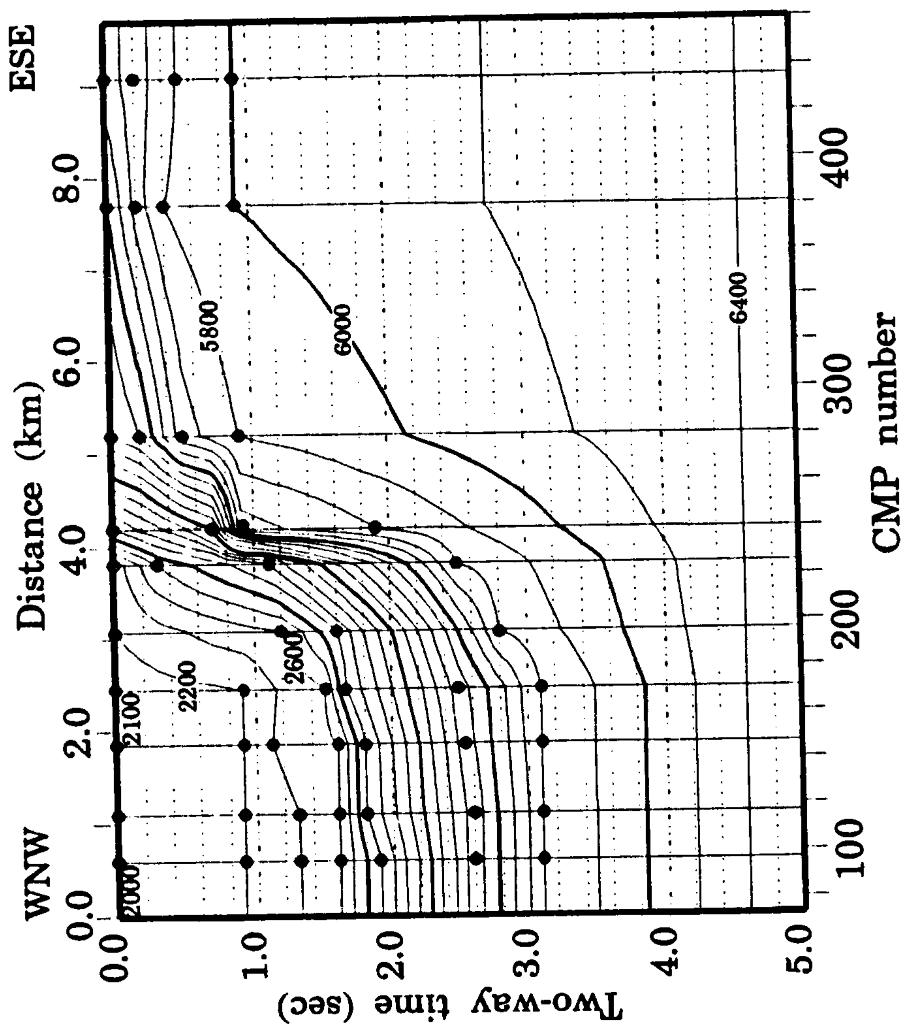

Fig. 2.20: Interpolated rms stacking velocity field of line 671/87. Shaded dots indicate velocity specification points.

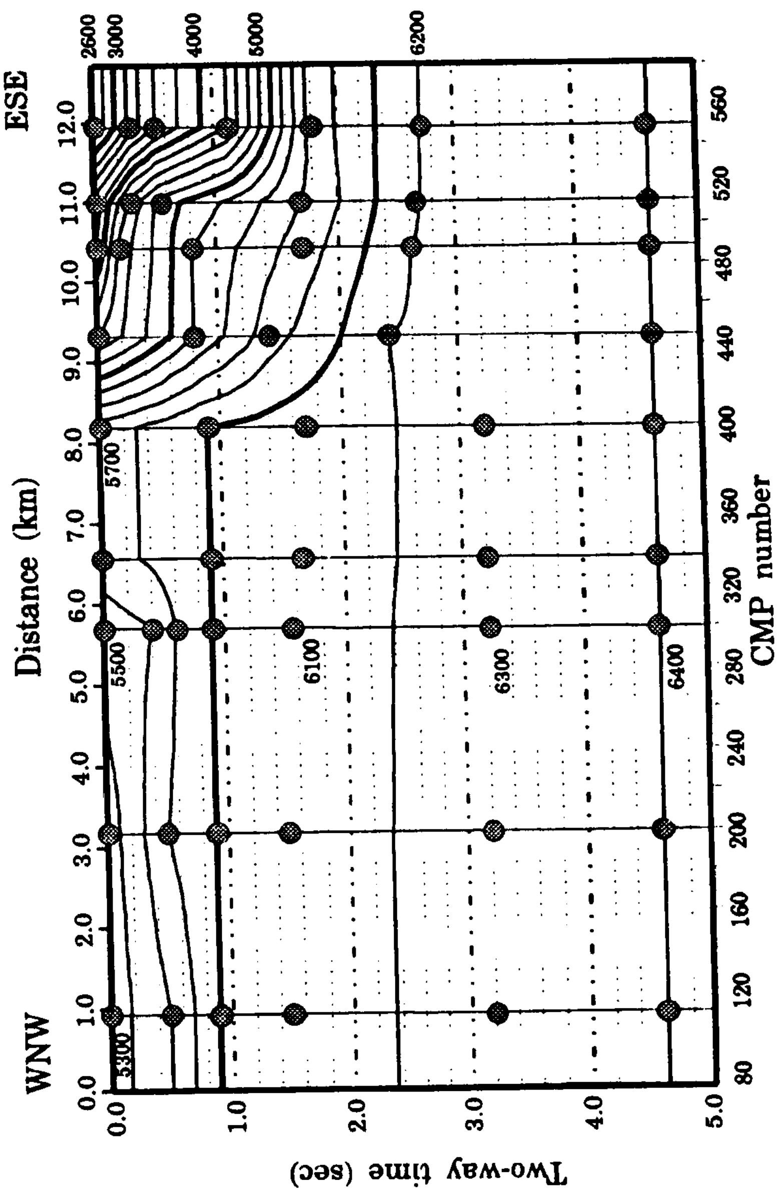

Fig. 2.21: Interpolated rms stacking velocity field of line 671A/87. Shaded dots indicate velocity specification points.

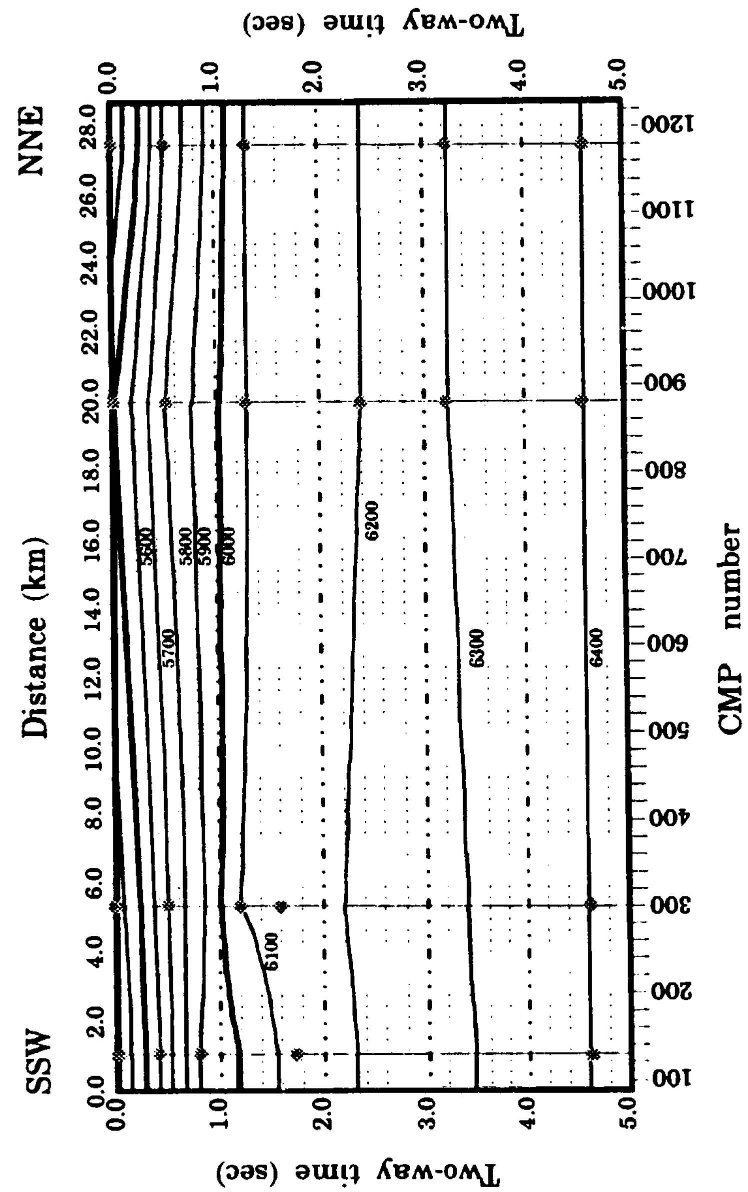

Fig. 2.22: Interpolated rms stacking velocity field of line 689/87. Shaded dots indicate velocity specification points.

reported from seismic refraction modelling (Beránek and Zátopek, 1981a). From the same seismic refraction survey, the velocity in the basement shows important lateral variations: while the 5.0 km/s isovelocity line rises only slightly from the Vienna basin to the West Danube basin, the 6 km/s refraction isovelocity can be modelled as rising sharply from about 13 km depth across the Peripieninian lineament to 5 to 6 km depth 25 to 30 km away under the Danube basin (Beránek and Zátopek, 1981a). This sharp lateral velocity variation makes the flat 6.4 km/s NMO isovelocity line at 4.6 sec TWT of the velocity field chosen inexact but we have no suitable reflector to define it more properly. The error is not critical since at high velocities the reflectors stack well for a wide range of velocities. Another source of error in velocity analysis is the anisotropy of the rocks of the Pezinok-Pernek group which reaches up to 17%, though it is usually lower than 10%. If distortion of the raypaths occurs because of rock anisotropy, the CMP gathering assumptions can be violated and reflectors displaced. However, this effect is probably only significant for near surface units in the first few hundred meters depth, since the Bratislava massif (MKM-2 borehole) does not show marked anisotropy in tri-directional velocity measurements from cubed rock samples from: at the bottom of the borehole, 603.7 m depth, VA = 5.490 km/s, VB = 5.860 km/s and VC = 5.868 km/s (Dvořaková, 1987); though slightly more anisotropic readings were obtained uphole; thus the anisotropy should not be critical.

To compensate for the absence of application of a strong gain function before stacking, diversity stacking was used. The 12 second data length of each trace was divided into four windows and to each window on the trace, a processor-calculated weight was applied according to the inverse of its energy, or rms amplitude. This provided a gentle trace equalization that also reduced the weight of high amplitude noisy traces in the stacked section as they were not relatively boosted.

This pre-stack processing improves the quality of the data. It is also possible to improve the appearance of the stacked section with post-stack processing. After NMO correction, a pass of residual statics would perhaps have improved the section across the Vienna Basin end of line 671/87, where there is a strong reflector for the residual static algorithm to cue on. However, residual statics is a midpoint-consistent processor and so needs the centroid of traces in bin easting, the centroid of traces in bin northing, the trace midpoint easting and the trace midpoint northing. These data were not available so there was no way to apply residual statics corrections using STARPAK software. To generate dummy values of the missing information we would need to know the exact position of shot and receiver stations along the line relative to the changes in orientation as well as the size of the bins. The precision and resolution of the location map (Plate 1) does not allow computation of these values. The Vienna basin part of line 671/87 would have been the only part of the data containing reflector segments long enough to carry through the residual statics.

2.3 POST-STACK PROCESSING

2.3.1 Lateral trace balancing

Trace amplitudes were laterally normalized using the average amplitude of a window from 1 to 2 sec TWT, i.e. within this window, a scale factor was calculated so that average amplitude equals the sum of the amplitudes divided by the number of samples included in the window. Each sample from a given trace was multiplied by a scalar equal to a user specified level divided by the average amplitude.

2.3.2 Coherency filtering

The goal of coherency filtering is to enhance reflectors over incoherent background noise. However, it can degrade data very much if overdone as it will create artificial reflectors everywhere. The application of coherency filtering was started at one second TWT to avoid unnecessarily disturbing reflectors at the top of the section.

Coherency filtering keeps the event times and amplitudes. It uses subwindows from adjacent traces to locate coherent events (see algorithm in Table 2.4). The subwindow length chosen is 16 ms, allowing preservation of steeply dipping events because events with lags of up to 16 ms are considered in the correlation. In this case,

Table 2.4: Coherency filtering algorithm.

Using a user specified number of adjacent traces, the reference trace being the current trace:
1) Input a window of user specified length from the reference trace and the adjacent traces.
2) Compute cross-correlation of each trace window with reference trace.
3) Search for largest peak in cross-correlation.
4) Shift trace windows by this peak lag time to align coherent events.
5) Multiply trace amplitude by user specified weights, the middle weight being that of reference trace.
6) Apply Hanning taper to the window.
7) Sum the windowed segments of the traces.
8) Replace the data in the current window from the reference trace by the sum calculated in step 7.
9) Move 1/2 window length down the trace and go back to step 1.
Repeat down to the bottom of the trace.
(STARPAK Processing manual, :CANE)

dips of up to 160 ms/km are kept as CMP interval is 25 m and 5 traces are used. Consecutive sub-windows were thus overlapping by 8 ms.

The number of traces to be correlated and the choice of weight allows the user to limit smearing of data. The weights are scalars by which the amplitude of each sample of the trace is multiplied, the central weight being that of the reference trace, the next ones the adjacent traces and so on. The weights used were 0.005 0.5 1 1 1 0.5 0.005 with a 200 ms window length. The very low weight of the two external traces are just a 'trick' to avoid floating point errors that were occurring during processing. Coherency filtering did not enhance much of the data but it did reduce random noise in the lower part of the sections (Figs 2.23 and 2.24). This is only a modest cosmetic improvement which does not change interpretation.

Final coherency filteres stacked section are presented as Plates 5 to 7 (pocket B at the rear). Reduced copies are located as Figs. 2.25, 2.29 and 2.30. These give a condensed view of the data, but give an appearance of reduced dynamic range due to the reduction process.

2.3.3 Migration

Because of large lateral velocity variations in lines 671/87 and 671A/87, wave-equation finite-difference migration (:WEM) was attempted only on the top 4.5 seconds of line 689/87. Though migration is known to yield poor results on strike lines because of sideswipes (Tucker and Yorston, 1973), none of these events were clearly identified on this line. Migration was attempted with stacking velocity and with velocities ± 15% from the stacking velocity. The small number of reflectors, steep velocity gradient, low signal-to-noise ratio and complex geology may explain the only modest improvement

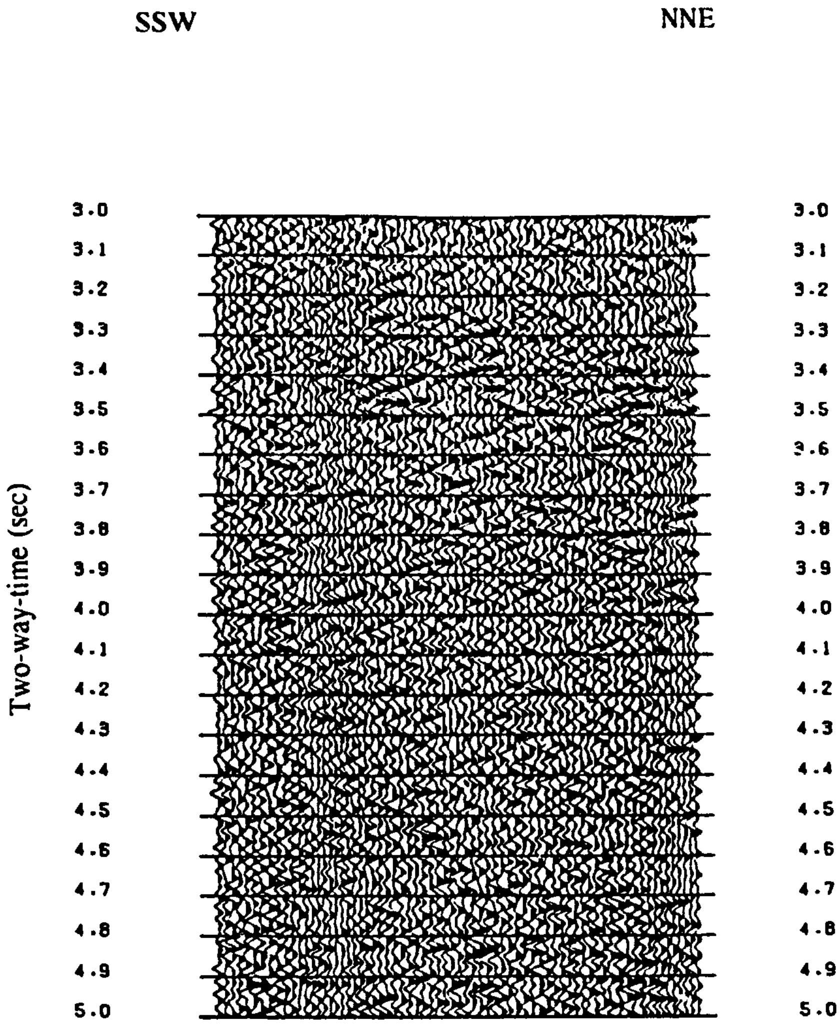

Fig. 2.23: Segment of line 689/87 between 3 and 5 sec TWT (vertical scale) and CMPs 730 to 880 before coherency filtering.

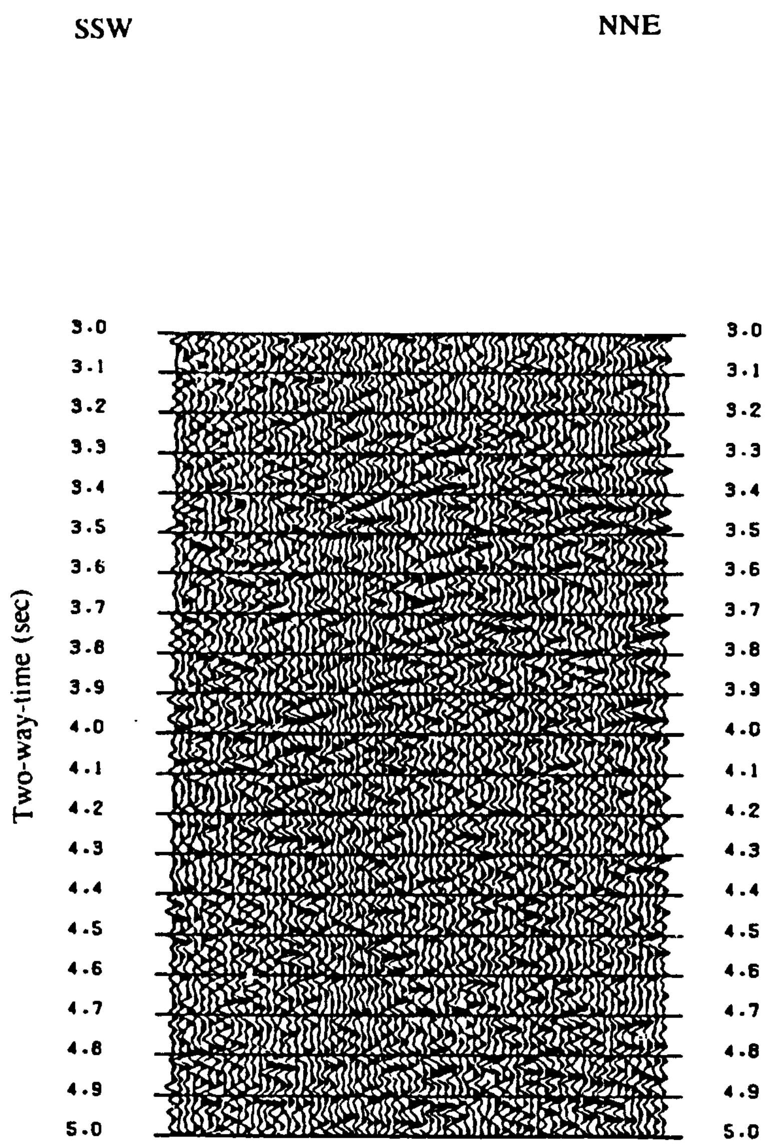

Fig. 2.24: Segment of line 689/87 between 3 and 5 sec TWT (vertical scale) and CMPs 730 to 880 after coherency filtering.

obtained from the migration (Figs. 2.26 to 2.28) as compared to the unmigrated section of line 689/87 (Fig. 2.25 and Plate 7). An event was chosen for comparison of the four versions of line 689/87: unmigrated (Plate 7), migrated with stacking velocity (Fig. 2.26), migrated with stacking velocity -15% and migrated with stacking velocity +15%. Its two-way time stays almost constant around 600 ms. This event is slightly more detached from neighbouring events on the section migrated with stacking velocity -15%, especially when compared with the unmigrated section. This discontinuity has been taken into consideration when the section was digitized for interpretation (Plates 8 to 10). There are some criss-crossing "smiles" on the bottom of the migrated sections and other edge effects on the sides, especially on the section migrated with stacking velocity +15% (Fig. 2.28). Two-way-time of reflectors has not changed significantly after migration though some diffractions may have collapsed. The migration did not improve the stacked section significantly and the smearing it introduced is annoying for geologic interpretation of the seismic section. Interpretation was thus carried on the unmigrated section (Figs. 2.25, 2.29 and 2.30 and Plates 5 to 7). For detailed geological interpretation (see next chapter), line drawings (Plate 8 to 10) are at the same scale as the large seismic sections (Plates 5 to 7) on which they are based.

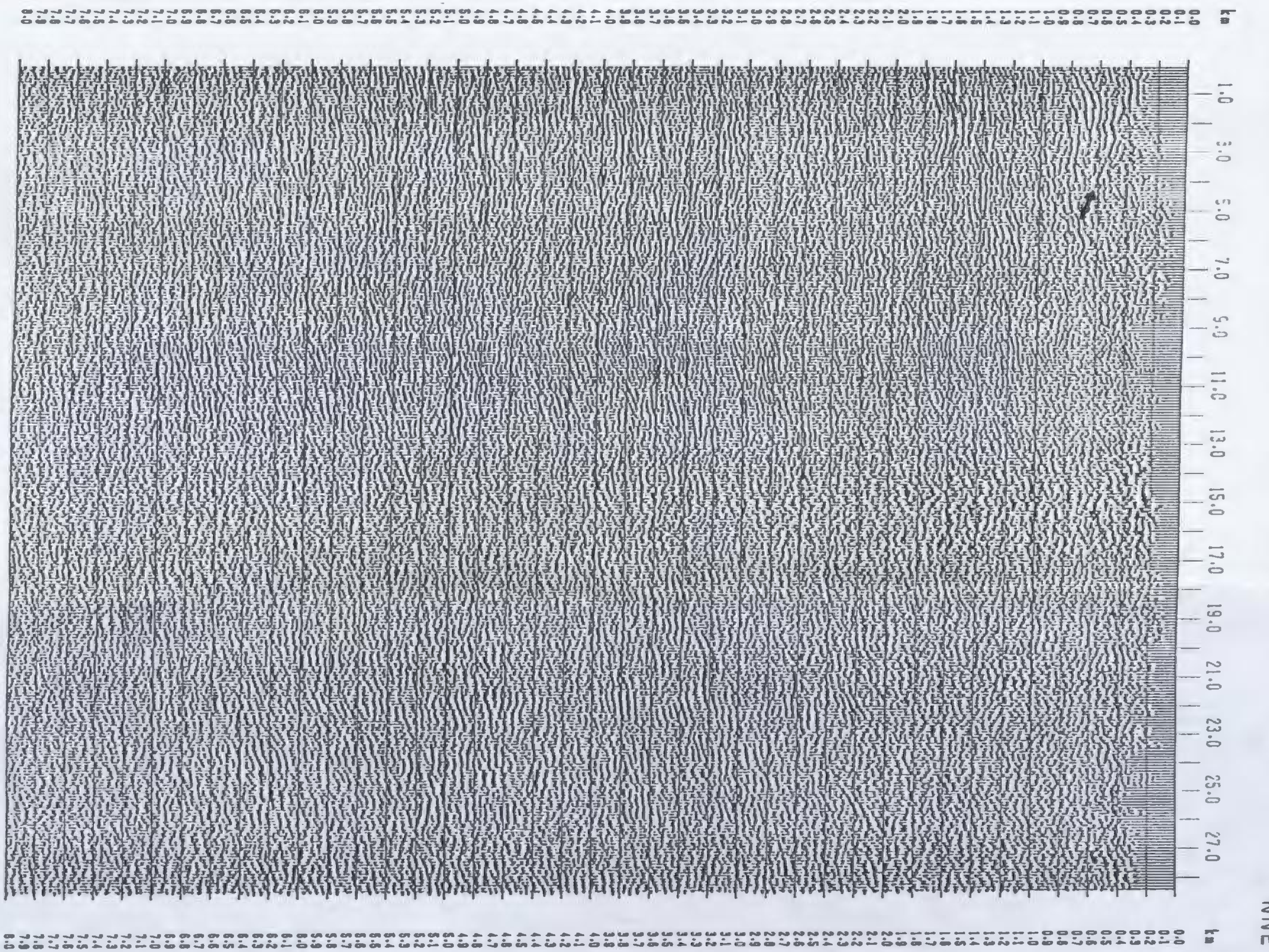

Two-way-time (sec)

Fig. 2.25: Final stack of line 689/87. Larger variable area plus wiggle trace copy of this figure is folded in pocket B. The arrow indicates an event that is compared when migration is applied with different velocity field. Vertical scale is two-way time (sec).

Fig. 2.26: Migration of line 689/87 with stacking velocity. The arrow indicates an event that is compared when migration is applied with different velocity field. Its position is almost unchanged relative to the unmigrated section (Fig. 2.26). Vertical scale is two-way time (sec).

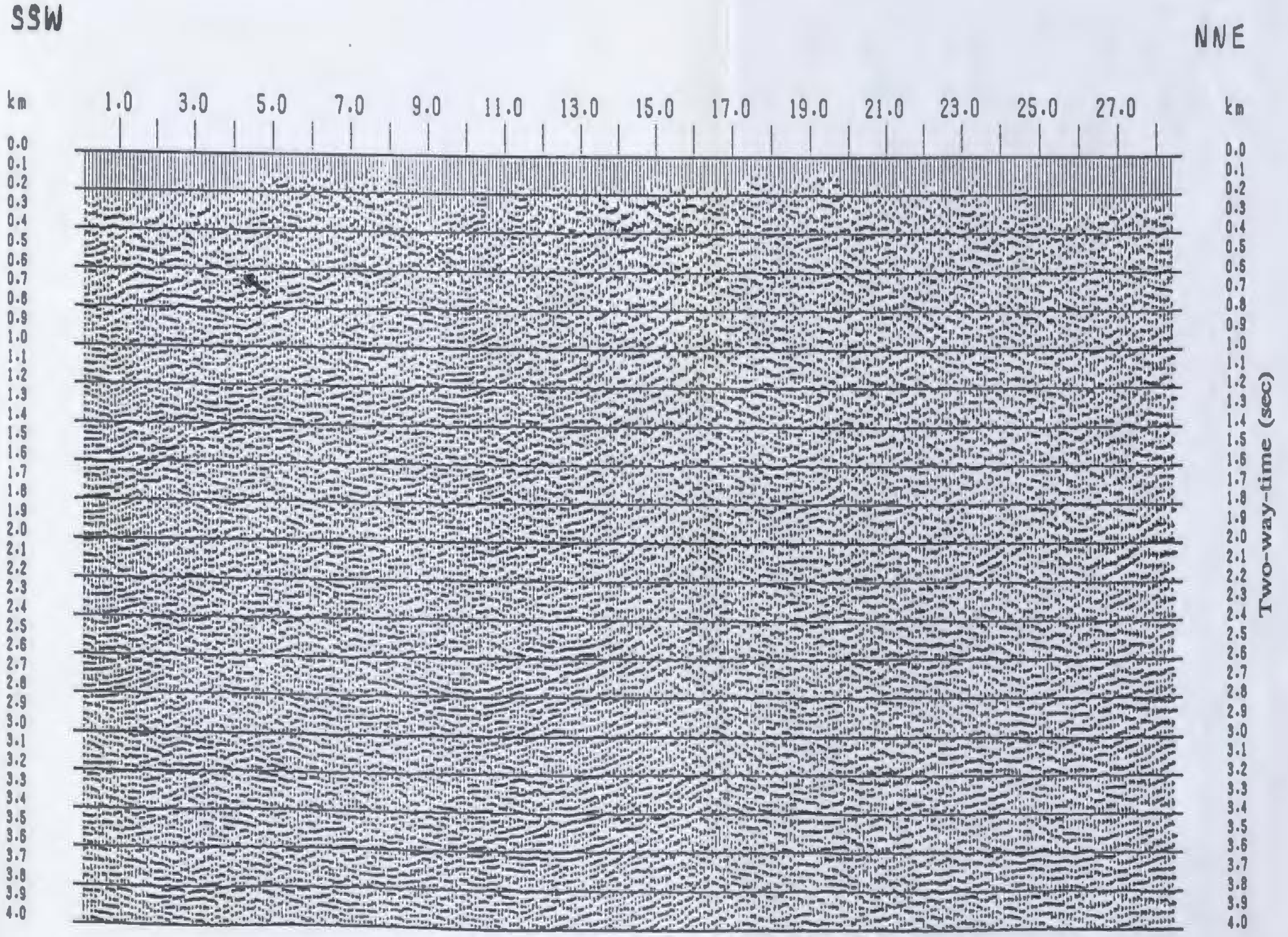

Fig. 2.27: Migration of line 689/87 with stacking velocity -15%. The arrow indicates an event that is compared when migration is applied with different velocity field. Its position is almost unchanged relative to the unmigrated section (Fig. 2.26). Vertical scale is two-way time (sec).

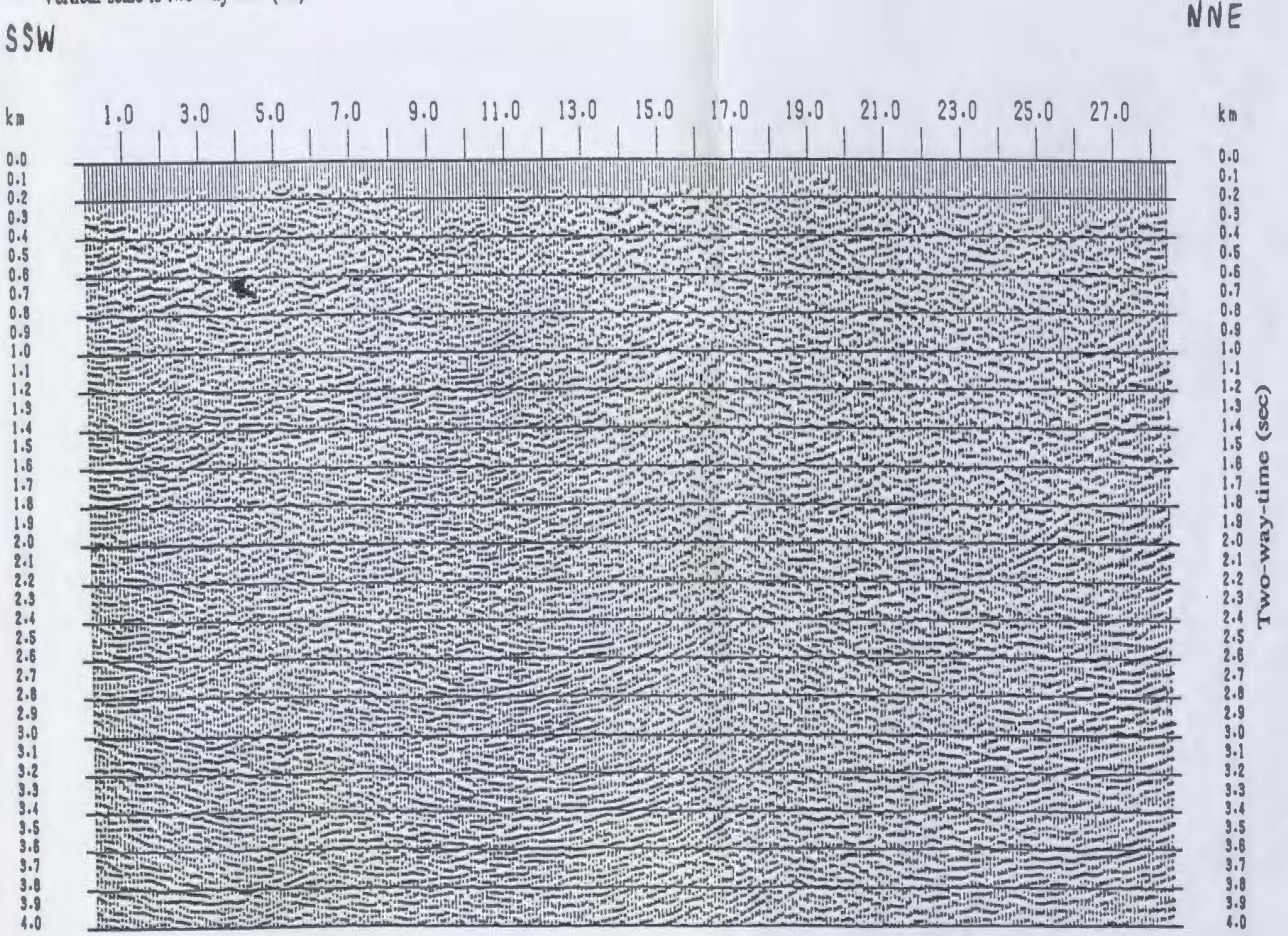

Fig. 2.28: Migration of line 689/87 with stacking velocity +15%. The arrow indicates an event that is compared when migration is applied with different velocity field. Its position is more detached from diffractions than on to the unmigrated section (Fig. 2.26) and other migrated sections (Fig. 2.27 and 2.28). Vertical scale is two-way time (sec).

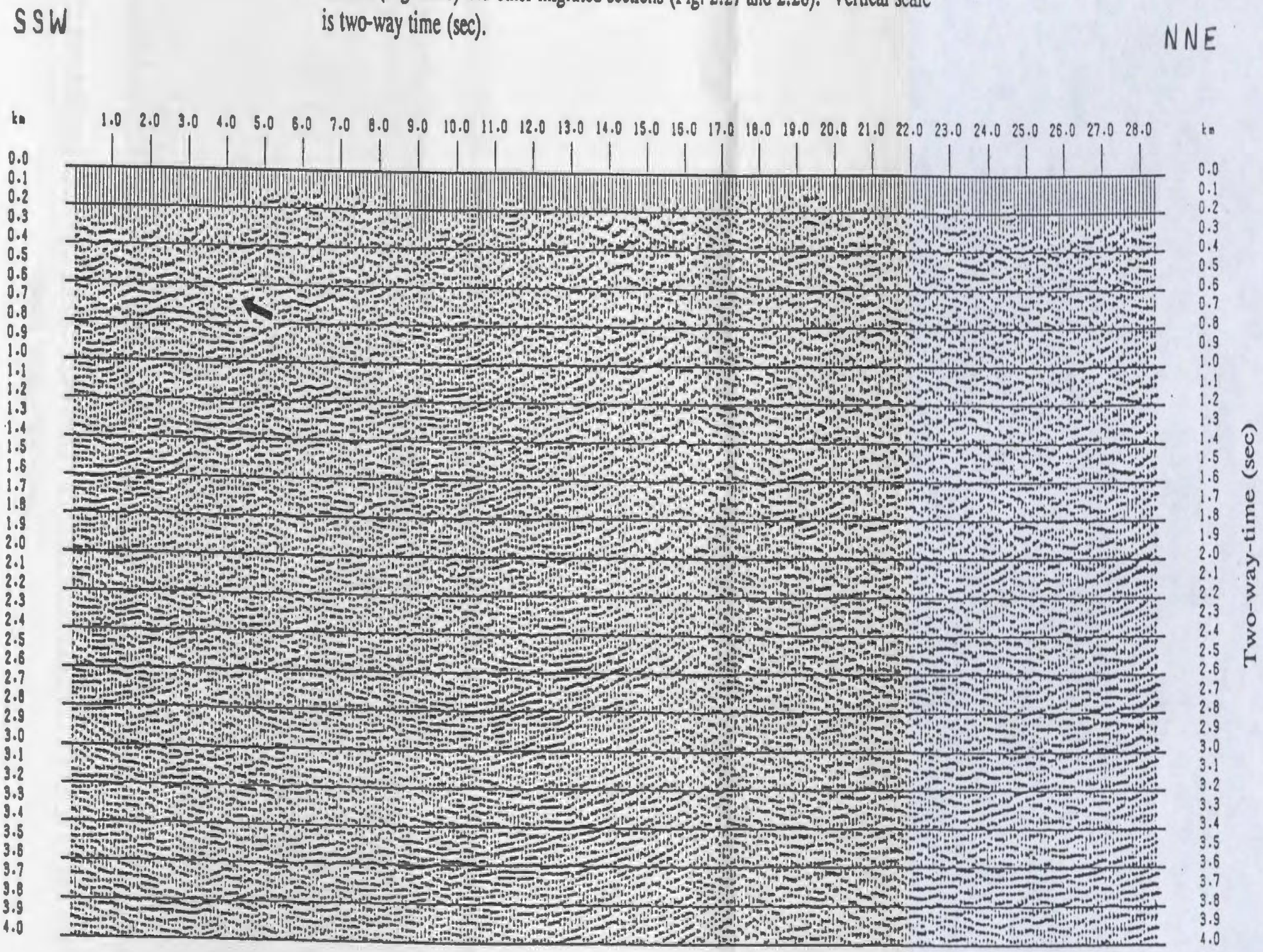

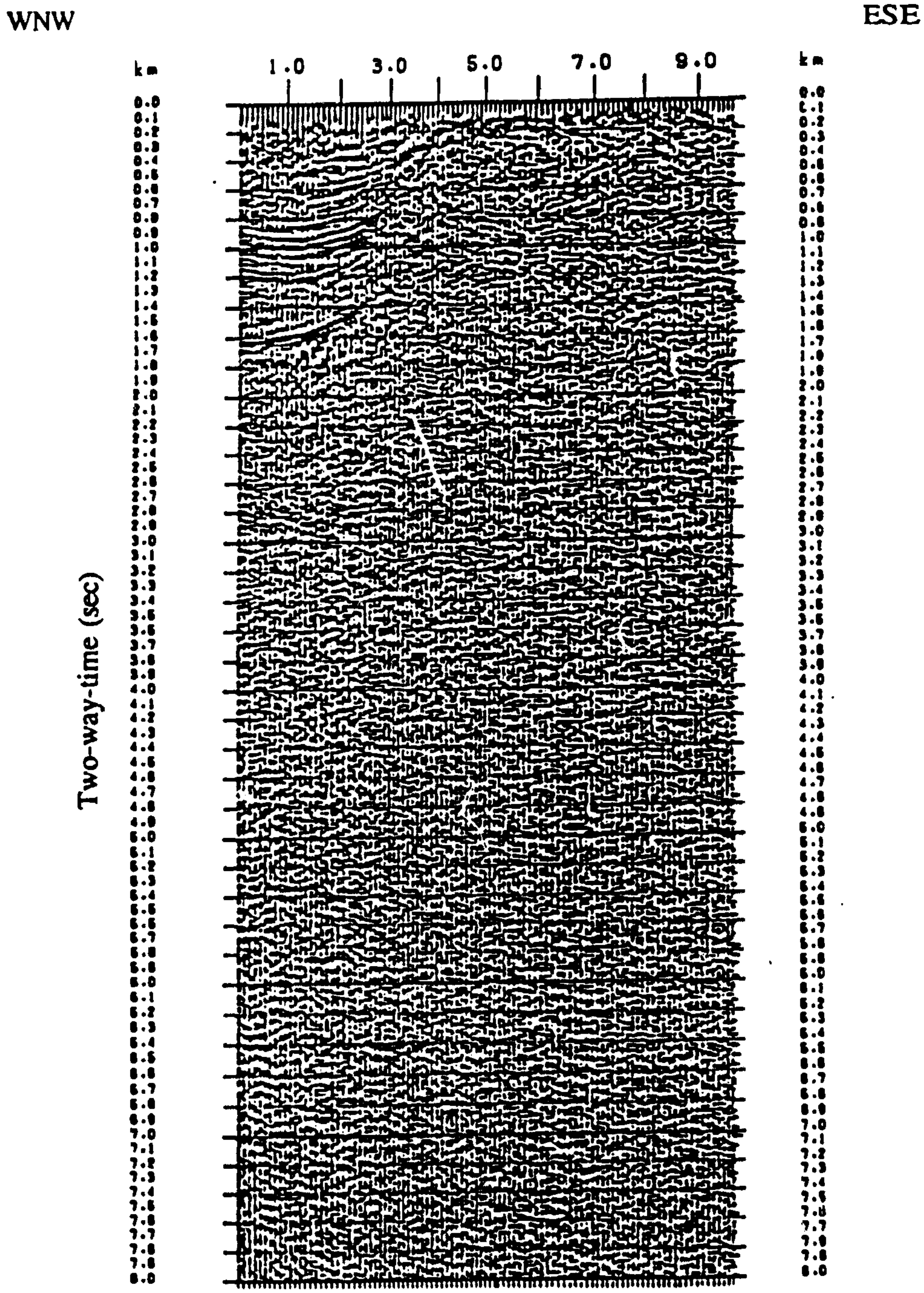

Fig. 2.29: Final stack of line 671/87. Vertical scale is two-way-time (sec). A larger variable area plus wiggle trace copy of this figure is folded in pocket B.

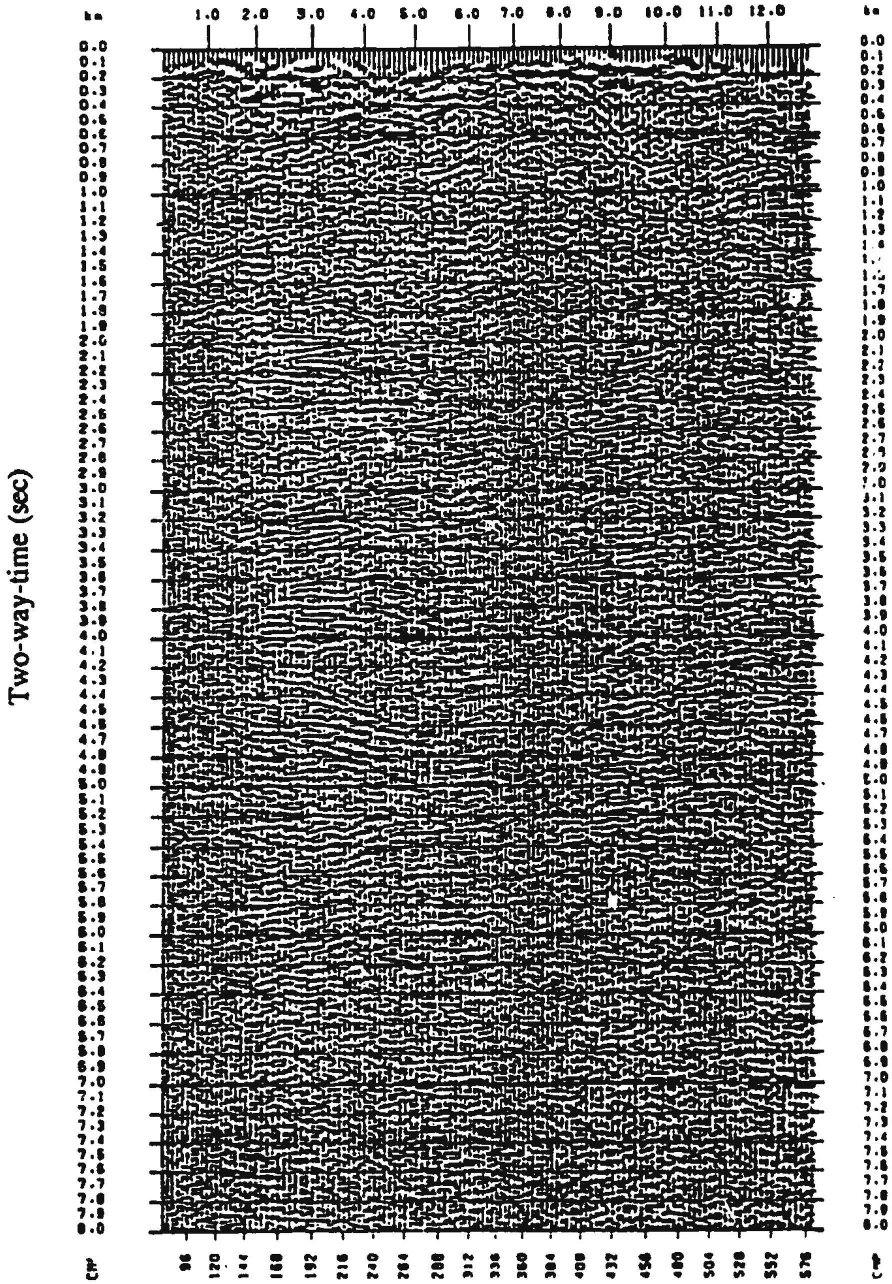

Fig. 2.30: Final stack of line 671A/87. Vertical scale is two-way-time (sec). A larger variable area plus wiggle trace copy of this figure is folded in pocket B.

3. INTERPRETATION AND DISCUSSION

The objective of this interpretation is to image sub-surface structures related to the formation of the Little Carpathians. First, the general character of the section is discussed. Then, reflections are identified among the various events present on the stacked sections (Fig. 3.1). Finally a geologic interpretation of the reflections (Plates 8 to 10) is made from comparison of the reprocessed seismic lines with geological map (Plate 1, Mahel' et al., 1961, 1972), with the seismic reflection lines 3T (Plate 11) and 8HR (Plate 12) and with Neogene paleostress data (Fodor et al., 1990; Nemčok et al., 1989).

The number of events dramatically decreases below 4 sec TWT. This may be caused in part by the low signal-to-noise ratio of the original CMP gathers but also by the structure of the study area. At greater depths, reflections originate from a larger area. Since interfaces such as older fault planes and shear zones have been broken down by Miocene horst and graben formation and strike-slip movement, pre-existing interfaces have become too small to create reflections strong enough on the CMP gathers to be stacked properly.

An obvious feature of the three seismic lines is the presence of vertical bands of low and high reflectivity. Such bands are often explained by different attenuation coefficients of the rocks close to the surface. On lines 671/87, 671a/87 and 689/87 there is no one-to-one correlation between these bands of high and low reflectivity and

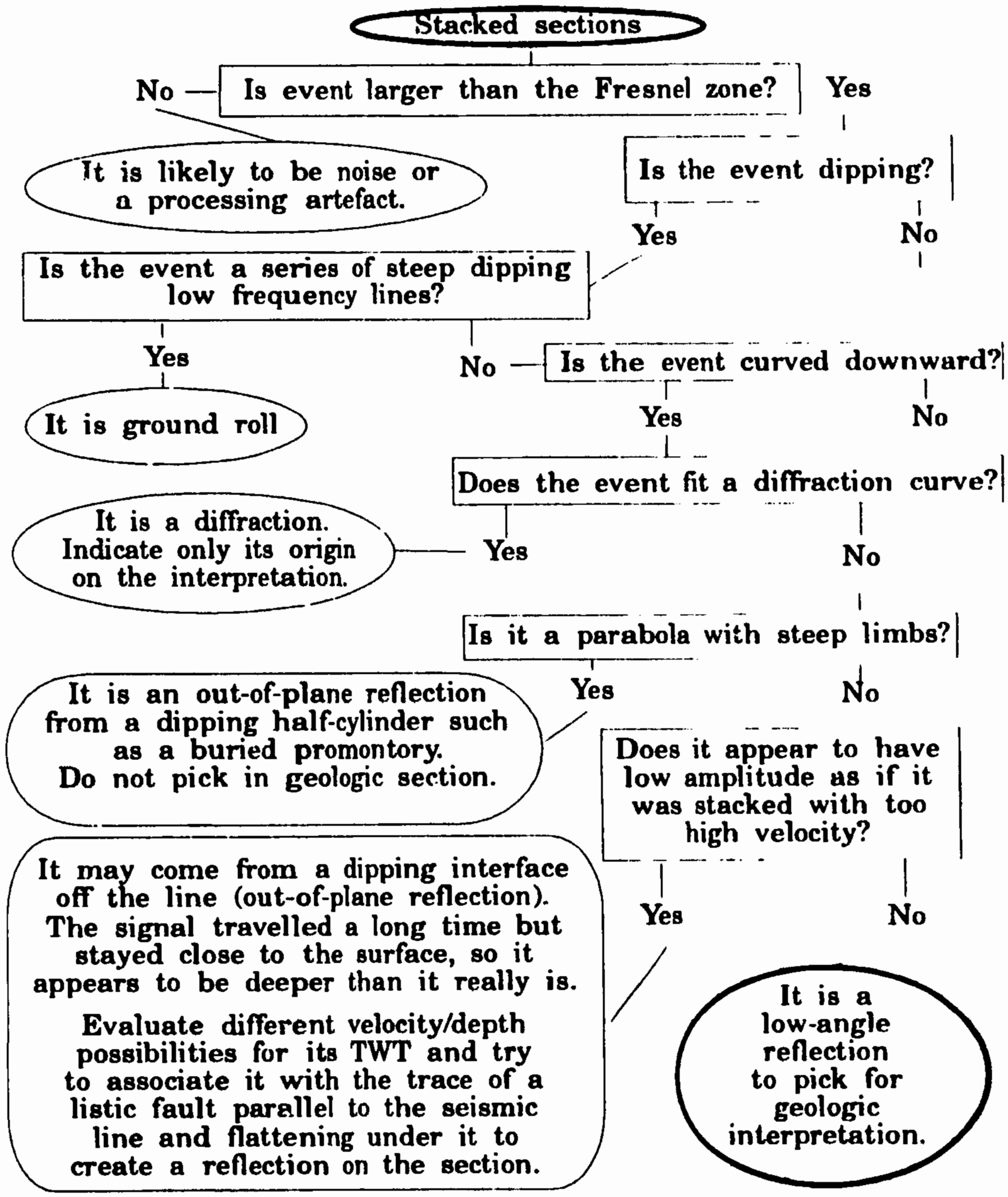

Fig. 3.1: Flow-chart describing the identification of reflections on a stacked section.

distribution of crystalline and carbonate units along the seismic lines (Table 3.1). These bands are therefore not exclusively caused by a greater attenuation of the seismic signal in carbonate rocks than in crystalline rocks closest to the surface, at least not on line 689/87. These bands may be related to the originai signal-to-noise ratio of the CMPs, especially on line 689/87. The attenuation may occur very close to the surface in natural unconsolidated fill, road fill, or be caused bu source or receiver coupling with the ground. These phenomena are common for surface sources such as Vibroseis. Since AGC has been used, relative amplitudes are not geologically significant anymore.

Table 3.1: Distribution of crystalline and sedimentary rocks compared to occurrence of zones of high and low reflectivity along line 671A/87.

Distance from beginning of line 689/87 (km)	Type of rock at the surface (Mahel' et al., 1972)	Distance from beginning of line 689/87 (km)	Reflectivity
0.0 - 1.7	Calcareous sedimentary rocks	0.0 - 2.0	Low
1.7 - 7.7	Crystalline	2.0 - 4.5	High
7.7 - 9.0	Sedimentary rocks	4.5 - 8.5	Low
9.0 - 10.8	Crystalline	8.5 - 9.5	High
10.8 - 12.7	Neogene sediments	9.5 - 12.7	Medium

3.1 IDENTIFICATION OF REFLECTORS

The first step in the interpretation of seismic reflection data is to pick the events which extend horizontally over a distance exceeding the diameter of the Fresnel zone. A reflection is created when a wavefront hits a zone of abrupt velocity change. The amplitude of the reflection depends on the reflector planarity over an area around the raypath reflection point with a diameter of the Fresnel zone. The radius Fr of the Fresnel zone depends on the average velocity V to the reflector, the two-way time t and the dominant frequency f of the reflection (Dobrin and Savit, 1988).

$$Fr = \frac{V}{4}\sqrt{\frac{t}{f}} \qquad (1)$$

If the planaritu of the reflector does not 'cover' the Fresnel zone, the reflection will be reduced in amplitude. Thus with typical reflection data sets, observable events tend to come from plane reflectors of diameter greater than the Fresnel zone. The corollary of this is that spectral reflections have lateral extents usually exceeding the diameter of the Fresnel zone. Events shorter than the Fresnel zone are not spectral reflections. The amplitude of these "small body diffractions" or "Fresnel diffractions" falls between the amplitude of spectral reflection and the amplitude of point or line diffractions. They may or may not be imaged as the size of the Fresnel zone is also dependant on the signal-to-noise ratio. They also can be either noise, scattering, reflections affected by mutual interference or processing artifacts. Figs. 3.2 and 3.3 show variation of the width of Fresnel zone as a function of two-way-time for two CMPs. The velocity fields at these

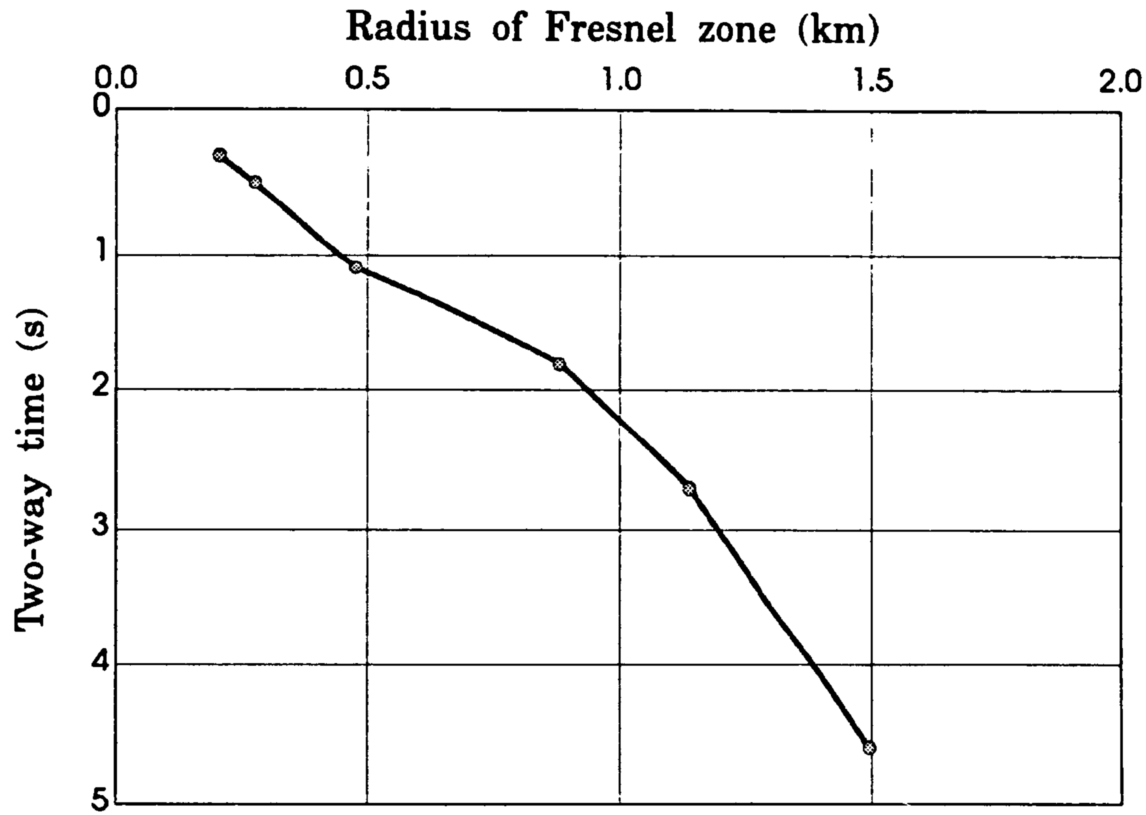

Fig. 3.2: Width of Fresnel zone for velocity field defined at CMP 550 of line 671/87.

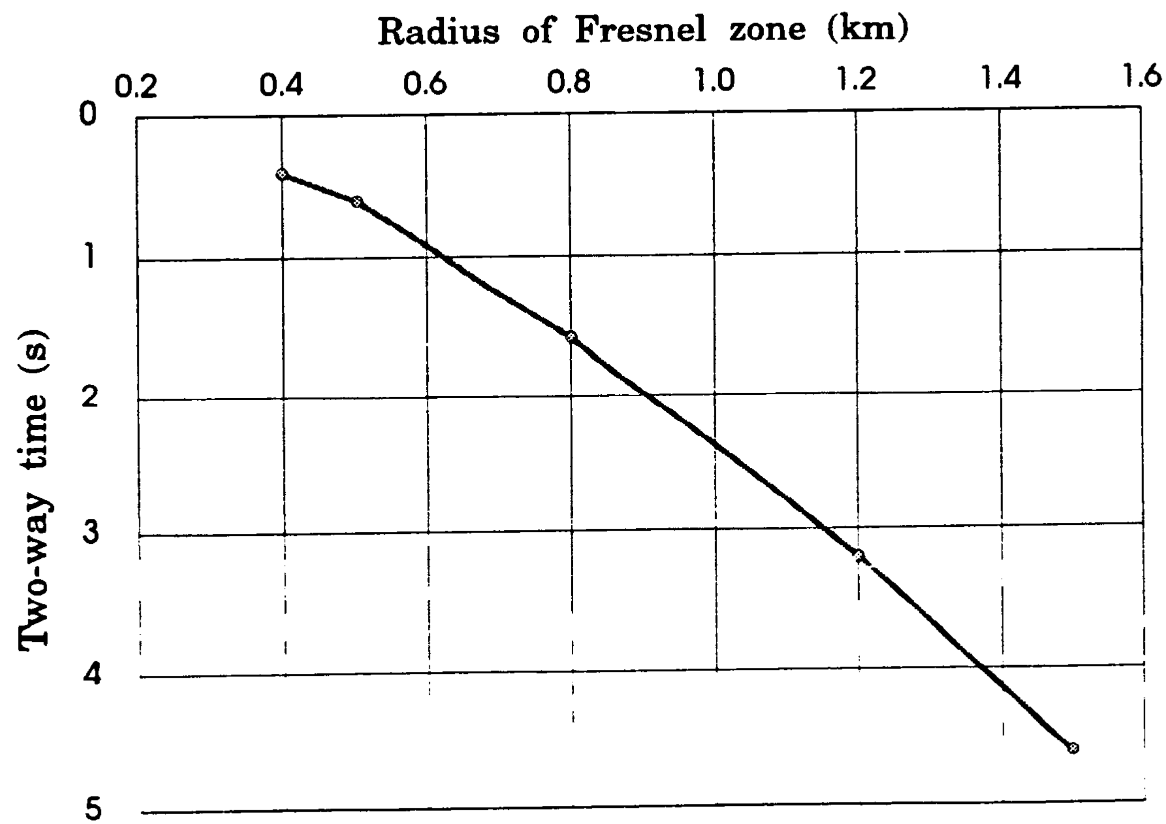

Fig. 3.3: Width of Fresnel zone for velocity field defined at CMP 330 of line 671A/87.

CMPs appear on Figs. 2.20 and 2.21. As radius of the Fresnel zone between 3 and 4 sec TWT increases from 1.2 to 1.4 km, most of the coherent events in this range are shorter than the Fresnel zone. This explains why there are fewer events on the interpreted seismic sections (Plates 8 to 10) than on the reprocessed sections (Plates 5 to 7). Some events that were not picked are not certainly something else than reflections but cannot be identified as reflections with certitude.

There are many events with lateral extent larger than the diameter of the Fresnel zone. Some of them are not reflections but diffractions or out-of-plane reflections. To discriminate reflectors from diffractions, we can compare their curvature with that of a diffraction at corresponding depth and rms velocity. On a stacked section, for a diffraction with an origin at t_0 sec, where the rms velocity is V and the depth h, the time of the diffraction t'_d at x meters offset from the origin will be:

$$t_d = \frac{2(x^2 + h^2)^{1/2}}{V} \qquad (2)$$

(Sheriff and Geldart, 1982). But since the depth h of the diffracting point is unknown,a diffraction equation using the normal moveout time shift must be used, such as

$$t_d \approx t_0 + 4\Delta t_n = t_0 + \frac{4x^2}{2V^2 t_0} \qquad (3)$$

where t_0 is the time corresponding to the diffracting point and Δt_n is the normal moveout time shift (Telford et al., 1976). As depth increases, the diffractions will flatten and the difference between diffractions and reflections will decrease. It will also be quite difficult to evaluate offset x and t_0 as only a very small part of the hyperbola will be seen. Since the NMO velocity changes in the top 3.5 sec TWT, a few diffraction curves were calculated for each fragment of hyperbola found on the sections, after estimation of a range of possible CMP and TWT of the diffracting point. If the segment of hyperbola fitted one of the calculated curves, it was identified as a diffraction. Below 3.5 sec TWT, the NMO velocity fields of lines 671/87, 671A/87 and 689/87 show only minor lateral variation and the influence of original two-way-time diminishes, so calculation of a few curves at 200 ms interval was sufficient to identify diffractions. Clusters of diffractions often occur when a zone is densely faulted, like in a horst and graben structure. The corners of buried crystalline blocks are strong diffracting points. Many diffracting points, identified as open circles on Plates 8 to 10, indeed appear close to the projected trace of faults or near reflectors. Four diffracting points form a peculiar subvertical plane under a low-angle thrust under the eighth kilometre of line 671A/87 (Plate 6). There is no fault trace corresponding to these diffracting points on the geologic maps consulted (Mahel' et al., 1961; Mahel' et al., 1972) though many faults have been mapped in recent years in this area (Nemčok et al, 1990). Information is insufficient to determine if this feature is geologically significant or not.

Out of plane reflections occur when the seismic energy is reflected on a dipping plane. As the wavefront is spherical, the strike of the fault plane may have any direction relative to the line. However, it is easier to explain when the strike of fault plane is

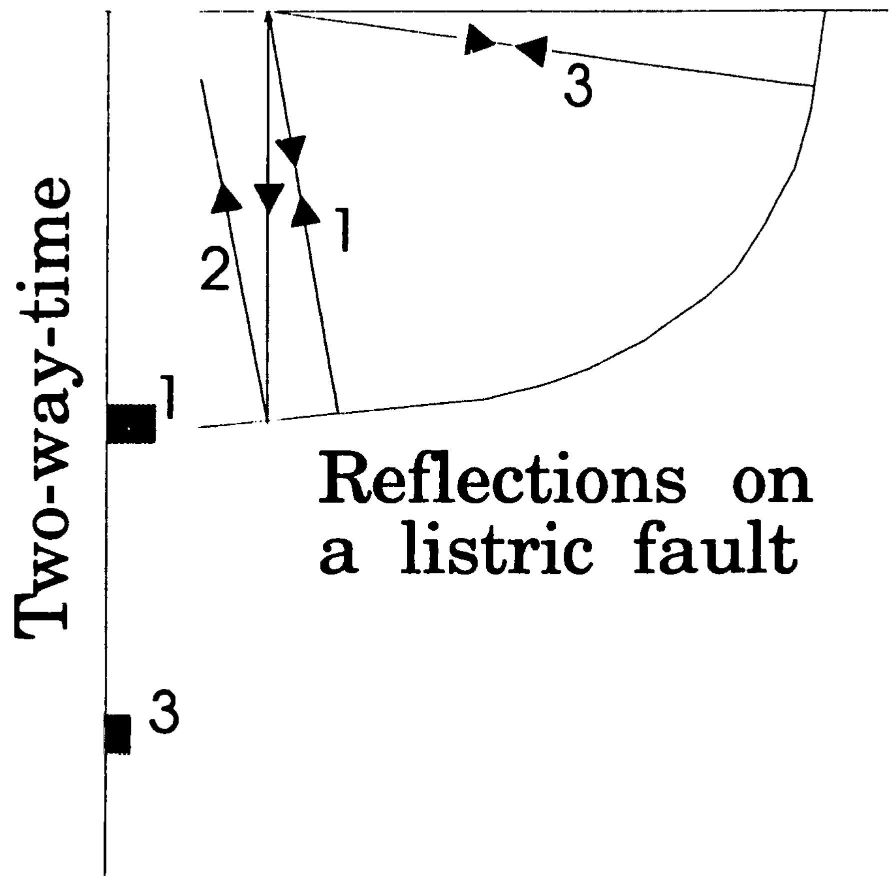

Fig. 3.4: Ray-path and two-way-time of in-plane (1) and out-of-plane (3) reflections on a listric fault plane. Reflections from vertical incidence rays (2) come to the surface our-of plane and cannot be recorded. Reflections from out-of-plane interfaces are produce only for specific (depth, angle of dip) combinations. Event 3 appears at late two-way-time because velocity close to the surface is lower than along the path of the in-plane reflection (1).

parallel to the line. Along the strike of a dipping plane with constant dip along the line, the energy coming back to the line is reflected on a point oblique relative to the line (trace 1 of Fig. 3.4). With a very steep plane, such as a buried valley or cliff wall, the energy could have travelled close to the surface but appear at late two-way times (Fig. 3.4). If the reflecting surface is not a plane but a dipping half-cylinder, the reflections will appear as a parabola with steep limbs, which will discriminate it from a diffraction. No out-of-plane reflection was clearly identified on the seismic sections though there maybe one from 1 to 1.2 sec TWT, between 5.3 to 6.2 km from the start of line 671/87 (Plate 2).

Ground roll still appears on the reprocessed line 671A/87 (Plate 6), close to the surface just before the Danube basin margin on line 671A/87.

3.2 COMPARISON OF SEISMIC LINES BEFORE AND AFTER REPROCESSING

There is a +200 ms or so static shift between the three reprocessed lines and the original lines. Its cause is not clear. It is not voluntary. It may come from a change in the datum level of the static corrections or from the change in stacking velocity. This shift is annoying for interpretation because the identification of the events could change if one level or the other is used. However, as the datum level obtained seems consistent with surface geology and borehole R-1 (Fig. A.2 and Table A.1), it is probably correct.

The comparison between the original section of line 671/87 (Plate 2) and the reprocessed section (Plate 5) is meaningless out of the Vienna basin and its immediate vicinity as there is no reflector outside that zone except maybe two short segments between 0 and 1.5 km at about 2.8 to 2.9 sec TWT on the reprocessed section (Plate 5). There seems to be a break in the sedimentary layering at about 1.2 km from the NW end of the reprocessed line (Plate 5) that did not appear before (Plate 2). At about 750 ms TWT, 3 to 4.3 km on the reprocessed line (Plate 5), there are short segments of low frequency signal that seem to form a reflector. It is probably an artefact since there is no hint of it in the CMP gathers.

The major feature of the line 671/87 is a graben of the Vienna Basin. A splay fault segment related to the Záhorie-Humenné deep fault, related to the Peripieninian lineament, corresponds to the right termination of the basin reflectors. At this termination there is a very important diffracting point (1.3 to 1.4 sec TWT, 3 km offset on Plate 5), close to a distance of 3 km and a depth of 4 km (open circle on Plate 8). The amplitude of the diffractions, with limbs appearing from 1.6 to 2.0 sec TWT (Plate 5) are lower on the reprocessed section. This indicates that the velocities originally chosen were too high in this area (Plate 2). The diffraction may be linked to the double reflection at a distance of 4 km from 1.3 to 1.4 sec TWT (event 1 on Plates 5 and 8). This group of diffractions indicates a zone of irregularity near the fault plane. The curved event at the top of the fault is not vertical enough to be a diffraction, but it is also too vertical to be a reflector and too shallow to be an out-of-plane reflection. It may be a processing artefact caused by inappropriate muting at that specific point. Since front mutes were interpolated between values, specified at a few CMPs having a clear direct wave and good data quality, interpolation may not yield appropriate front mute TWT at some specific CMPs.

On line 671A/87, many reflectors appear more clearly in the top middle of the reprocessed section (Plate 6) than on the original section (Plate 3). Layering at the margin of the West Danube Basin (event 7) is still not clear on the reprocessed line (Plate 6) but its basement top appears as a series of discrete segments. This is different from the original section (Plate 3) where dipping events identified as ground roll and diffractions were dominating. There is still some ground roll behind the basin margin however. The fold is so low at the edge of the section that energy appearing over the basement of the basin edge may be noise or artefact, though some events correspond to possible sedimentary units in this area. The reprocessed line 671A/87 (Plate 6) may be considered more suitable for geologic interpretation than the original section (Plate 3).

The quality of the original line 689/87 (Plate 4) was already good so the reprocessed line (Plate 7) is quite similar to the original line. Many diffractions have been identified on line 689/87 both before (Plate 4) and after (Plate 7) reprocessing (open circles on Plate 10). Some seem to have their diffracting points aligned. On the reprocessed section (Plate 7), the reflector at about 1.58 sec TWT (event 1 between 3 and 4 km depth, 2.1 to 2.5 km offset on Plate 10) terminates in a diffraction at 2.1 km offset. This may indicate an abrupt termination such as block displacement.

In general, reprocessing improved the signal-to-noise ratio in some zones and removed diffractions at the margin of the Vienna and West Danube basin. The main objectives of reprocessing have been realized, though the extent of improvement is modest.

3.3 GEOLOGIC INTERPRETATION OF SEISMIC LINES

This section presents a comparison of the reprocessed seismic lines (Plates 5 to 7) with geological map (Plate 1, Mahel' et al., 1961, 1972), with the seismic reflection lines 3T (Plate 11) and 8HR (Plate 12) and with Neogene paleostress data (Fodor et al., 1990; Nemčok et al., 1989). From the synthesis of this information, the interpreted sections (Plates 8 to 10) were drawn. Past tense is used in the text for information from referenced publications while present tense is otherwise used.

The aim of deep crustal seismic reflection data is to image deep structures. There are a few deep events on lines 671A/87 and 689/87. On the reprocessed line 689/87 (Plates 7 and 10), the reflectors at 1.6 sec TWT (events from group 1) that were identified as a detachment horizon or low angle normal fault could be the bottom of the Envelope nappe, as uplift and erosion has removed more than one kilometre of rock since the nappe thrusting over autochthonous or para-autochthonous carbonate formations in late Early Cretaceous to early Late Cretaceous (Late Albian to Early Coniacian time, around 95 to 91 Ma, Fig. B.6 and B.7) (Hovorka et al., 1982). The Bratislava and Modra massifs of the Envelope nappe were also eroded between their formation during Late Carboniferous and the Early Triassic (Fig. B.3 and B.4), as indicated by the presence of Permian arkosic conglomerate on its SSW edge (Mahel' et al., 1961, Plate 1), so it would be likely that the massifs would have of a thickness of less than 5 km. The base of the Envelope nappe was estimated at 6.4 to 7 km depth from gravity and refraction modelling (Table 1.2) (Blížkovský, 1989). However, corresponding reflectors do not appear at the same two-way-time under the NNE end of line 689/87 nor under line 671A/87 (Plates 6 and 9). Another candidate for the bottom of the Envelope nappe is the group of reflectors at 2 sec TWT (6 km equivalent depth), between 0 and 4 kilometres from the start of line 671A/87 (Plates 6 and 9). Thrust structures were imaged much deeper on line 3T (event no 3 on Fig. 1.4, seismic section on Plate 11, Tomek et al., 1987), at 4 to 5 sec TWT (12 to 15 km equivalent depth) under the West Danube basin (Tomek and Thon, 1988). If we remove the depth of Neogene sediments over the structure, these deep thrust structures should appear at 7 to 8 km under the Little Carpathians, which is close to the depth of the bottom of the Envelope nappe in Table 1.4. Reflectors at 1.6 sec TWT (5 km depth for a stacking velocity of 5 km/s, events of group 1 on Plates 7 and 10) are probably not the base of the nappe containing the intrusives but some structure within the Envelope nappe. Moreover Pliocene to Quaternary uplift of the Little Carpathians (Kvitkovič and Plančar, 1981) cannot explain the difference in depth between the thrust structure under the West Danube basin and these reflectors under the Little Carpathians. The base of the Envelope nappe is thus either the reflector at 2 sec TWT (6 km depth, event 4 on Plates 6 and 9) or it is not imaged because the velocity contrast between the Envelope nappe (metasediments and granodiorite) and the calcareous, and likely metamorphosed, rocks under it was too weak.

On line 671/87 (Plates 5 and 8), some reflectors are interpreted as part of the nappe complex overlying the Modra massif of the Envelope nappe. From surface dips and structural interpretation by Mahel' et al. (1972), the two reflectors at 0.6 sec TWT between 4 and 6 km from the start of the line are interpreted as the thrust plane between the Envelope nappe and the Križna nappe (the two middle events of group number 2 on Plate 8). A reflector at 0.780 sec TWT (lower reflector of group 2 on Plate 8) is interpreted as the interface between the top of the Modra massif intrusive with maybe Proterozoic to Devonian metasediments over it (Figs. B.1 and B.2), and its Early Triassic to Middle Cretaceous sedimentary cover of the Little Carpathian group (Figs. B.4 to B.6).

From borehole R-1 (Fig. A.1 and table A.1), the lowermost long concave reflector on line 671/87 (Plates 5 and 8), at 1.6 to 1.7 sec TWT (around 5 km depth for 6 km/s stacking velocity, event 4 on Plates 2, 5 and 8) is also related to Early Cretaceous thrusting (Fig. B.5). It was identified as a thrust plane between two subnappes of the

Northern Limestone Alps (Tomek, 1992, personal communication), as it underlies a line of reflectors with a position that matches the depth of the top of the Northern Limestone Alps, which is the allochthonous basement of the Vienna basin west of the main strike-slip fault. The amplitude of this reflector seems very strong for a thrust plane separating units of Triassic limestone (Table A.1), especially when compared to the reflectivity of thrust planes under the Little Carpathians. But because of the TWT of the reflection and borehole data, no other identity for this reflector is proposed: though migration raises the reflector toward 0 sec TWT, 1.6 sec TWT is quite deep for the top of the Northern Limestone Alps, drilled at 2.8 km depth. The top of the Northern Limestone Alps formations is then more likely to be event 3 (Plates 2, 5 and 8) though it has lower amplitude. The termination of this reflector against the projected trace of the normal fault precludes identification of event 4 as the detachment horizon of this normal fault. Comparison of line 671/87 with line 8HR (Plate 12) indicates that the northern limit of the deep graben is located between these two lines as the basement appears at shallower depth on line 8HR (event 8) than on line 671/87 (event 3), as indicated by depth of Cretaceous and Triassic rocks in boreholes near Lakšárska Nová Ves (Table A.1). A normal fault subparallel to line 8HR appears south of line 8HR on Plate 1. This fault is likely to be the northern boundary of the deep graben. The southern boundary of the deep graben lies between line 3T (Plate 11) and line 671/87 as reflections from the base of the Vienna basin is shallower on line 3T (event 7) than on line 671/87 (event 3).

The best defined set of reflectors on line 671A/87 (Plates 3, 6 and 9) shows complex relations between low-angle planes (events of group 1) projected into faults mapped by Mahel' et al. (1972) and other reflections that are subhorizontal or dipping in an opposite direction (events of group 2). From the geometry of the reflectors and surface geology, these reflectors are interpreted as thrust faults and conjugate faults respectively. The mapped faults are interpreted as a trailing imbricate fan, a structure associated with thrusting: as the rocks of the Little Carpathian group, which were originally overlying the Modra massif, now appear below the higher thrust fault, the three thrust faults form a trailing imbricate fan. This structure indicates that the Envelope nappe is in fact broken into subnappes. This fault could have been initiated during late Early Cretaceous to early Late Cretaceous (Coniacian) formation of the accretionary prism (Figs. B.6 to B.9, Tomek, 1988). From the strike of the thrust faults and the change in paleostress orientation though the Neogene in the Little Carpathians (Fig. B.9) (Nemčok et al., 1989), this thrust was probably reactivated in Palaeocene to Lower Miocene age (early Karpatian). The maximum compressional stress was then NW-SE as the nappes from the European margin were overriding the North European platform.

The major feature of the strike-line 689/87 (Plates 7 and 10) is the dipping reflector (event 2) between 0.3 to 0.7 sec TWT (1 to 2 km depth) at 9 to 10 km from the SSW end of the line. It is interpreted as the contact between two Hercynian granitoid intrusives, the Bratislava massif to the south and the Modra massif to the north. This contact was previously identified as a Late Cretaceous thrust fault along which the

Bratislava massif was pushed from the south over the Modra massif during the formation of the accretionary prism (Tomek, 1992, personal communication) as suggested by the low angle dip of the fault and the greater erosion of the Little Carpathian group over the Bratislava massif than over the Modra massif. When projected to the surface, it also corresponds to a SSW dipping Lower Miocene normal fault related to the northward slip of the Modra massif along the N-S strike-slip faults (Nemčok et al., 1989) (see Fig. 1.3 for fault orie· tation in Neogene). When the paleostress orientation changed in Lower to Middle Miocene, this fault accommodated right-slip movement (Nemčok et al., 1989). The Late Cretaaceous thrust fault between the Modra massif and the Bratislava massif has thus been reactivated into a low-angle dip-slip fault. On the interpreted section (Plate 10), this fault is continued to the SSW into a group of reflectors at the SSW end of line 689/87 (leftmost event 2). The thickness of the Bratislava massif, which is part of a granitoid intrusive severed from its root in Cretaceous time, is thus estimated between 1 and 2 km.

Event 3 is composed of N to NE dipping reflectors at about 0.3 sec TWT (1 equivalent kilometre). As there was horst and graben formation in Middle to Late Miocene, it is likely to be a segment of a low-angle normal fault cutting the surface SSW of the line.

Other reflectors are identified as Lower Miocene or younger features. There are two possible explanations for lowermost reflectors on lines 671A/87 (events of groups

4 and 5, Plates 6 and 9) and 689/87 (events of group 4 on Plates 7 and 10). First, they are likely to be segments of a low-angle normal fault identified on line 3T, flattening at about 3 sec TWT under the margin of the West Danube basin (Fig. 1.4; Tomek, 1988; Tomek et al., 1987; Tomek and Thon, 1988). On line 3T, this fault cuts the Pre-Neogene basement under the West Danube basin and reaches under the Little Carpathians with a strike about parallel to that of line 689/87. They could also be thrust structures within the Inner West Carpathian nappes as the group of reflectors no 3 on fig 1.4.

The SSE end of line 671A/87 (Plates 6 and 9) crosses the margin of the West Danube basin. Though the fold of CMPs gathers is low in this area, two main groups of events (6 and 7) can be identified, using borehole data and interval velocities approximated from stacking velocities. According to borehole Vistük-2 (Fig. A.3, Table A.3) located about 2 km away from the end of line 671A/87 (Fig. A.1), they are most likely the interface between early Middle Miocene (more exactly early to middle Middle Badenian, which was around 15 Ma) gravel and overlying sand, and later clay to clayey shale. The break between the two main groups of small reflections projects into a normal fault mapped by Mahel' et al. (1961) (Plate 1). The left edge of the left group of reflectors projects into the normal fault defining the edge of the West Danube basin. The lower projection of this fault is not clearly defined but is made to match basement depth at borehole Vistük-2 (Fig. A.3). Unfortunately, line 671A/87 does not reach far enough into the West Danube basin to allow comparison with lines 3T and 8HR. Line 3T (Plate 11, events 11 - Sarmatian/Pannonian interface and 12 - Pannonian/Pontian interface) and

8HR (Plate 12, events 9 to 13) both show sediment layers dipping toward the Pannonian basin. The fan-like structure of the sediment layers at the edge of the basin is caused by thermal subsidence. Events 8 and 9 may be broken by faults older than overlying sediments, though the apparent faulting may be caused by strong amplitudes above. However buried faults are also observed on line 3T, especially on both sides of a horst indicated by number 5 (Faults A and B).

On line 671/87 (Plates 5 and 8), many closely spaced reflectors appear between 0.6 and 1.2 sec TWT from 0 to 2.5 km from the start of the line (reflections between events 3 and 5). According to borehole Rohožník-1, about 1 km SW of the end of line 671/87, it is likely to be caused by numerous interfaces into the early Middle Miocene (Karpatian and lower Badenian, 17.5 to 16 or 15.5 Ma) sediments, mostly composed of clay with thin sand beds. According to Fig. A.2, reflections in and after the Late Middle Miocene (Upper Badenian and over) are likely caused by intra unit beds of sandstone or sandy limestone. This is why the interpreted unit limits do not overlie the reflections. Instead, unit limits are positioned using the relative thickness of units and the depth of potentially reflective beds inside them. Though Sarmatian and older sediments are labelled as post-rift, the second phase of extension, from 13 Ma to present (Tomek and Thon, 1988) was not controlled by subsidence but by movement on a different set of faults after rotation of the Little Carpathians as the nappes were pushed against the Bohemian massif around 17 Ma (Karpatian time) (Fig. B.9). The steep normal fault inferred at the margin of the basin by following the termination of Vienna basin reflectors corresponds to a mapped fault (Plate 1) and is consistent with Late Miocene to Pliocene changes in paleostress orientation (Nemčok et al., 1989). The two other faults near it are drawn from surface geology.

The reflections on the reprocessed lines are in agreement with the allochthonous nature of the Bratislava and Modra Hercynian granodiorite intrusives suggested by many authors (Hovorka et al., 1982; Hrouda, 1986), However, the basement of the Envelope nappe, containing the granodiorite intrusives and Proterozoic-Palaeozoic metasediments, was not clearly identified. The reflection sections also suggest that the faults that were activated as the paleostress directions changed through the Neogene (Fodor et al., 1990; Nemčok et al., 1989) were often reactivated thrust planes as they correspond to reflectors flattening at shallow depth, identified as Late Cretaceous thrust faults. From line 671A/87, it is likely that the Envelope nappe which contains the intrusives is in fact made up of a set of smaller nappes because a trailing imbricate fan was imaged within it, and an old thrust may have been reactivated as a shallow normal fault on line 689/87. The partial breaking of the Envelope nappe into subnappes must have occurred when the Envelope nappe was already close to its present position relative to underlying formations since the thrust faults do not seem to have a great lateral extension on the geologic map (Plate 1). Line 671/87 shows the steepness of the Vienna basin margin. Its dipping sedimentary interfaces are broken by faults. This style of margin is very different from the West Danube basin margin which shows sedimentary layers dipping like in a fan toward the Pannonian basin, a structure caused by thermal subsidence followed by uplift of the horst. Few faults break the sedimentary interfaces. This structure is associated with thermal subsidence. The Vienna basin was probably too far from the partial melt zones of the Pannonian basin to undergo thermal subsidence and to evolve into a back-arc basin such as the Danube and Pannonian basins.

A summary of new conclusions and observations appears on Table 3.2. Reviewing the features we were looking for to confirm the geological model proposed (section 1.3), most of them are indeed imaged. A deep detachment horizon detaching the block rotation above it is not clearly identified but deep reflectors are indeed imaged despite the low signal-to-noise ration of the data set. Some of the deep reflectors are identified as listric faults related to the formation of the NNE trending horst and graben structure (lines 689/87 and 671A/87). We image large offset on both sides of the Little Carpathians horst: a large offset on the steep normal fault bordering the Vienna basin, and a seemingly shallower one on the fault at the margin of West Danube. On line 689/87, the thrust fault between the Bratislava massif and the Modra massif is imaged, indicating that the Bratislava massif is only 1 to 2 km thick. This low-angle fault also corresponds to Lower to Middle Miocene normal and then right-slip movement caused by paleostress orientation contemporary to the formation of NNW horst and graben structure. Many diffractions were indeed imaged but their position was not clearly indicating the breaking of the Little Carpathians horst into smaller blocks by a NNW horst and graben structure. Given the quality of this seismic data set, the geological model proposed is sustained by seismic reflection data.

Table 3.2: New observations and conclusion

Observations that were not made before:

1) First seismic reflection images of shallow thrust structures within the Little Carpathian horst (Plates 9 and 10) though they were known from geological mapping and structural analysis (such as Mahel' et al., 1972).

2) First seismic reflection image of a trailing imbricate fan within the Envelope nappe of the Little Carpathian horst (Plate 9).

3) First estimation of the thickness of the Bratislava massif: 1 to 2 km (Plate 10).

Conclusion:

The thrust structures imaged within the Little Carpathian horst supports the hypothesis that this horst is part of an accretionary prism as most thrust faults are dipping NNW and seem to flatten at similar depths.

3.4 SUGGESTIONS FOR FURTHER WORK

To strengthen the proposed geological model, further geophysical work could be attempted.

To constrain the dip and depth of the Hercynian granodiorite intrusives, and the lower boundary of the Proterozoic-Palaeozoic metasediments they intruded through, simultaneous modelling of coincident closely spaced gravity (residual Bouguer anomaly) and magnetic measurements along the three reprocessed seismic lines and line 3T could be a good choice. The magnetic susceptibility of granodiorite is in average about ten times higher than the magnetic susceptibility of phyllite and gneiss (Telford et al., 1976). The ƒgf^x unit (see Plate 1 for location) of the Pezinok-Pernek group contains both pyrite and graphite. The rocks of the Harmonia group contain significant quantities of graphite which would create low susceptibility anomalies. It would thus be possible to evaluate the subsurface extent of the Proterozoic-Palaeozoic formations, especially under the Križna and Choč nappes, and maybe find some more evidence of strike-slip displacement through them. Limestones also have weaker magnetic susceptibilities than metamorphic rocks. Coincident gravity and magnetic modelling may help us better evaluate the dip of the nappes. However, the presence of numerous power lines along the seismic lines may reduce the validity of a magnetic survey. If the presence of the power lines would not disturb too many magnetic field measurements they would greatly add to the 1:200 000 scale 5 mGal interval residual Bouguer anomaly data already available in Czechoslovakia (Ibrmajer, 1981) that we were unable to obtain for this study. Sections along the seismic lines through these residual anomaly maps may be sufficiently precise for this purpose. To produce better a constrained model of the Little Carpathians from the magnetic and gravity data, the magnetic measurement stations along the three seismic lines should be closely spaced, discarding all unreliable stations (power lines, underground metal pipes etc.). Density of many samples from each rock unit should be evaluated.

Though often used to help gravity modelling, reversed refraction surveys may bring limited results because of the small velocity contrast between units which would not provide many high-velocity paths for refracted waves, and because of the high amplitude of railroad noise. The 12.5 Hz noise would indeed fall into the higher amplitudes of the refraction survey and greatly reduce the usefulness of the data.

Though the signal-to-noise ratio of the Vibroseis lines was low and the small velocity contrasts did not create many reflections, dynamite data collected by Geofyzika Brno across the West Carpathians consistently had higher signal-to-noise ratio than Vibroseis data, as exemplified by line 3T (Plate 11). High resolution 4 sec TWT reflection with shorter sampling rate (1 or 2 ms) with an explosive source may be most useful to image the margins of the Vienna and West Danube basins since with higher frequencies, a clearer image of the sedimentary interfaces could be obtained. However, more borehole data through the Neogene sediments would be required to increase the reliability of the interpretation. Variations in the rate of uplift of the Little Carpathian horst block could then be evaluated using the angle of the reflections from the sedimentary interfaces at the margin of the West Danube basin. Though the signal-to-noise ratio would still be low in the pre-Neogene formations, the higher frequency (with a narrower Fresnel zone and finer vertical separation) could help delineate the NNW-SSE normal faults of the Lower Miocene and Lower to Middle Miocene extension episodes in the Little Carpathians, and determine the importance of reactivated Cretaceous to Palaeogene thrust faults among them.

Studies of fractures and slickensides (Fodor et al., 1990; Kovač et al., 1989; Nemčok et al., 1989) have brought a lot of new information about the Neogene history of the Little Carpathians but such traces of earlier events have been obliterated by Neogene activity. Geophysical surveys would maybe yield a hint of the nappe formation and emplacement of the basement block over carbonate nappe.

CONCLUSION

Comparison of the seismic sections before and after reprocessing shows that the signal-to-noise ratio has improved in many places and that diffractions have faded at the margin of the basins due to closer spaced velocity analysis. Ringing in the Vienna basin has also diminished through deconvolution. Although the range of improvement is modest, the seismic objectives of reprocessing were thus met, given the limits imposed by the lack of binning information and the presence of strong white noise.

The interpretation of line drawings from the reprocessed lines confirmed the proposed geological model. Moreover, interesting thrust structures were imaged suggesting that the Envelope nappe may be divided in subnappes, further supporting the allochthonous nature of the Little Carpathians.

BIBLIOGRAPHY

ADAM, A., 1980. The change of electrical structure between an orogenic and an ancient tectonic area (Carpathians and Russian Platform). *J. Geomag. Geoelectr.*, 32: 1-46.

ANDRUSOV, D. and O. Fusán, 1968. Harmonia. *Lexique stratigraphique international*, vol. I: Europe (P. Pruvost, dir.), no 6b :Tchécoslovaquie, 2nd ed.), part 6b2: Région karpatique (D. Andrusov, dir.), Union internationale des sciences géologiques, Centre national de la recherche scientifique, Paris: 113-114.

ARTYUSHKOV, E.V. and M.A. Baer, 1986. Mechanism of formation of fold belts, the Alpine-Carpathian regions. *The Origin of Arcs* (Wezel, F.C., ed.) in the collection Developments in Geotectonics, Elsevier, Amsterdam, Netherlands, 21: 191-232.

BALLA, Z., 1988. Clockwise paleomagnetic rotations in the Alps in the light of structural pattern of the Transdanubian Range (Hungary). *Tectonophysics*, 145: 277-292.

BALLA, Z., 1987. Tertiary paleomagnetic data for the Carpatho-Pannonian region in the light of Miocene rotation kinematics. Laurasian paleomagnetism and tectonics (D.V. Kent, ed. et al.) *Tectonophysics*, 139(1-2): 67-98.

BEER, M.A., 1983. The Carpathians and Dinarids in the Mesozoic. *Geotectonics*, 17(2): 123-132.

BERÁNEK, B. and A. Zátopek, 1981a. Earth's crust structure in Czechoslovakia and in Central Europe by methods of explosion seismology. *Geophysical Syntheses in Czechoslovakia*. Veda, Bratislava: 243-264.

BERÁNEK, B. and A. Zátopek, 1981b. Preliminary results of geophysical synthesis in Czechoslovakia and Central Europe based on exploration seismology until 1980. *Geophysical Syntheses in Czechoslovakia*. Veda, Bratislava: 469-497.

BERGERAT, F., 1989. From pull-apart to the rifting process: the formation of the Pannonian Basin. *Tectonophysics*, 157: 271-280.

BIELY, A., 1988. The Geological Structure of the West Carpathians. *Evolution of the Northern Margin of Tethys: The Results of IGCP Project 198*, vol. I (Rakús, M., Dercourt, J. and Nairn, A.E.M., eds.). Occasional Publications ESRI, New Series, No. 3, Earth Sciences and Resources Institute, University of South Carolina:: 137-140.

BLIŽKOVSKÝ, M., 1989. The Lithospheric Structure in Czechoslovakia. 6th International Mathematical Geophysics Seminar, Free University of Berlin, 1988. *Inverse Modelling in Exploration Geophysics: Proceedings*. F.Vieweg and Sohn - Braunschweig. Theory and Practice of Applied Geophysics, v. 3: 513-531.

BLIŽKOVSKÝ, M., O. Fusan, J. Ibrmajer, J. Plančár and M. Suk, 1986. Geophysical phenomena of the deep structure in Czechoslovakia. *Journ. of Geodynamics*, 5(2): 165-178.

BOTT, M.H.P., 1982. *The Interior of the Earth: Its Structure and Evolution*, 2nd edition. Elsevier, New York: 403 p.

BURCHART, J., B. Cambel and J. Král', 1987. Isochron reassessment of K-Ar dating from the West Carpathian crystalline complex. *Geologický Zborník: Geologica Carpathica*, 38(2): 131-170.

BURCHFIEL, B.C. and L. Royden, 1982. Carpathian foreland fold and thrust belt and its relation to Pannonian and other basins. *Bull. Am. Assoc. Petrol. Goel.*, 66: 1179-1195.

BYSTRICKÝ, J., 1968. Havrania Skala. *Lexique stratigraphique international*, vol. I: Europe (P. Pruvost, dir.), no 6b :Tchécoslovaquie, 2nd ed.), part 6b2: Région karpatique (D. Andrusov, dir.), Union internationale des sciences géologiques, Centre national de la recherche scientifique, Paris: 115-116.

ČERMÁK, V., 1981. Heat flow investigations in Czechoslovakia. *Geophysical Syntheses in Czechoslovakia.* Veda, Bratislava: 427-439.

CERV, V., J. PEK and O. Praus, 1984. Models of geoelectrical anomalies in Czechoslovakia. *J. Geophys.*, 55: 161-168.

CHALOUPSKÝ, J., 1989. Major tectonostratigraphic units of the Bohemian Massif. *Terranes in the Circum-Atlantic Paleozoic Orogen* (R.D. Dallmeyerr ed.). Geological Society of America Special Paper 230: 101-114.

DEBALMAS, J. and M. Sandulescu, 1987. Transformante nord-pennique et problèmes de corrélation palinspatique entre les Alpes et les Carpathes. *Bull. Soc. géol. France*, (8), III(2): 403-408.

DOBRIN, M.B. and C.H. Savit, 1988. *Introduction to Geophysical Prospecting*, 4th ed., McGraw-Hill: 867 p.

DVOŘÁKOVÁ, V., 1987. Fyzikální vlastnosti hornin na vrtech MKM - 2 Jur pri Brastislave a MKM - 6 Pernek. Geofyzika n.p. Brno, Brno, Czechoslovakia, 58 p.

FODOR, L., F. Marko and M. Nemčok, 1990. Evolution microtectonique et paléo-champs de contraintes du Bassin de Vienne. *Geodinamica Acta (Paris)*: 4(3): 147-158.

FÖLDVARY, G.Z., 1988. *Geology of the Carpathian Region*. World Scientific Publishing Co., New Jersey. 571 p.

FUSÁN, O., J. Ibrmajer and J. Plančár, 1979. Neotectonic blocks of the West Carpathians. Geodynamic Investigations in Czechoslovakia. Veda, Bratislava: 187-193.

GUTDEUTSCH, R. and K. Aric, 1988. Seismicity and Neotectonics of the East Alpine-Carpathian and Pannonian Area, *The Pannonian Basin: A Study in Basin Evolution*, AAPG Memoir 45 (edited by Leigh H. Royden and Ferenc Horvath), The American Association of Petroleum Geologists and The Hungarian Geological Society: 183-194.

HAMILTON, W.B., 1990. On Terrane analysis. *Phil. Trans. R. Soc. Lond. A.*, 331: 511-522.

HATTON, L., M.H. Worthington and J. Makin, 1986. *Seismic Data Processing, Theory and Practice*. Blackwell Scientific Publications: 177 p.

HORVATH, F., 1984. Neotectonics of the Pannonian Basin and the surrounding mountain belts: Alps, Carpathians and Dinarides. The Alpine-Meditte-ranean region (Kahle, H.G. ed. et al.) *Annales Geophysicae*, 2(2): 147-154.

HOVORKA, D., P. Pitoňák and J. Spišiak, 1982. Mesozoic Basalts of the Malé Karpaty Mts (the Western Carpathians) - Their Significance for the Tectonic Interpretation of the Variscan Granodiorite Massif, *Veröffentlichungen des Zentralinstituts für Physik der Erde*, 73: 5-13.

HOVORKA, D. and J. Spišiak. 1988. West Carpathian Mesozoic Volcanic Activity: Paleogeographic Aspects. *Evolution of the Northern Margin of Tethys: The Results of IGCP Project 198*, vol. I (Rakús, M., Dercourt, J. and Nairn, A.E.M., eds.). Occasional Publications ESRI, New Series, No. 3, Earth Sciences and Resources Institute, University of South Carolina: 137-140.

HROUDA, F., 1986. The magnetic fabric of sedimentary rocks of the Malé Karpaty Mts. and its tectonic implications. *Sbor. Geol. Věd, užitá Geofyz.*, 20: 155-167.

IBRMAJER, J., 1981. Geological interpretation of gravity maps of Czechoslovakia. Geophysical syntheses in Czechoslovakia. Veda, Praha: 135-143.

JIŘIČEK,R. and Tomek, 1981. Sedimentary and structural evolution of the Vienna Basin, *Earth Evol. Sci.*, 1(3): 195-204.

KARNIK, V., V. Schenk and Z. Schenkova, 1984. Earthquake provinces of Central and Eastern Europe. *Geophysics: Proceedings of the 27th International Geological Congress*, Moscow 4-14 August 1984, Vol. 8. VNU Science Press, Utrecht, The Netherlands: 15-256.

KÓKAI, J. and Gy. Pogácsás, 1991. Hydrocarbon plays in Mesozoic nappes, Tertiary wrench basins and interior sags in the Pannonian Basin. *First Break*, 9(7): 315-334.

KOVÁC, M., I. Barath, I. Holicky, F. Marko and I. Tunyi, 1989. Basin opening in the lower Miocene strike-slip zone in the SW part of the Western Carpathians, *Geologický Zborník: Geologica Carpathica*, 40(1): 37-62.

KOVÁC, M., I. Krystěk, J. Seneš and D. Vass, 198. Origin, migration and disappearance of West Carpathians sedimentary basins in Lower Miocene. *Giornale di Geologia*, Ser. 3, 48(1-2): 317-322.

KRS, M., 1981. Paleomagnetic Research in Eurasia. *Geophysical Syntheses in Czechoslovakia*. Veda, Bratislava: 317-333.

KRS, M., P. Muška, O. Orlický and P. Pagáč, 1979. Palaeomagnetic investigations in the West Carpathians. *Geodynamic Investigations in Czechoslovakia*. Veda, Bratislava: 207-214.

KVITKOVIČ, J. and J. Plančár, 1979. Recent Vertical Movement Tendencies of the Earth's Crust in the West Carpathians. *Geodynamic Investigations in Czechoslovakia*. Veda, Bratislava: 193-200.

MAHEL, A., T. Buday, O. Fusán and, 1961. *Geological Map of Czechoslovakia.* Ustredni ustav geologicky, Praha. Scale 1:200 000. Sheets M-34 XXV, M-34 XXVII, M-34 XXII and XXVIII with legend, stratigraphic and geological section.

MAHEL', A., T. Buday, B. Cambel, R. Halouzka, A. Matějka, M. Peržel, A. Sabol and J. Vozár, 1972. Malých Karpatych Geologický Mapa. Geologický ustav Dionýza Štura, Bratislava. Scale 1:50 000.

MICHALÍK, J., 1988. Early Cretaceous Carbonate Platform development in the West Carpathian Realm. *Evolution of the Northern Margin of Tethys: The Results of IGCP Project 198*, vol. I (Rakús, M., Dercourt, J. and Nairn, A.E.M., eds.). Occasional Publications ESRI, New Series, No. 3, Earth Sciences and Resources Institute, University of South Carolina: 137-140.

MICHALÍK, J. and J. Soták, 1990. Lower Cretaceous shallow marine buildups in the Western Carpathians and their relationship to pelagic facies. *Cretaceous Research*, 11: 211-227.

MIŠÍK, M. and R. Marschalko, 1988. Exotic conglomerate in Flysch sequences, West Carpathians. *Evolution of the Northern Margin of Tethys: The Results of IGCP Project 198*, vol. 1 (Rakús, M., Dercourt, J. and Nairn, A.E.M., eds.). Occasional Publications ESRI, New Series, No. 3, Earth Sciences and Resources Institute, University of South Carolina: 95-113.

NAGYMAROSY, A., 1981. Chrono- and Biostratigraphy of the Pannonian Basin: A Review Based Mainly on Data from Hungary. *Earth Evol. Sci.*, 1(3): 183-194.

NEMČOK, M., F. Marko, M. Kovác and L. Fodor, 1989. Neogene Tectonics and Paleostress Changes in the Czechoslovakian Part of the Vienna Basin. *Jahrb. Geol. Bundes A.*, Wien, 132(2):443-458.

NG, M., 1990. Noise reduction methods - A tutorial. *Can. Soc. Expl. Geophys. Recorder.* XV(4): 8-33.

NIKOLAEV, V.G., D. Vass and D. Pogácsás, 1989. Neogene-Quaternary Pannonian Basin : a structure of labigenic type. *Origin and Evolution of Sedimentary Basins and Their Mineral and Energy Resources* (R.A. Price ed.), Geophysical Monograph 48, IUGG, vol. 3: 187-196.

RAKÚS, M. and the IGCP National Working Groups, 1988. Stratigraphic sections. *Evolution of the Northern Margin of Tethys: The Results of IGCP Project 198*, vol. II (Rakús, M., Dercourt, J. and Nairn, A.E.M., eds.). Occasional Publications ESRI, New Series, No. 3, Earth Sciences and Resources Institute, University of South Carolina:

RAKÚS, M., M. Mišík, J. Michalík, R. Mock, T. Ďurkovič, T. Koráb, R. Marschalko, J. Mello, M. Polák and J. Jablonský, 1988. Paleogeographic Development of the West Carpathians: Anisian to Oligocene. *Evolution of the Northern Margin of Tethys: The Results of IGCP Project 198*, vol. III (Rakús, M., Dercourt, J. and Nairn, A.E.M., eds.). Occasional Publications ESRI, New Series, No. 3, Earth Sciences and Resources Institute, University of South Carolina: 39-62.

RAMIREZ, R.W., 1985. *The FFT, Fundamentals and Concepts.* Prentice-Hall, Englewood Cliffs, N.J., U.S.A., 178 p.

RATSCHBACHER, L., W. Frisch, H.G. Linzer and O. Merle, 1991. Lateral extrusion in the eastern Alps, Part 2: Structural analysis. *Tectonics*, 10(2): 257-271.

RATSCHBACHER, L., J.H. Behrmann and A. Pahr, 1990. Penninic windows at the eastern end of the Alps and their relation to the intra-Carpathian basins. *Tectonophysics*, 172: 91-105.

RÖGL, F. and C. Müller, 1978. Middle Miocene salinity crisis and paleogeography of the Paratethys (Middle and Eastern Europe). *DSDP* Vol. XLII, part 1: 985-990.

ROYDEN, L.H., 1988. Late Cenozoic Tectonics of the Pannonian Basin System. *The Pannonian Basin: A Study in Basin Evolution*, AAPG Memoir 45 (L.H. Royden and F. Horváth, eds.), The American Association of Petroleum Geologists and The Hungarian Geological Society: 27-48.

ROYDEN, L.H., 1985. The Vienna Basin: a thin-skinned pull-apart basin. *Strike-slip deformation, basin formation and sedimentation*, (Biddle, K.T., ed. et al), Special Publication - Society of Economic Paleontologists and Mineralogists, 37: 319-338.

ROYDEN, L.H. and T. Báldi, 1988. Early Cenozoic Tectonics and Paleogeography of the Pannonian and Surrounding Regions. *The Pannonian Basin: A Study in Basin Evolution*, AAPG Memoir 45 (L.H. Royden and F. Horváth, eds.), The American Association of Petroleum Geologists and The Hungarian Geological Society: 1-16.

ROYDEN, L.H. and B.C. Burchfiel, 1989. Are Systematic Variations in Thrust Belt Style Related to Plate Boundary Processes? (The Western Alps versus the Carpathians). *Tectonics*, 8(1):51-61.

ROYDEN, L.H. and P. Dovenyi, 1988. Variations in Extensional Styles at Depth Across the Pannonian Basin System. *The Pannonian Basin: A Study in Basin Evolution*, AAPG Memoir 45 (L. H. Royden and F. Horváth, eds.), The American Association of Petroleum Geologists and The Hungarian Geological Society: 235-255.

ROYDEN, L.H., F. Horváth and B.C. Burchfiel, 1982. Transform faulting, extension and subduction in the Carpathian Pannonian Region. *Geological Society of America Bulletin*, 93: 717-725.

RUDAKOV, S.G., 1985. Correlation of principal tectonic boundaries in Pre- Alpine evolution of the Carpatians and Eastern Alps. *Geotectonics*, 19(5): 397-403.

SANDULESCU, M., 1988. Cenozoic Tectonic History of the Carpathians. *The Pannonian Basin: A Study in Basin Evolution*, AAPG Memoir 45 (L.H. Royden and F. Horvath, eds.), The American Association of Petroleum Geologists and The Hungarian Geological Society: 17-26.

SCLATER, H.G., L. Royden, F. Horvath, B.C. Burchfield, S. Semken and L. Stegena, 1980. The formation of Intra-Carpathian basins as determined from subsidence data. *Earth Planet. Sci. Lett.*, 51: 139-162.

SHERIFF, R.E. and L.P. Geldart, 1982. *Exploration Seismology volume 1: History, theory and data acquisition*. Cambridge University Press, 253 p.

STANLEY, W.D., 1989. Comparison of geoelectrical/tectonic models for suture zones in the western U.S.A. and eastern Europe: are black shales a possible source of high conductivities? *Phys. Earth and Planet. Int.*, 53: 228-238.

STARPAK PROCESSING MANUAL, 1990. Texaco Corp., 3 vol.

STARPAK REFERENCE MANUAL, 1990. Texaco Corp.

STEININGER, F.F., C. Müller and F. Rögl, 1988. Correlation of Central Paratethys, Eastern Paratethys, and Mediterranean Neogene Stages. *The Pannonian Basin: A Study in Basin Evolution*, AAPG Memoir 45 (L. H. Royden and F. Horvath, eds.), The American Association of Petroleum Geologists and The Hungarian Geological Society: 79-88.

SUK, M., 1987. Some results of geophysical and drilling investigations into upper lithosphere in Czechoslovakia. *Observation of the continental crust through drilling II*, Proceedings of the international symposium, Springer-Verlag, Berlin, FRG: 77-80.

TOLLMANN, A., 1988. Eastern Alpine Sector, Northern margin of Tethys. *Evolution of the northern margin of Tethys: The Results of IGCP Project 198*, Volume II. (Rakús, M., Dercourt, J. and Nairn, A.E.M., eds.). Occasional Publications ESRI, New Series, No. 3, Earth Sciences and Resources Institute, University of South Carolina: 25-46.

TOMEK, Č., 1988. Geophysical investigation of the Alpine-Carpathian Arc. *Evolution of the northern margin of Tethys: The Results of IGCP Project 198*, Volume I. (Rakús, M., Dercourt, J. and Nairn, A.E.M., eds.). Occasional Publications ESRI, New Series, No. 3, Earth Sciences and Resources Institute, University of South Carolina: 167-199.

TOMEK, Č., L. Dvoraková, I. Ibrmajer, R. Jiřiček and T. Koráb, 1987. Crustal profiles of active continental collisional belt: Czechoslovak deep seismic reflection profiling in the West Carpathians. *Geophys. J. R. astr. Soc.*, 89: 383-388.

TOMEK, Č. and A. Thon, 1988. Interpretation of Seismic Reflection Profiles from the Vienna Basin, the Danube Basin, and the Transcarpathian Depression in Czechoslovakia, *The Pannonian Basin: A Study in Basin Evolution*, AAPG Memoir 45 (L.H. Royden and F. Horvath,eds.), The American Association of Petroleum Geologists and The Hungarian Geological Society: 171-182.

TRÜMPY, R., 1988. A possible Jurassic-Cretaceous transform system in the Alps and the Carpathians. *Processes in Continental lithospheric deformation* (Clark, S.P., ed et al.), Geological Society of America Special Paper 218. Boulder, Colorado: 93-107.

VASS. D., Z. Stranik and I. Krystek, 1987. Tectonomagmatic Activity in the Western Carpathians (Czechoslovak Part) from Pyrenean to Rhodanian Epochs. *Global Correlation of Tectonic Movements* (Leonov, Yu.G. and Khain, V.E.) IGCP project no 107. John Wiley & Sons Ltd.: 159-171.

WERNICKE, B., 1985. Uniform-sence normal simple shear of the continental lithosphere, *Can. J. Earth Sci.*, 22: 108-125.

WESSELY, G., 1988. Structure and Development of the Vienna Basin in Austria, *The Pannonian Basin: A Study in Basin Evolution*, AAPG Memoir 45 (edited by Leigh H. Royden and Ferenc Horvath), The American Association of Petroleum Geologists and The Hungarian Geological Society: 333-346.

YILMAZ, O., 1988. *Seismic Data Processing*. Society of Exploration Geophysicists, Tulsa Oklahoma, 526 p.

APPENDIX A: BOREHOLE DATA

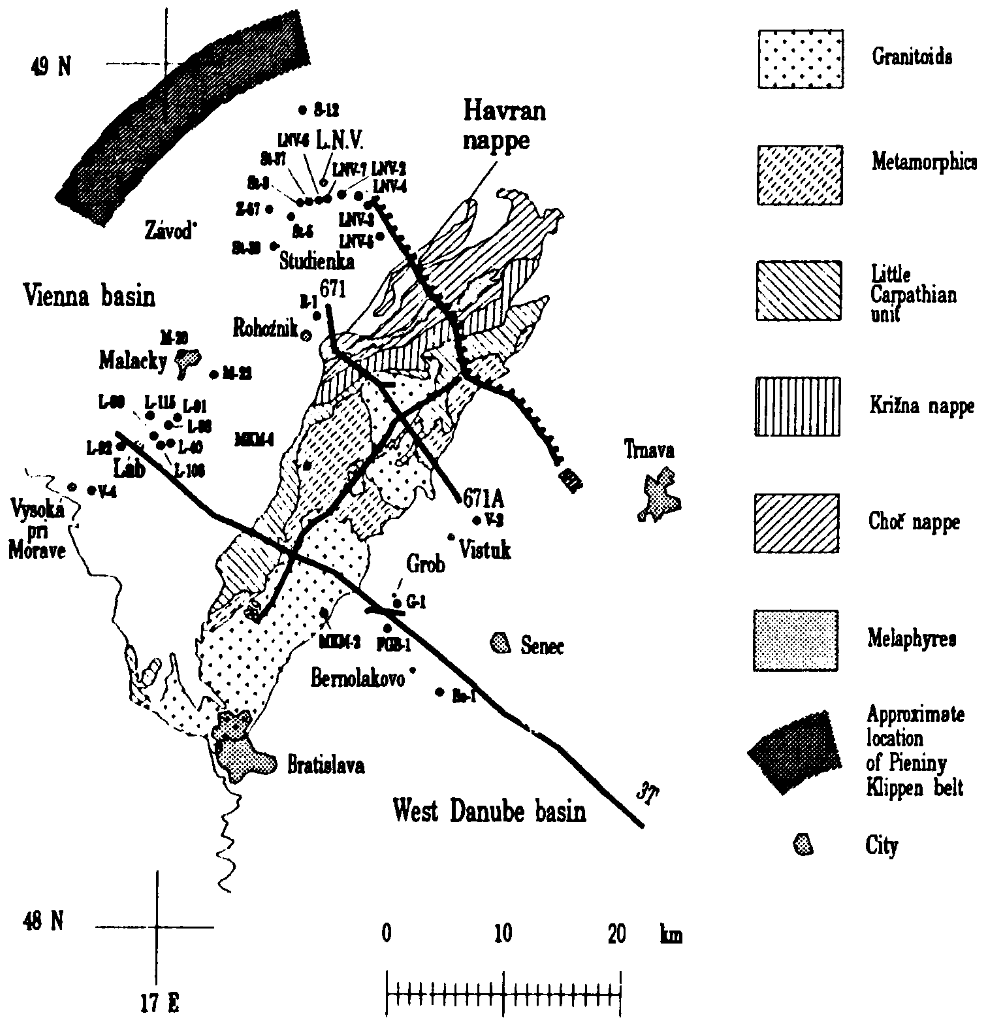

Fig. A.1: Borehole location map with limit of nappe distribution in the Little Carpathians (modified from Hrouda, 1986; Jiříček and Tomek, 1981; Tomek, 1991, personal communication). The Granitoids and Little Carpathians group form the Envelope nappe.

A.1 VIENNA BASIN

Table A.1: Borehole data for the Vienna Basin					
Nearest Town	Borehole	Unit	Depth of top (m)	Depth drilled (m)	Unit
Vysoké pri Morave	V-4	T_3	2886	3085	T_3
Láb	L-40	T	2300	2601	T
	L-90	T	2218	2673	T
	L-91	T	2730	3000	T
	L-92	T	2810	2908	T
	L-93	T_3	2345	2650	T
	L-106	T	2145	2300	T
	L-115	T_3	2555	4204	T
Malacky	M-20	T_3	3177	3500	T_3
	M-22	T	2633	3000	T
Studienka	St-3	Pg	1693	1760	K_1
	St-5	T_3(?)	2333	2593	K_1
	St-37	K_1	1677	1948	K_1
	St-39	Pg(?)	3260	3365	Pg(?)
Závod	Z-57	Pg	3165	4023	K_1

Table A.1: Borehole data for the Vienna Basin					
Nearest Town	Borehole	Unit	Depth of top (m)	Depth drilled (m)	Unit
Lakšárská nová Ves	LNV-2	Neogene	1277	1360	T
	LNV-3	T_2	799	1683	Pg
	LNV-4	T	1115	2002	T
	LNV-5	Pg	935	1008	T_3
	LNV-6	Neogene	1545	1800	K_3

(Tomek, 1991 - personal communication)

Table A.1: Borehole data for the Vienna Basin			
Nearest Town	Borehole	Unit	Depth to bottom (m)
Šaštin	Š-12	Neogene	2195
		Triassic (depth drilled)	6502
Lakšárská nová Ves	LNV-7	Neogene	1564
		Senonian Brezová Furrow	1857
		Triassic (depth drilled)	6405

(Jiříček and Tomek, 1981)

Table A.1: Borehole data for the Vienna basin				
Nearest town	Borehole	Unit	Age (Ma)	Depth (m)
Rohožník	R-1	Pannonian	11.5-8.5	0-1150
		Sarmatian	13.6-11.5	1150-1510
		Upper Badenian	15.5-13.6	1510-1860
		Lower Badenian	16.5-15.5	1860-1963
		Karpatian	17.2-16.5	1963-2700
		Eggenburgian	23-19	2700-2780
		Upper Triassic (Northern Limestone Alps)	229-204	2780-2900

(Tomek, 1992, personal communication)

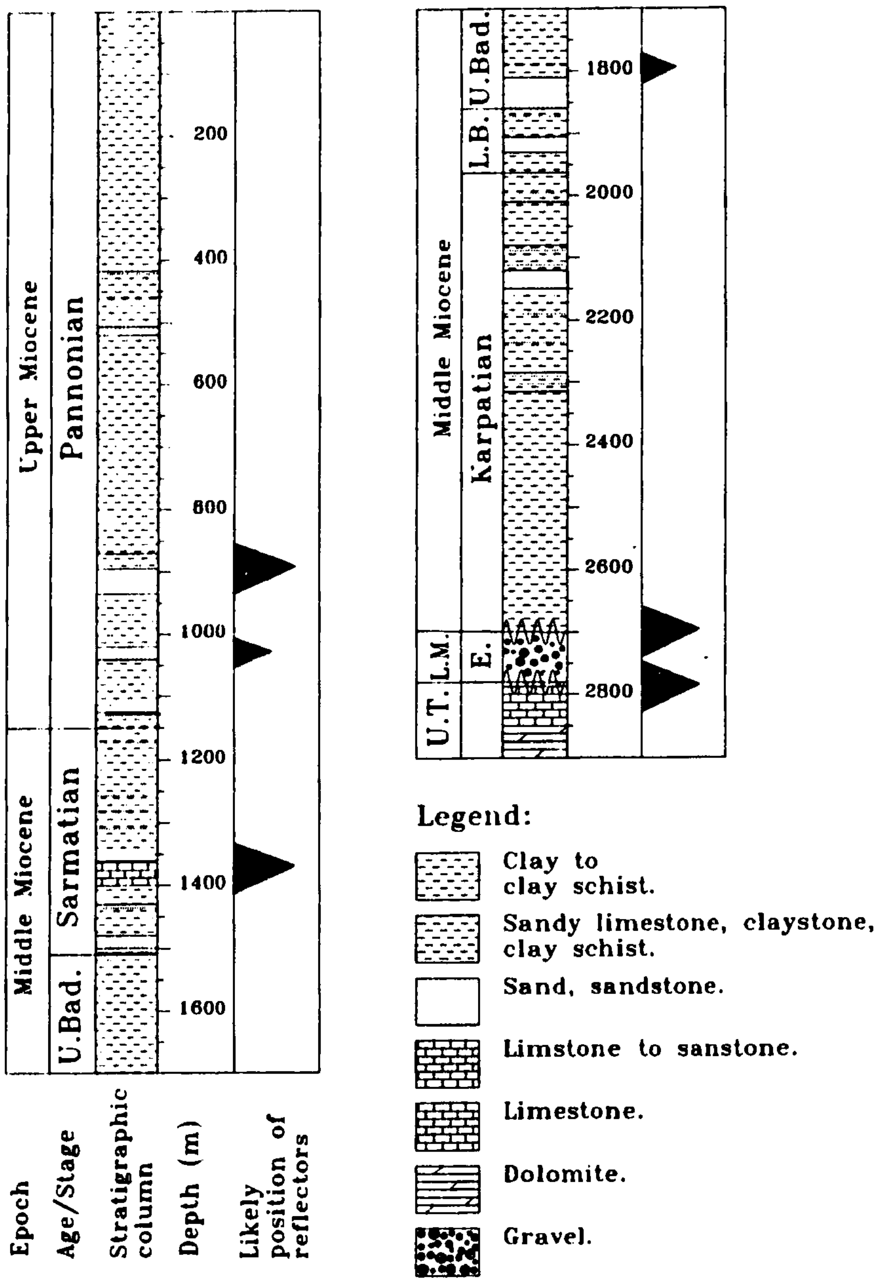

Fig. A.2: Borehole data for borehole Rohožník-I in the Vienna basin. Tomek, 1992, personal communication. The wiggle indicates a break in sedimentation.

A.2 LITTLE CARPATHIANS

Table A.2: Borehole data for the Little Carpathians			
Nearest Town	Borehole	Depth interval (m)	Units
Jur pri Bratislave	MKM-2	0-604	Crystalline Basement
Pernek	MKM-6	0-218	Devonian phyllite
		218-300	Mesozoic
		300-650	Late Paleozoic with tuff and phyllite

(Tomek, 1991, personnal communication)

A.3 DANUBE BASIN

Table A.3: Borehole data for the West Danube basin

Nearest town	Borehole	Unit	Depth to top (m)	Depth Drilled (m)	Unit
Grob	G-1	Paleozoic basement	1283	1336	Paleozoic basement
Bernolákovo	Be-1	Crystalline	1792	1797	Gneiss
Chorvátský Grob	FGB-1	Paleozoic	1197	1231	Paleozoic

(Tomek, 1991, personnal communication)

Table A.3: Borehole data for the Vienna basin

Nearest town	Borehole	Unit	Age (Ma)	Depth (m)
Vistük	V-2	Dacian	5.6-4	0- 208
		Pontian	8.5-5.6	208-380?
		Pannonian	11.5-8.5	380?-550
		Sarmatian	13.6-11.5	550-947?
		Upper Badenian	15.5-13.6	947?-1617
		Lower Badenian	16.5-15.5	1617?-2273
		Crystalline basement	Proterozoic-Paleozoic	2273-2335

(Tomek, 1992, personal communication)

Table A.3: Borehole data for the West Danube basin			
Nearest town	Borehole	Unit	Depth to base (m)
Grob	G-1	Pontian	240
		Pannonian	480
		Sarmatian	708
		Badenian	1283
		Miocene Depth drilled	1336
Senec	S-1	Dacian	500
		Pontian	784
		Pannonian	1238
		Sarmatian	1875
		Badenian	2540
		Miocene Depth drilled	2579

(Tomek and Thon, 1988)

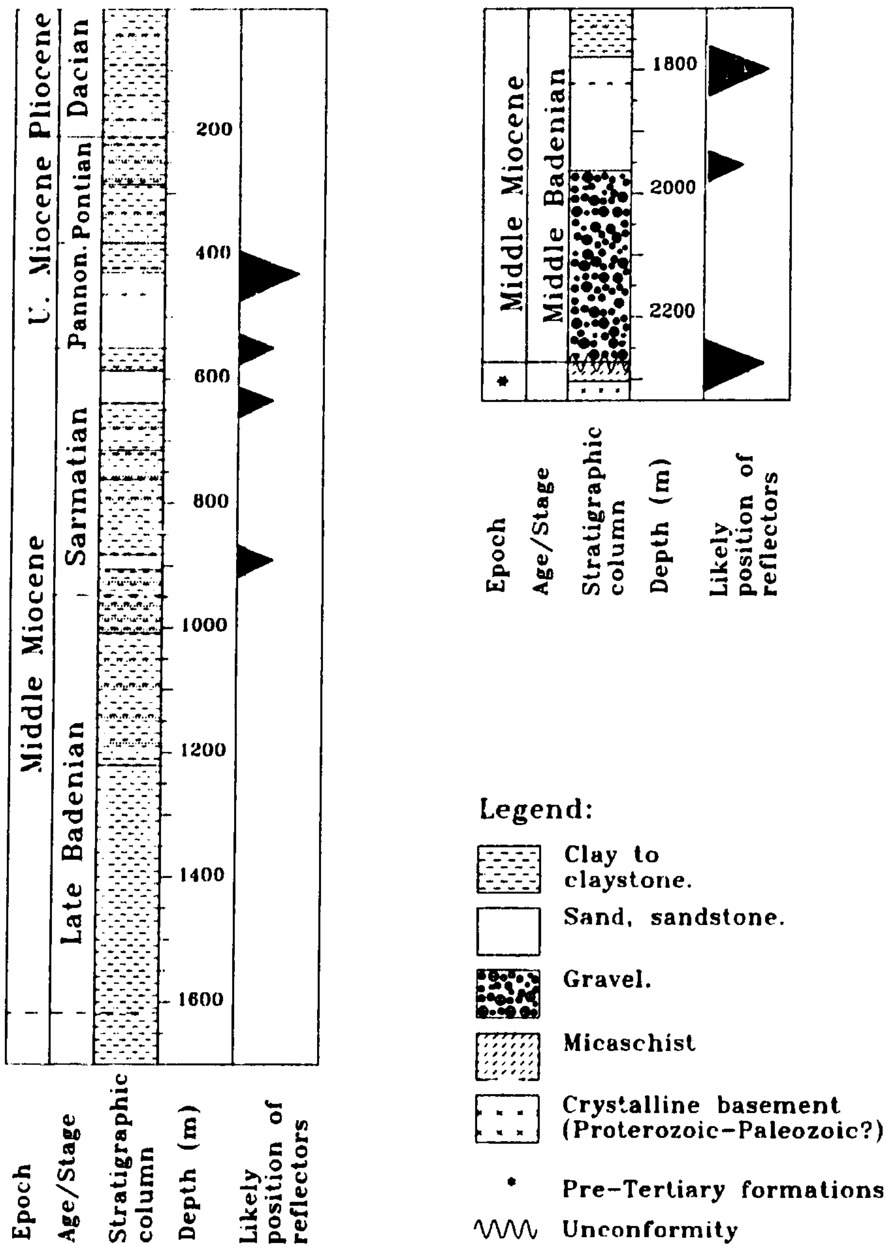

Fig. A.3: Borehole data for borehole Vistük-2 in the West Danube basin. Tomek, 1992, personal communication. The wiggle indicates a break in sedimentation.

APPENDIX B: TECTONOSTRATIGRAPHIC CHARTS

Charts in this appendix show tectonic and stratigraphic events in units that were used to reconstruct the history of the northwestern Carpathian-Pannonian area, on both European and African/Apulian margins. There is much more documentation available on the European margin than on the African/Apulian margin. It is thus useful to compare them to get a broader understanding of the tectonic history of the area. The time scale is from Ménager (1989). In the Palaeogene and the Neogene charts, local stages (Nagymarosy, 1981; Steininger et al., 1988) were also used to be consistent with publications referred to.

Blocks and units are laid out from the northwest to the southeast, from the European margin to the African margin. Letters in stratigraphic columns refer to legend of plate 1.

The synthese from publications listed below was modified to take into account the more mobilistic model now favored (Hamilton, 1990; Tomek, 1992, personal communication). Parenthesed numbers correspond to the following references: 1) Adam, 1980; 2) Andrusov and Fusán, 1968; 3) Artyushkov and Baer, 1986; 4) Balla, 1988; 5) Beer, 1983; 6) Beránek and Zátopek, 1981b; 7) Bergerat, 1989; 8) Biely, 1988; 9) Bližkovský et al., 1986; 10) Burchart et al., 1987; 11) Burchfiel and Royden, 1982; 12) Bystrický, 1968; 13) Čermák, 1981; 14) Cerv, 1984; 15)

Chaloupsky, 1989; 16) Debalmas and Sandulescu, 1987; 17) Dvořaková, 1987; 18) Fodor et al., 1988; 19) Földvary, 1988; 20) Fusán et al., 1979; 21) Gutdeutsh and Aric, 1988; 22) Horvath, 1984; 23) Hovorka et al., 1982; 24) Hovorka and Spišiak, 1988; 25) Hrouda, 1986; 26) Jiříček and Tomek, 1981; 27) Kokai and Pogacsás, 1991; 28) Kováč et al., 1989; 29) Kováč et al., 1986 30) Krs, 1981; 31) Krs et al., 1979; 32) Kvitkovič and Plančar, 1979; 33) Mahel' et al., 1972; 34) Mahel' et al., 1961; 35) Michalík, 1988; 36) Michalík and Soták, 1990; 37) Mišík and Marshalko, 1988; 38) Nemčok et al., 1989; 39) Nikolaev et al., 1989; 40) Rakús and the IGCP National Working Groups, 1988; 41) Rakús et al., 1988; 42) Ratschbacher et al., 1989; 43) Ratschbacher et al., 1991; 44) Royden, 1988; 45) Royden, 1985; 46) Royden and Baldí, 1988; 47) Royden and Burchfiel, 1989; 48) Royden and Dövenyi, 1988; 49) Rudakov, 1985; 50) Sclater et al., 1980; 51) Stanley, 1989; 52) Tomek, 1988; 53) Tomek et al., 1987; 54) Tomek et al., 1987; 55) Tomek and Thon, 1988; 56) Trümpy, 1988; 57) Vass et al., 1987; 58) Wessely, 1988.

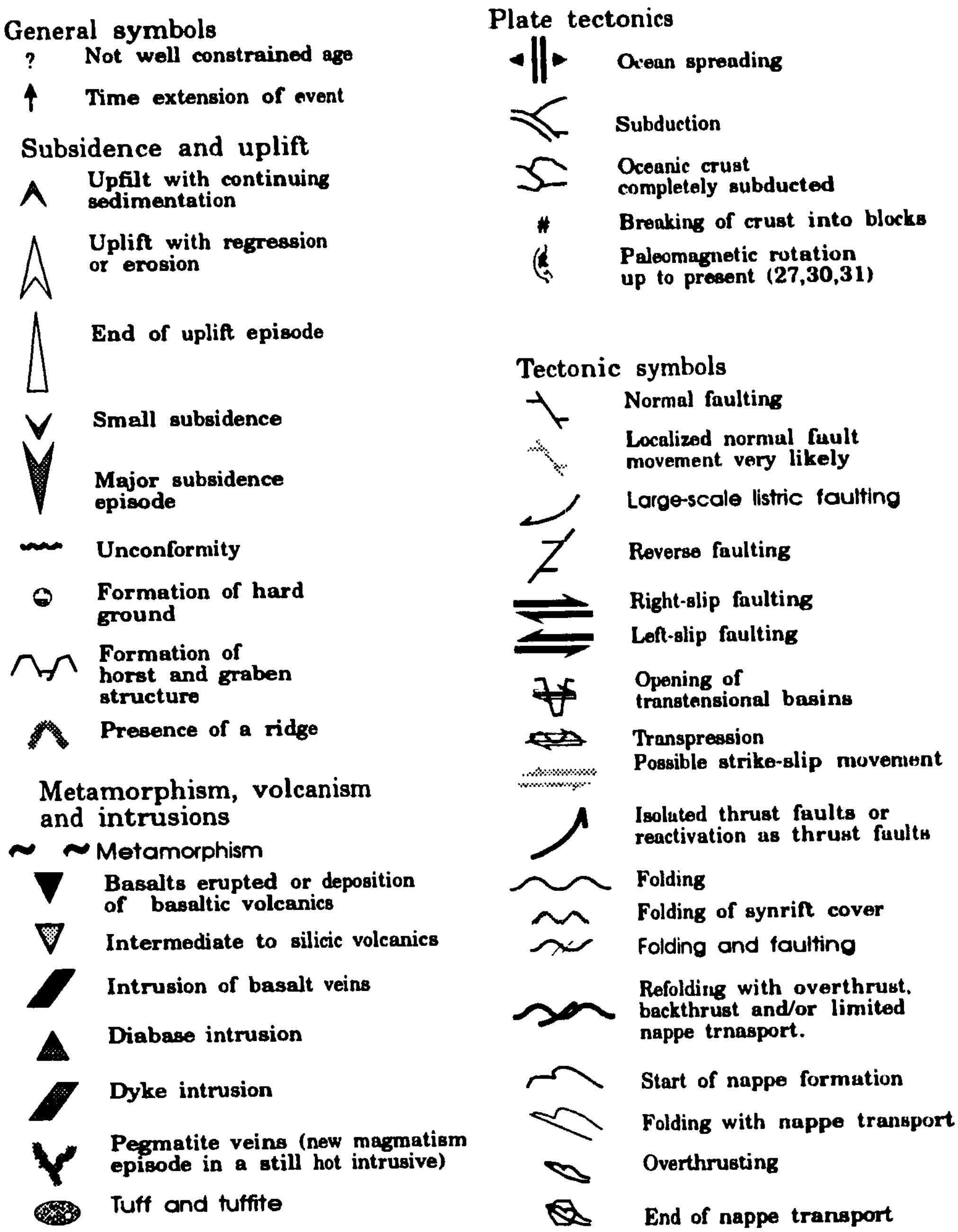

Fig. B.1: List of symbols used in appendix B.

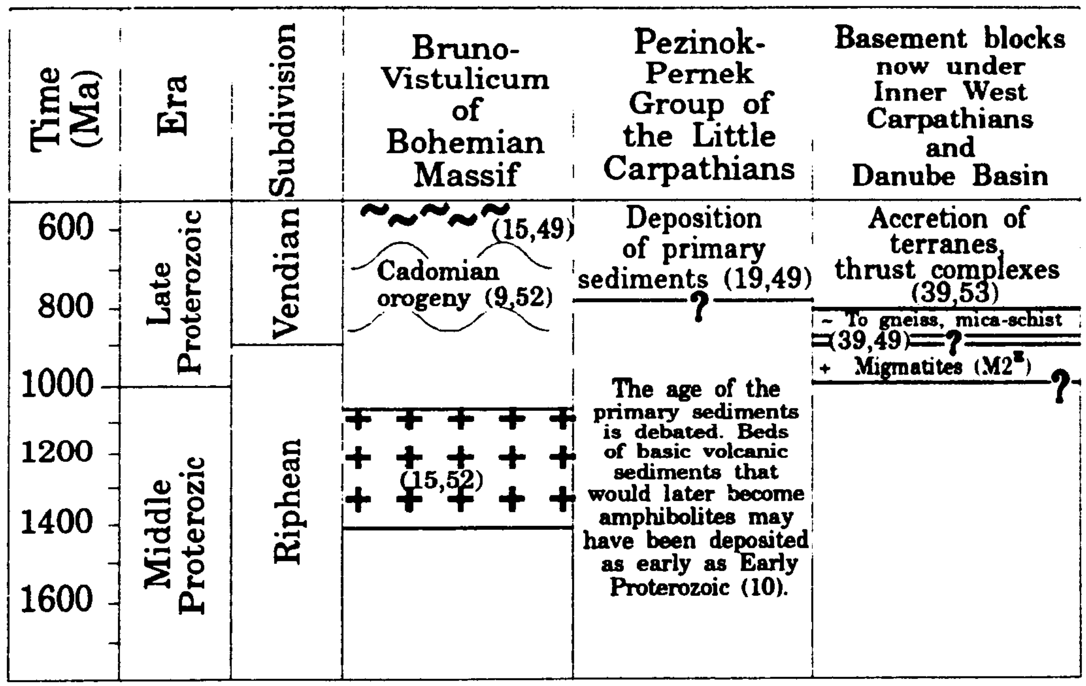

Fig. B.2: Precambrian events of Northwestern Carpathian-Pannonian area. + = plutonism.

Legend:

Formation of deep granitoid intrusives of Bratislava and Modra massives in the Little Carpathians (302 + 40 Ma) and similar massives in other ranges of the Inner West Carpathians (10). Pegmatite veins, at end of Permian? (34).

Shallow water deposits (3,5).

Arkosic conglomerate (33).

Tm: sandstone, shale and arkose (19,25,33,34).

β'T: Diabases, melaphyres, quartz porphyries (19,25,33,34,49).

Fig. B.3: Paleozoic events of Northwestern Carpathian-Pannonian area.

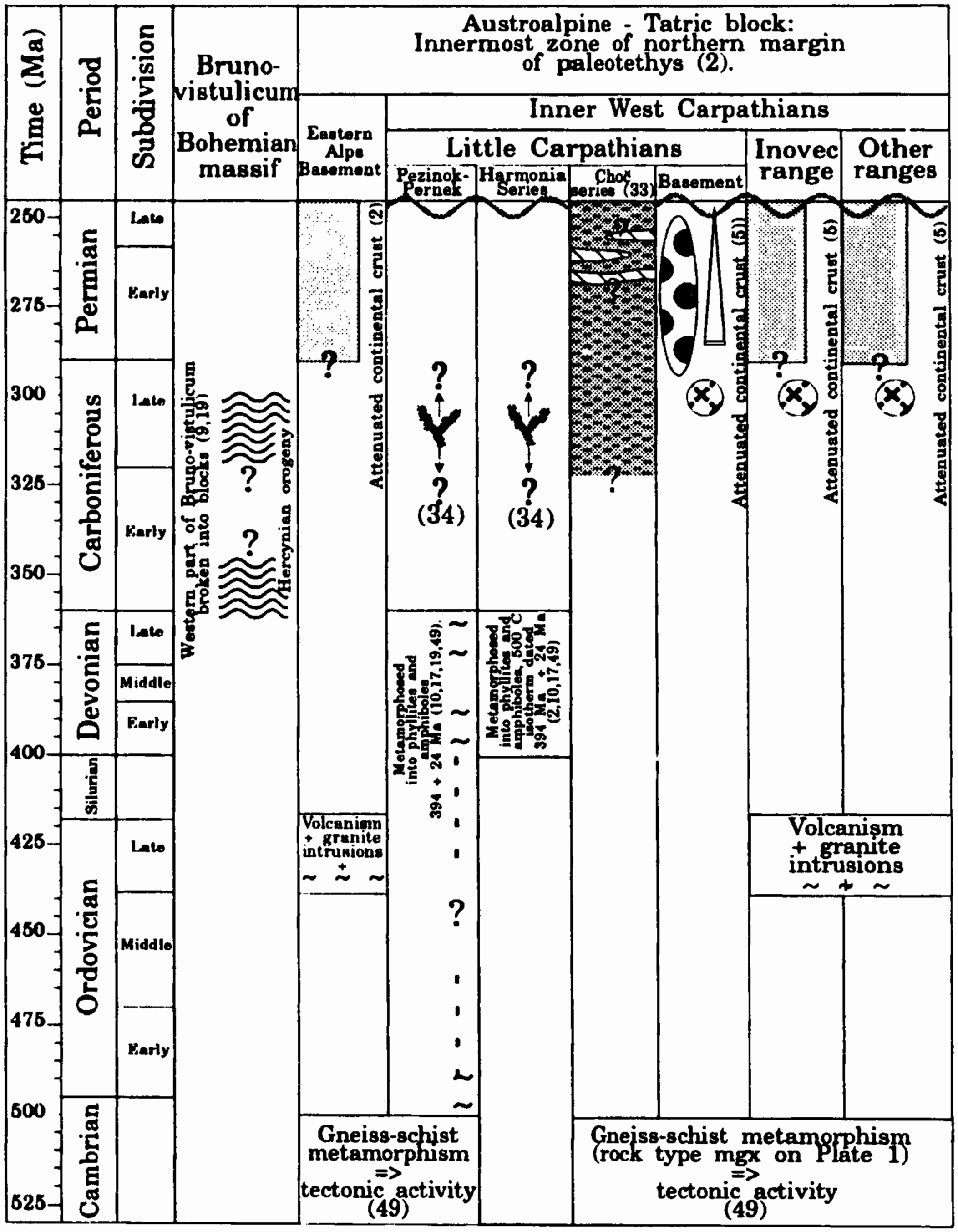
Time (Ma)
Period
Subdivision
Bruno-vistulicum of Bohemian massif
Austroalpine - Tatric block: Innermost zone of northern margin of paleotethys (2).
Eastern Alps Basement
Inner West Carpathians
Little Carpathians
Inovec range
Other ranges
Pezinok-Pernek
Harmonia Series
Choč series (33)
Basement
250
275
300
325
350
375
400
425
450
475
500
525
Permian
Carboniferous
Devonian
Silurian
Ordovician
Cambrian
Late
Early
Late
Early
Late
Middle
Early
Late
Middle
Early
Western part of Bruno-vistulicum broken into blocks (9,19)
Hercynian orogeny
Attenuated continental crust (2)
Attenuated continental crust (5))
Attenuated continental crust (5)
Attenuated continental crust (5)
(34)
(34)
Metamorphosed into phyllites and amphiboles 394 + 24 Ma (10,17,19,49).
Metamorphosed into phyllites and amphiboles, 500 C isotherm dated 394 Ma + 24 Ma (2,10,17,49)
Volcanism + granite intrusions
Volcanism + granite intrusions
Gneiss-schist metamorphism => tectonic activity (49)
Gneiss-schist metamorphism (rock type mgx on Plate 1) => tectonic activity (49)

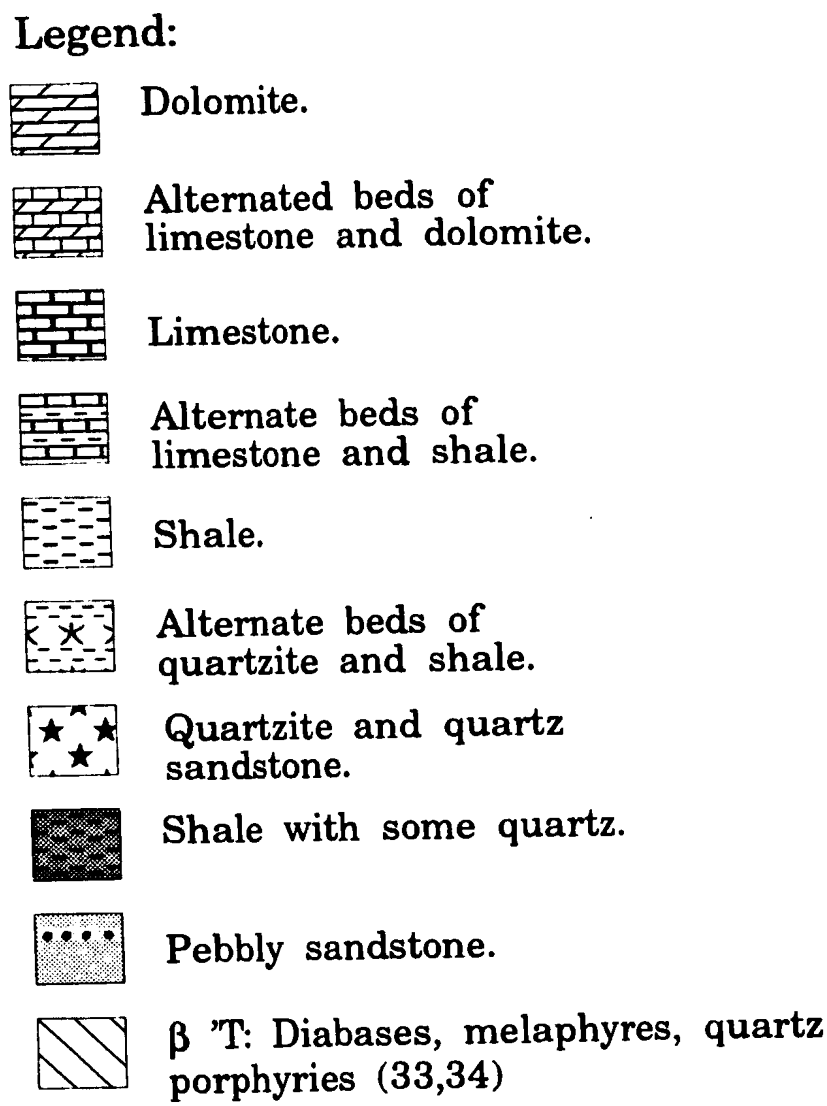

Fig. B.4: Triassic events of Northwestern Carpathian-Pannonian area.

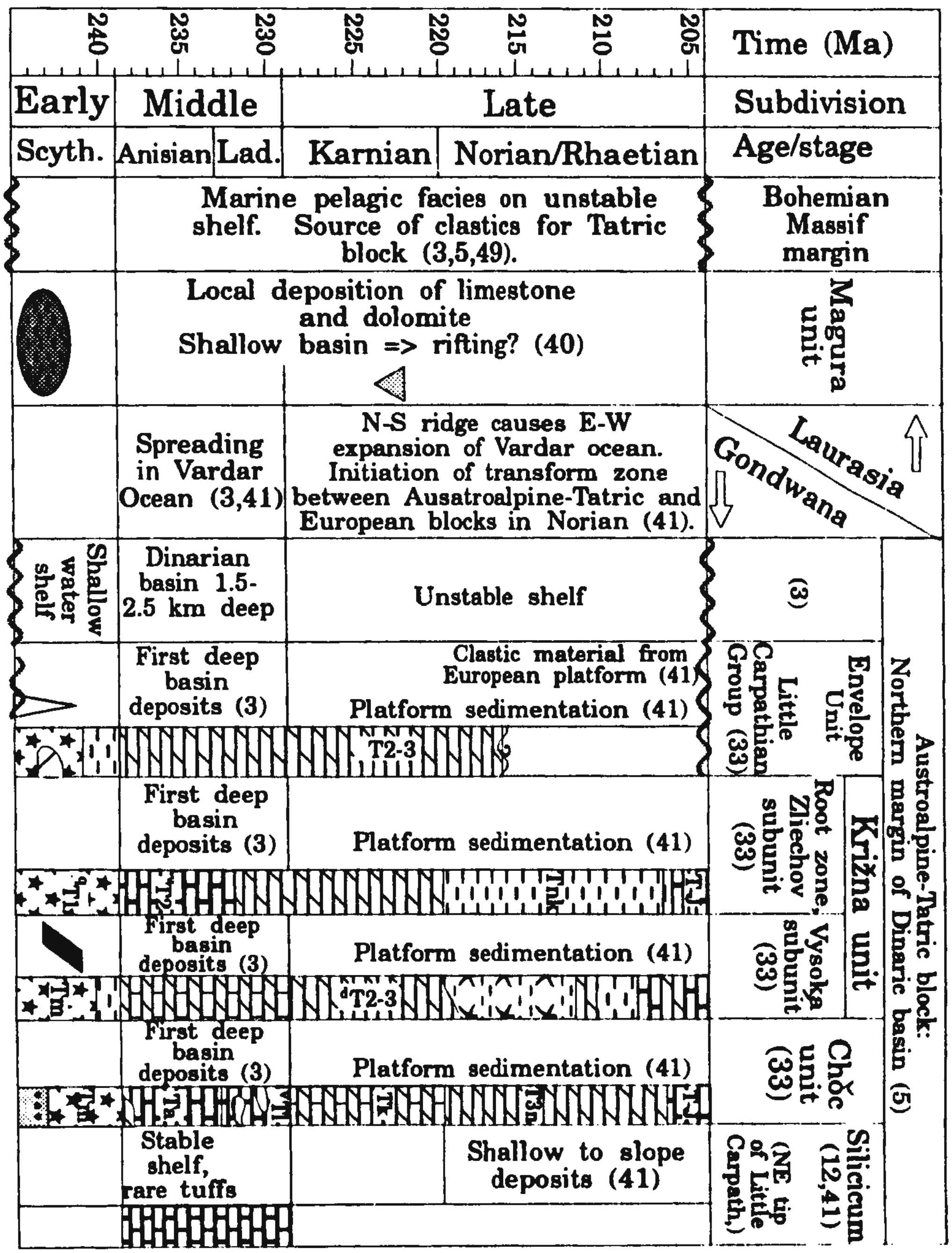

Time (Ma)
240
235
230
225
220
215
210
205
Subdivision
Early
Middle
Late
Age/stage
Scyth.
Anisian
Lad.
Karnian
Norian/Rhaetian
Bohemian Massif margin
Marine pelagic facies on unstable shelf. Source of clastics for Tatric block (3,5,49).
Magura unit
Local deposition of limestone and dolomite
Shallow basin => rifting? (40)
Laurasia
Gondwana
Spreading in Vardar Ocean (3,41)
N-S ridge causes E-W expansion of Vardar ocean. Initiation of transform zone between Ausatroalpine-Tatric and European blocks in Norian (41).
Austroalpine-Tatric block: Northern margin of Dinaric basin (5)
(3)
Shallow water shelf
Dinarian basin 1.5-2.5 km deep
Unstable shelf
Envelope Unit
Little Carpathian Group (33)
First deep basin deposits (3)
Clastic material from European platform (41)
Platform sedimentation (41)
T2-3
Križna unit
Root zone, Zliechov subunit (33)
First deep basin deposits (3)
Platform sedimentation (41)
T1s
T2
Tnk
TJ
Vysoka subunit (33)
First deep basin deposits (3)
Platform sedimentation (41)
Tm
T2-3
Choč unit (33)
First deep basin deposits (3)
Platform sedimentation (41)
Tm
Ta
Tl
Tk
T3n
TJ
Silicicum (12,41) (NE tip of Little Carpath.)
Stable shelf, rare tuffs
Shallow to slope deposits (41)

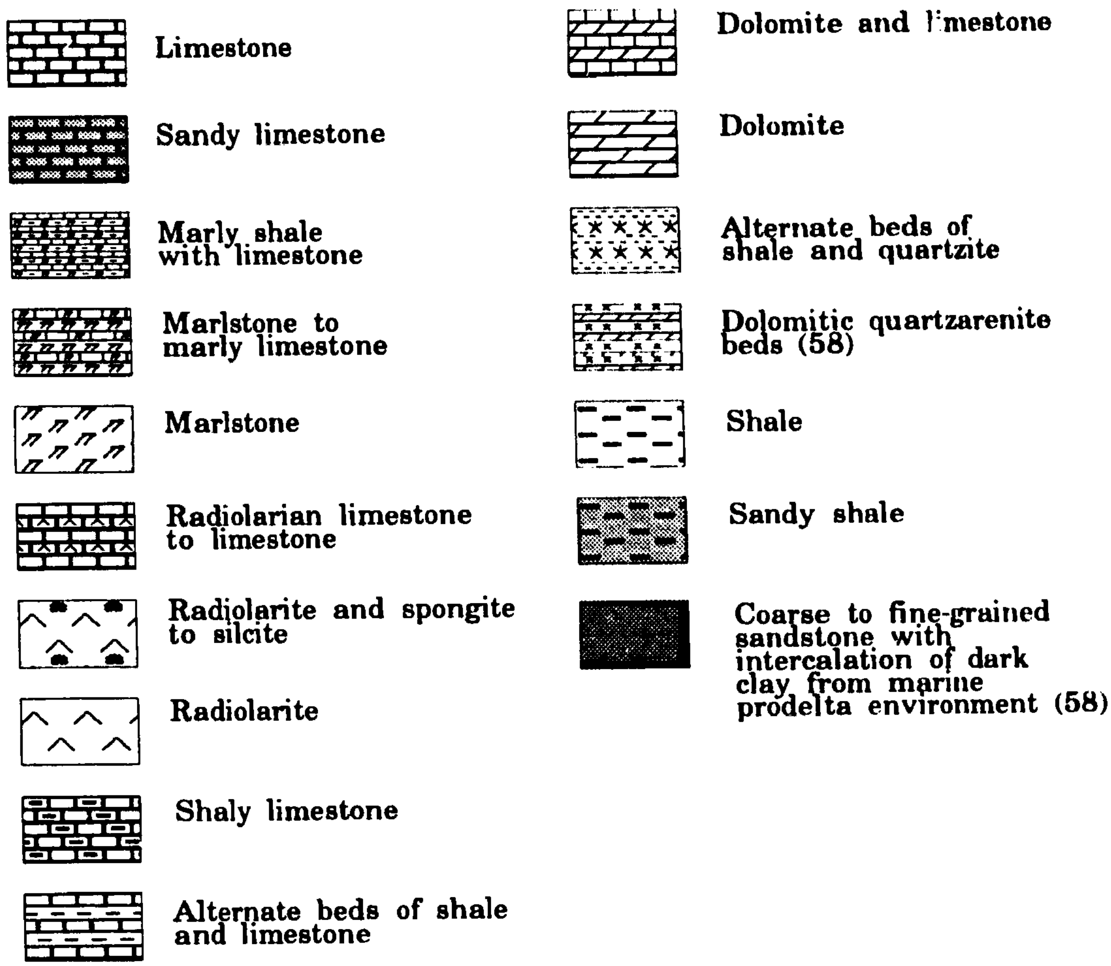

Fig. B.5: Jurassic events of the northwestern Carpathian-Pannonian area.

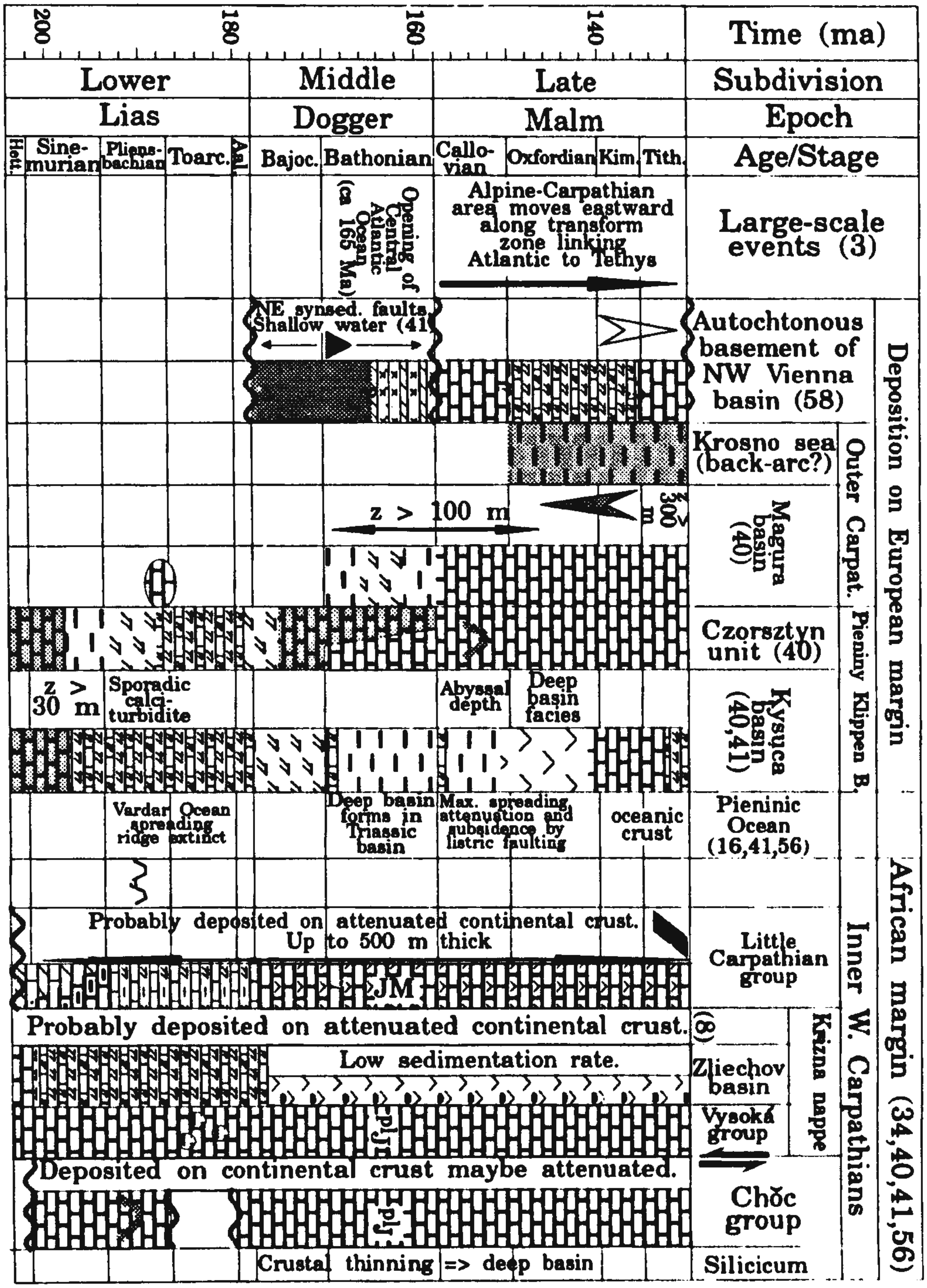

Time (ma)
200
180
160
140
Subdivision
Lower
Middle
Late
Epoch
Lias
Dogger
Malm
Age/Stage
Hett.
Sine-murian
Pliens-bachian
Toarc.
Aal.
Bajoc.
Bathonian
Callo-vian
Oxfordian
Kim.
Tith.
Large-scale events (3)
Opening of Central Atlantic Ocean (ca 165 Ma)
Alpine-Carpathian area moves eastward along transform zone linking Atlantic to Tethys
Autochtonous basement of NW Vienna basin (58)
NE synsed. faults. Shallow water (41)
Krosno sea (back-arc?)
Magura basin (40)
z > 100 m
300 m
Czorsztyn unit (40)
Kysuca basin (40,41)
z > 30 m
Sporadic calci-turbidite
Abyssal depth
Deep basin facies
Pieninic Ocean (16,41,56)
Vardar Ocean spreading ridge extinct
Deep basin forms in Triassic basin
Max. spreading, attenuation and subsidence by listric faulting
oceanic crust
Little Carpathian group
Probably deposited on attenuated continental crust. Up to 500 m thick
JM
Probably deposited on attenuated continental crust.
(8)
Zliechov basin
Low sedimentation rate.
Vysoká group
Krizna nappe
Deposited on continental crust maybe attenuated.
Chŏc group
Silicicum
Crustal thinning => deep basin
Outer Carpat.
Pieniny Klippen B.
Inner W. Carpathians
Deposition on European margin
African margin (34,40,41,56)

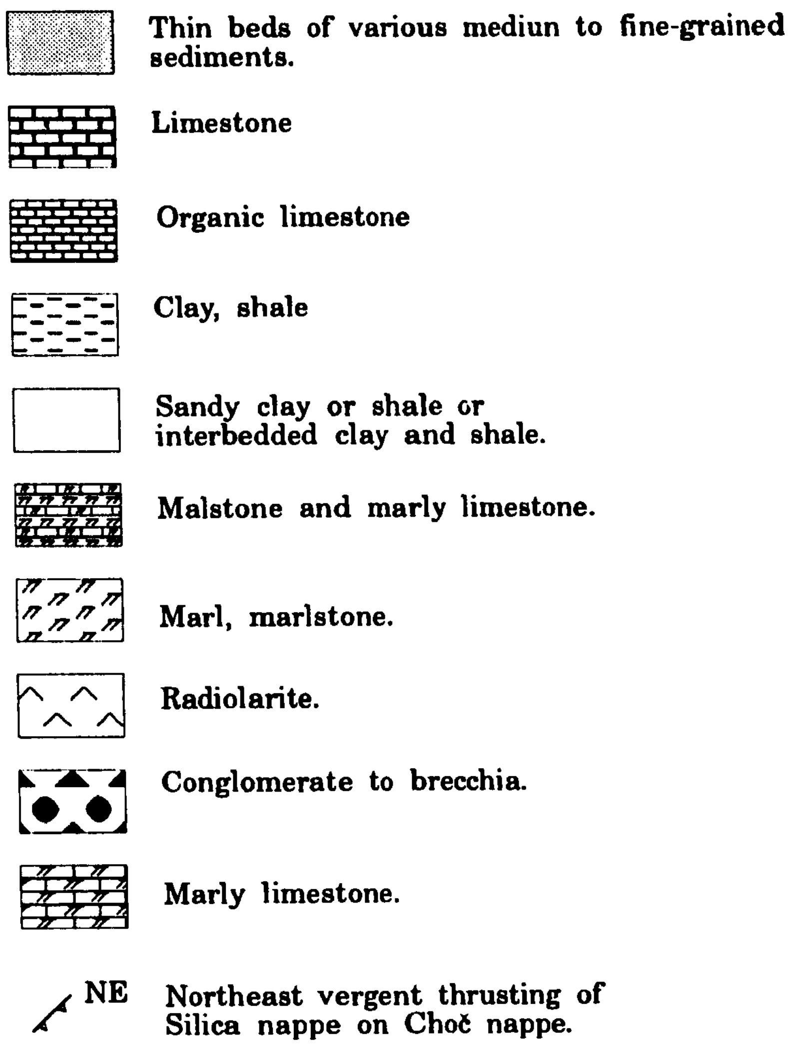

Fig. B.6: Early Cretaceous events of the Northwestern Carpathian-Pannonian area.

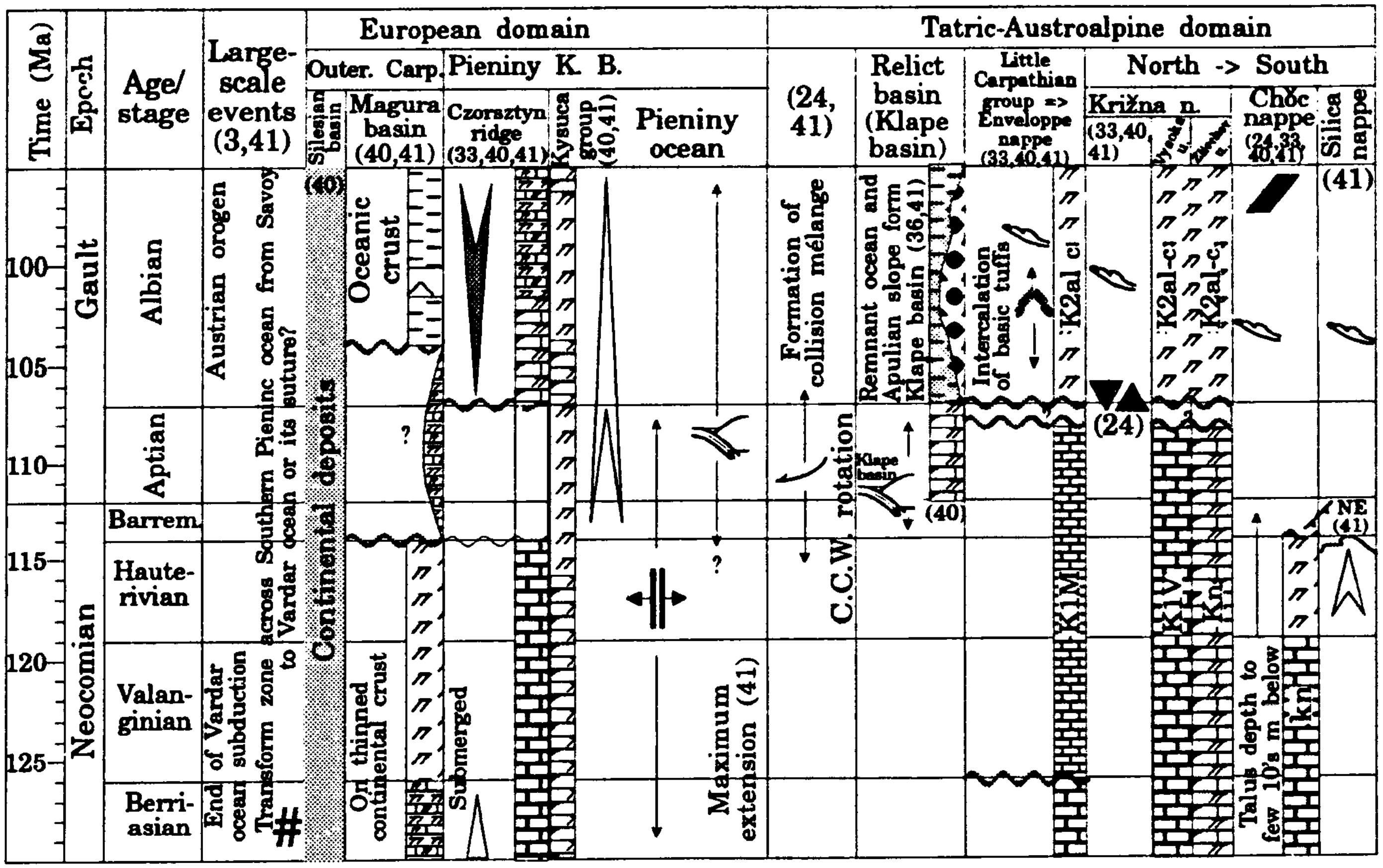
Time (Ma)
Epoch
Age/ stage
Large-scale events (3,41)
European domain
Outer. Carp.
Pieniny K. B.
Silesian basin
Magura basin (40,41)
Czorsztyn ridge (33,40,41)
Kysuca group (40,41)
Pieniny ocean
Tatric-Austroalpine domain
(24, 41)
Relict basin (Klape basin)
Little Carpathian group => Enveloppe nappe (33,40,41)
North -> South
Križna n. (33,40, 41)
Choc nappe (24,33, 40,41)
Silica nappe
100
105
110
115
120
125
Gault
Neocomian
Albian
Aptian
Barrem.
Haute-rivian
Valan-ginian
Berri-asian
Austrian orogen
Southern Pieninc ocean from Savoy across Transform zone to Vardar ocean or its suture?
End of Vardar ocean subduction
(40)
Continental deposits
Oceanic crust
On thinned continental crust
Submerged
Maximum extension (41)
Formation of collision mélange
C.C.W. rotation
Remnant ocean and Apulian slope form Klape basin (36,41)
Klape basin
(40)
Intercalation of basic tufts
K2al-c1
K1M
(24)
K2al-c1
K1V
Kn
Talus depth to few 10's m. below
Kn
(41)
NE (41)

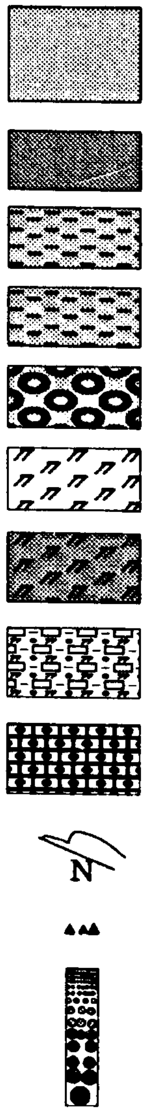

Flysh sediments: syntectonic sediments produced by the erosion of uplifting fold structures. The grain size varies in time and space from conglomerate to clay.

Sandstone.

Shale and clay.

Sandy clay or interbedded clay and sandstone.

Conglomerate and gravel

Marl, marlstone

Sandy marlstone.

Calcareous sanstone to calcareous-argileous shale, conglomerate to shale (33).

Pebbly limestone

North-vergent thrusting

Breccia

Conglomerate to sandstone.
Retrograding source.

Fig. B.7: Late Cretaceous events of the Northwestern Carpathian-Pannonian area.

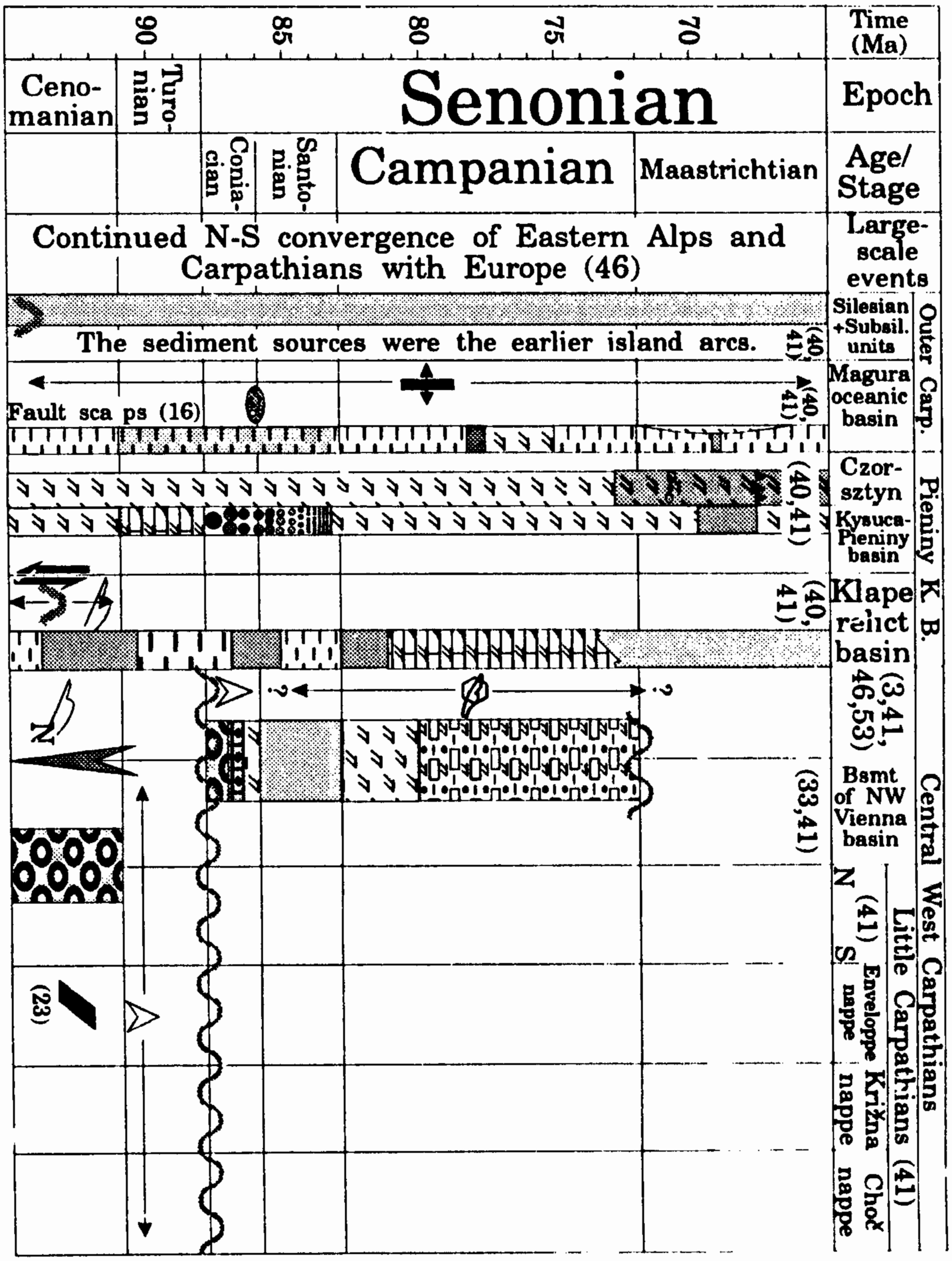
Time (Ma)
90
85
80
75
70
Epoch
Ceno-manian
Turo-nian
Senonian
Age/ Stage
Conia-cian
Santo-nian
Campanian
Maastrichtian
Large-scale events
Continued N-S convergence of Eastern Alps and Carpathians with Europe (46)
Silesian +Subsil. units
Outer Carp.
The sediment sources were the earlier island arcs.
(40, 41)
Magura oceanic basin
Fault scarps (16)
(40, 41)
Czor-sztyn
Kysuca-Pieniny basin
Pieniny
(40,41)
Klape relict basin
K. B.
(40, 41)
(3,41, 46,53)
?
?
N
Bsmt of NW Vienna basin
(33,41)
Central West Carpathians
Little Carpathians (41)
N
S
(41)
Envelope nappe
Križna nappe
Choč nappe
(23)

Geologic units:

Variegated fine-grained sediments

Sand and sandstone.

Conglomerate and gravel.

Argileous limestone.

Conglomerate, breccia to pebbly limestone.

Marl, marlstone.

Clay, shale, schist.

Sandy clay or interbedded clay and sand.

Limestone.

Abbreviations:

P.A.L.: Initiation of Peri-Adriatic lineament in Southern Alps, From then on, the collision of Africa against Europe does not cause direct compression in the Carpathians (5).

S.E.A.: Shortening n Eastern Alps because of counter-clockwise rotation of Apulia block (42,43).

T.E.: NNE tectonic escape of crustal blocks form between the Eastern Alps and Southern Alps to the Pannonian basin (42,43).

Fig. B.8: Palaeogene events of the Northwestern Carpathian-Pannonian area.

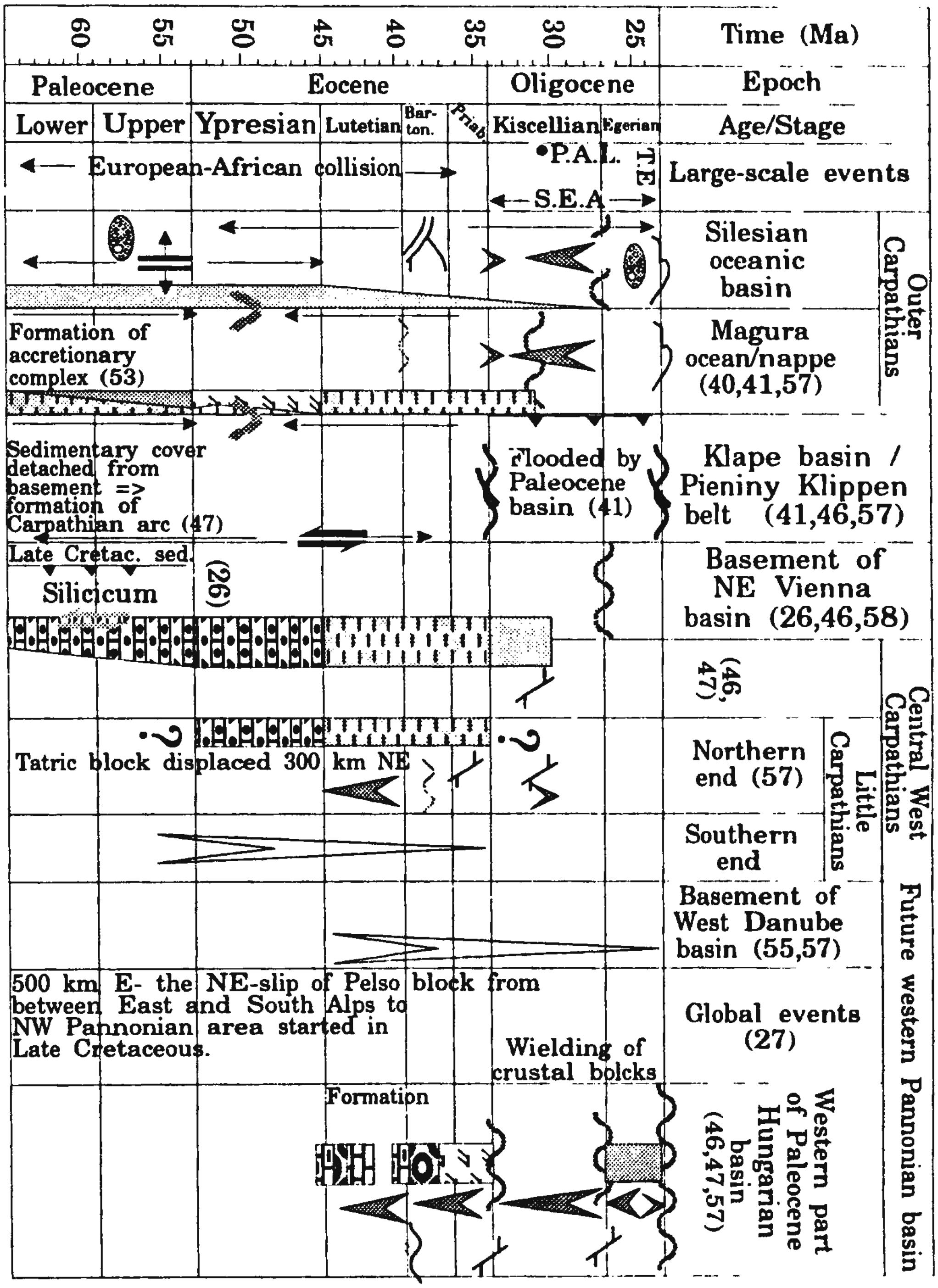
Time (Ma)
60
55
50
45
40
35
30
25
Epoch
Paleocene
Eocene
Oligocene
Age/Stage
Lower
Upper
Ypresian
Lutetian
Bar-ton.
Priab.
Kiscellian
Egerian
Large-scale events
European-African collision
•P.A.L.
T.E
S.E.A
Silesian oceanic basin
Outer Carpathians
Magura ocean/nappe (40,41,57)
Formation of accretionary complex (53)
Klape basin / Pieniny Klippen belt (41,46,57)
Sedimentary cover detached from basement => formation of Carpathian arc (47)
Flooded by Paleocene basin (41)
Basement of NE Vienna basin (26,46,58)
Late Cretac. sed.
Silicicum
(26)
(46, 47)
Central West Carpathians
Little Carpathians
Northern end (57)
Tatric block displaced 300 km NE
Southern end
Basement of West Danube basin (55,57)
Future western Pannonian basin
Global events (27)
500 km E- the NE-slip of Pelso block from between East and South Alps to NW Pannonian area started in Late Cretaceous.
Wielding of crustal bolcks
Western part of Paleocene Hungarian basin (46,47,57)
Formation

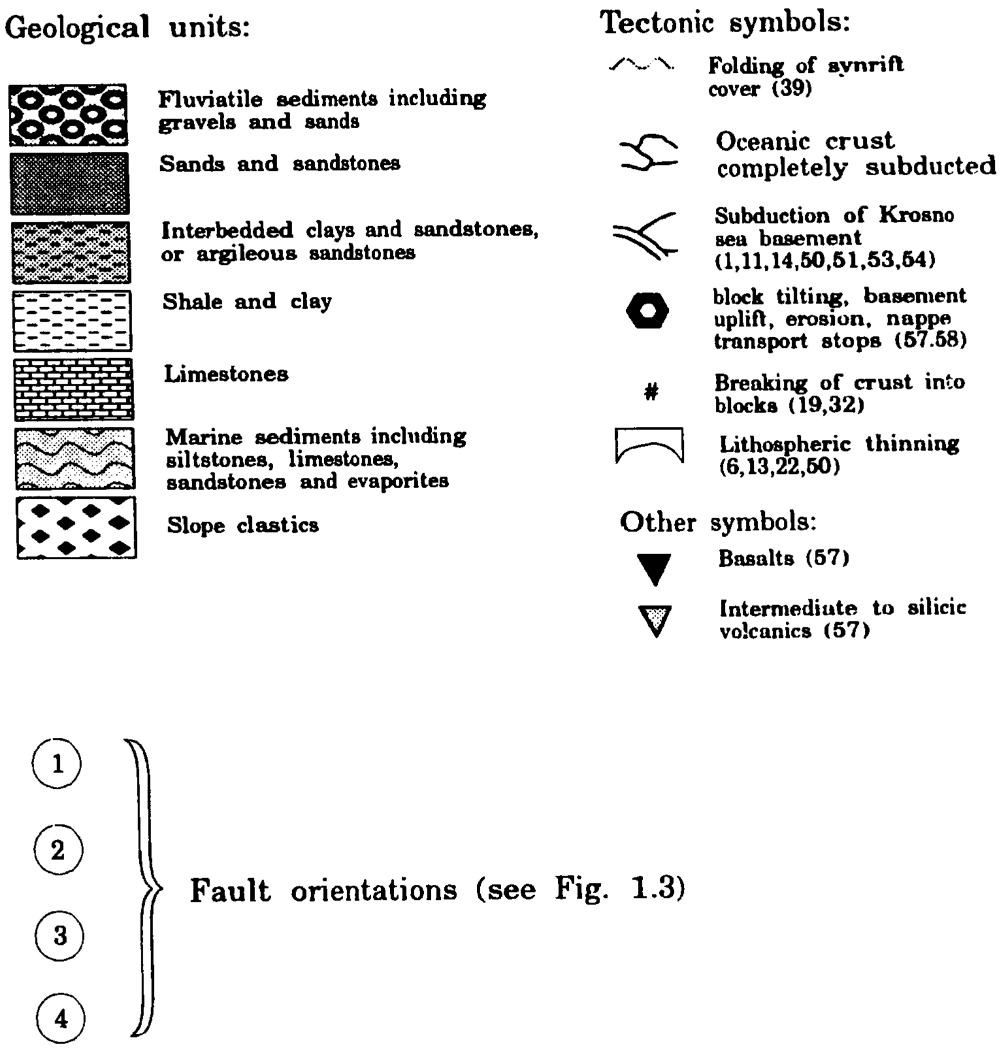

Fig. B.9: Neogene events of the Northwestern Carpathian-Pannonian area.

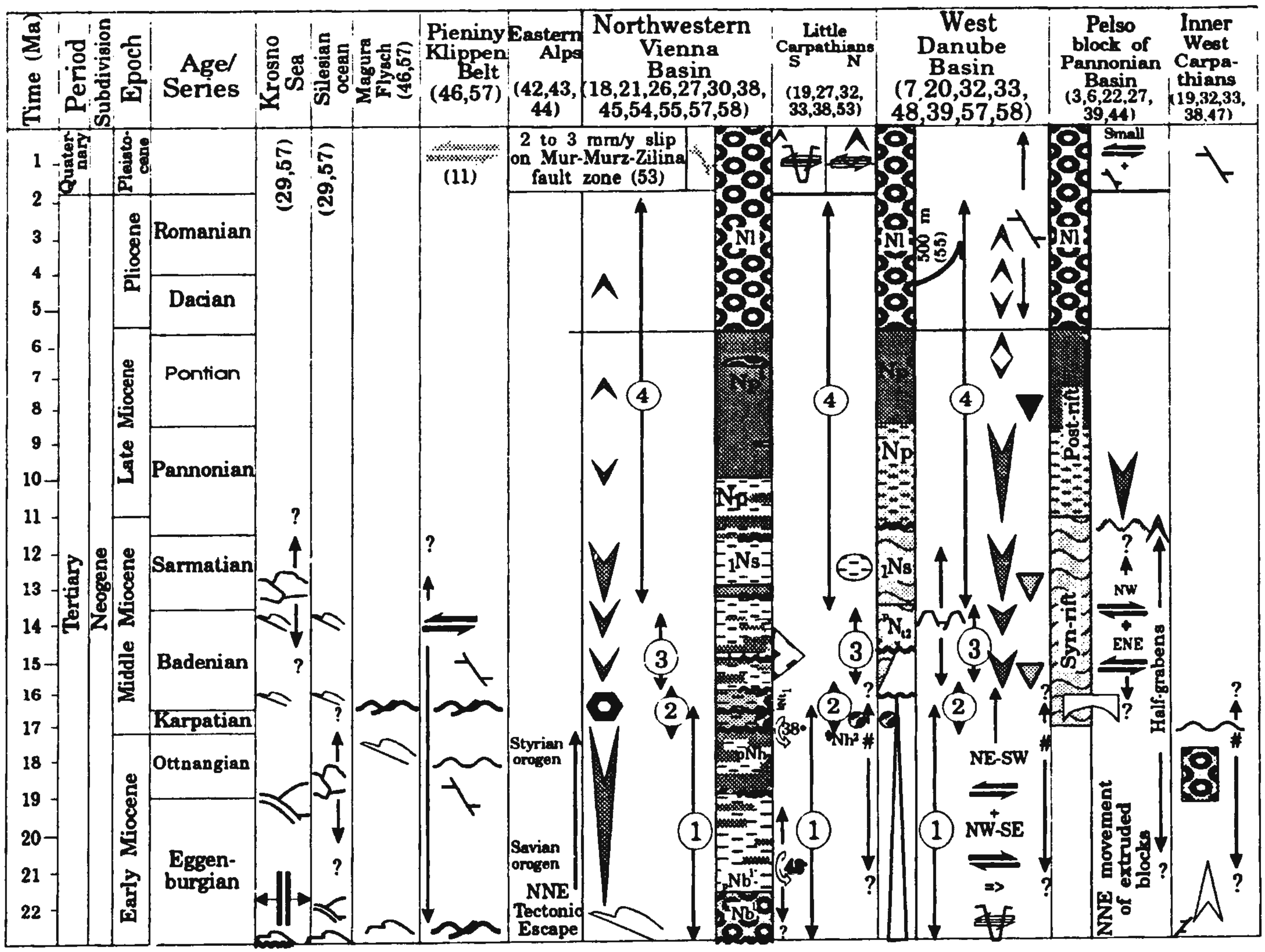
Time (Ma)
Period
Subdivision
Epoch
Age/ Series
Krosno Sea
Silesian ocean
Magura Flysch (46,57)
Pieniny Klippen Belt (46,57)
Eastern Alps (42,43, 44)
Northwestern Vienna Basin (18,21,26,27,30,38, 45,54,55,57,58)
Little Carpathians S N (19,27,32, 33,38,53)
West Danube Basin (7,20,32,33, 48,39,57,58)
Pelso block of Pannonian Basin (3,6,22,27, 39,44)
Inner West Carpa-thians (19,32,33, 38,47)
Quaternary
Tertiary
Neogene
Pleistocene
Pliocene
Late Miocene
Middle Miocene
Early Miocene
Romanian
Dacian
Pontian
Pannonian
Sarmatian
Badenian
Karpatian
Ottnangian
Eggen-burgian
(29,57)
(29,57)
(11)
2 to 3 mm/y slip on Mur-Murz-Zilina fault zone (53)
Styrian orogen
Savian orogen
NNE Tectonic Escape
Nl
Np
Ns
Nb
500 m (55)
NE-SW
NW-SE
Small
NW
ENE
Syn-rift
Post-rift
NNE movement of extruded blocks
Half-grabens


Zavod
Malacky
3

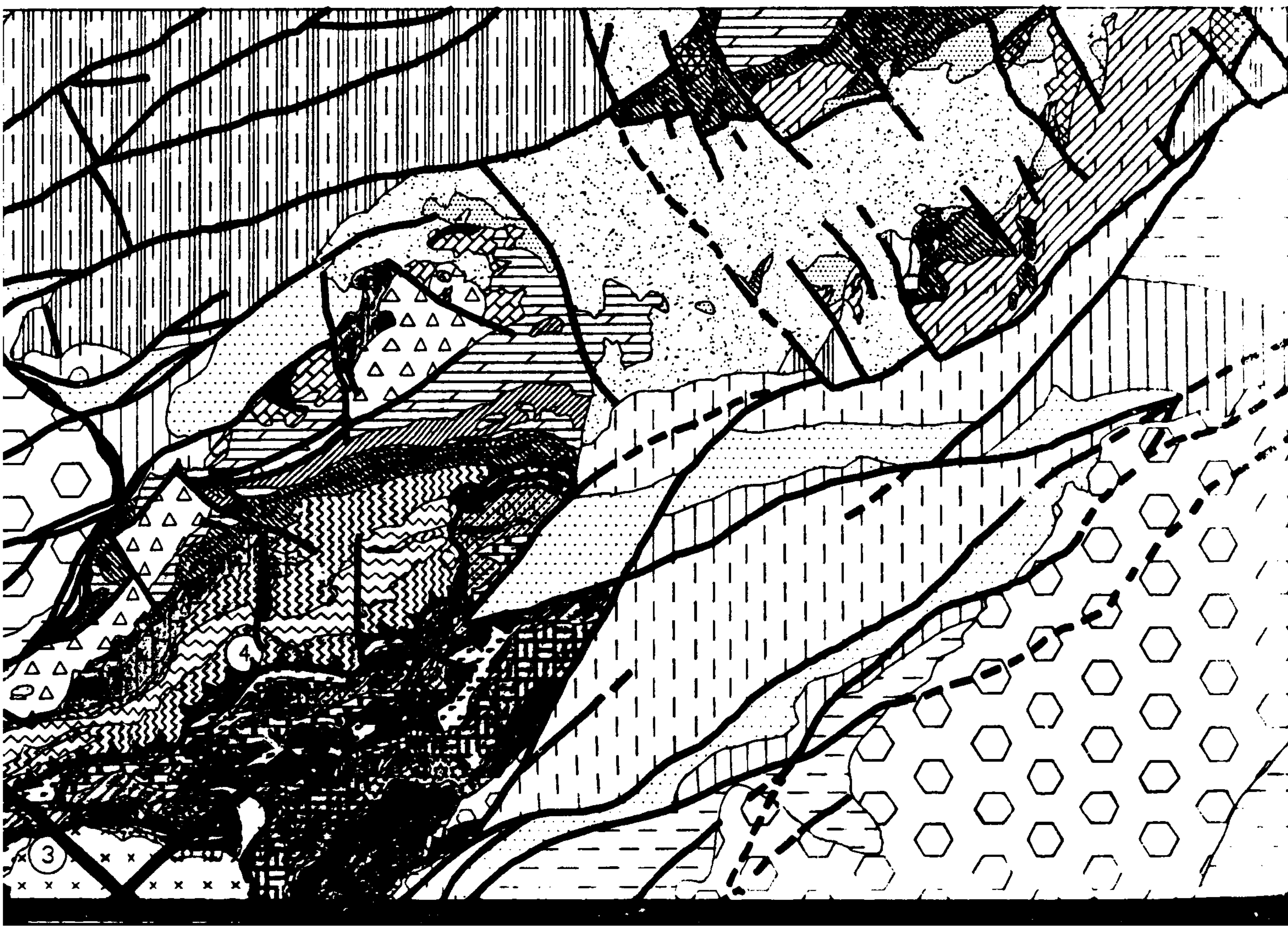
4
3

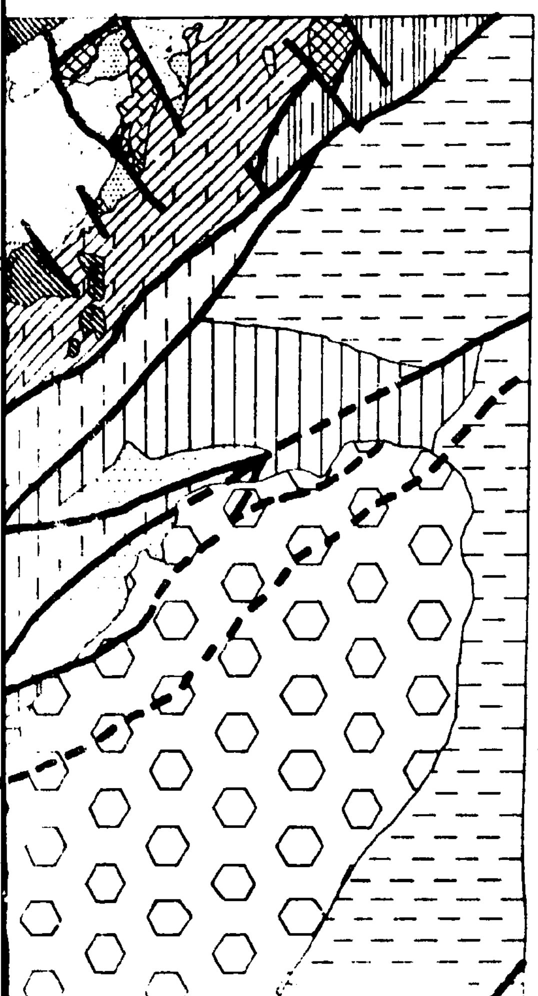

Legend:

TERTIARY

Pliocene

N2: Upper Pliocene sediment

N1: Gravel and sand, variegate

Miocene:

Npt: Pontian: variegated clays

Np: Pannonian: Calcarous clay

$_1$Ns: Sarmatian: calcarous clay gravel and conglomerate. Lo

^{P}Nt^2: Middle to Upper Badeni clays, subordinate sandstone.

^{k}Nt^1. Lower Badenian conglon

Geologic map with location of seismic lines. Modified from Mahel' et al, 1961; Tomek, 1

ments.

egated clays and gravel in Vienna Basin.

clays, subordinate gravel and sand.

clay and clay, sand, gravel.

clay and sand, sandstone, coquina,
Locally some volcanic material.

denian calcarous, finely sandy
one.

nglomerate and gravel

Jurassic

hJ: Marlstone, marly limestone, radio
of Zliechov Group.

J: Slate, marlstone, limestone of Litt

pl J: Cherty to crinoidal limestone a
and Choc Group.

JM: Middle to Late Jurassic cherty li

Lower Jurassic marl, variegated lime
some dolomite and breccia.

Triassic

Upper Triassic to Lower Jurassic

T2–J1: Limestone, *dolomite*, brecciat
Little Carpathian Group, Devinska be

odified from Mahel' et al, 1961; Tomek, 1990, personal communication; Tomek and Thon, 1988.

hJ: Marlstone, marly limestone, radiolarian limestone, radiolarite of Zliechov Group.

J: Slate, marlstone, limestone of Little Carpathian Group.

pl J: Cherty to crinoidal limestone and spongestone of Vysoka and Choc Group.

JM: Middle to Late Jurassic cherty limestone of Little Carpathian Group.

Lower Jurassic marl, variegated limestone, sandstone, with some dolomite and breccia.

Triassic to Lower Jurassic

T2–J1: Limestone, dolomite, brecciate limestone, breccia Little Carpathian Group, Devinska beds.

Lower Triassic do

$^{v}T_1$: I

Tm: P
Varieg

β'T:
melap

PROTEROZOIC AND
Permian

P: Pe

Hercynian granit

Grani
of pe

ic down to Upper Paleozoic

T : Lower Triassic: Quartzite, metamorphosed quartz conglomerate
1 with some schist.

'm: Permian to Lower Triassic, Melaphyre formation.
/ariegated sandstone, schist and arkose with melaphyre clasts.

3'T: Permian? to Lower Triassic. Basic igneous rocks such as
nelaphyre, quartz porphyry, augitic prophyry etc.

; AND PALEOZOIC

P: Permian arkose, conglomerate to porphyroid lightly metamorphosed .

ranitoids

iranite to Granodiorite of Bratislava Massif. Locally shows veins
of pegmatite. Small zone of mylonitization to the NW.

... Massif with local mylonitization

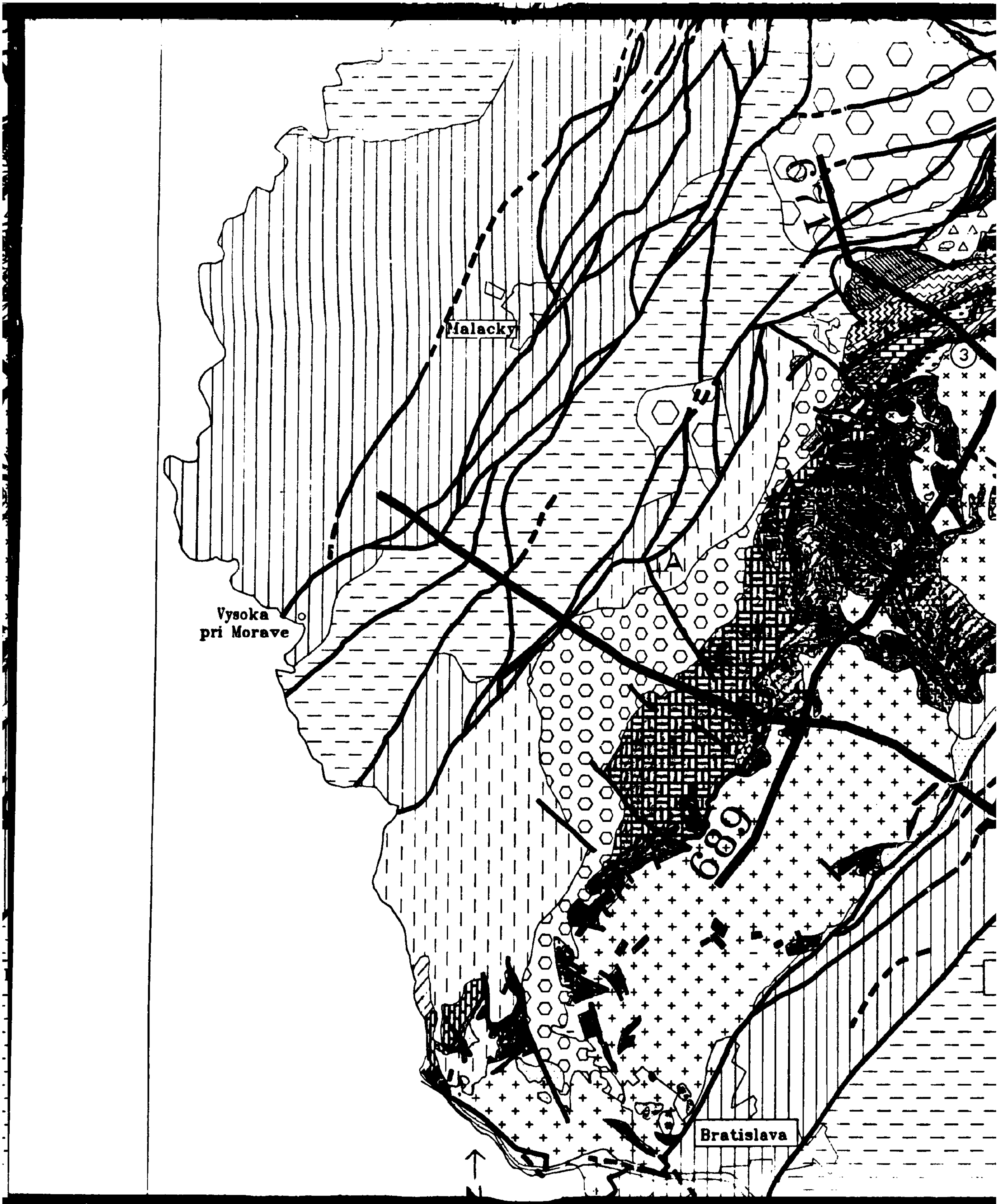
Malacky
Vysoka
pri Morave
Bratislava
689

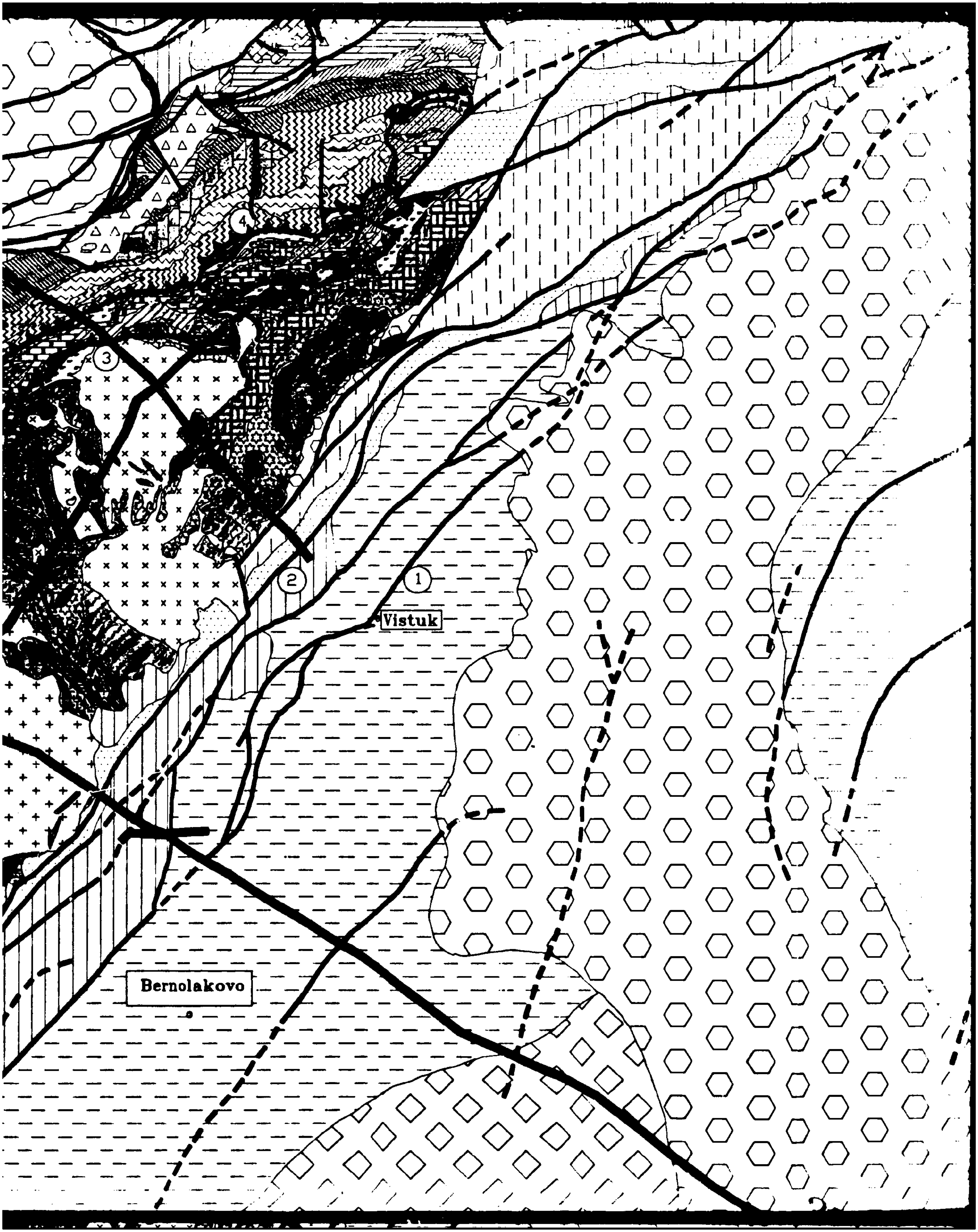
Vistuk
Bernolakovo
1
2
3
4

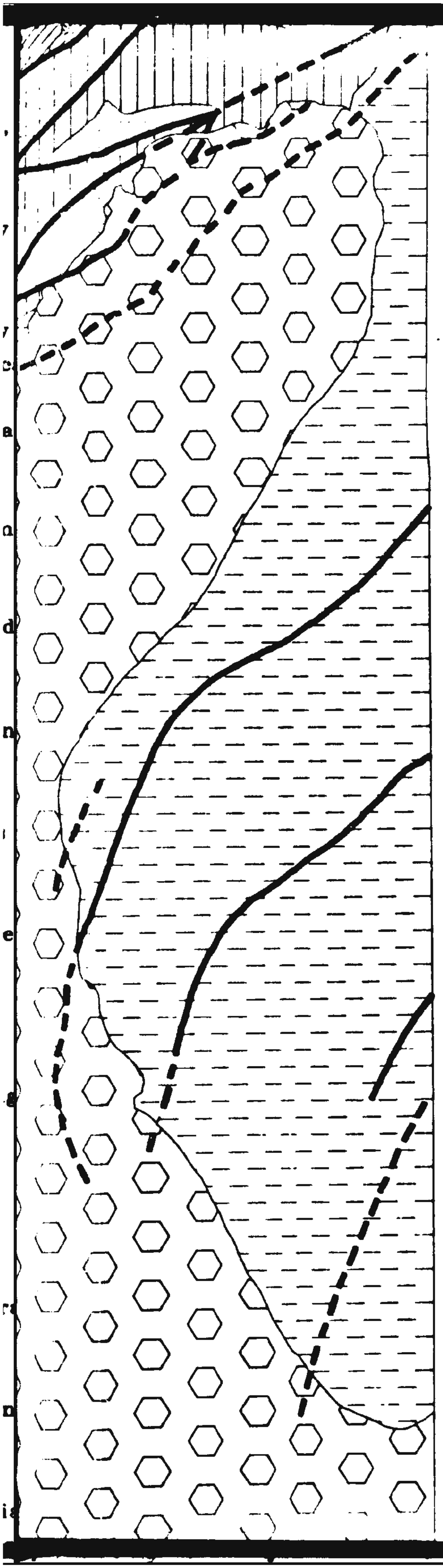

Miocene:

Npt: Pontian: variegated clays

Np: Pannonian: Calcarous clay

$_1$Ns: Sarmatian: calcarous clay
gravel and conglomerate. Lo

^{p}Nt^2: Middle to Upper Badeni
clays, subordinate sandstone.

^{k}Nt^1: Lower Badenian conglon

$_p$Nh^2: Calcarous clay, clay an

^{k}Nh^2: Ottnangian to Karpatia
and sand of Jablonoca beds.

$_p$Nb^1: Eggenburgian calcarous

^{k}Nb^1: Eggenburgian carbonac

Eocene

Sand and clays on basal con

MESOZOIC
Cretaceous

Kcn: Carbonaceous conglome
Gosau formation.

K2al-c: Albian to Cenomania
and calcarous sandstone.

K1-2: Tithonian to Cenoman

clays, subordinate gravel and sand.

clay and clay, sand, gravel.

clay and sand, sandstone, coquina,
Locally some volcanic material.

idenian calcarous, finely sandy
one.

nglomerate and gravel

y and sand. Flysch formation.

patian conglomerate, gravel
eds.

arous clay.

onaceous conglomerate and sandstone.

l conglomerate, breccia and sandy limestone.

omerate, pebbly limestone, marl

ianian: Marly shale, marlstone

manian: Limestone, locally cherty, marly

^{Pl}J: Cherty to crino... ...
and Choc Group.

JM: Middle to Late Jurassic cherty li

Lower Jurassic marl, variegated lim
some dolomite and breccia.

Triassic

Upper Triassic to Lower Jurassic

T2–J1: Limestone, dolomite, brecciat
Little Carpathian Group, Devinska be

T–J: Rhaetian limestone, oolithic lim
Choc Series.

Tnk: Norian Carpathian keuper: Vari
dolomite and sandstone.

T3: Karnian to Norian dolomite.

^{v}Tk: Carnian limestone of Havran m

Tk: Shale and sandstone.

Middle to Upper Triassic

^{d}T2–3: Dolomite.

T2–3: Limestone.

Middle Triassic

^{v}T2: Grey to dark-grey limestone.

pl J: Cherty to crinoidal limestone and spongestone of Vysoka and Choc Group.

JM: Middle to Late Jurassic cherty limestone of Little Carpathian Group.

Lower Jurassic marl, variegated limestone, sandstone, with some dolomite and breccia.

...assic to Lower Jurassic

T2–J1: Limestone, dolomite, brecciate limestone, breccia Little Carpathian Group, Devinska beds.

T–J: Rhaetian limestone, oolithic limestone, fossiliferous limestone Choc Series.

Tnk: Norian Carpathian keuper: Variegated shales with interbedded dolomite and sandstone.

T3: Karnian to Norian dolomite.

v Tk: Carnian limestone of Havran nappe.

Tk: Shale and sandstone.

... Upper Triassic

d T2–3: Dolomite.

T2–3: Limestone.

...riassic

v T2: Grey to dark grey limestone

Variegated...

β'T: Per... melaphyr...

PROTEROZOIC AND PA...

Permian

P: Permia...

Hercynian granitoids

Granite t... of pegma...

Biotitic g... in the so...

Amphiboli...

Harmonia Series

Sericitic– biotitic c... siliceous

Pezinok–Pernek Seri...

fb^{x}: Devo...

mg^{x} and post–orog...

fgf^{x}: Pyri...

A^{x}: Amph...

Variegated sandstone, schist and arkose with melaphyre clasts.

β'T: Permian? to Lower Triassic. Basic igneous rocks such as melaphyre, quartz porphyry, augitic prophyry etc.

)IC AND PALEOZOIC

P: Permian arkose, conglomerate to porphyroid lightly metamorphosed.

granitoids

Granite to Granodiorite of Bratislava Massif. Locally shows veins of pegmatite. Small zone of mylonitization to the NW.

Biotitic granodiorite of the Modra Massif with local mylonitization in the south.

Amphibolitic to biotitic–amphibolitic diorite with quartzite.

Series

Sericitic–chloritic phyllite, graphitic to cherty biotitic phyllite, biotitic chert, schist. Locally crystalline limestone to calcareous–siliceous chert with pyroclastics. 394 + 24 Ma K/Ar metamorphic age.

ernek Series (Deposited in Proterozoic, metamorphosed in Paleozoic).

fb^x: Devonian phyllite, biotitic to sericitic–biotitic phyllite.

mg^x and $M2^x$: Biotitic gneiss to paragneiss with garnet and staurolite (mg^x) post–orogenic migmatite ($M2^x$) near Bratislava.

fgf^x: Pyritic graphitic phyllite with tuffitic actinolitic schist.

A^x: Amphibolite.

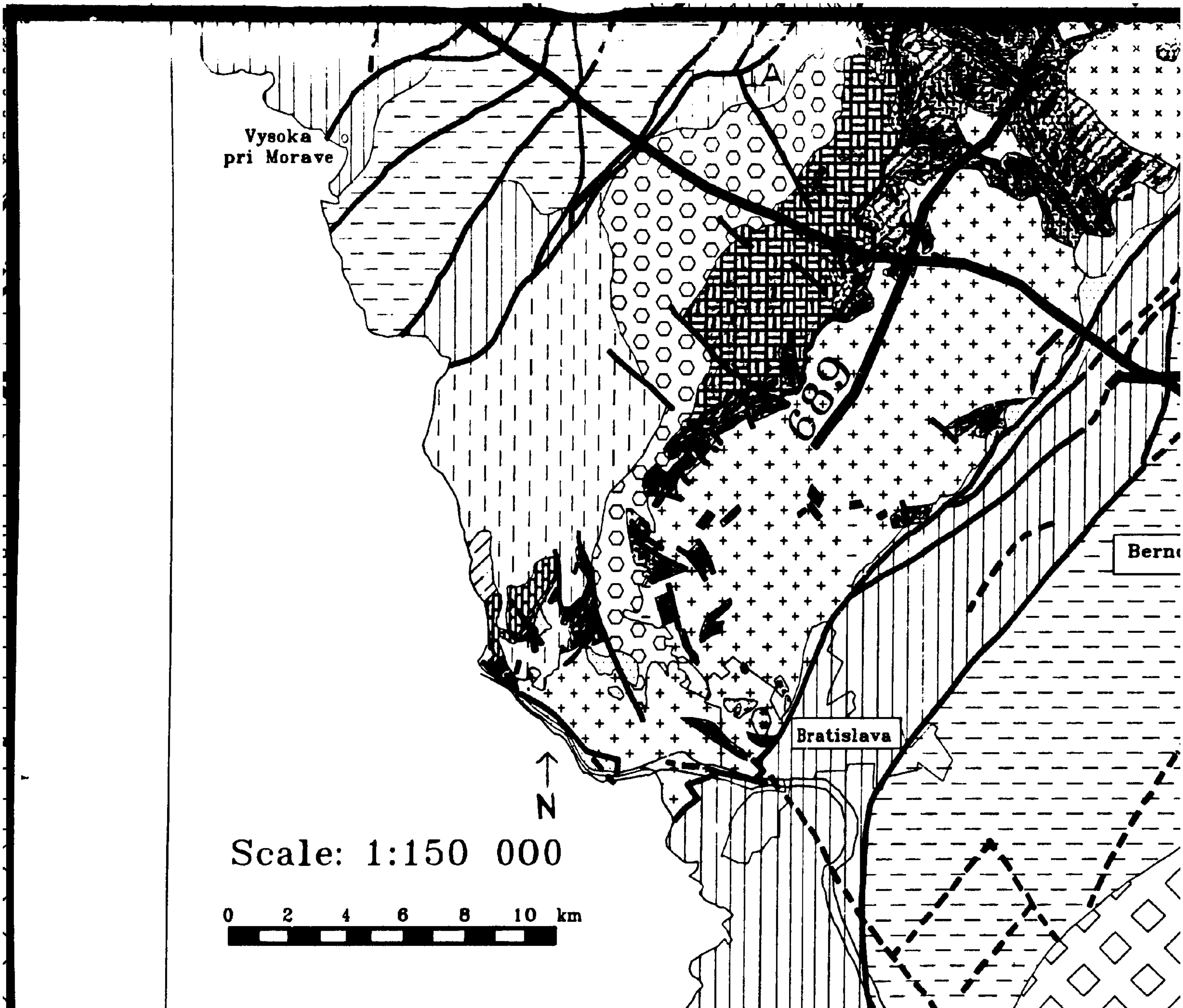

Plate 1: Geologic map with

Modified from Mahel' et al., 1961; To

Tomek and

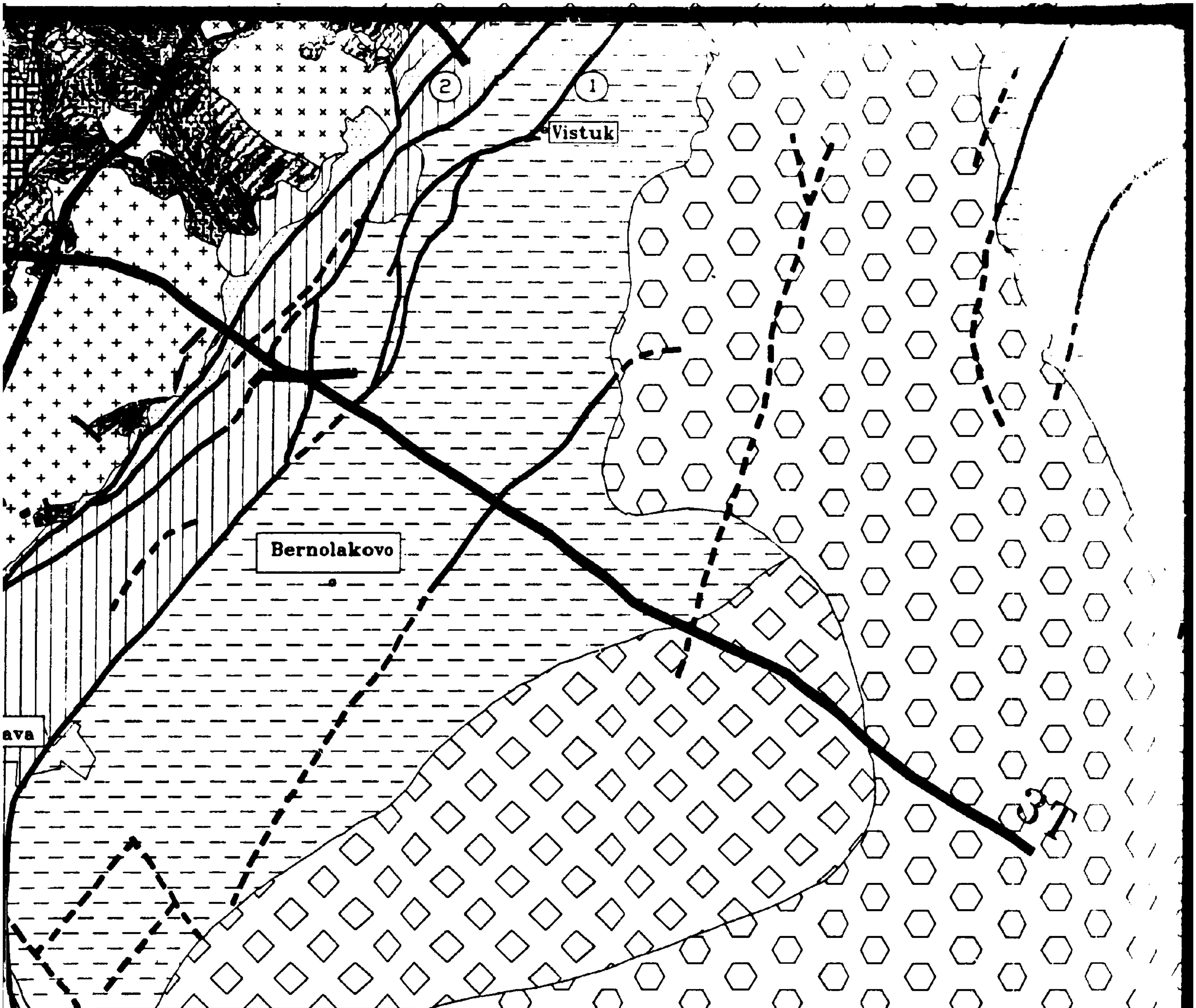

ologic map with location of seismic lines.

et al., 1961; Tomek, 1990, personal communication; Tomek and Thon, 1988.

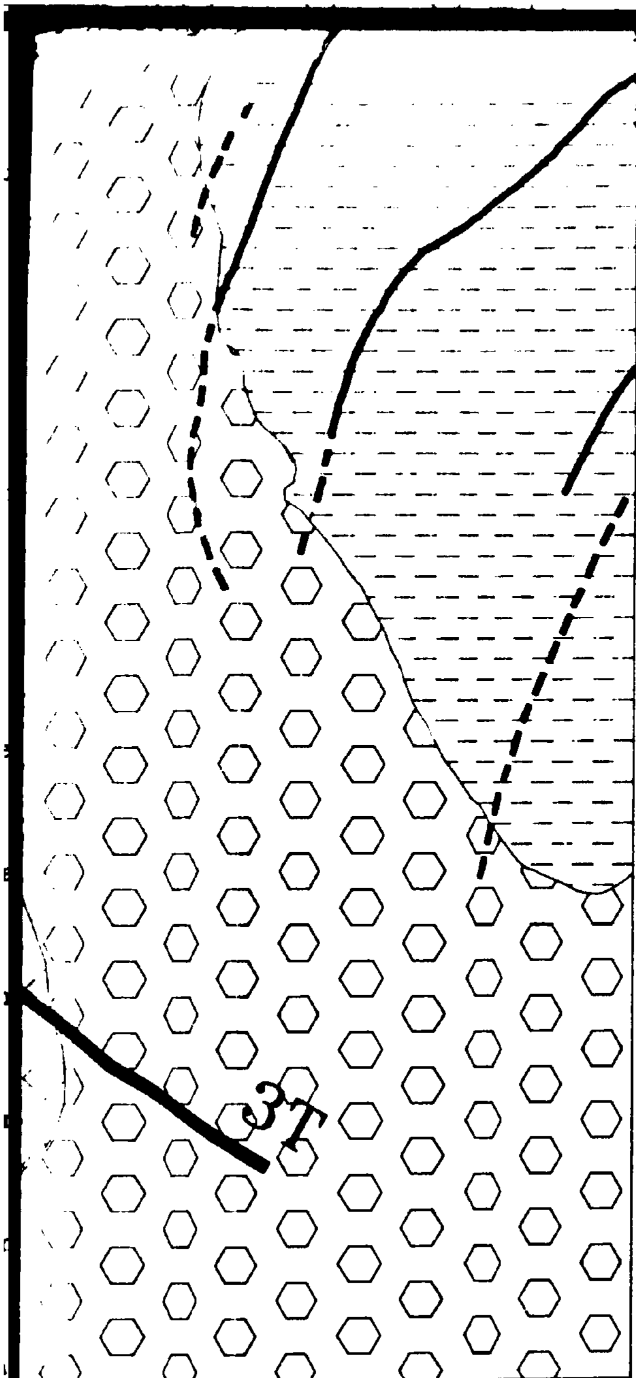

- and sand of Jablonoca beds
- pNb[1]: Eggenburgian calcarou
- kNb[1]: Eggenburgian carbona

Eocene

- Sand and clays on basal co

MESOZOIC

Cretaceous

- Kcn: Carbonaceous conglome Gosau formation.
- K2al–c: Albian to Cenomani and calcarous sandstone.
- K1–2: Tithonian to Cenomar with marly shale, calcarous
- Kn: Tithonian to Neoceomia
- K1V: Tithonian to Aptian lin chert and marl.
- K1M: Tithonian to Aptian ch the Little Carpathian Group.
- J2–K1: Dogger to Neocomian marly, cherty limestone of
- J–K2: Jurassic to Middle Cre Limestone.

es.

nmunication;

of Jablonoca beds.

nburgian calcarous clay.

nburgian carbonaceous conglomerate and sandstone.

clays on basal conglomerate, breccia and sandy limestone.

naceous conglomerate, pebbly limestone, marl
nation.

ian to Cenomanian: Marly shale, marlstone
ous sandstone.

onian to Cenomanian: Limestone, locally cherty, marly
shale, calcarous sandstone.

ian to Neoceomian: limestone, grey marl to marly limestone.

nian to Aptian limestone of Vysoka series with
marl.

nian to Aptian cherty limestone to chert of
Carpathian Group.

ger to Neocomian: Cherty limestone,
rty limestone of the Little Carpathian Group.

ssic to Middle Cretaceous, Vysoka and Zliechov group

T3: Karnian to Norian

^{v}Tk: Carnian limestone

Tk: Shale and sandstone

Middle to Upper Triassic

^{d}T2–3: Dolomite.

T2–3: Limestone.

Middle Triassic

^{v}T2: Grey to dark-grey lime

^{d}T2: Grey dolomite.

^{v}Tl: Ladinian limestone

Ta: Anisian limestone and

3: Karnian to Norian dolomite.

Tk: Carnian limestone of Havran nappe.

Tk: Shale and sandstone.

Jpper Triassic

^{d}T2–3: Dolomite.

T2–3: Limestone.

ssic

^{v}T2: Grey to dark–grey limestone.

^{d}T2: Grey dolomite.

^{v}Tl: Ladinian limestone.

Ta: Anisian limestone and chert.

Harmonia Series

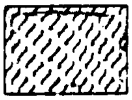

Sericitic–cl
biotitic che
siliceous cl

Pezinok–Pernek Series

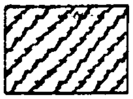

fb^{x}: Devoni

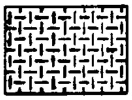

mg^{x} and M
post–oroger

fgf^{x}: Pyritic

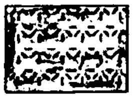

A^{x}: Amphib

SYMBOLS

Unit bound

Fault

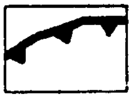

Thrust faul

Seismic

ia Series

Sericitic–chloritic phyllite, graphitic to cherty biotitic phyllite, biotitic chert, schist. Locally crystalline limestone to calcareous–siliceous chert with pyroclastics. 394 + 24 Ma K/Ar metamorphic age.

–Pernek Series (Deposited in Proterozoic, metamorphosed in Paleozoic).

fb^x: Devonian phyllite, biotitic to sericitic–biotitic phyllite.

mg^x and $M2^x$: Biotitic gneiss to paragneiss with garnet and staurolite (mg^x) post–orogenic migmatite ($M2^x$) near Bratislava.

fgf^x: Pyritic graphitic phyllite with tuffitic actinolitic schist.

A^x: Amphibolite.

Unit boundary

Fault

Thrust fault

Seismic line

(1) Vistuk fault

(2) Boleraz fault

(3) Boundary between Krizna and Male Karpaty nappe

(4) Boundary between Križna and Choč nappe

City or village

Large city

Plate 2: Line 671/87. Pre-stack processing by Geofyzika Brno.

Plate 2: Line 671/87. Pre-stack processing by Geofyzika Brno. Event 3 is the basement of the Vienna a thrust plane within the Northern Limestone Alps. Event 5 is the interface between early Middle Miocene conglomerate to sandstone alternating with clay and early Middle Miocene (Badenian) calcarous clay to f

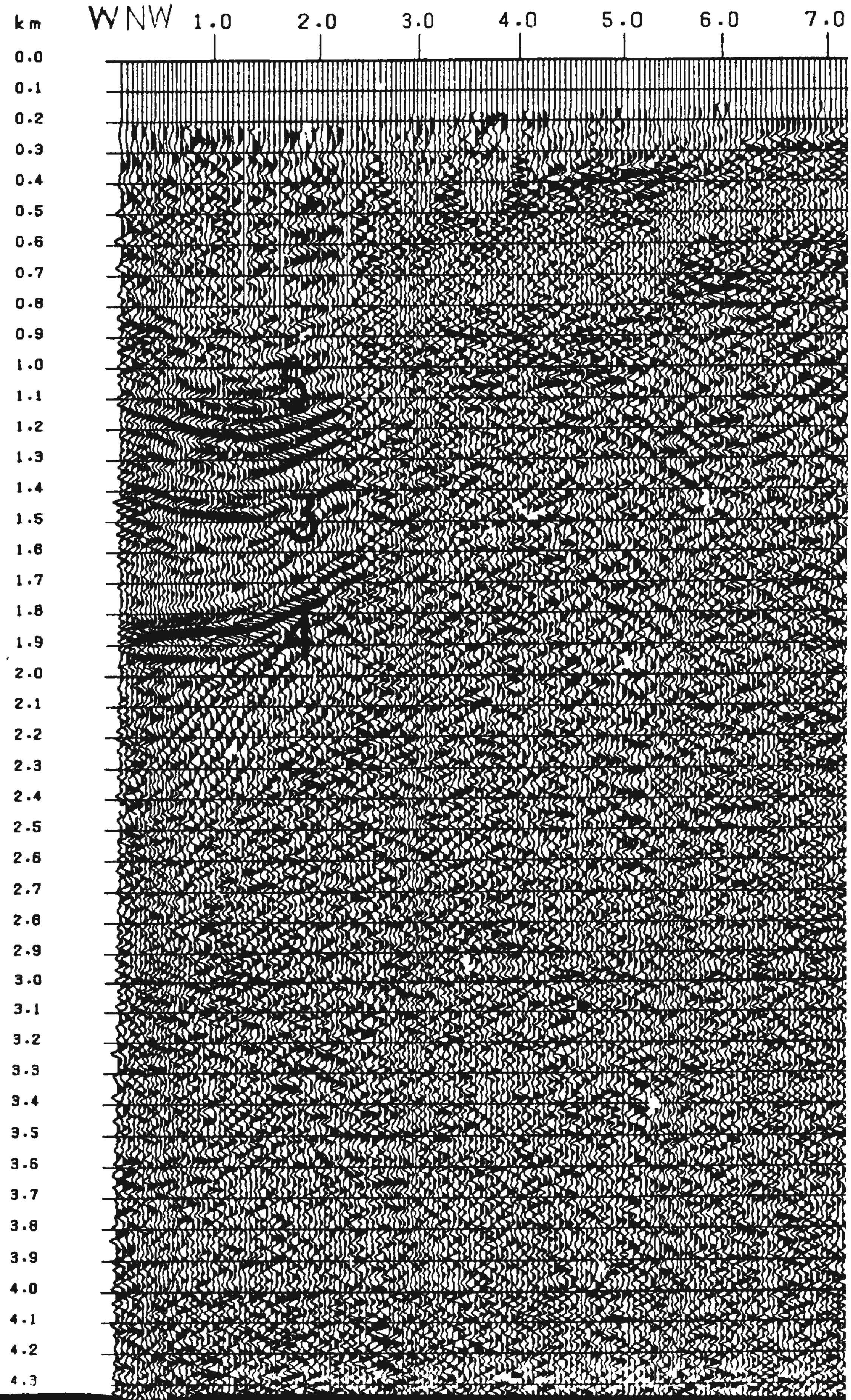

zika Brno. Event 3 is the basement of the Vienna basin. Event 4 is
nt 5 is the interface between early Middle Miocene (Lower Badenian)
ly Middle Miocene (Badenian) calcarous clay to fine gravel.

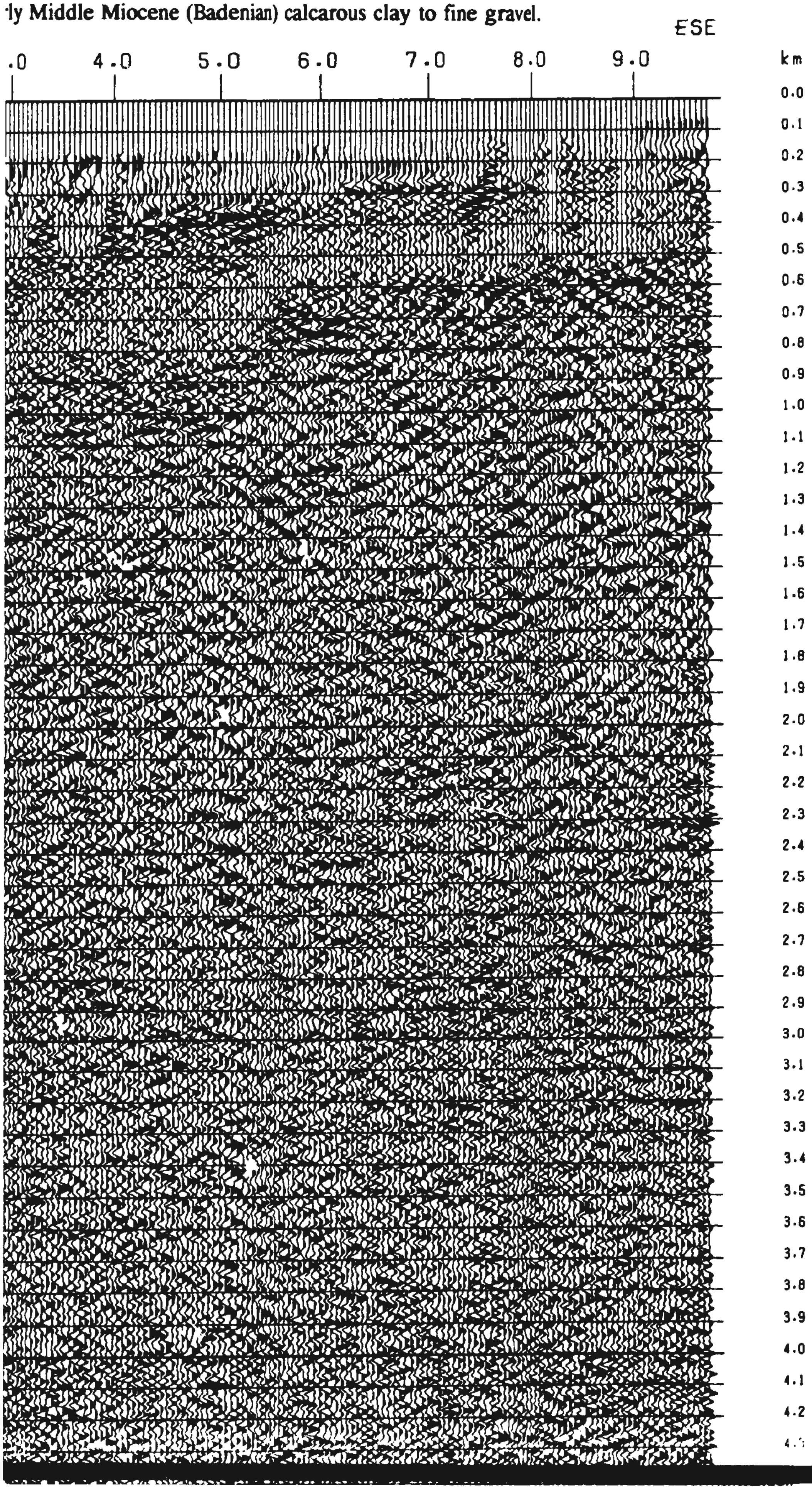

Plate 3: Line 671A/87. Pre-stack processing by Geofyzika Brno.

Plate 3: Line 671A/87. Pre-stack processing by Geofyzika Brno. Events
Cretaceous age that may have been reactivated in Early Miocene. Events
shear zones.

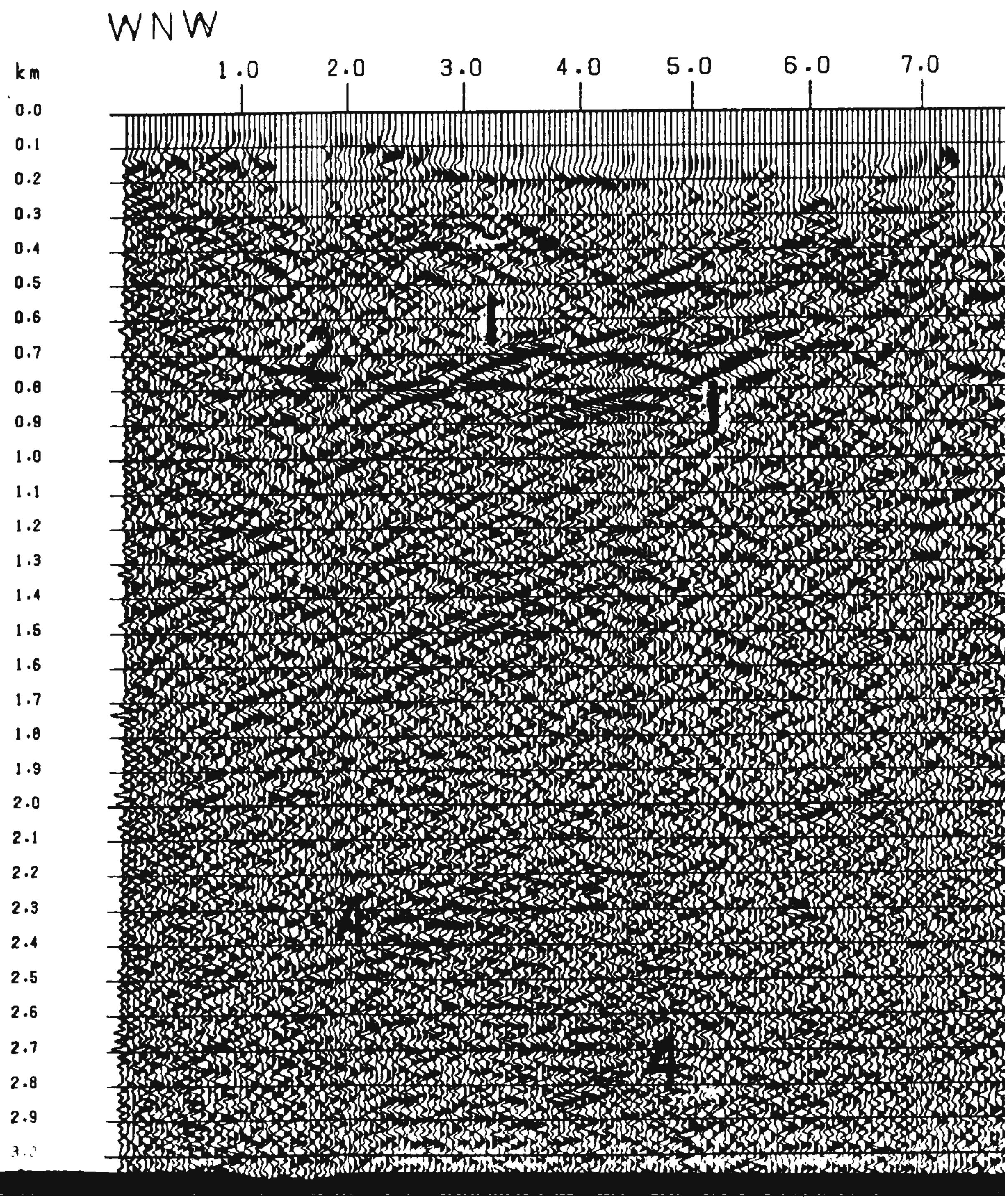

Pre-stack processing by Geofyzika Brno. Events 1 are segment of an imbricate trailing fan of Late
have been reactivated in Early Miocene. Events 2 are conjugated faults to events 1. Events 4 are

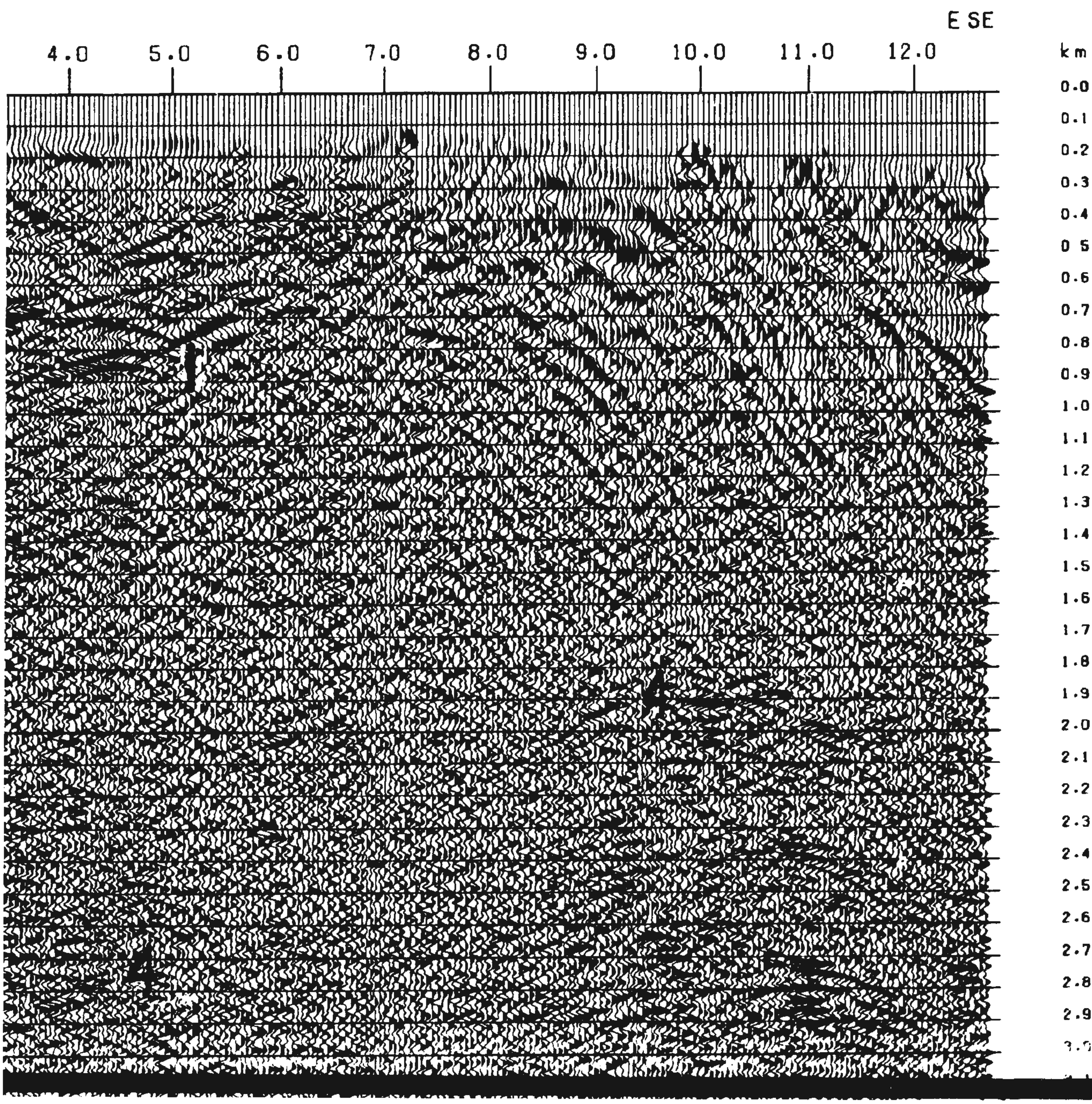

Plate 5: Reprocessed section of line 671/87.

Plate 5: Reprocessed section of line 671/87. Event 3 is the ba
basin. Event 4 is a thrust plane within the Northern Limestone
interface between early Middle Miocene (Lower Badenian) congl
alternating with clay and early Middle Miocene (Badenian) calcaro

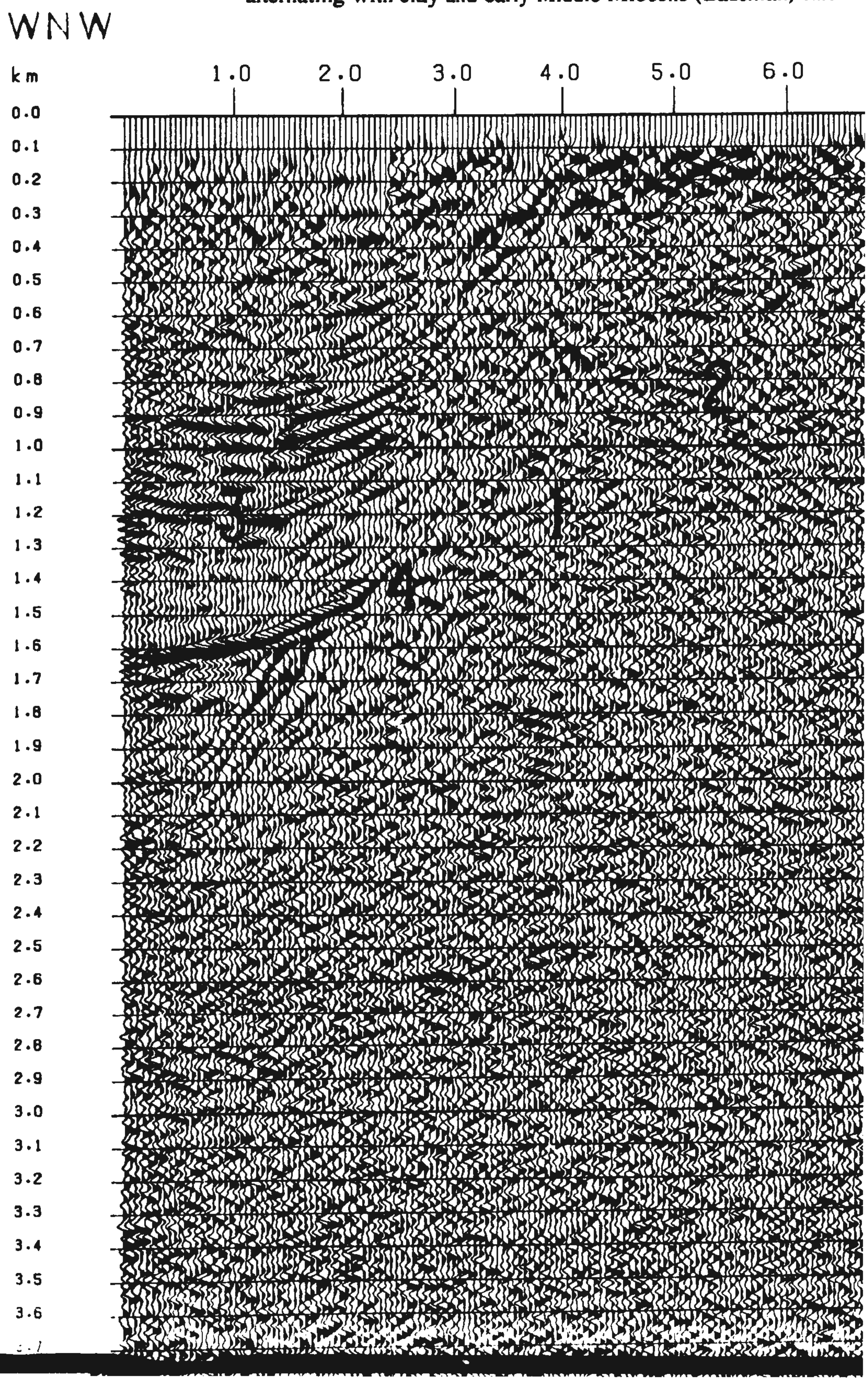

eprocessed section of line 671/87. Event 3 is the basement of the Vienna
t 4 is a thrust plane within the Northern Limestone Alps. Event 5 is the
ween early Middle Miocene (Lower Badenian) conglomerate to sandstone
ith clay and early Middle Miocene (Badenian) calcarous clay to fine gravel.

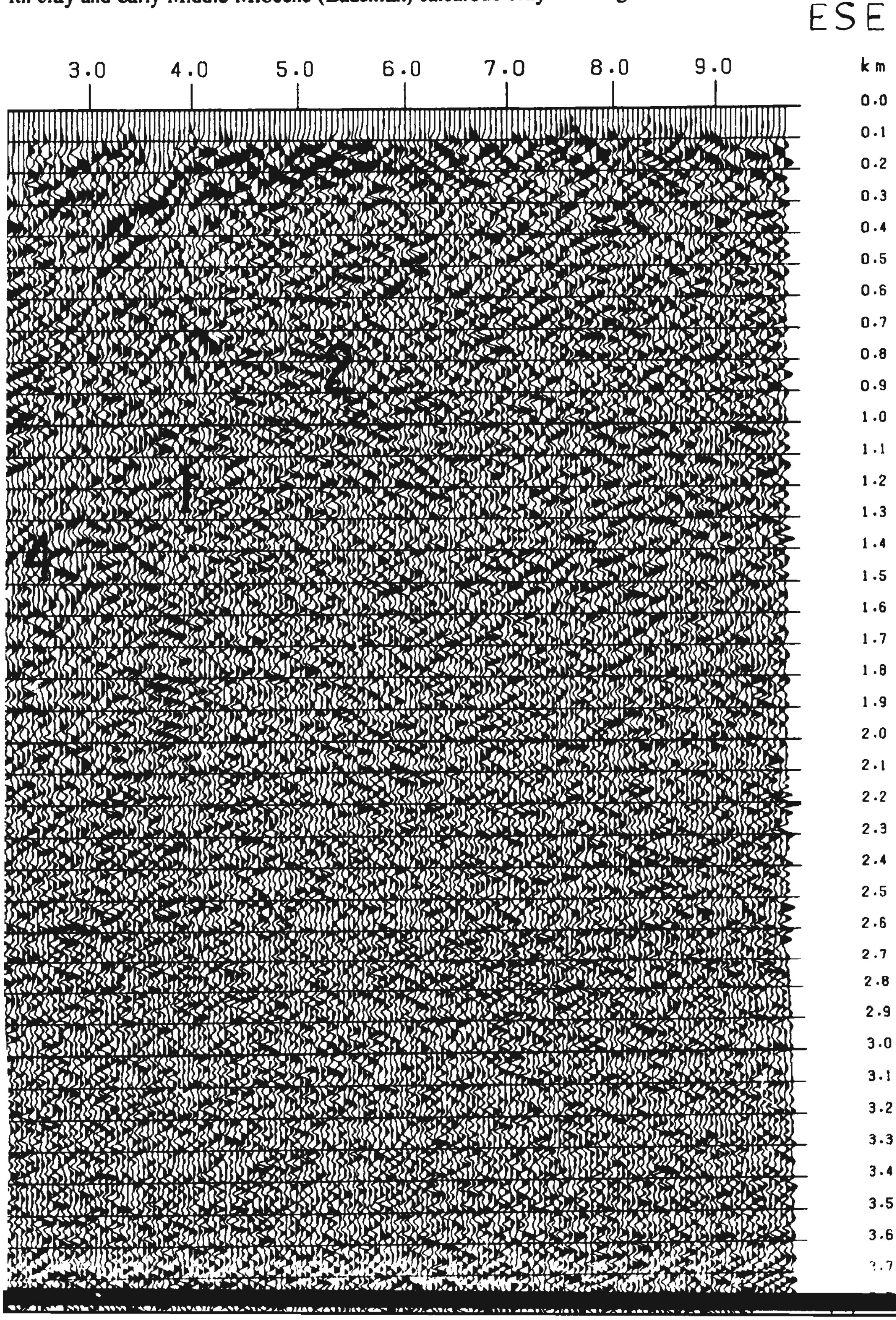

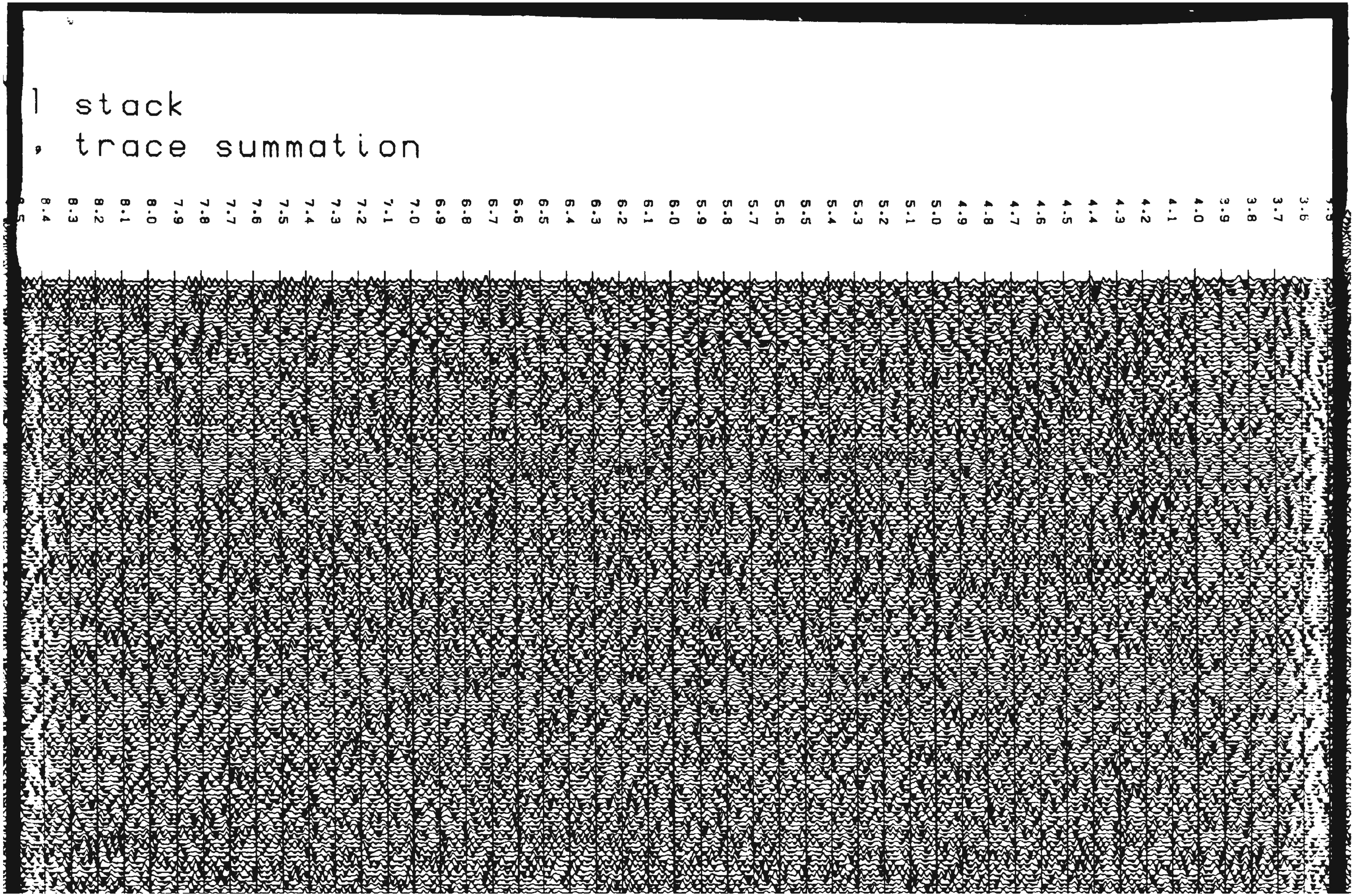
l stack
, trace summation
8.4 8.3 8.2 8.1 8.0 7.9 7.8 7.7 7.6 7.5 7.4 7.3 7.2 7.1 7.0 6.9 6.8 6.7 6.6 6.5 6.4 6.3 6.2 6.1 6.0 5.9 5.8 5.7 5.6 5.5 5.4 5.3 5.2 5.1 5.0 4.9 4.8 4.7 4.6 4.5 4.4 4.3 4.2 4.1 4.0 3.9 3.8 3.7 3.6

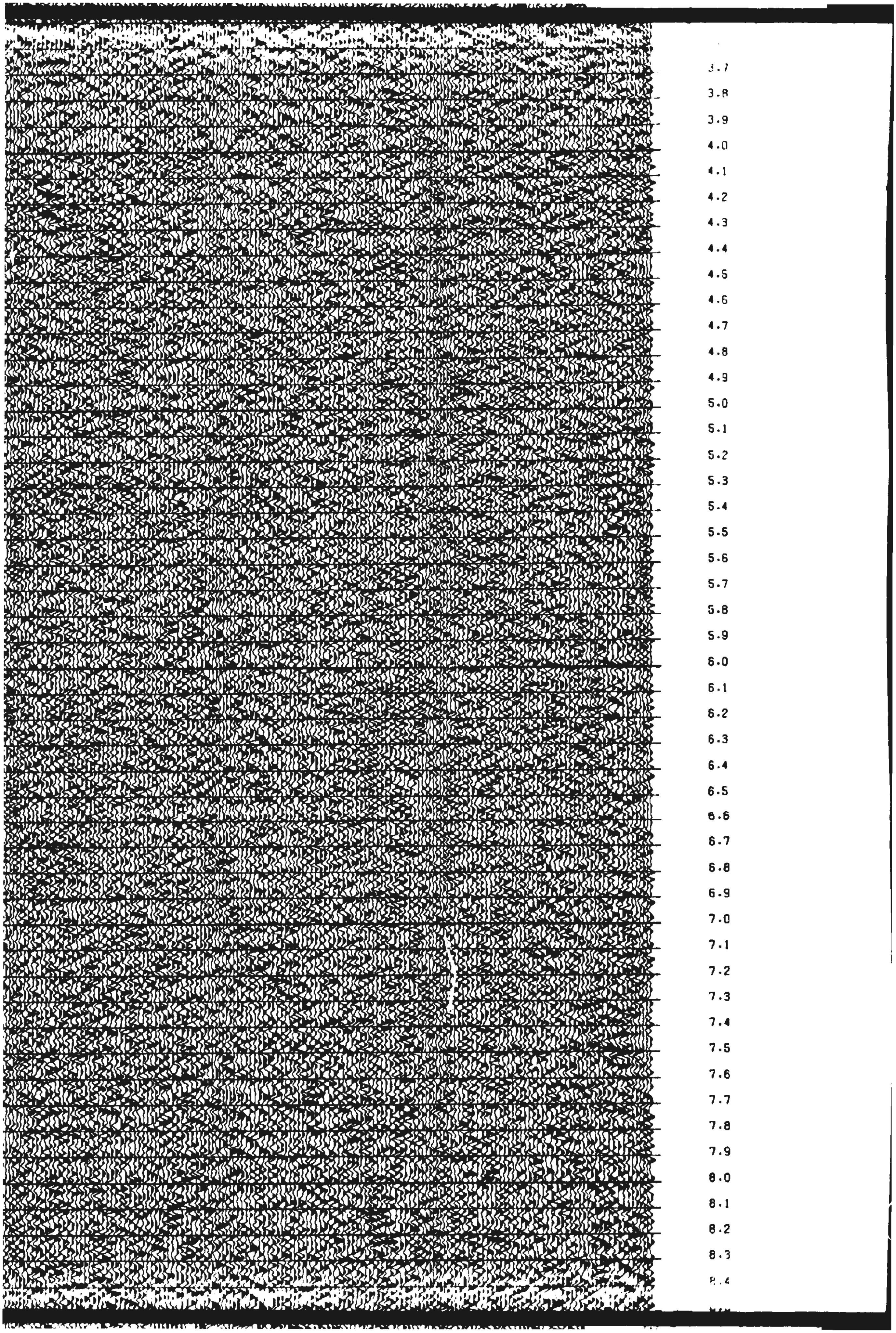

3.7
3.8
3.9
4.0
4.1
4.2
4.3
4.4
4.5
4.6
4.7
4.8
4.9
5.0
5.1
5.2
5.3
5.4
5.5
5.6
5.7
5.8
5.9
6.0
6.1
6.2
6.3
6.4
6.5
6.6
6.7
6.8
6.9
7.0
7.1
7.2
7.3
7.4
7.5
7.6
7.7
7.8
7.9
8.0
8.1
8.2
8.3

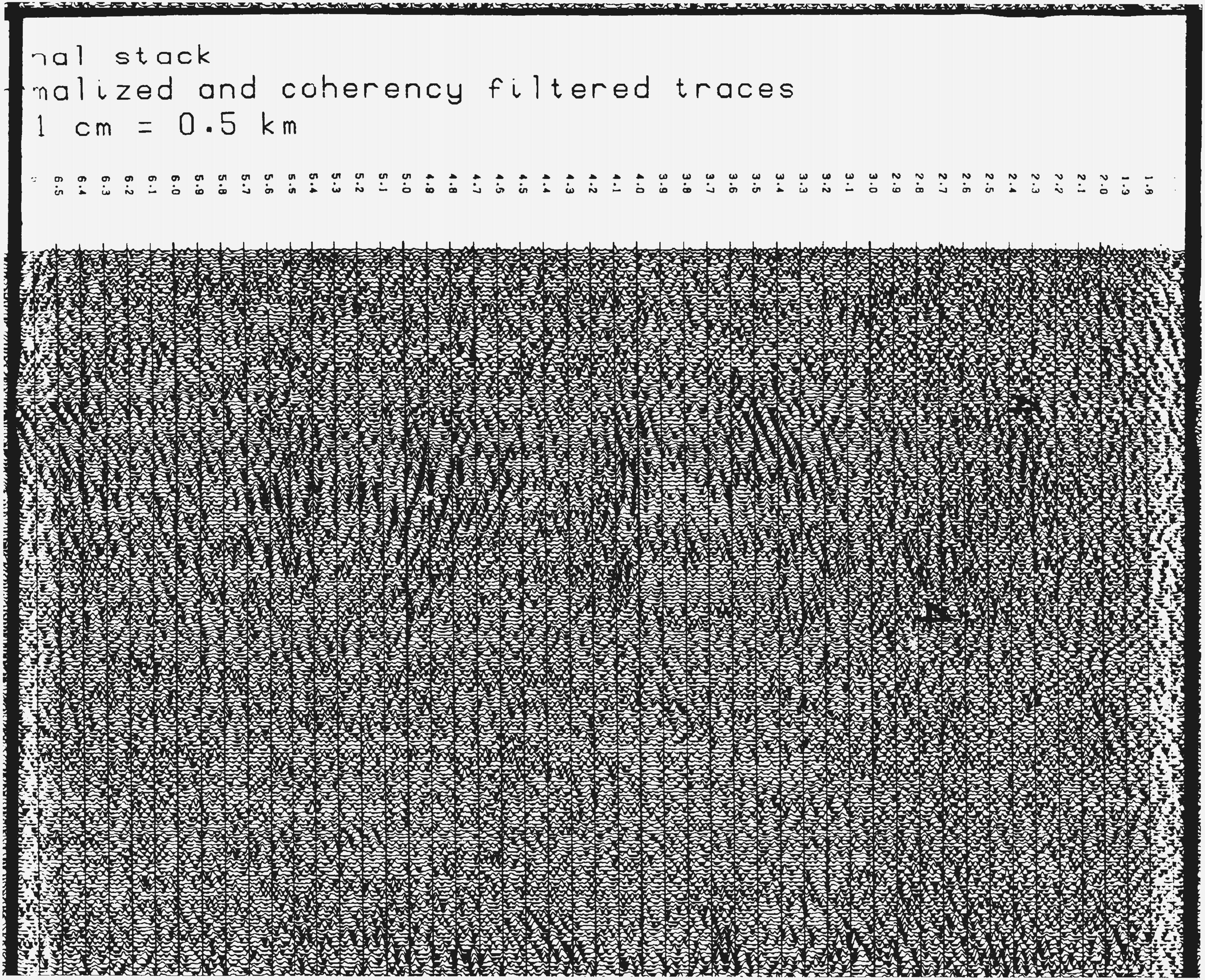
nal stack
malized and coherency filtered traces
1 cm = 0.5 km

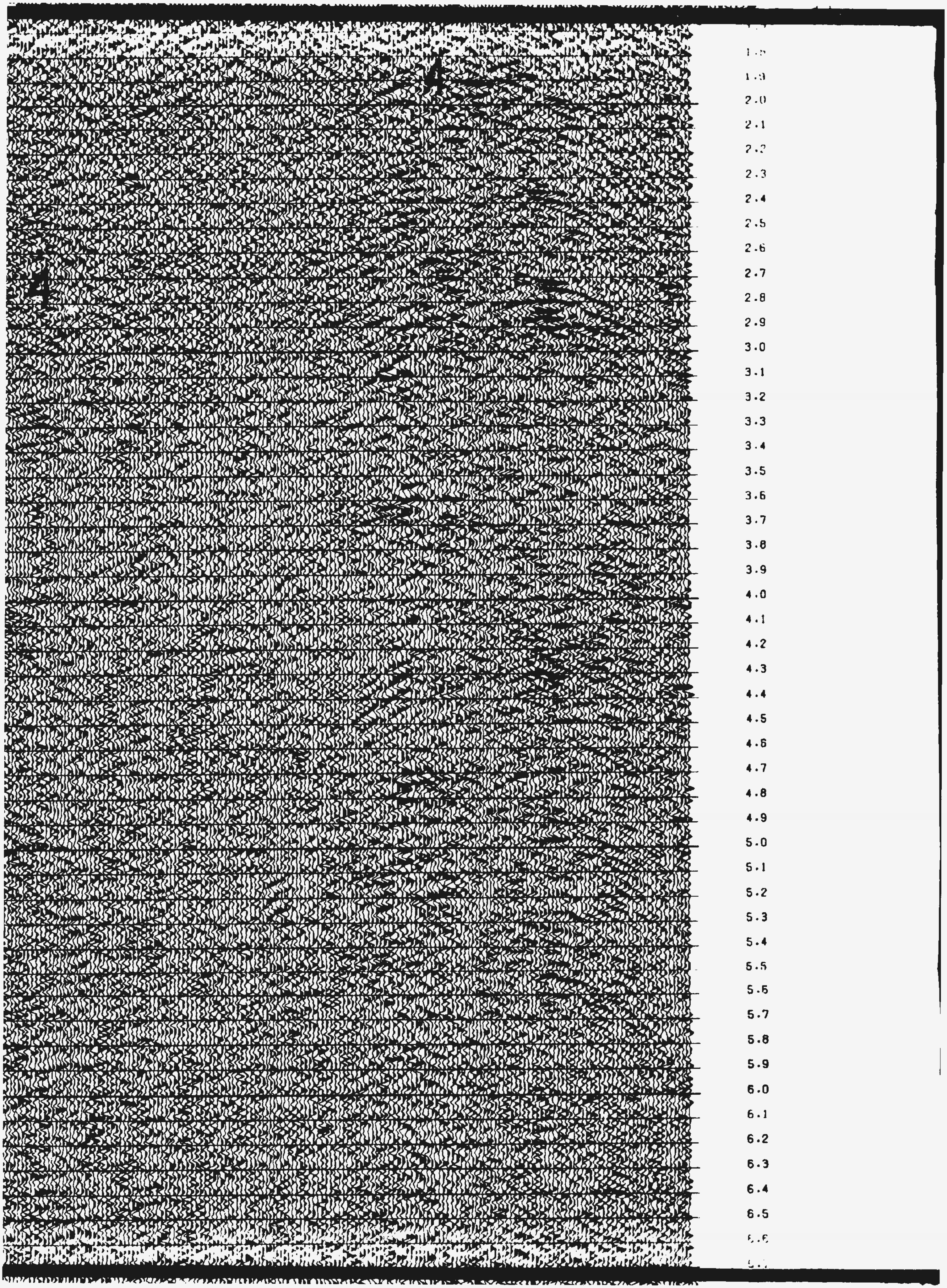
2.0
2.1
2.2
2.3
2.4
2.5
2.6
2.7
2.8
2.9
3.0
3.1
3.2
3.3
3.4
3.5
3.6
3.7
3.8
3.9
4.0
4.1
4.2
4.3
4.4
4.5
4.6
4.7
4.8
4.9
5.0
5.1
5.2
5.3
5.4
5.5
5.6
5.7
5.8
5.9
6.0
6.1
6.2
6.3
6.4
6.5

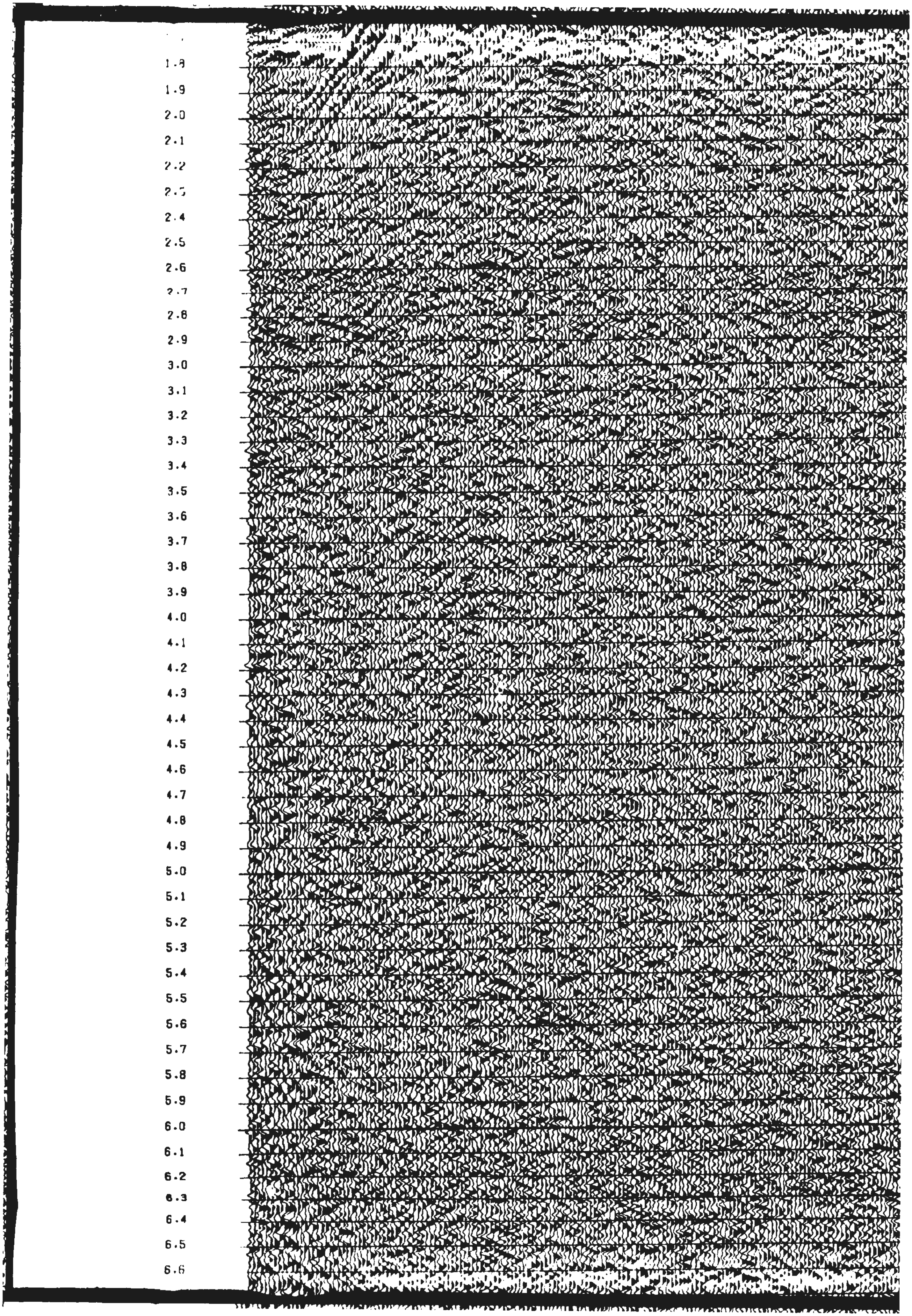
1.8
1.9
2.0
2.1
2.2
2.3
2.4
2.5
2.6
2.7
2.8
2.9
3.0
3.1
3.2
3.3
3.4
3.5
3.6
3.7
3.8
3.9
4.0
4.1
4.2
4.3
4.4
4.5
4.6
4.7
4.8
4.9
5.0
5.1
5.2
5.3
5.4
5.5
5.6
5.7
5.8
5.9
6.0
6.1
6.2
6.3
6.4
6.5
6.6

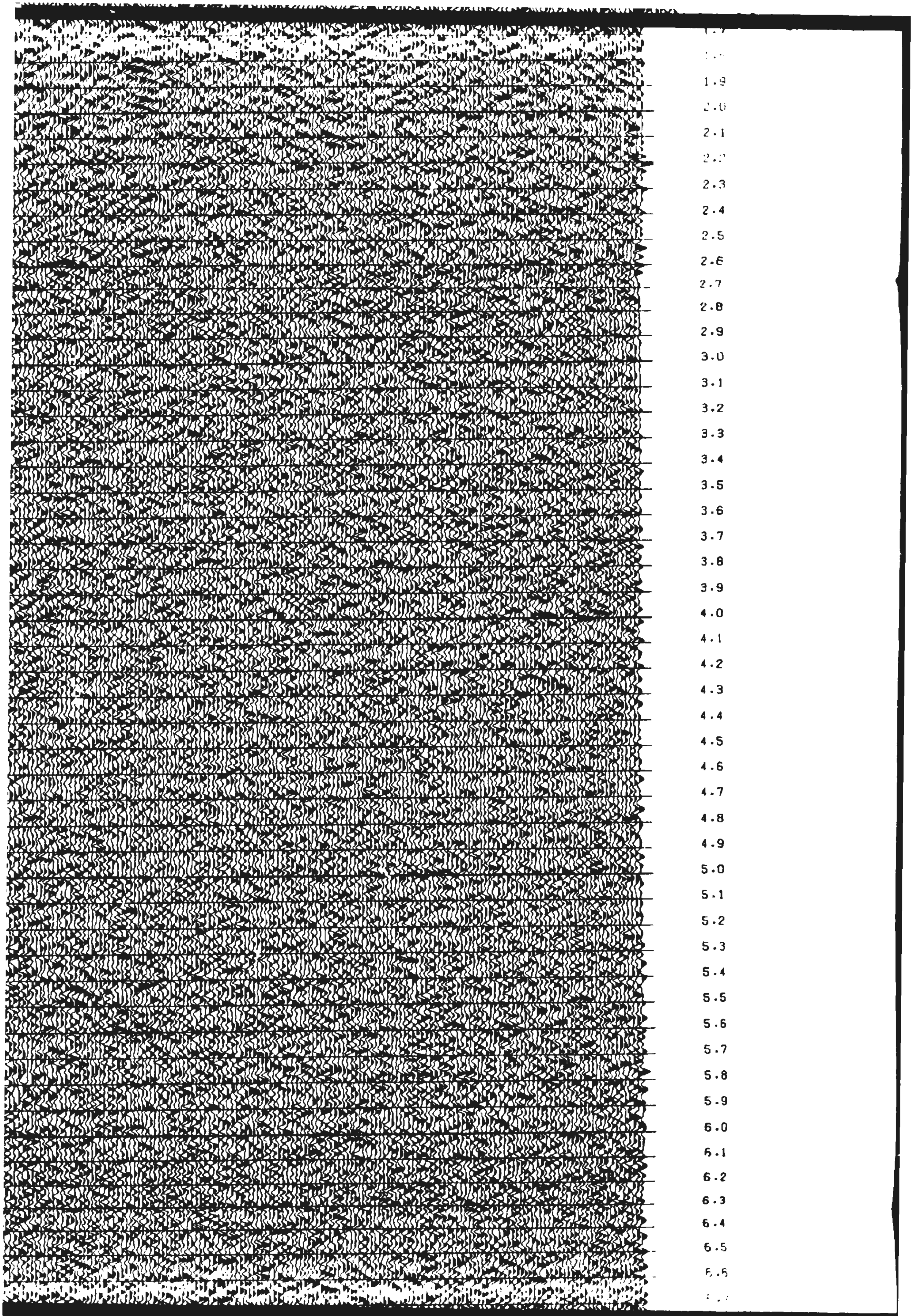
1.9
2.0
2.1
2.3
2.4
2.5
2.6
2.7
2.8
2.9
3.0
3.1
3.2
3.3
3.4
3.5
3.6
3.7
3.8
3.9
4.0
4.1
4.2
4.3
4.4
4.5
4.6
4.7
4.8
4.9
5.0
5.1
5.2
5.3
5.4
5.5
5.6
5.7
5.8
5.9
6.0
6.1
6.2
6.3
6.4
6.5
6.6

Line 671/87: 6 km/s 1:1 section, original stack

Trace normalization, coherency filtering, trace

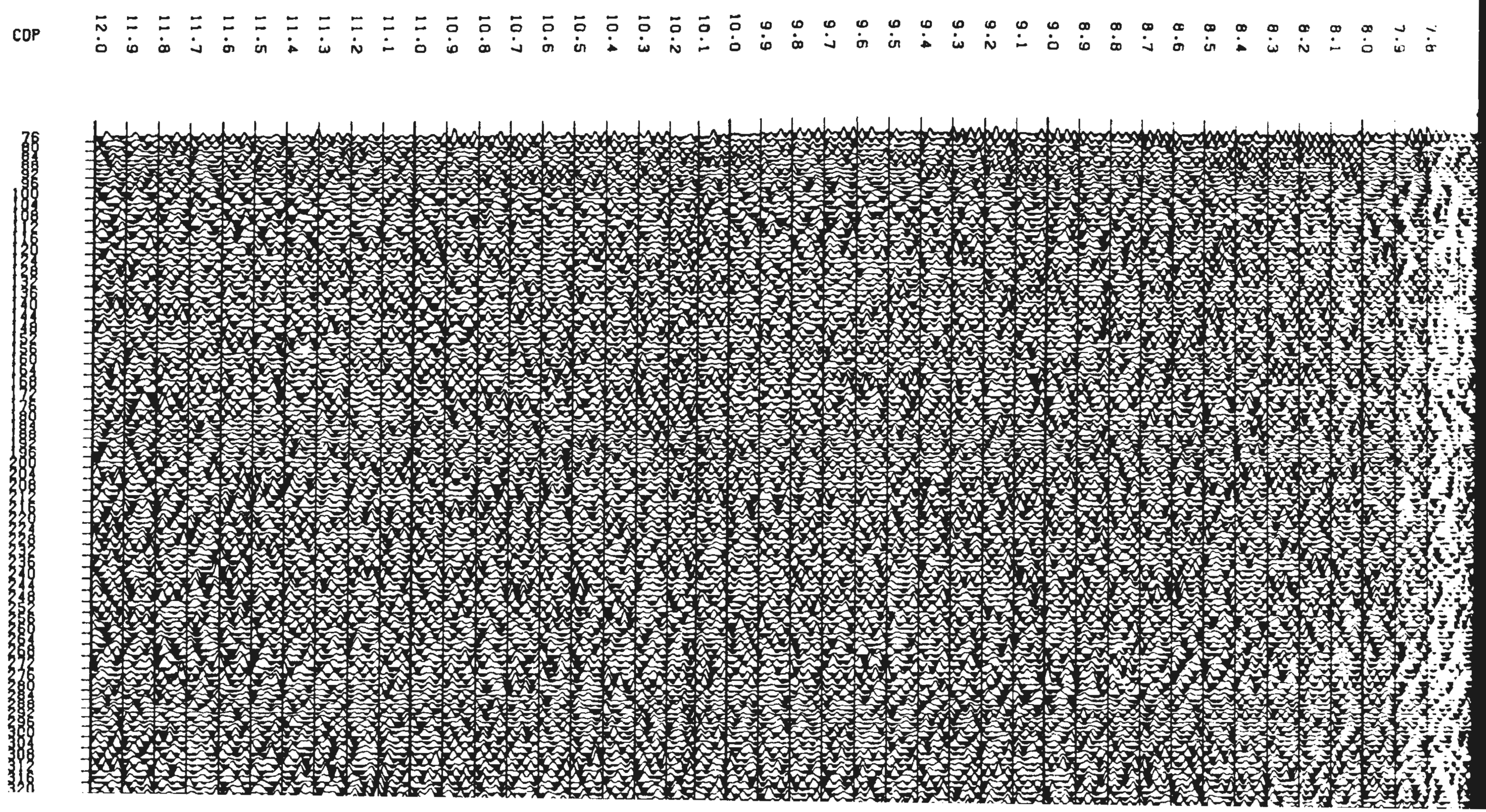

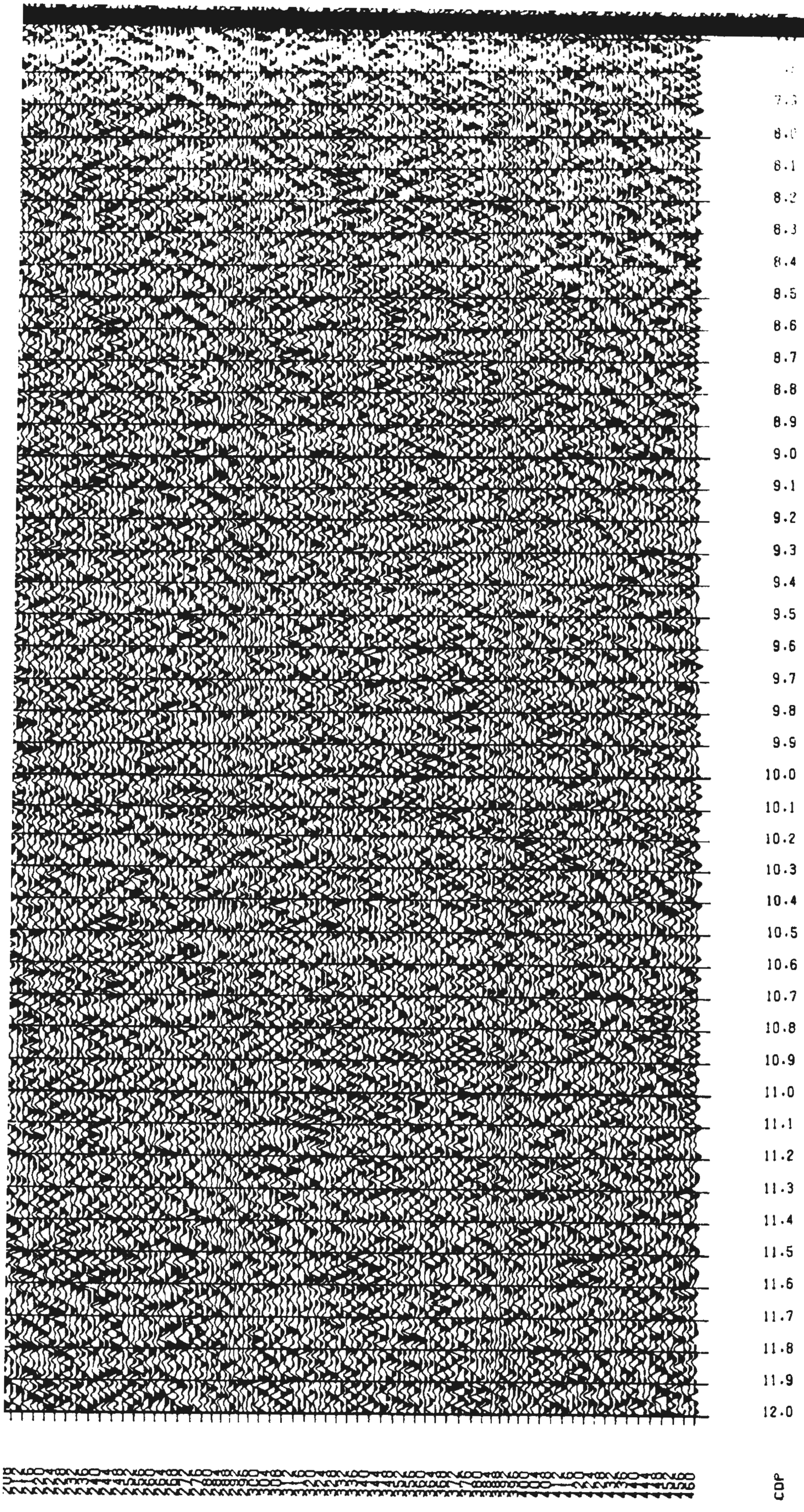

8.1
8.3
8.4
8.5
8.6
8.7
8.8
8.9
9.0
9.1
9.2
9.3
9.4
9.5
9.6
9.7
9.8
9.9
10.0
10.1
10.2
10.3
10.4
10.5
10.6
10.7
10.8
10.9
11.0
11.1
11.2
11.3
11.4
11.5
11.6
11.7
11.8
11.9
12.0
CDP

LINE 671a, original stack

Horizontally normalized and coherency filtered ...

For v = 6 km/s, 1 cm = 0.5 km

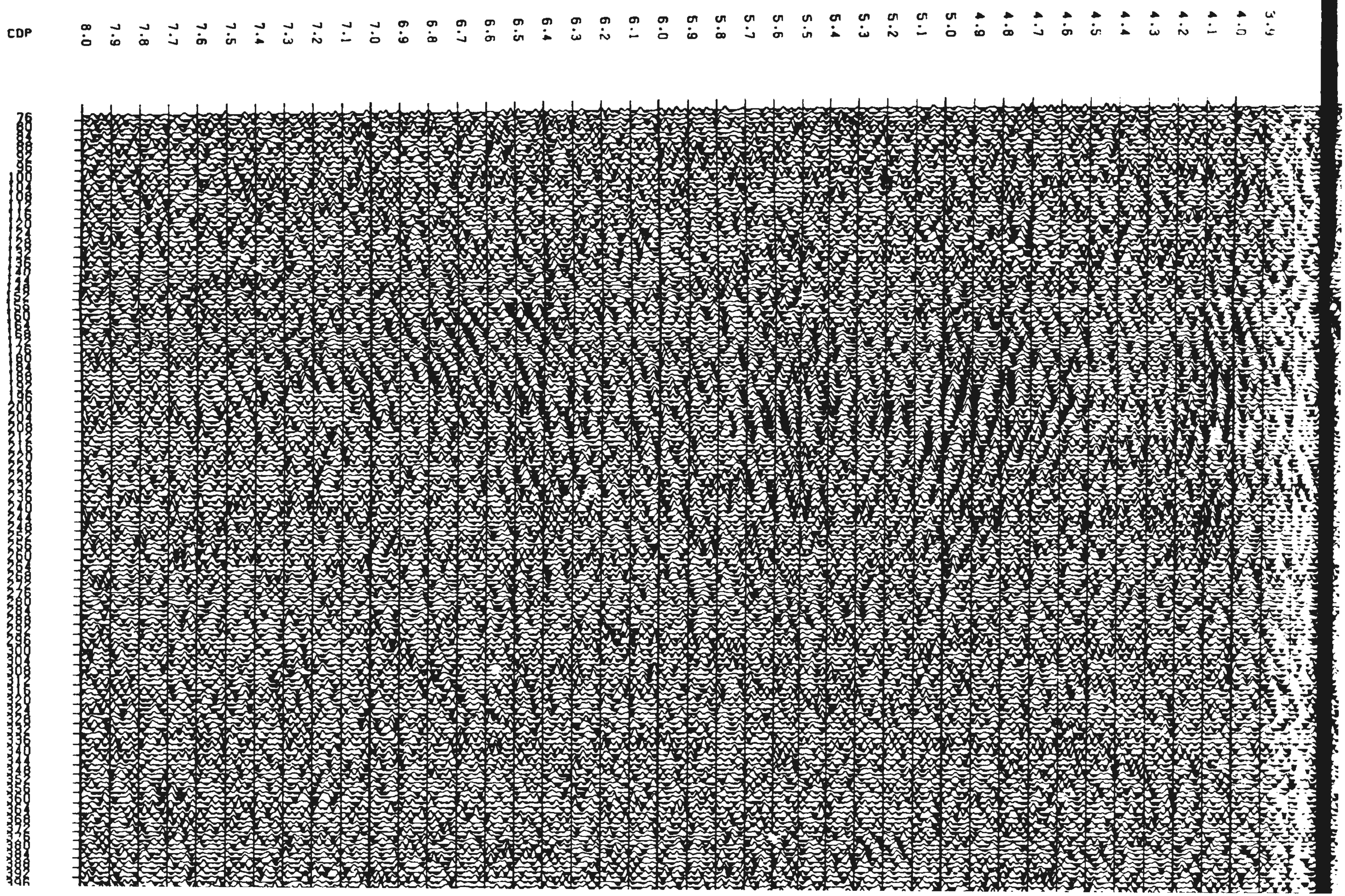

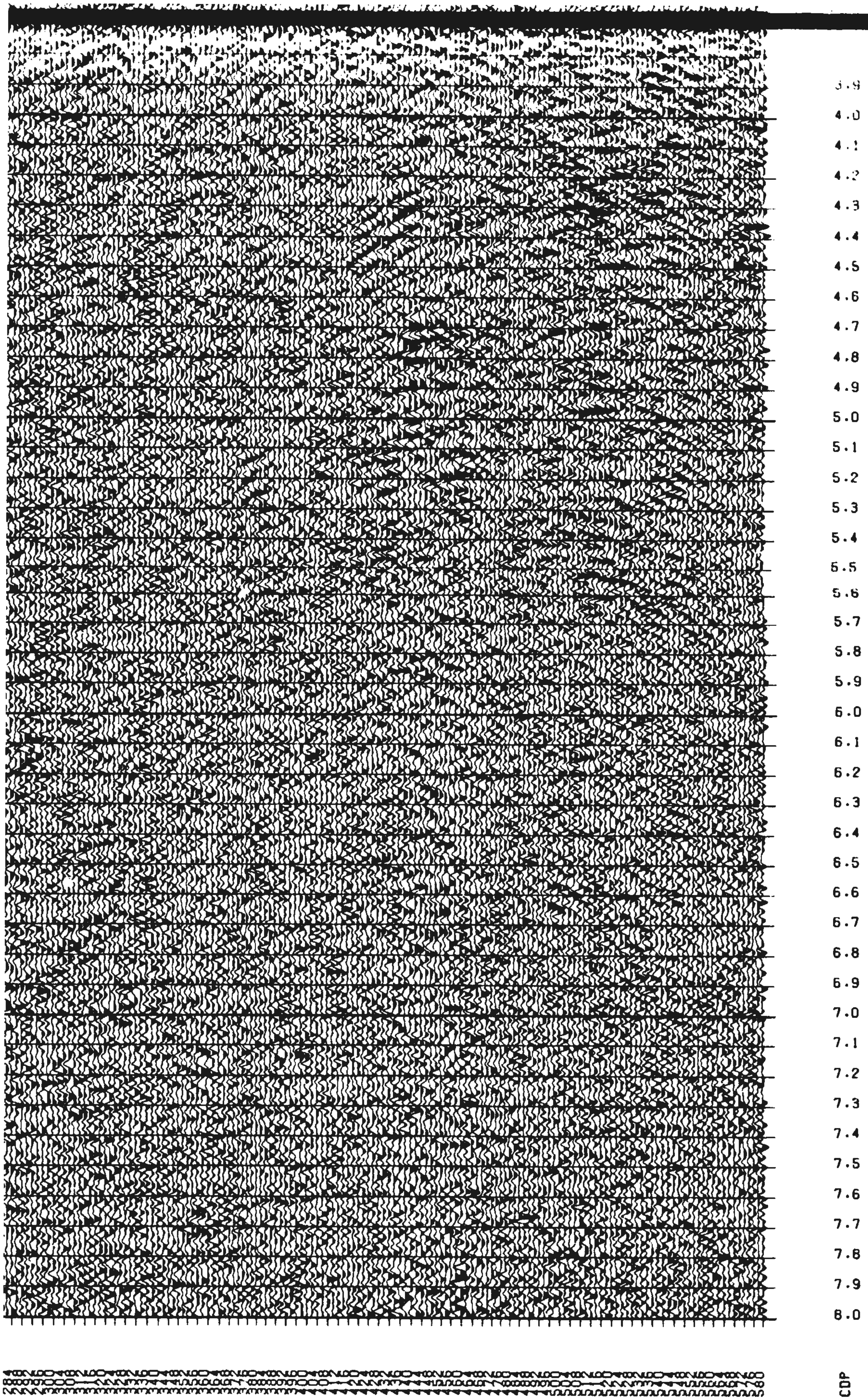
3.9
4.0
4.1
4.2
4.3
4.4
4.5
4.6
4.7
4.8
4.9
5.0
5.1
5.2
5.3
5.4
5.5
5.6
5.7
5.8
5.9
6.0
6.1
6.2
6.3
6.4
6.5
6.6
6.7
6.8
6.9
7.0
7.1
7.2
7.3
7.4
7.5
7.6
7.7
7.8
7.9
8.0
CDP

ering applied on reprocessed data

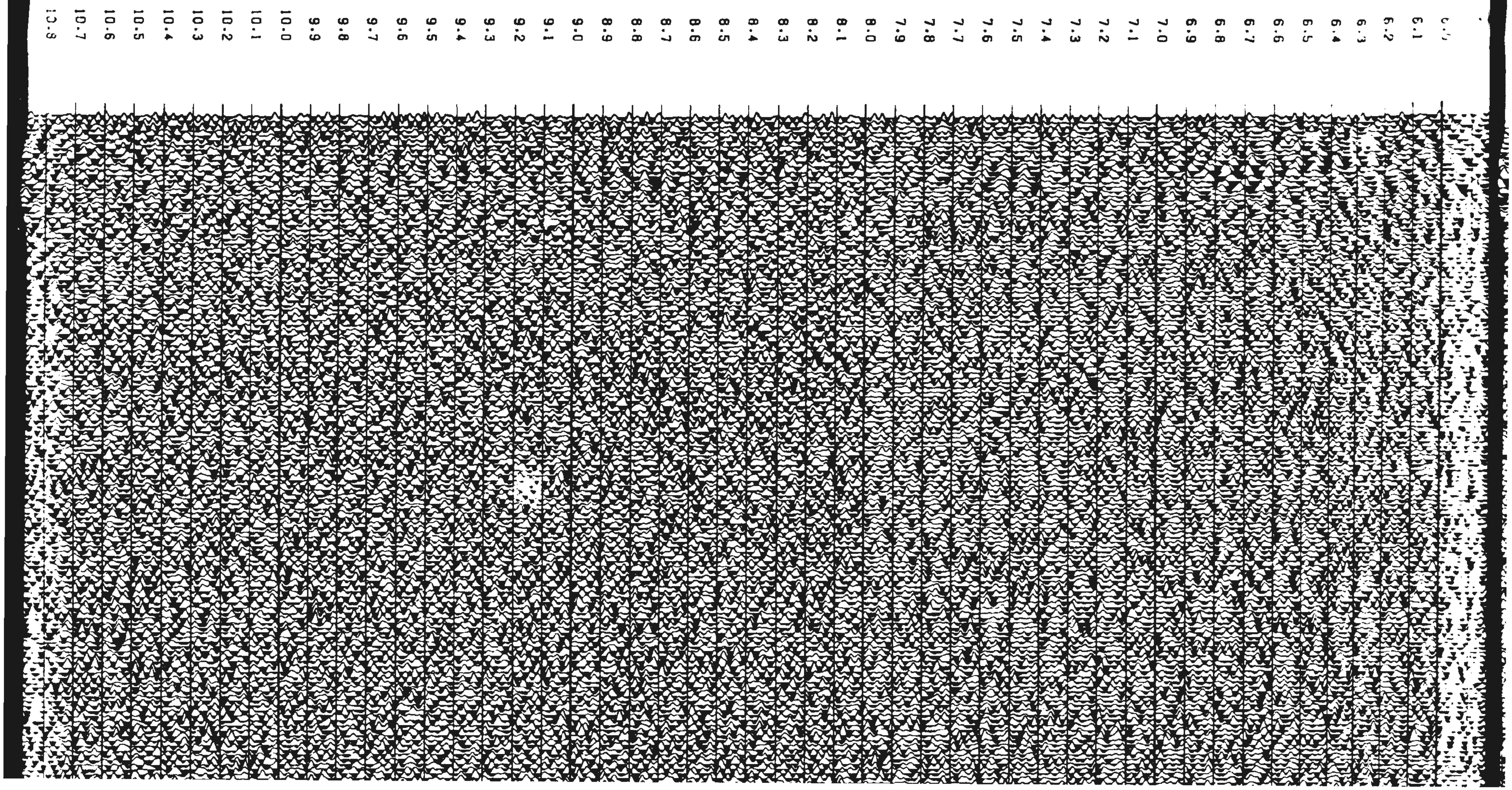

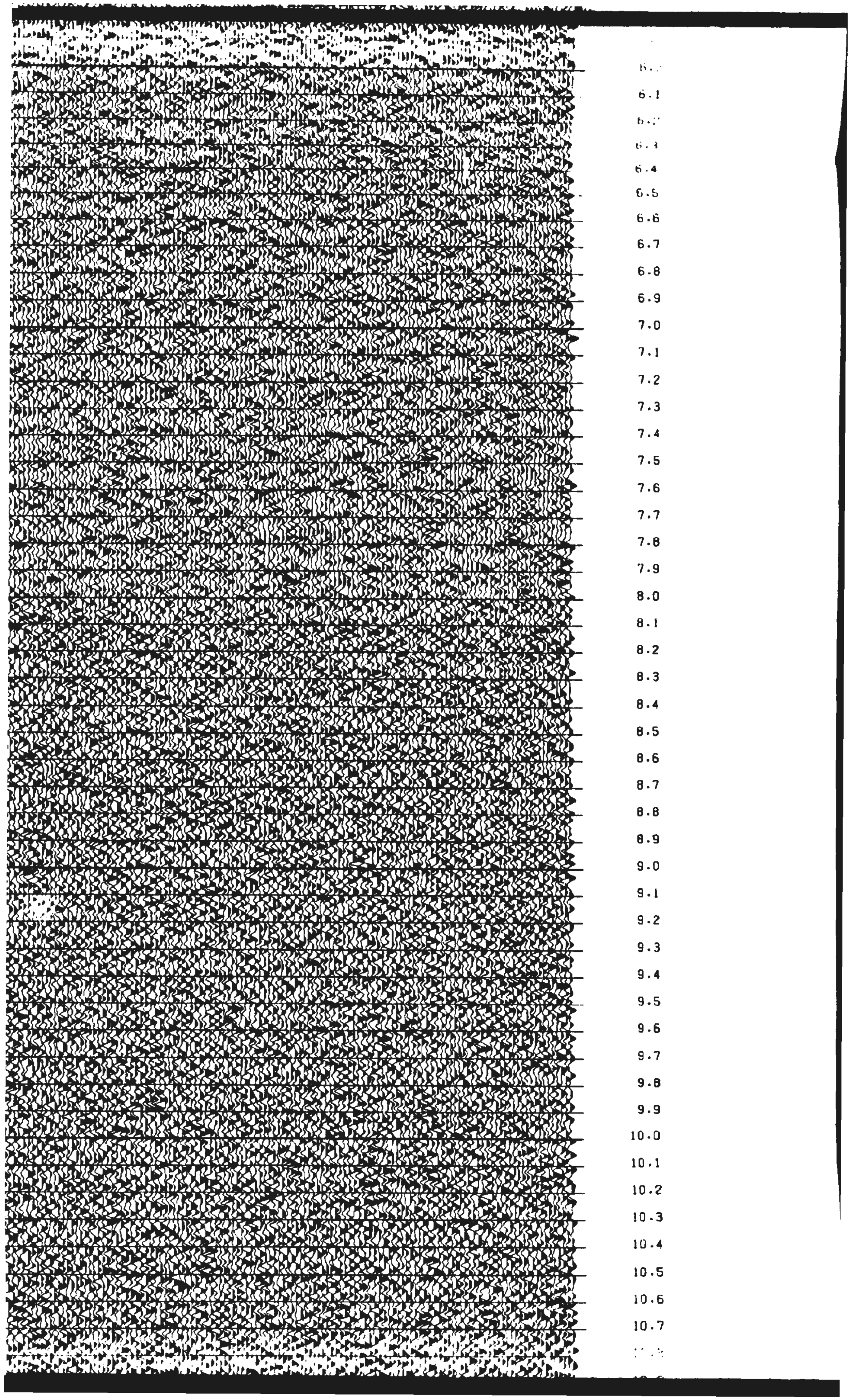
6.1
6.4
6.5
6.6
6.7
6.8
6.9
7.0
7.1
7.2
7.3
7.4
7.5
7.6
7.7
7.8
7.9
8.0
8.1
8.2
8.3
8.4
8.5
8.6
8.7
8.8
8.9
9.0
9.1
9.2
9.3
9.4
9.5
9.6
9.7
9.8
9.9
10.0
10.1
10.2
10.3
10.4
10.5
10.6
10.7

Line 671/87
Coherency filtering applied on reprocessed data

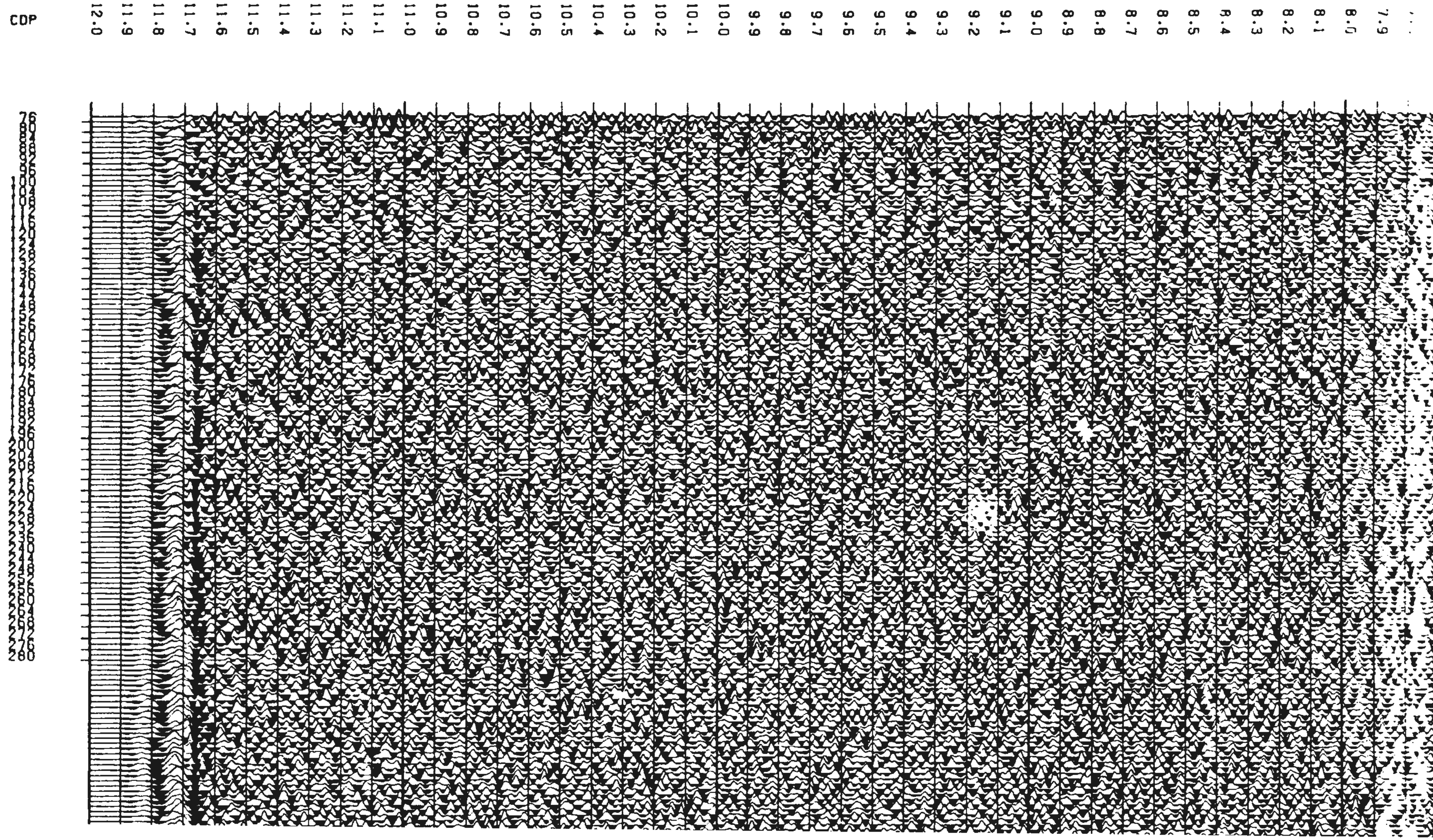

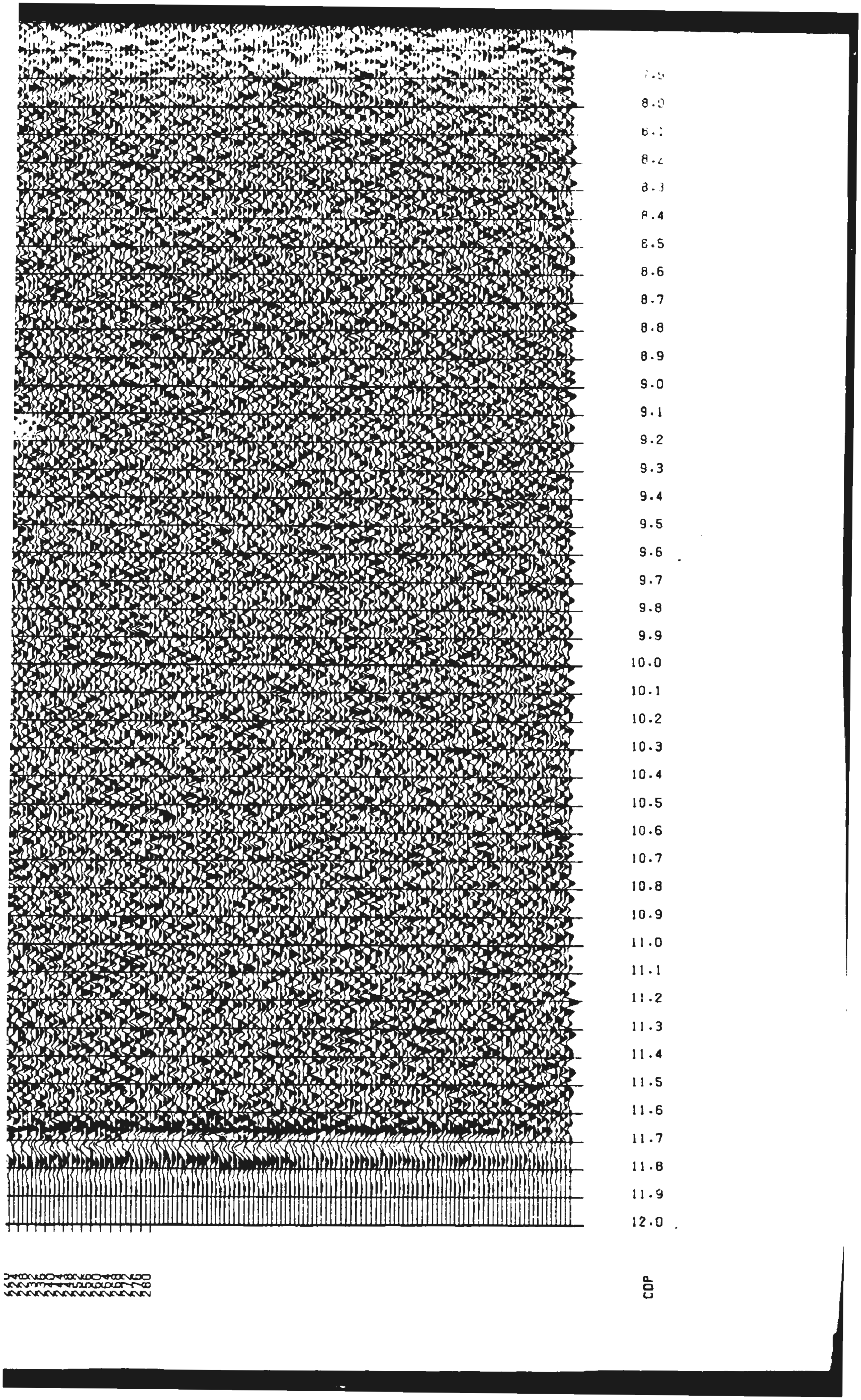

8.0
8.1
8.2
8.3
8.4
8.5
8.6
8.7
8.8
8.9
9.0
9.1
9.2
9.3
9.4
9.5
9.6
9.7
9.8
9.9
10.0
10.1
10.2
10.3
10.4
10.5
10.6
10.7
10.8
10.9
11.0
11.1
11.2
11.3
11.4
11.5
11.6
11.7
11.8
11.9
12.0
CDP

Plate 4: Line 689/87. Pre-stack processing by Geofyzika Brno.

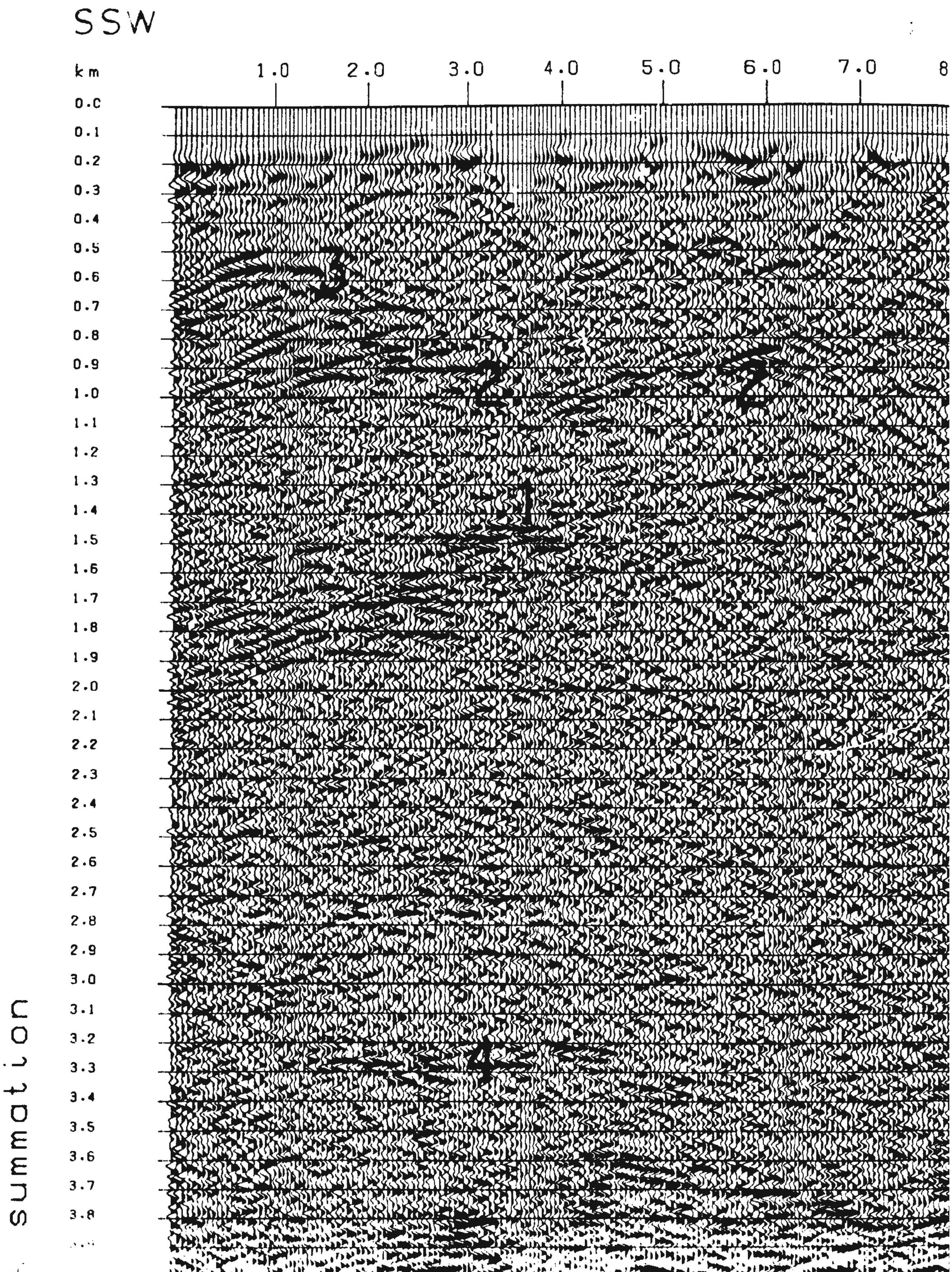

SSW
km
1.0
2.0
3.0
4.0
5.0
6.0
7.0
8
0.0
0.1
0.2
0.3
0.4
0.5
0.6
0.7
0.8
0.9
1.0
1.1
1.2
1.3
1.4
1.5
1.6
1.7
1.8
1.9
2.0
2.1
2.2
2.3
2.4
2.5
2.6
2.7
2.8
2.9
3.0
3.1
3.2
3.3
3.4
3.5
3.6
3.7
3.8
3
2
2
1
4
summation

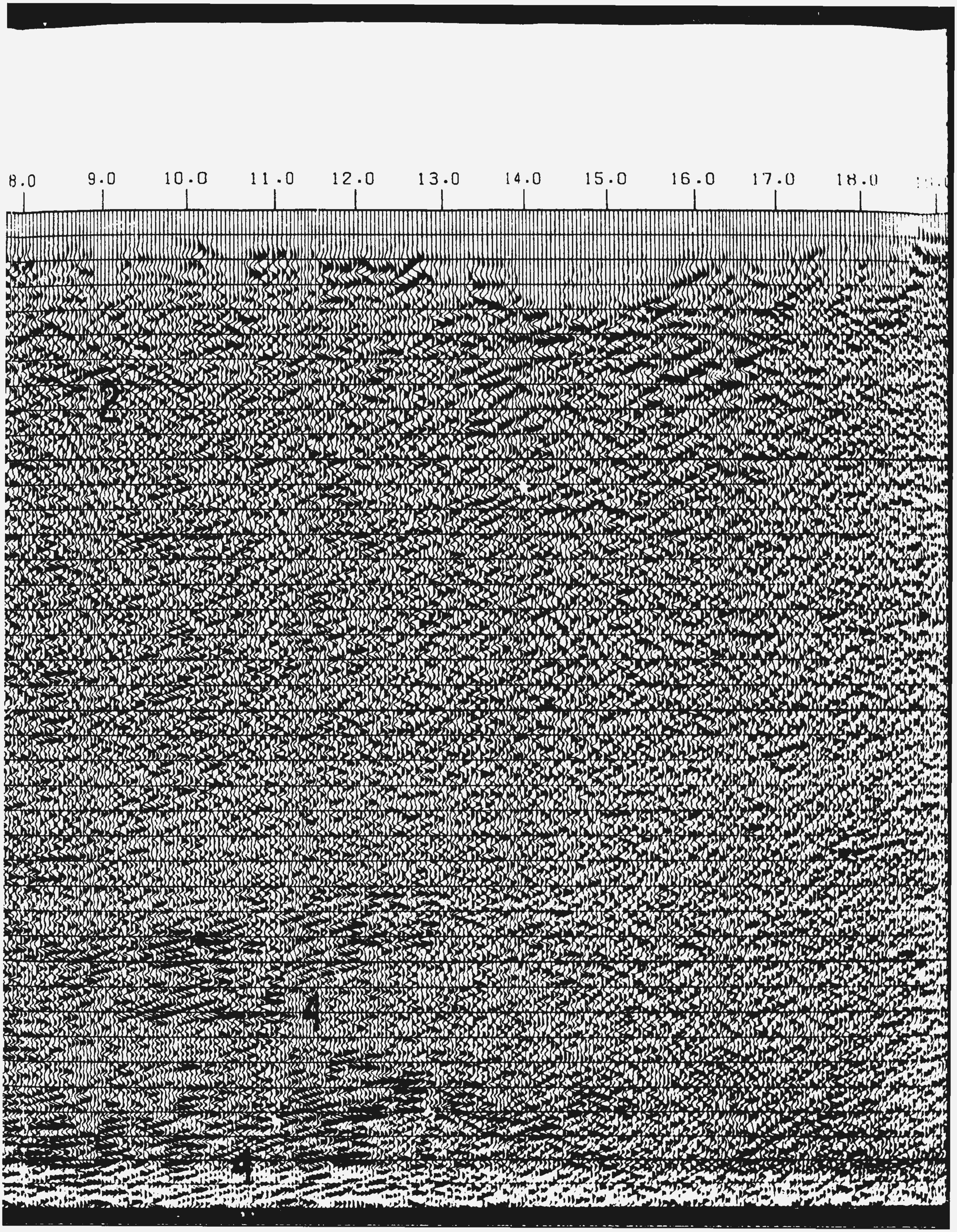
8.0
9.0
10.0
11.0
12.0
13.0
14.0
15.0
16.0
17.0
18.0

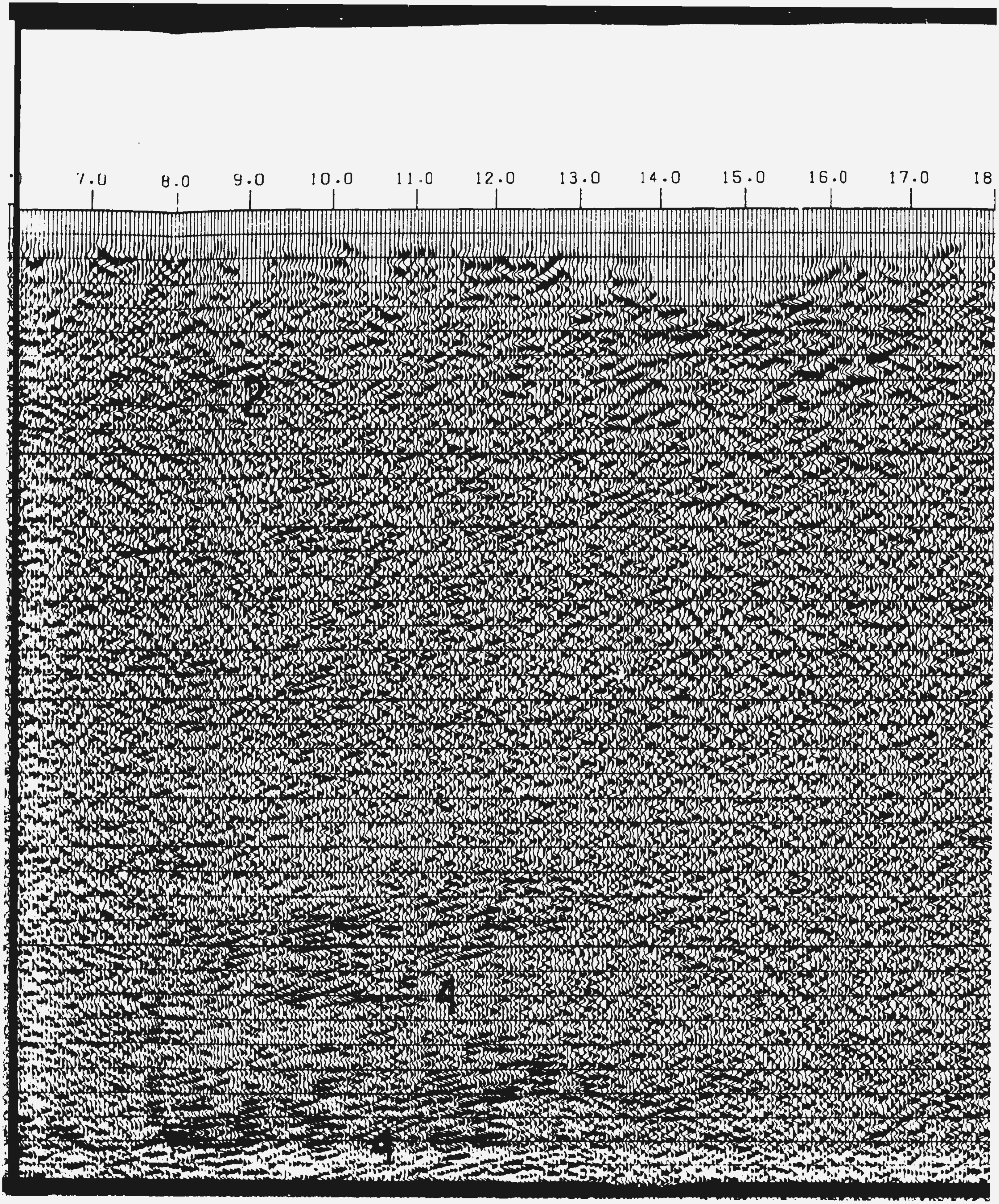
7.0
8.0
9.0
10.0
11.0
12.0
13.0
14.0
15.0
16.0
17.0
18
2
4

Plate 4: Line 689/87. Pre-stack processing by Geofyzika Brno. Events 1 are thrust planes within the Modra massif of the Envelope nappe, though the 1 at the left edge of the plate may be the base of the Modra massif. Events 2 are segments of the thrust plane between the Modra massif and overlying Bratislava massif. Event 3 is a conjugated fault to event 2. Events 4 are shear zones.

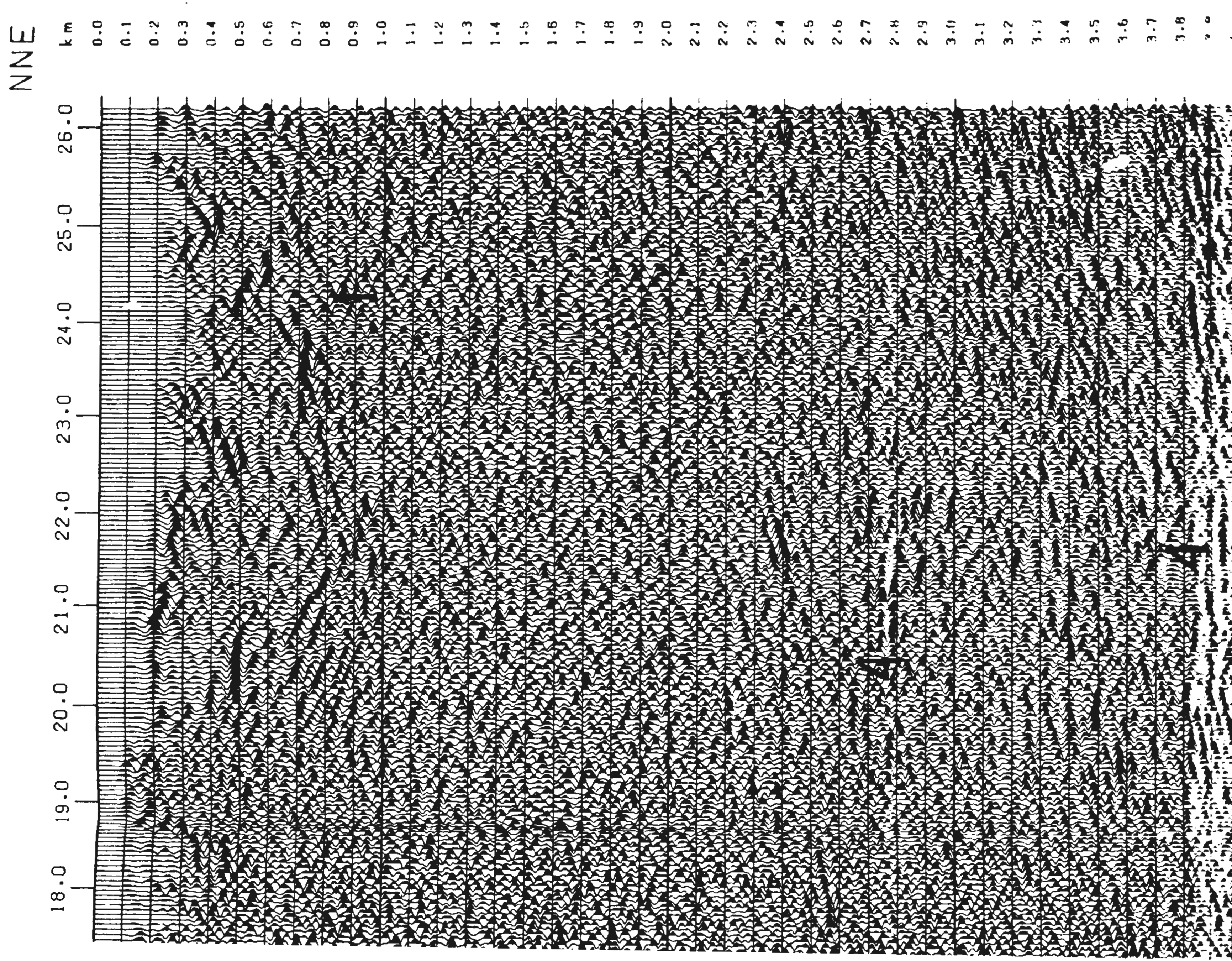

Plate 6: Reprocessed section of line 671A/87.

Plate 6: Reproocessed section of line 671A/87. Events 1 a
trailing fan of Late Cretaceous age that may have been rea
Events 2 are conjugated faults to events 1. Event 3 are thru
age. Events 4 are shear zones. Event 5 may be a segme
angle normal faults as these seen on lines 3T and 689/87. E
short reflectors interpreted as the interface between Middle
gravel and ovelying Middle Miocene calcareous sandy clay
crystalline basement of the West Danube margin.

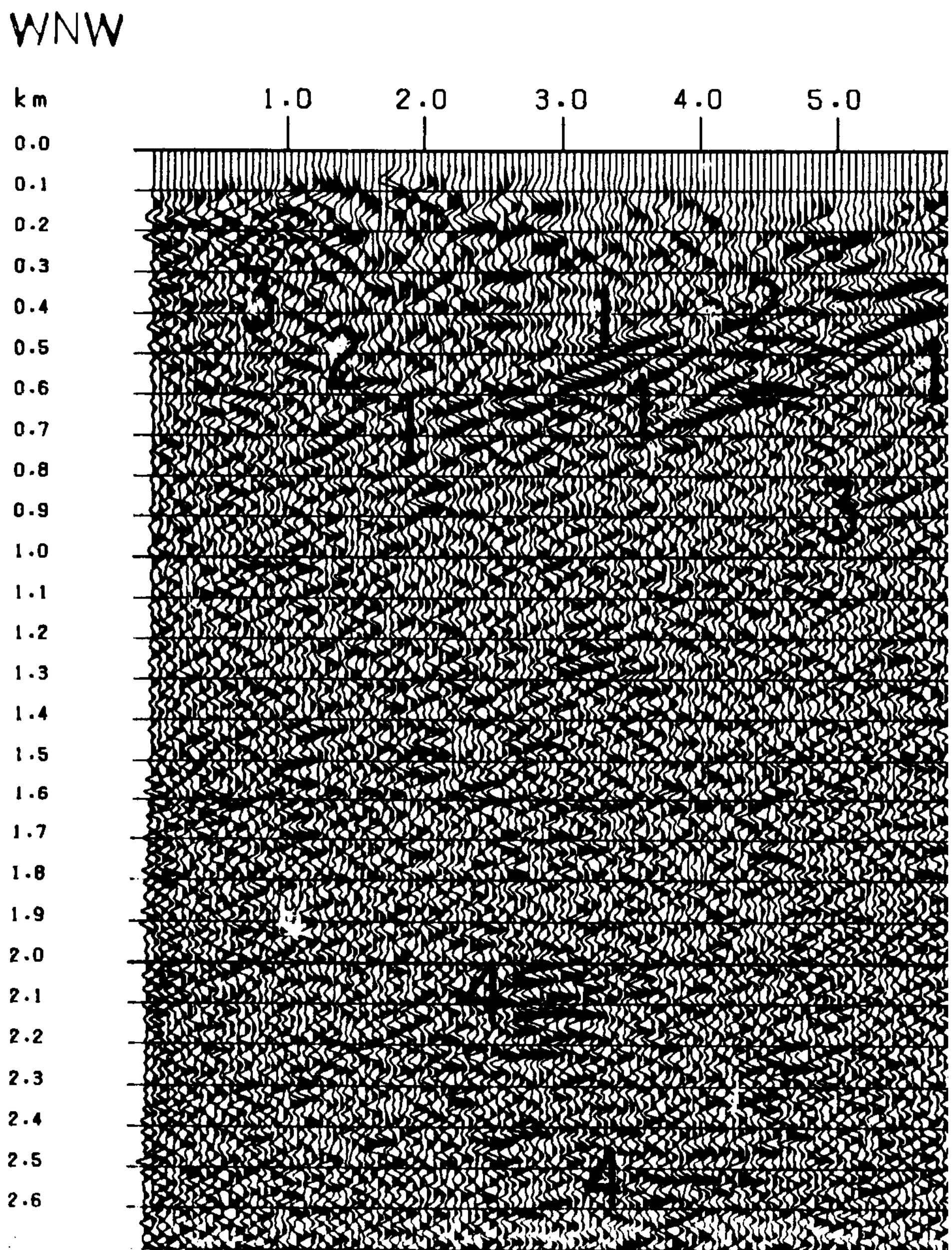

;ment of an imbricate
ed in Early Miocene.
es of Late Cretaceous
the same kind of low
6 and 7 are groups of
ene conglomerate and
:nt 8 is the top of the

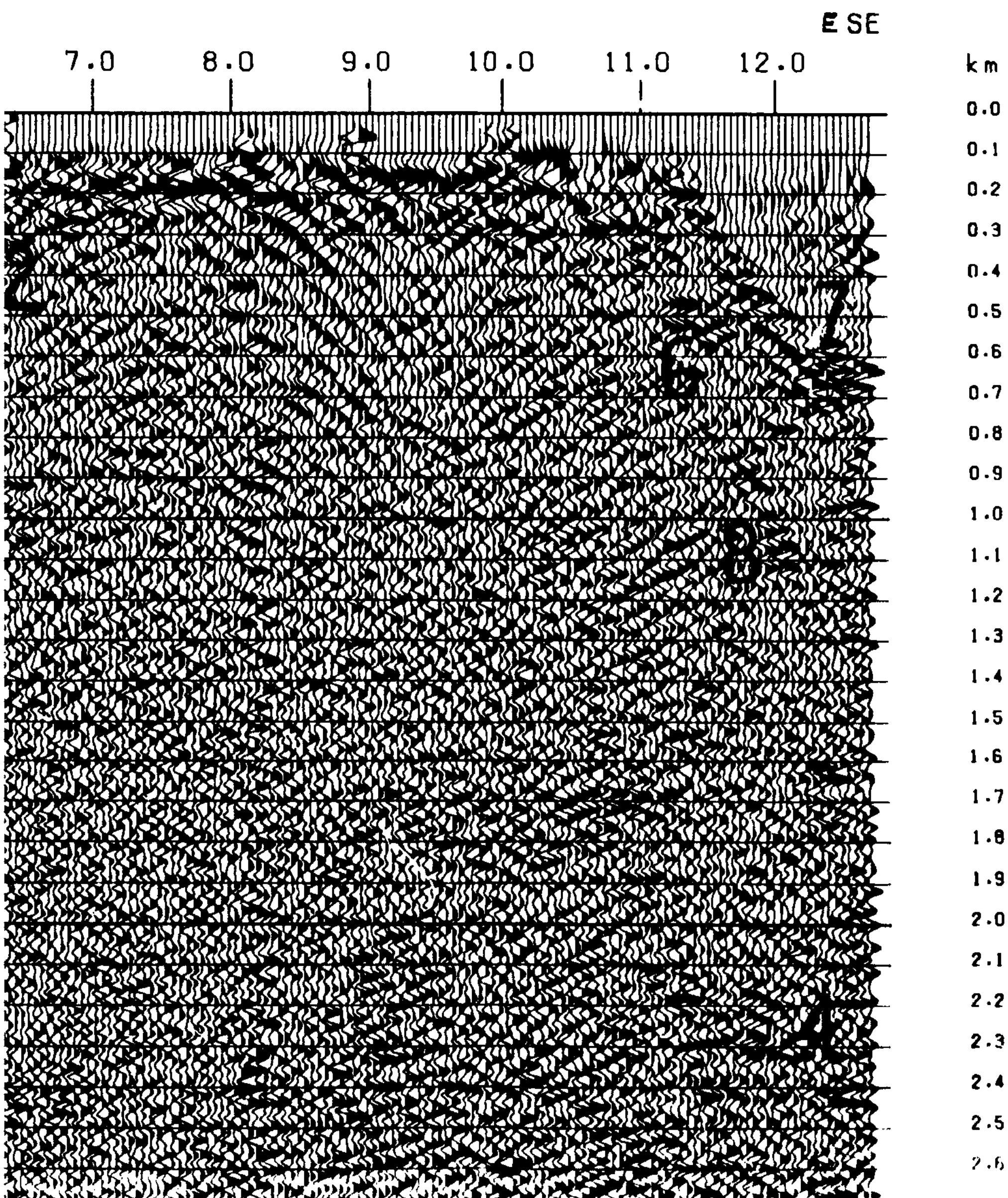

6 km/s 1:1 original section
ization, bandpass filtering, trace summation

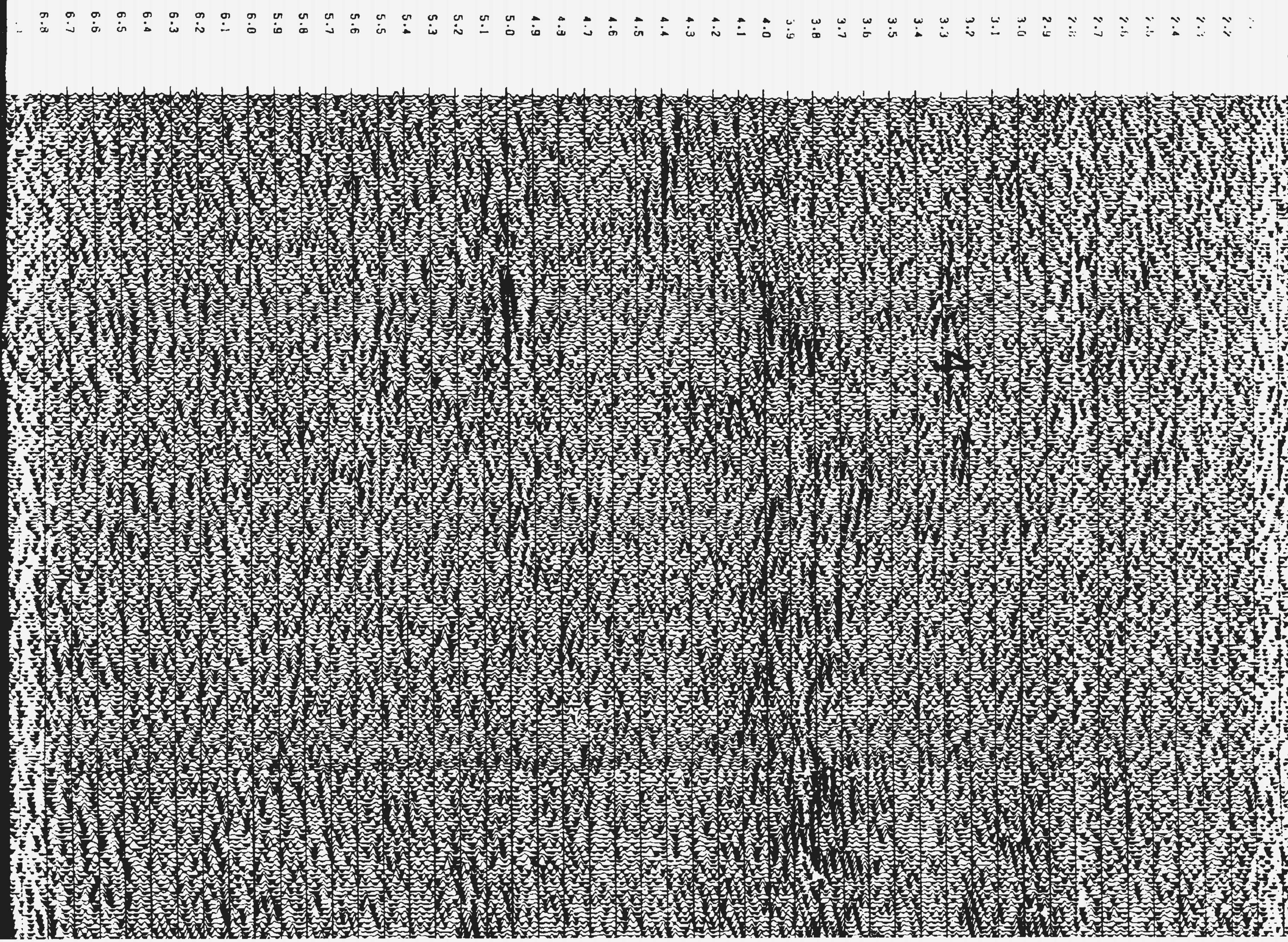

-89/87. Pre-stack processing by Geofyzika Brno. Events 1 are thrust
e Modra massif of the Envelope nappe, though the 1 at the left edge of
e the base of the Modra massif. Events 2 are segments of the thrust plane
dra massif and overlying Bratislava massif. Event 3 is a conjugated fault
ents 4 are shear zones.

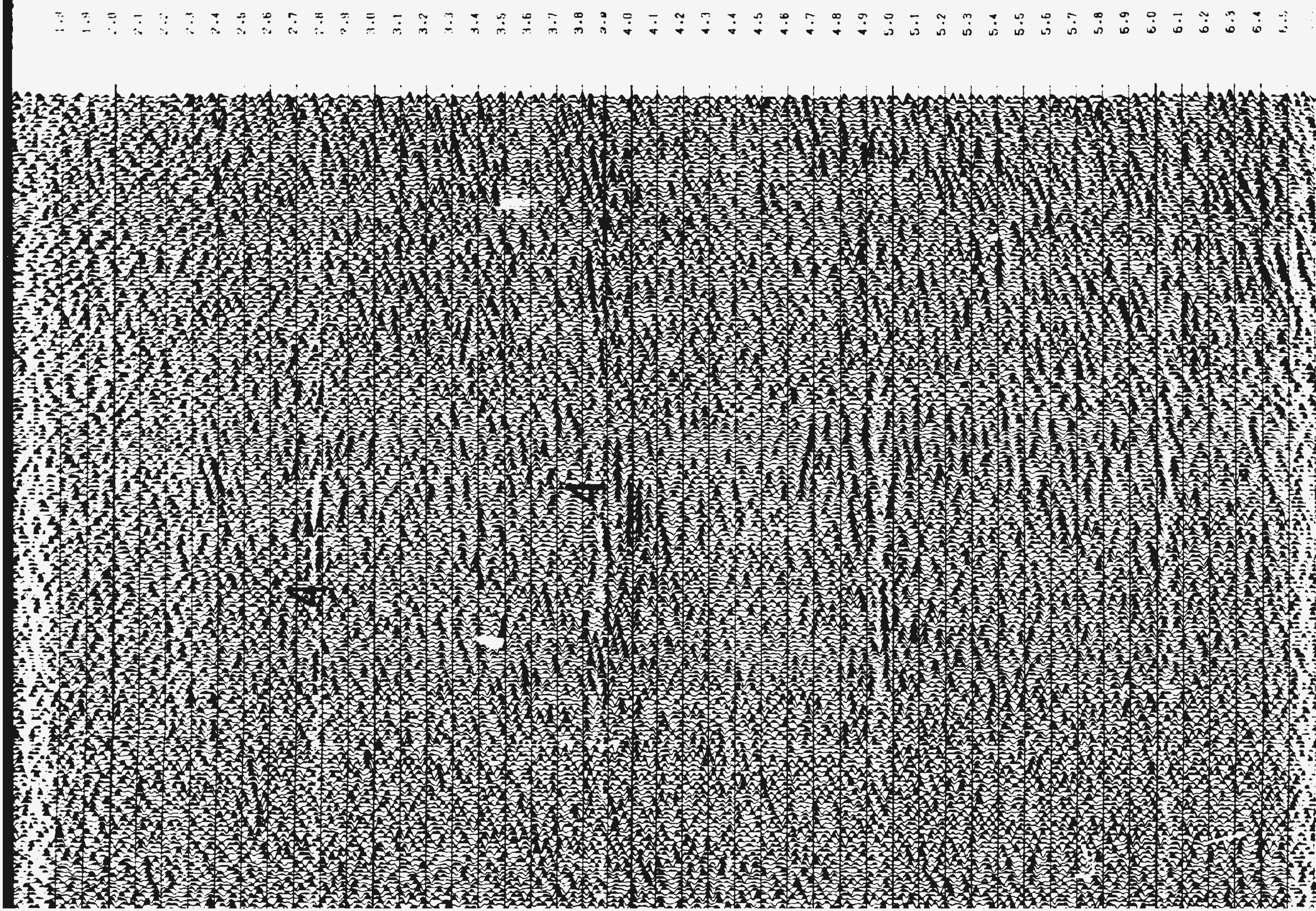

and coherency filtered traces
0.5 km

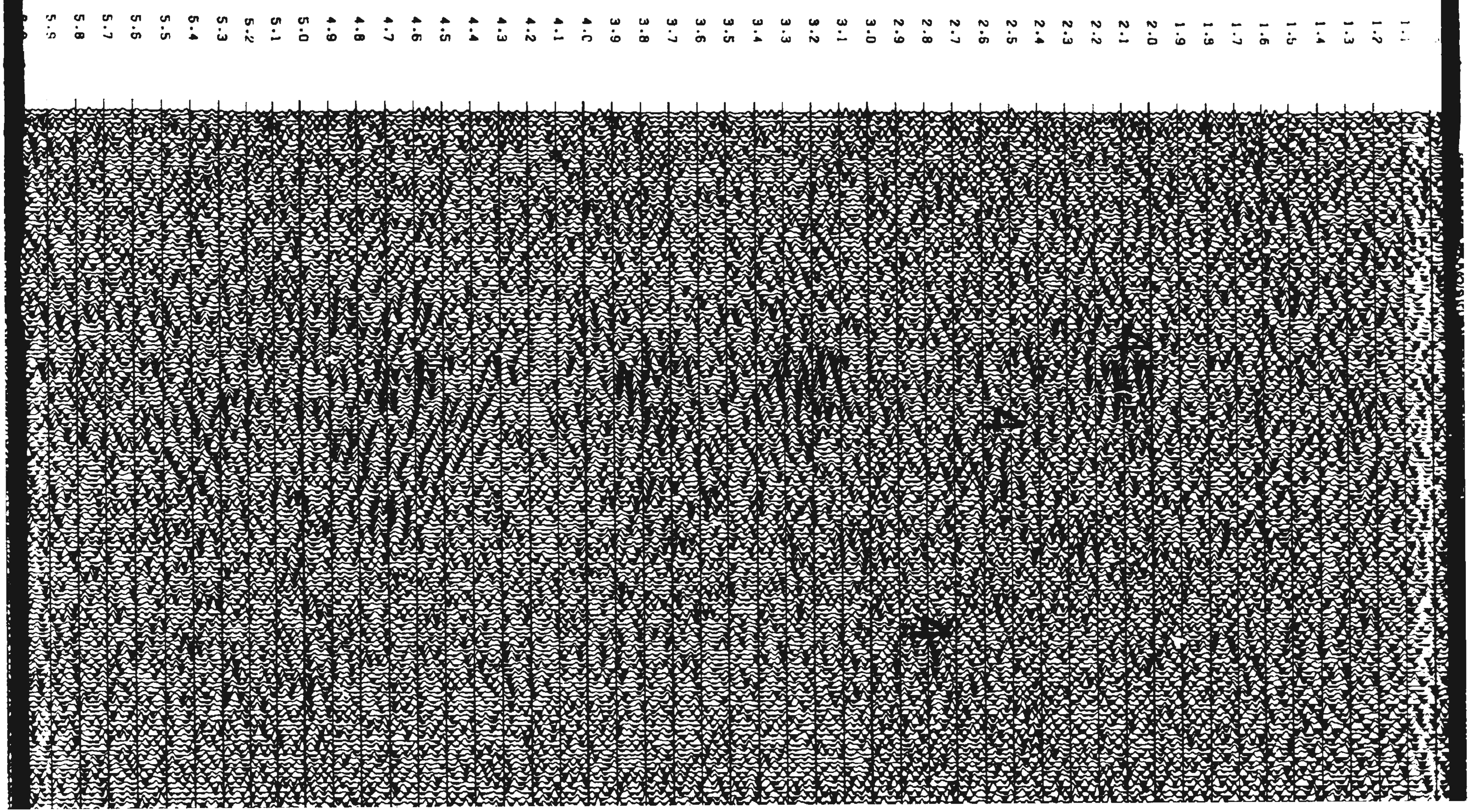

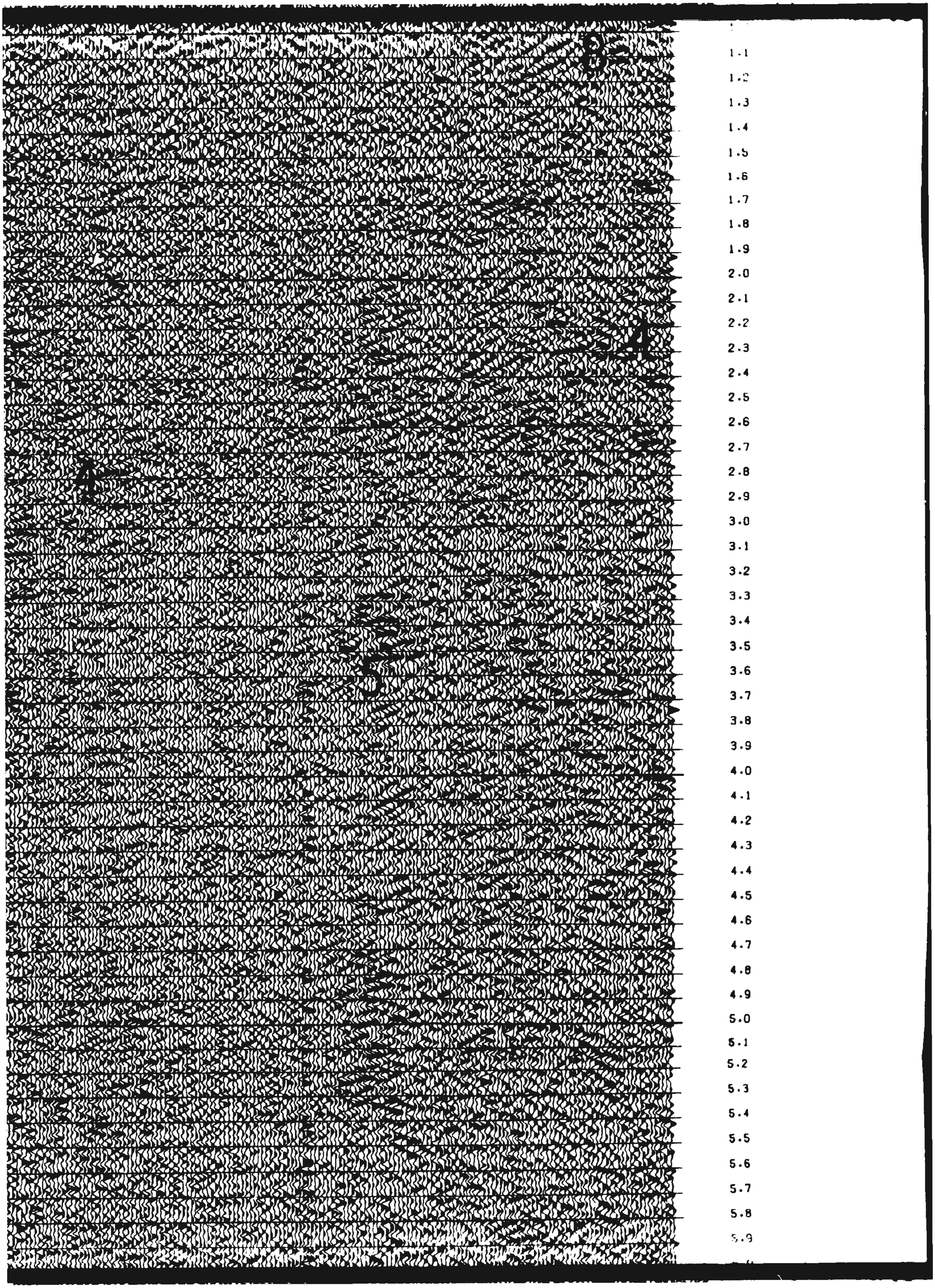
1.1
1.2
1.3
1.4
1.5
1.6
1.7
1.8
1.9
2.0
2.1
2.2
2.3
2.4
2.5
2.6
2.7
2.8
2.9
3.0
3.1
3.2
3.3
3.4
3.5
3.6
3.7
3.8
3.9
4.0
4.1
4.2
4.3
4.4
4.5
4.6
4.7
4.8
4.9
5.0
5.1
5.2
5.3
5.4
5.5
5.6
5.7
5.8
5.9

Line 689/87: 6 km/s 1:1 original section
Trace normalization, bandpass filtering, trace s

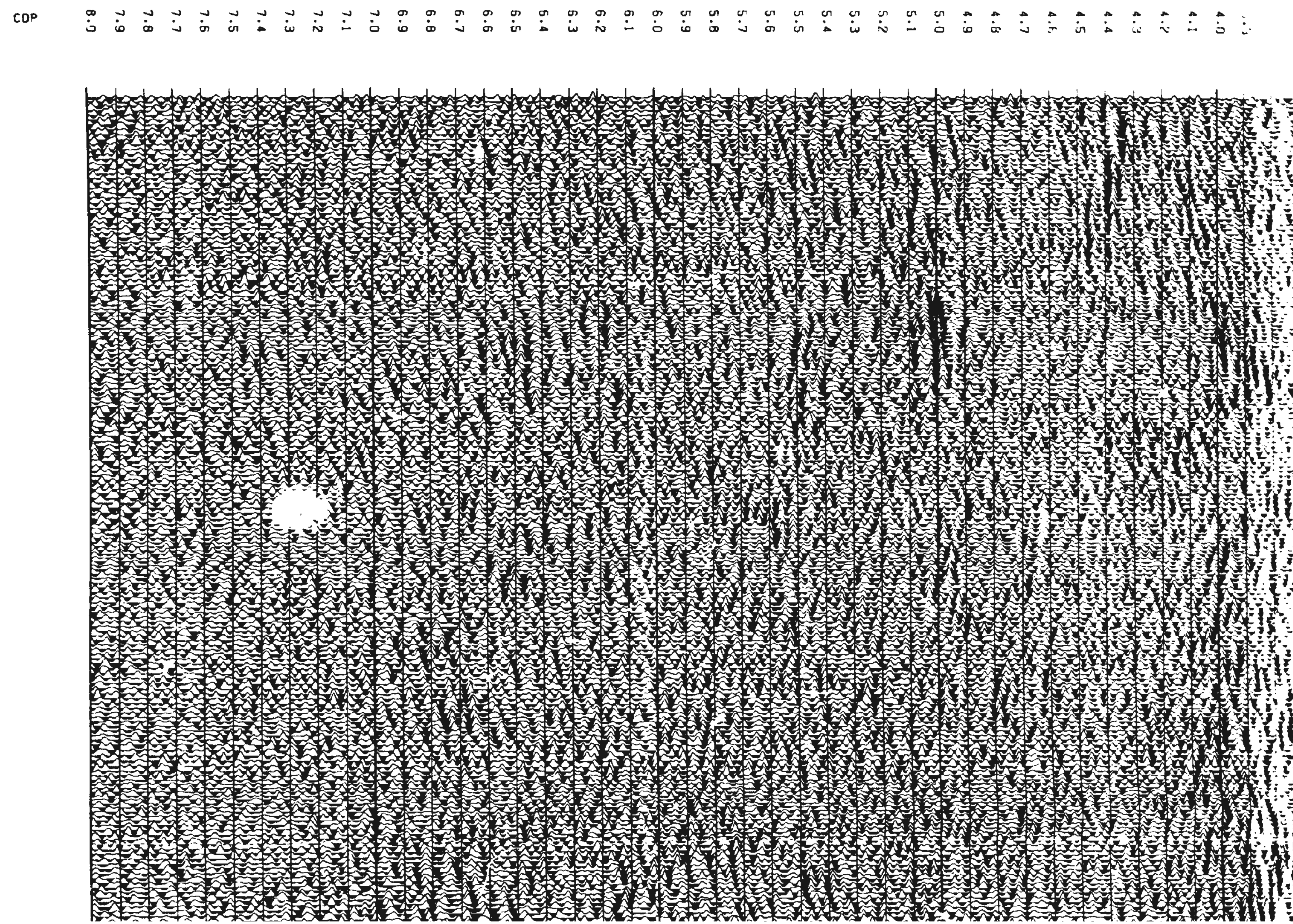

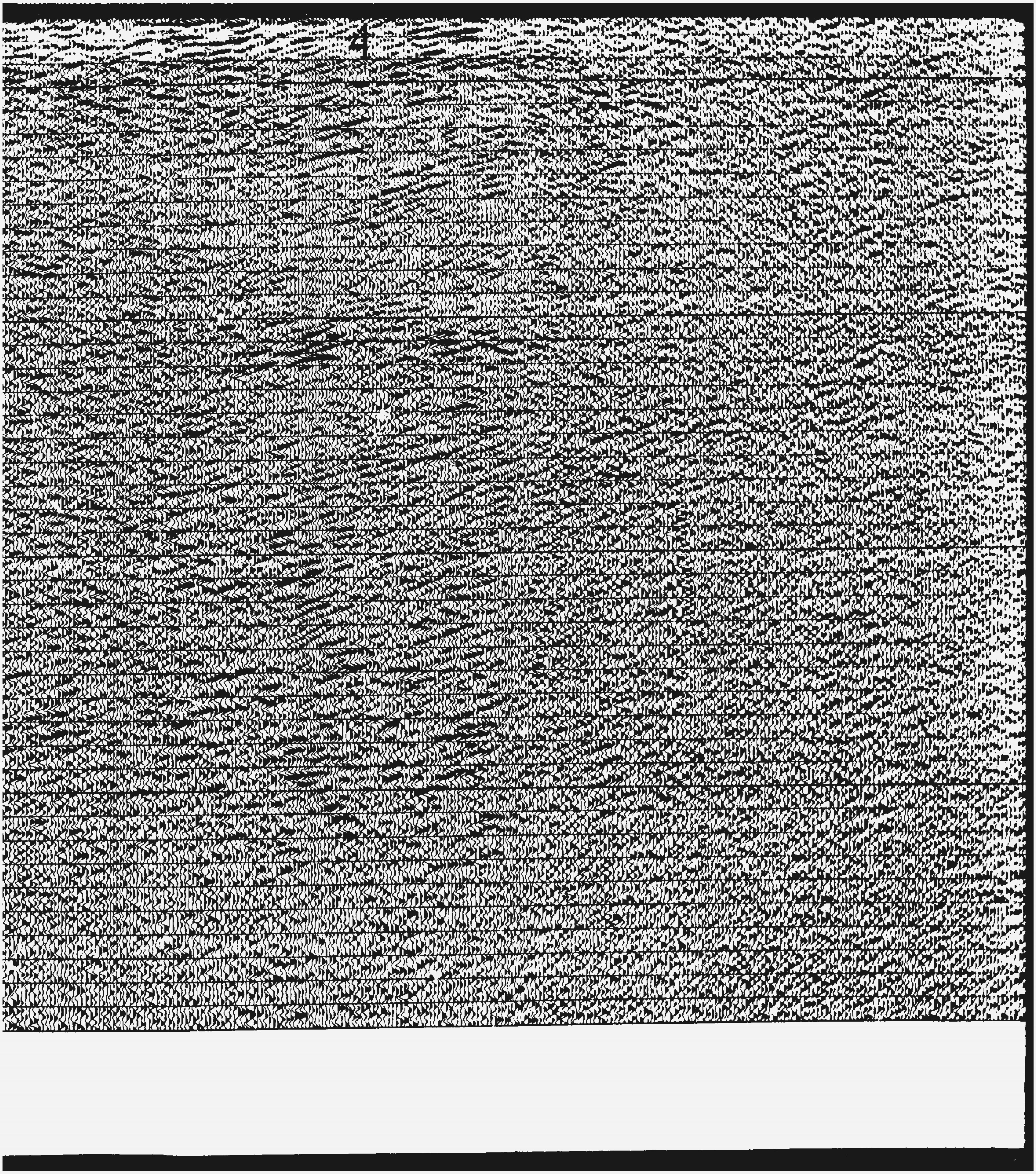

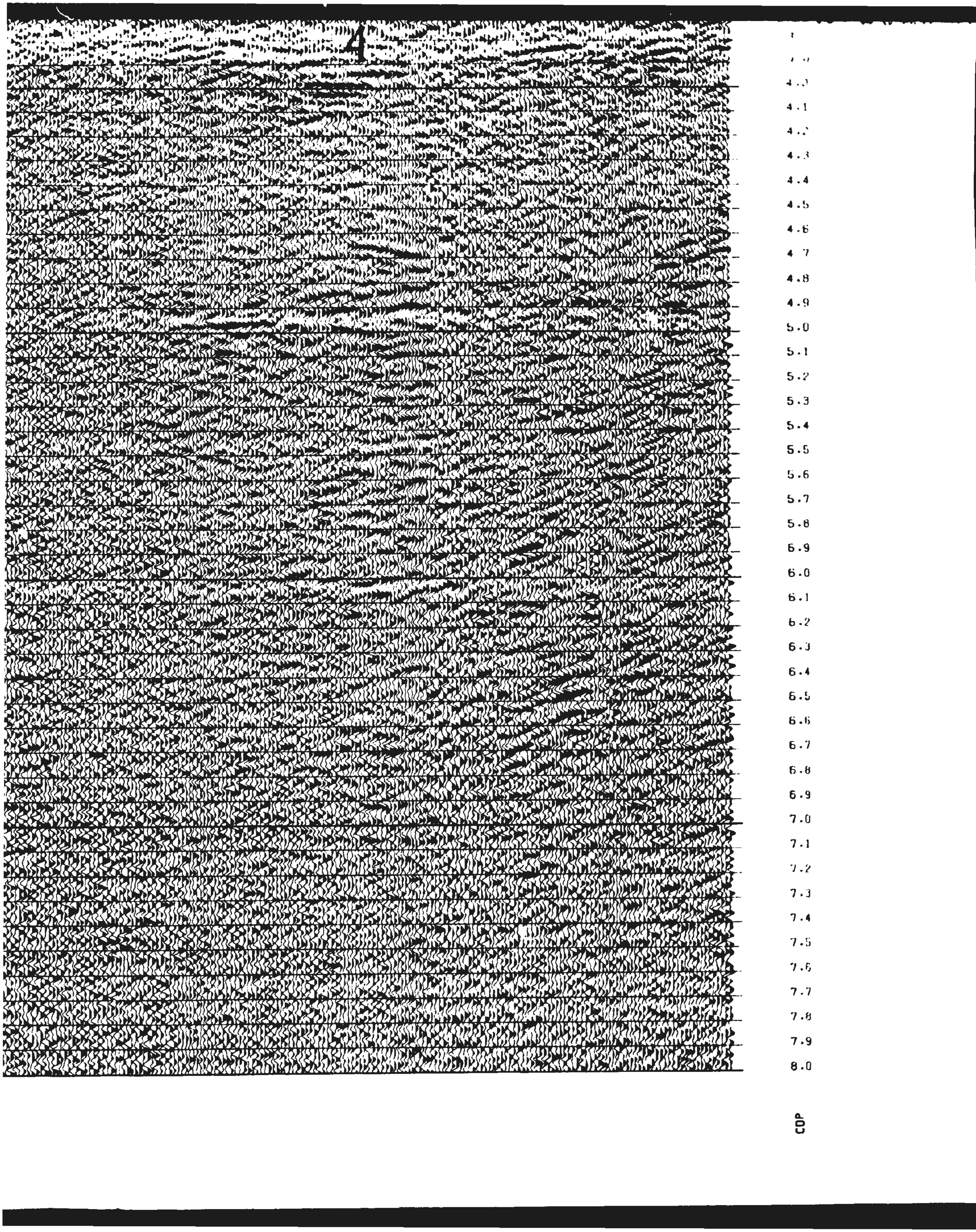
4
4.1
4.4
4.5
4.6
4.8
4.9
5.0
5.1
5.2
5.3
5.4
5.5
5.6
5.7
5.8
6.0
6.1
6.2
6.3
6.4
6.5
6.6
6.7
6.8
6.9
7.0
7.1
7.2
7.3
7.4
7.5
7.6
7.7
7.8
7.9
8.0
CDP

LINE 671a
Horizontally normalized and coherency filtered t
For v = 6 km/s, 1 cm = 0.5 km

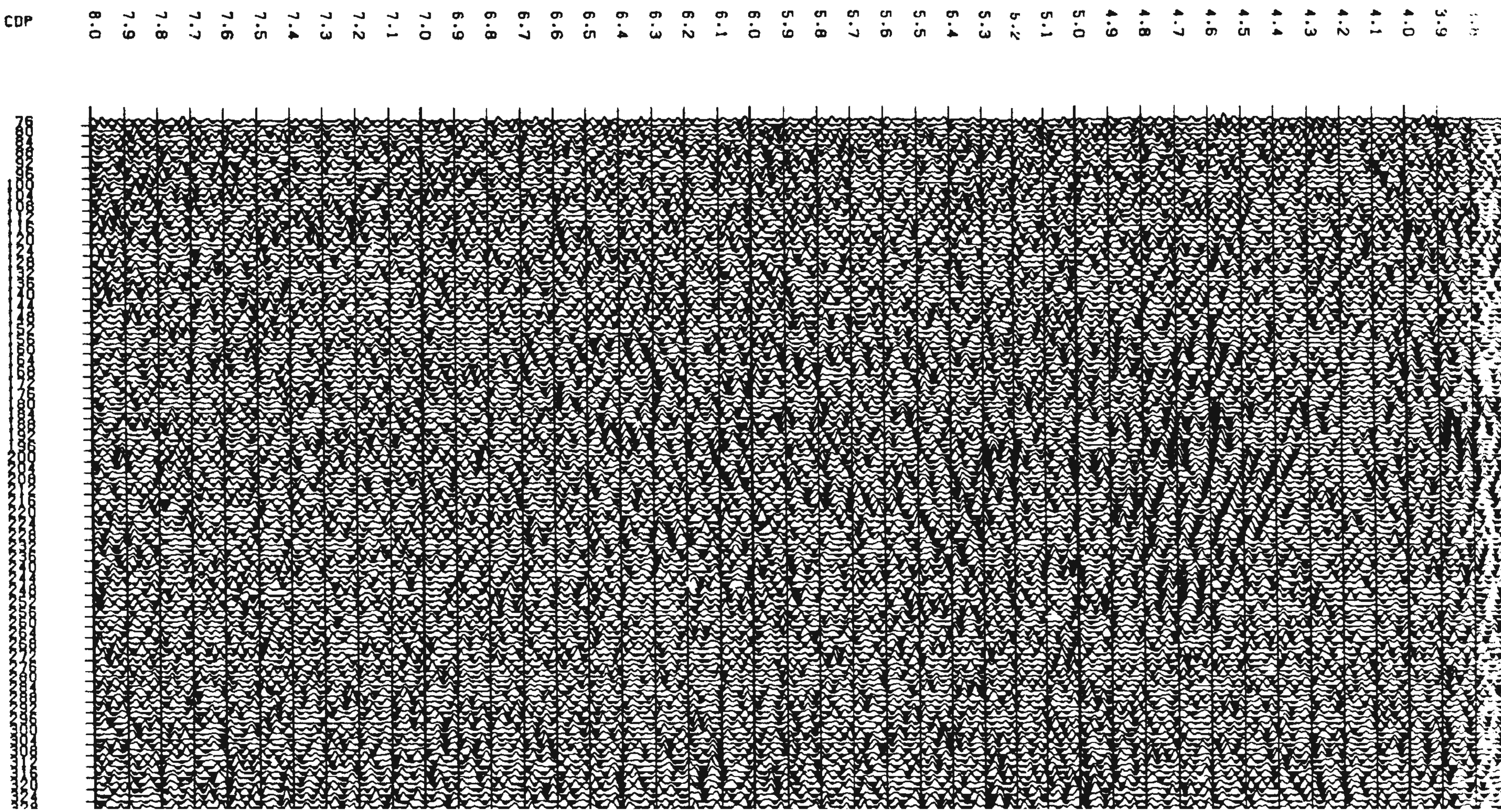

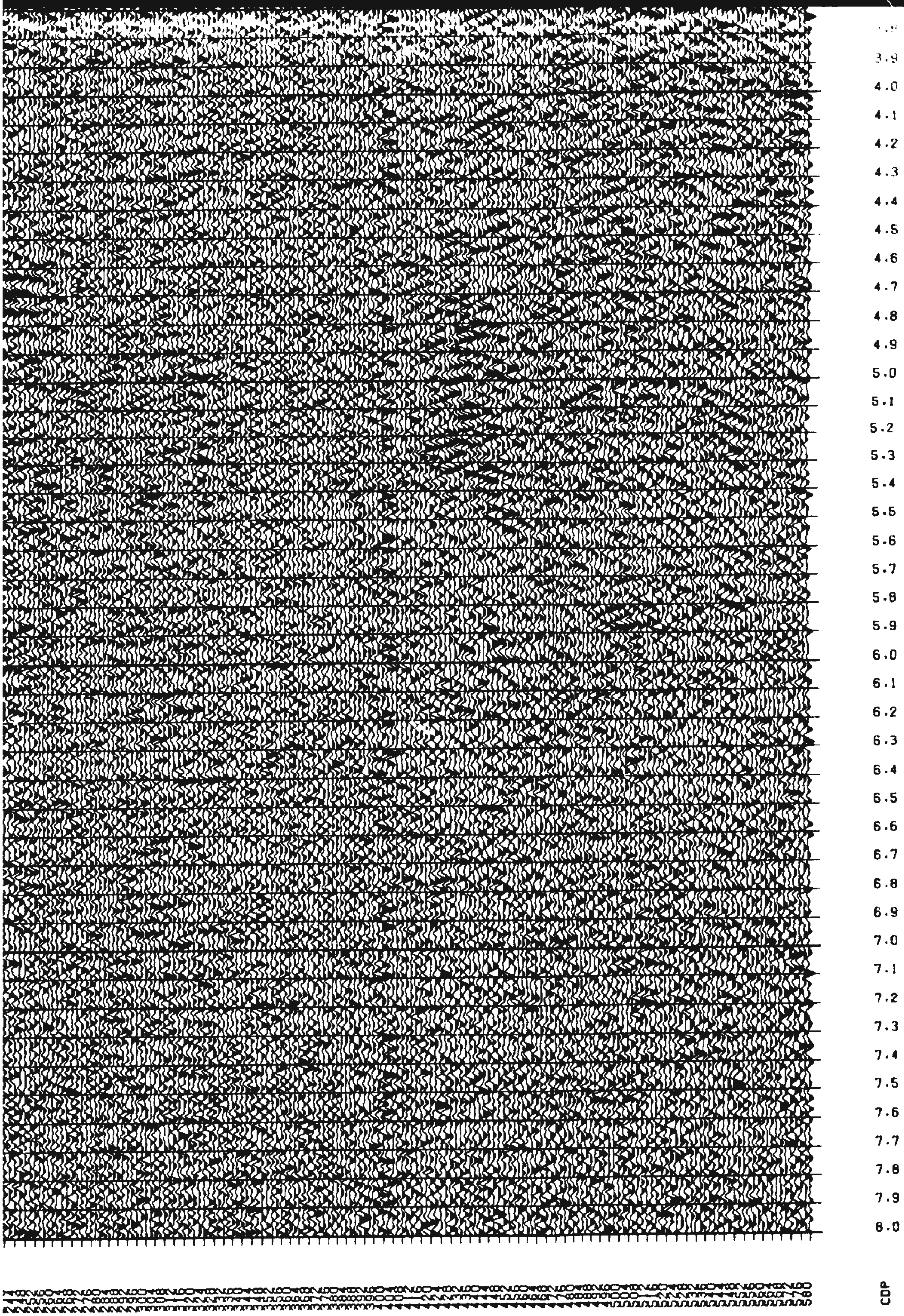
3.9
4.0
4.1
4.2
4.3
4.4
4.5
4.6
4.7
4.8
4.9
5.0
5.1
5.2
5.3
5.4
5.5
5.6
5.7
5.8
5.9
6.0
6.1
6.2
6.3
6.4
6.5
6.6
6.7
6.8
6.9
7.0
7.1
7.2
7.3
7.4
7.5
7.6
7.7
7.8
7.9
8.0
CDP

Plate 7: Reprocessed section of line 689/87.

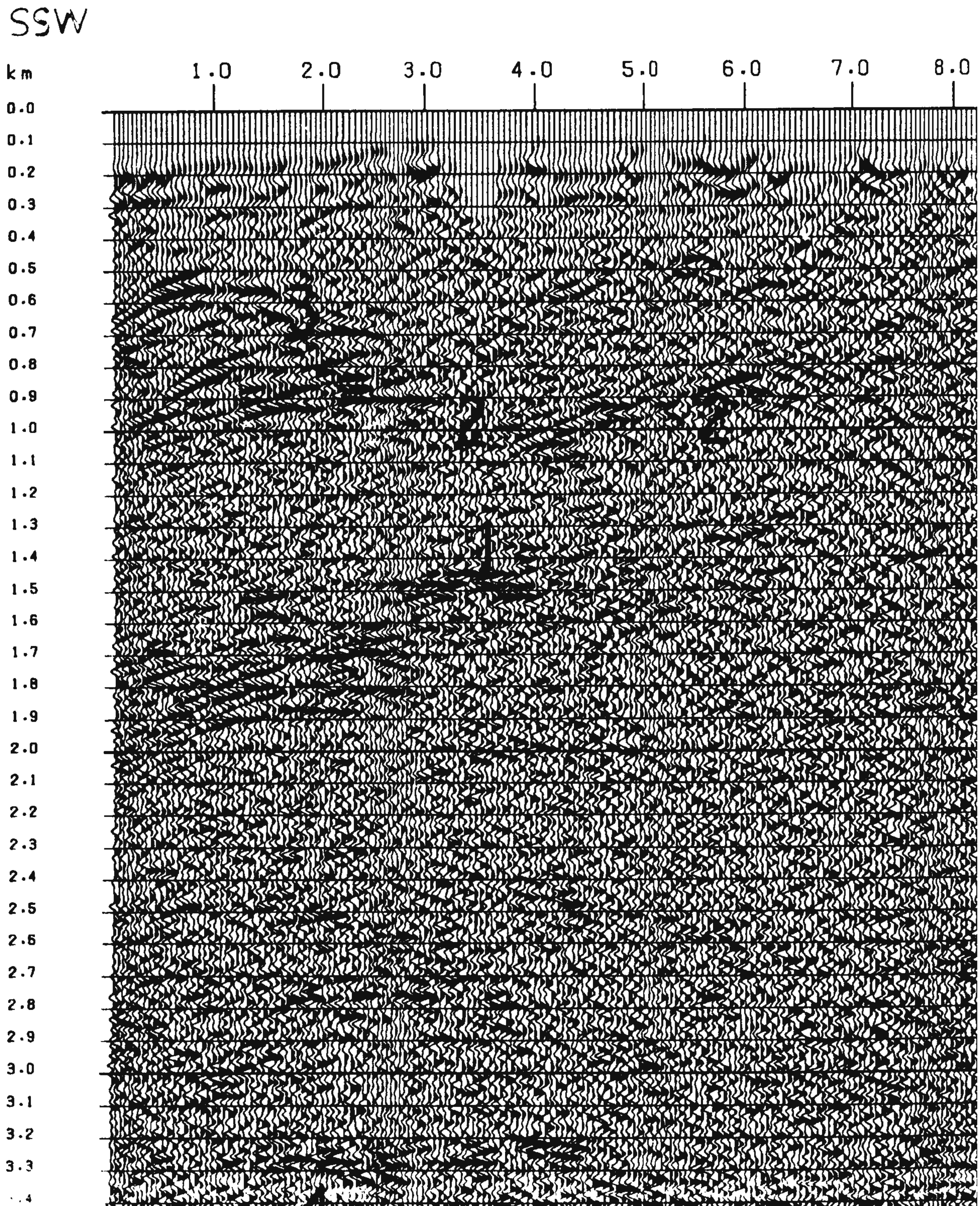
SSW
km
1.0
2.0
3.0
4.0
5.0
6.0
7.0
8.0
0.0
0.1
0.2
0.3
0.4
0.5
0.6
0.7
0.8
0.9
1.0
1.1
1.2
1.3
1.4
1.5
1.6
1.7
1.8
1.9
2.0
2.1
2.2
2.3
2.4
2.5
2.6
2.7
2.8
2.9
3.0
3.1
3.2
3.3

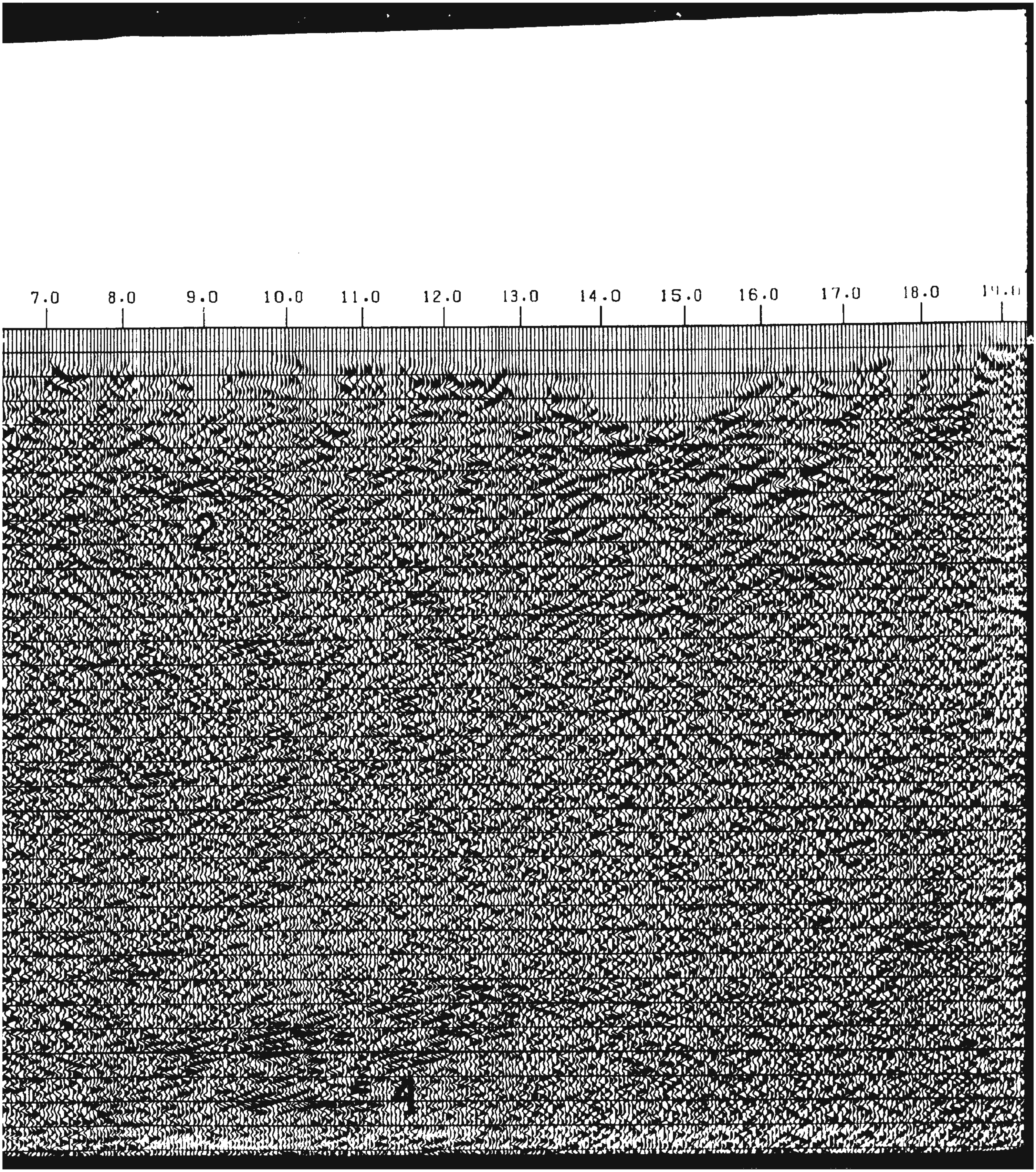
7.0
8.0
9.0
10.0
11.0
12.0
13.0
14.0
15.0
16.0
17.0
18.0
2
4

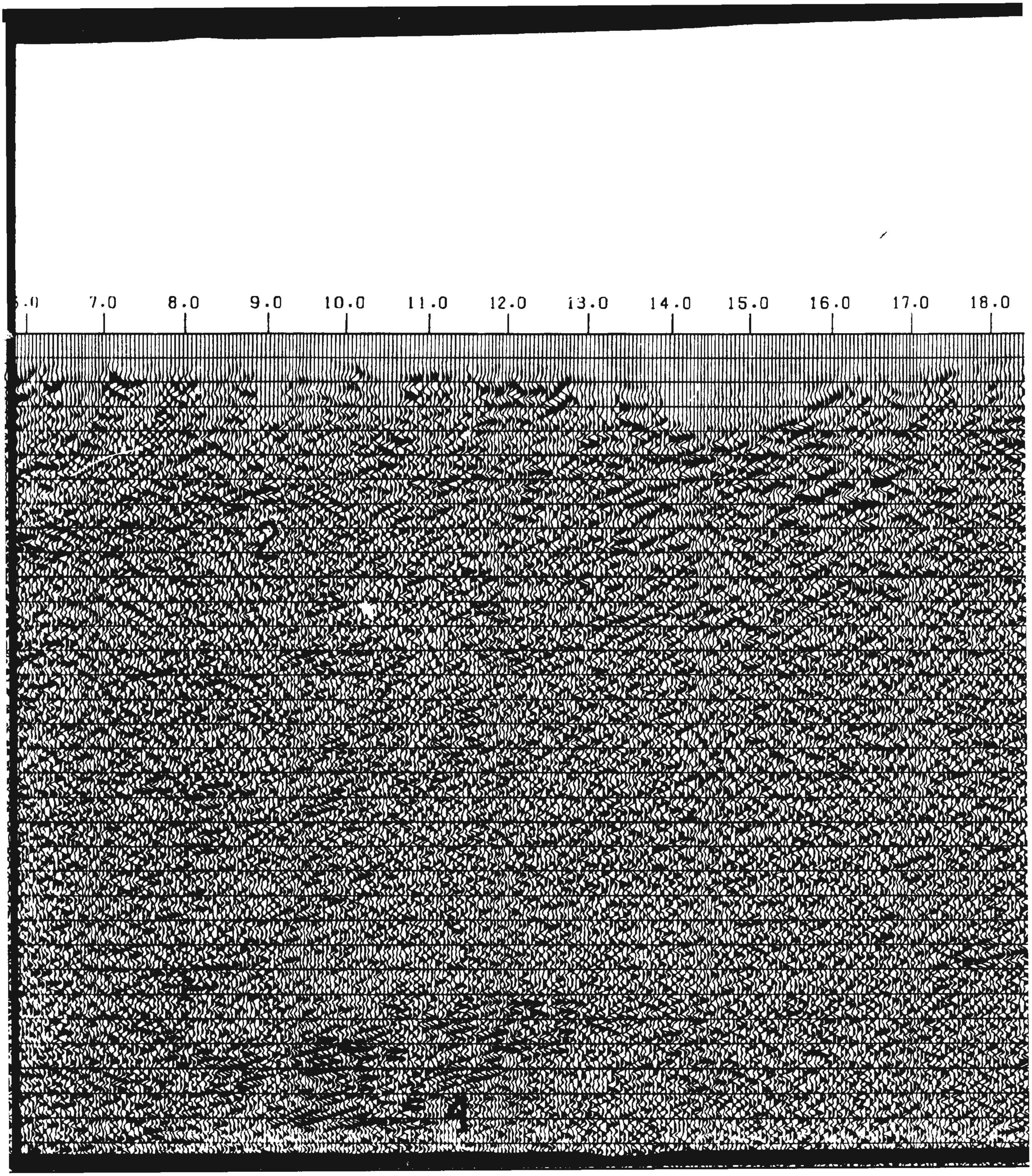
7.0 8.0 9.0 10.0 11.0 12.0 13.0 14.0 15.0 16.0 17.0 18.0

Plate 7: Reprocessed section of line 689/87. Pre-stack processing by Ga
Events 1 are thrust planes within the Modra massif of the Envelope napp
1 at the left edge of the plate may be the base of the Modra massif.
segments of the thrust plane between the Modra massif and overlying Bra
Event 3 is a conjugated fault to event 2. Events 4 are shear zones.

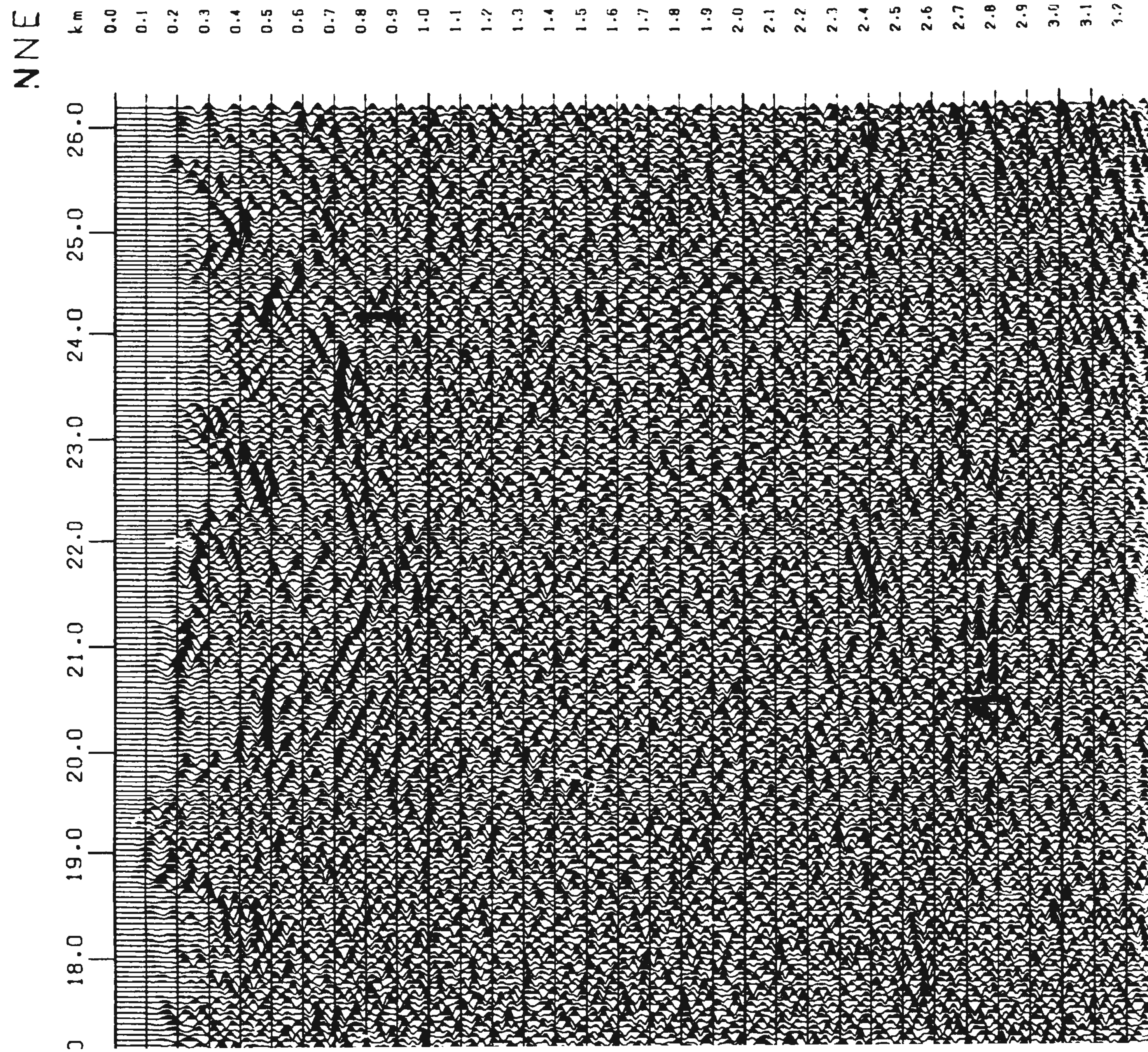

Plate 11: Dynamite source seismic line 3T.

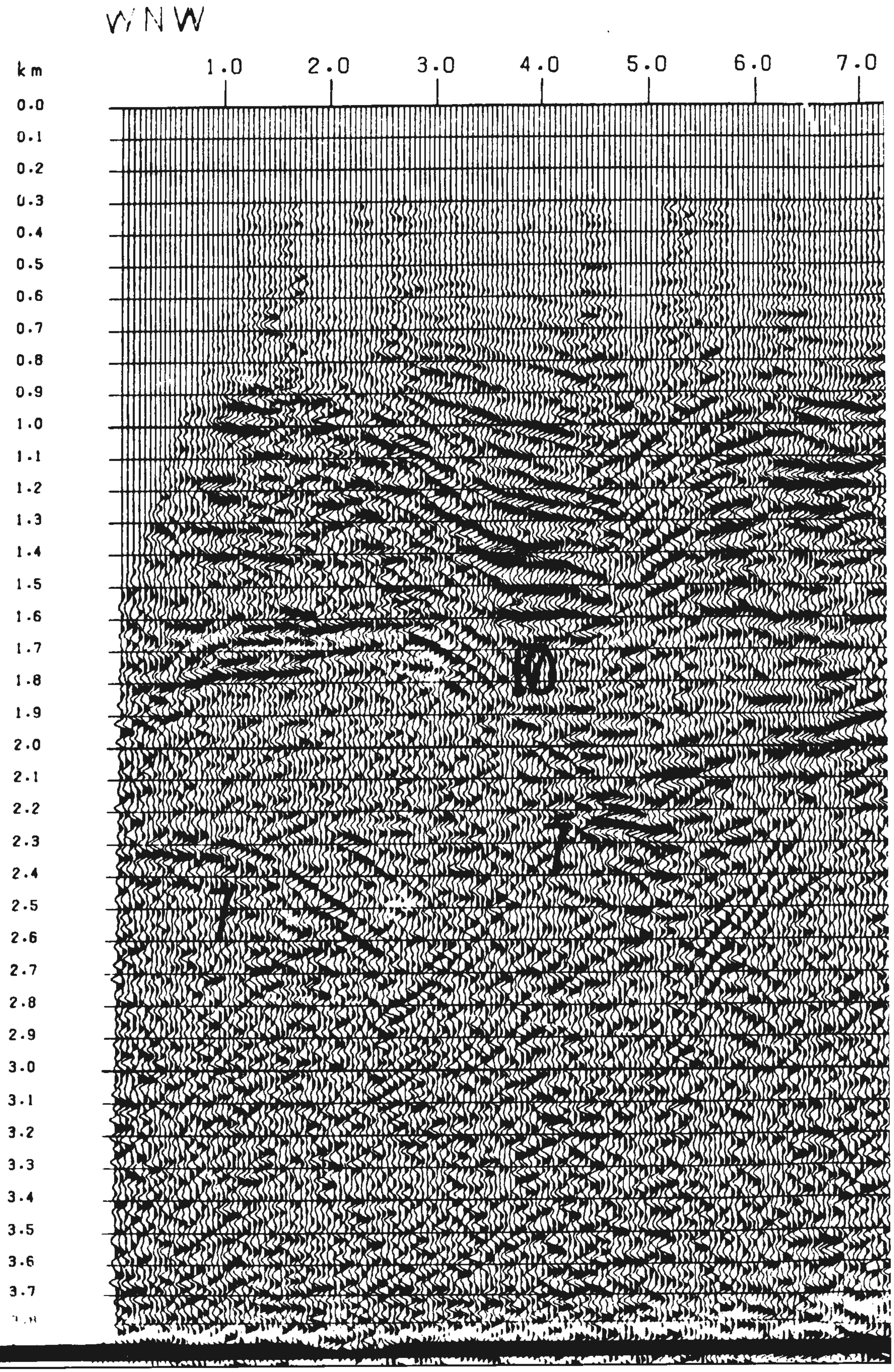
WNW
km
1.0
2.0
3.0
4.0
5.0
6.0
7.0
0.0
0.1
0.2
0.3
0.4
0.5
0.6
0.7
0.8
0.9
1.0
1.1
1.2
1.3
1.4
1.5
1.6
1.7
1.8
1.9
2.0
2.1
2.2
2.3
2.4
2.5
2.6
2.7
2.8
2.9
3.0
3.1
3.2
3.3
3.4
3.5
3.6
3.7
10
7
7

e basin

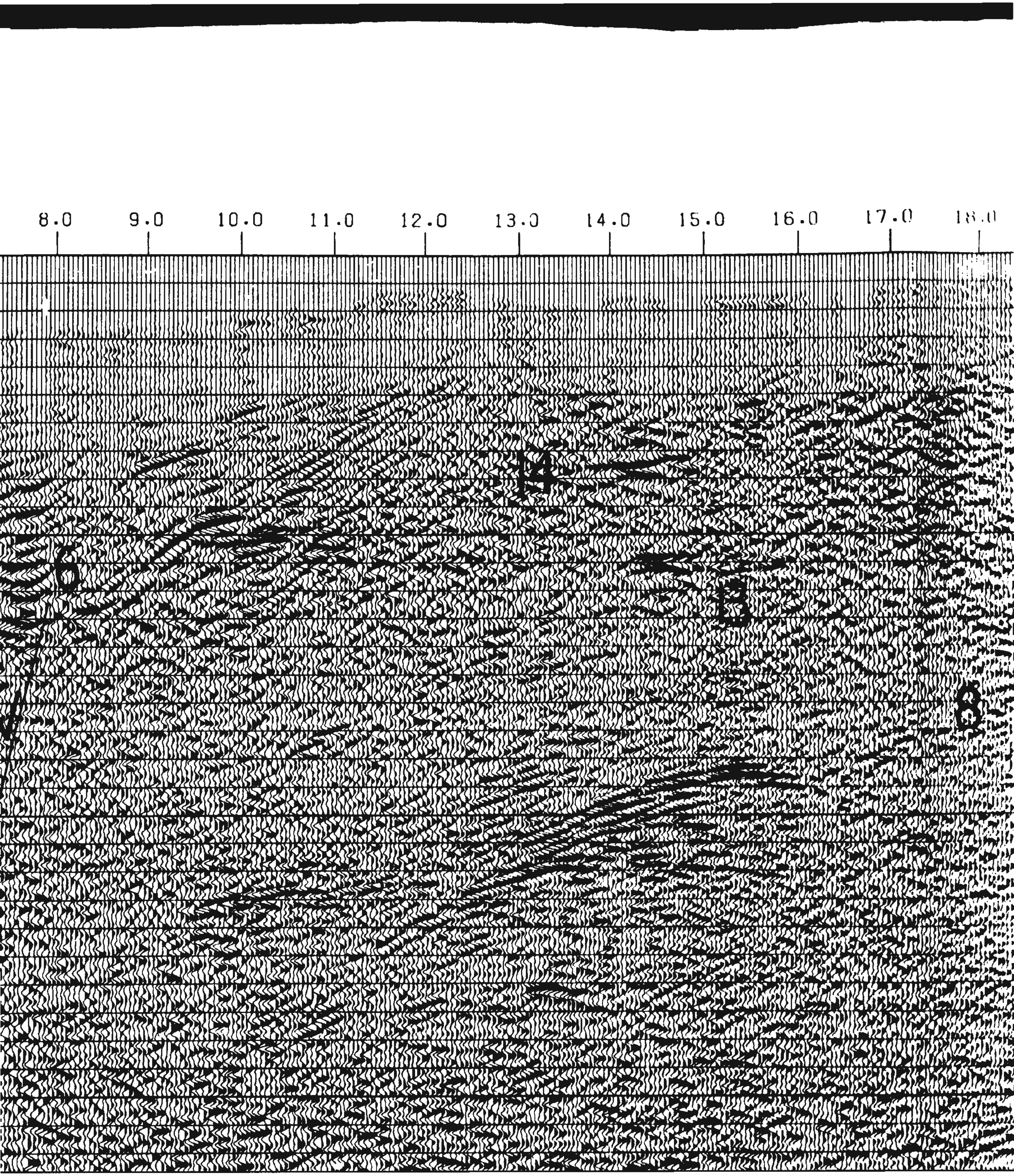
8.0
9.0
10.0
11.0
12.0
13.0
14.0
15.0
16.0
17.0
18.0
6
14
8

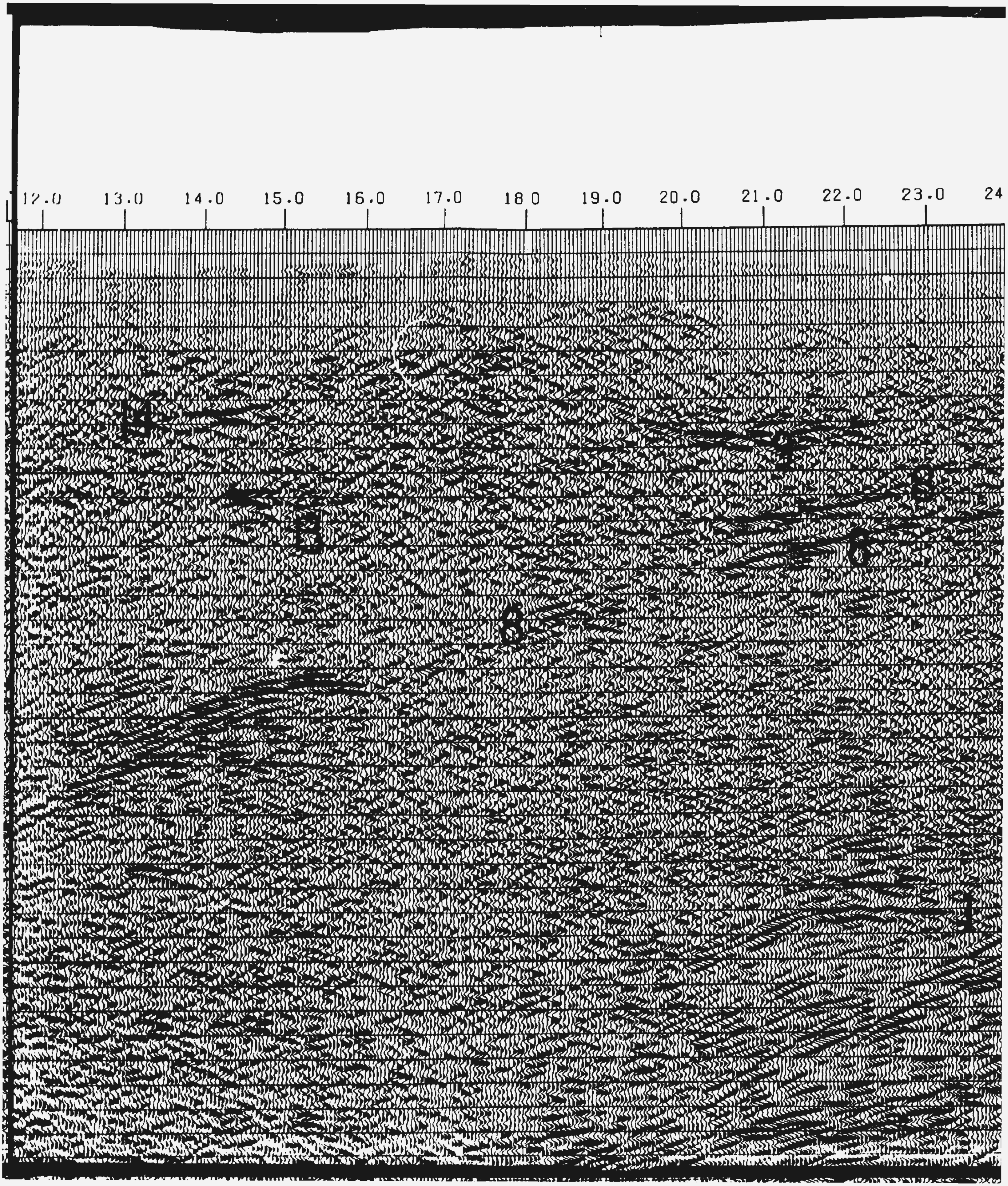
12.0
13.0
14.0
15.0
16.0
17.0
18 0
19.0
20.0
21.0
22.0
23.0
24

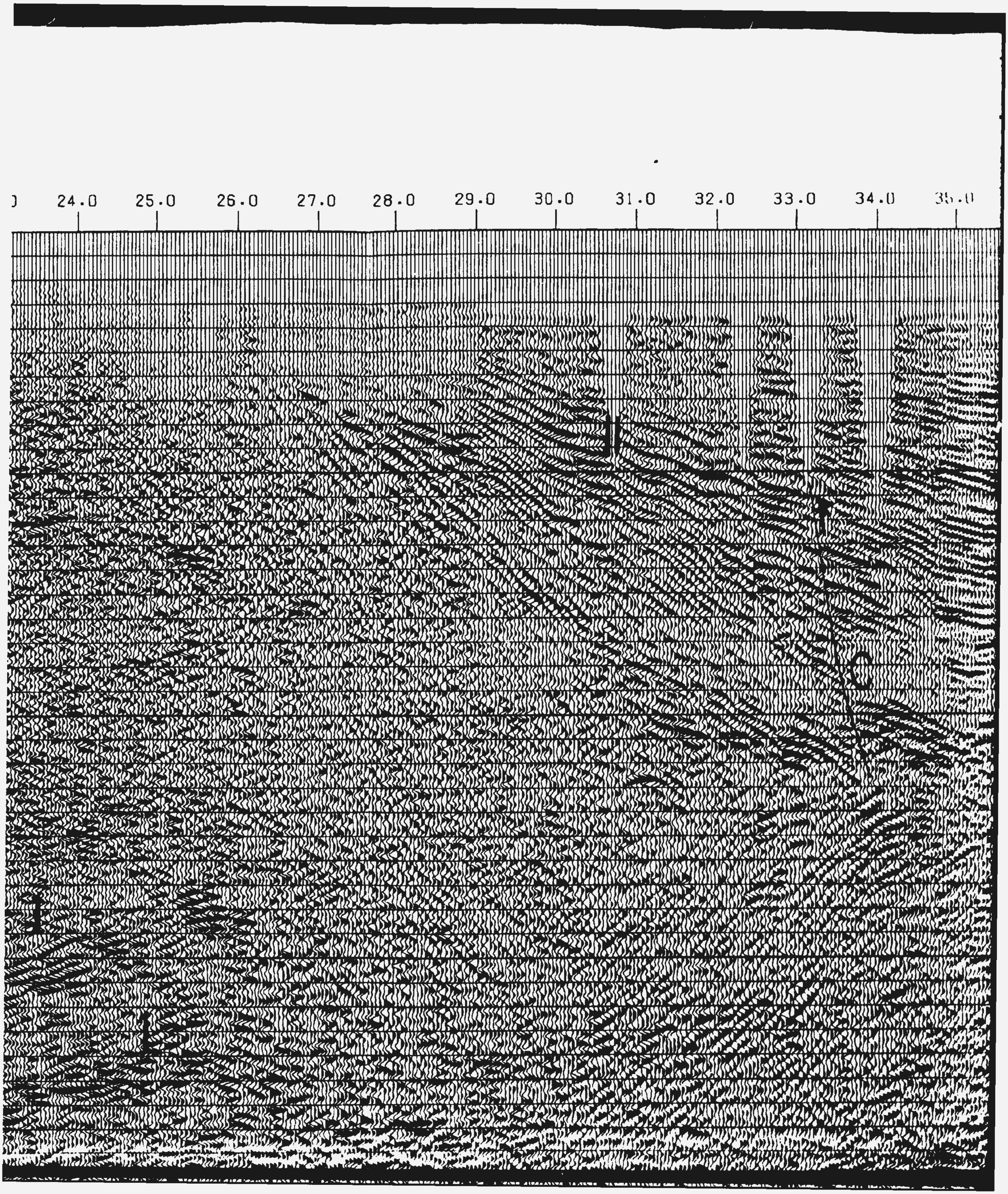
24.0
25.0
26.0
27.0
28.0
29.0
30.0
31.0
32.0
33.0
34.0

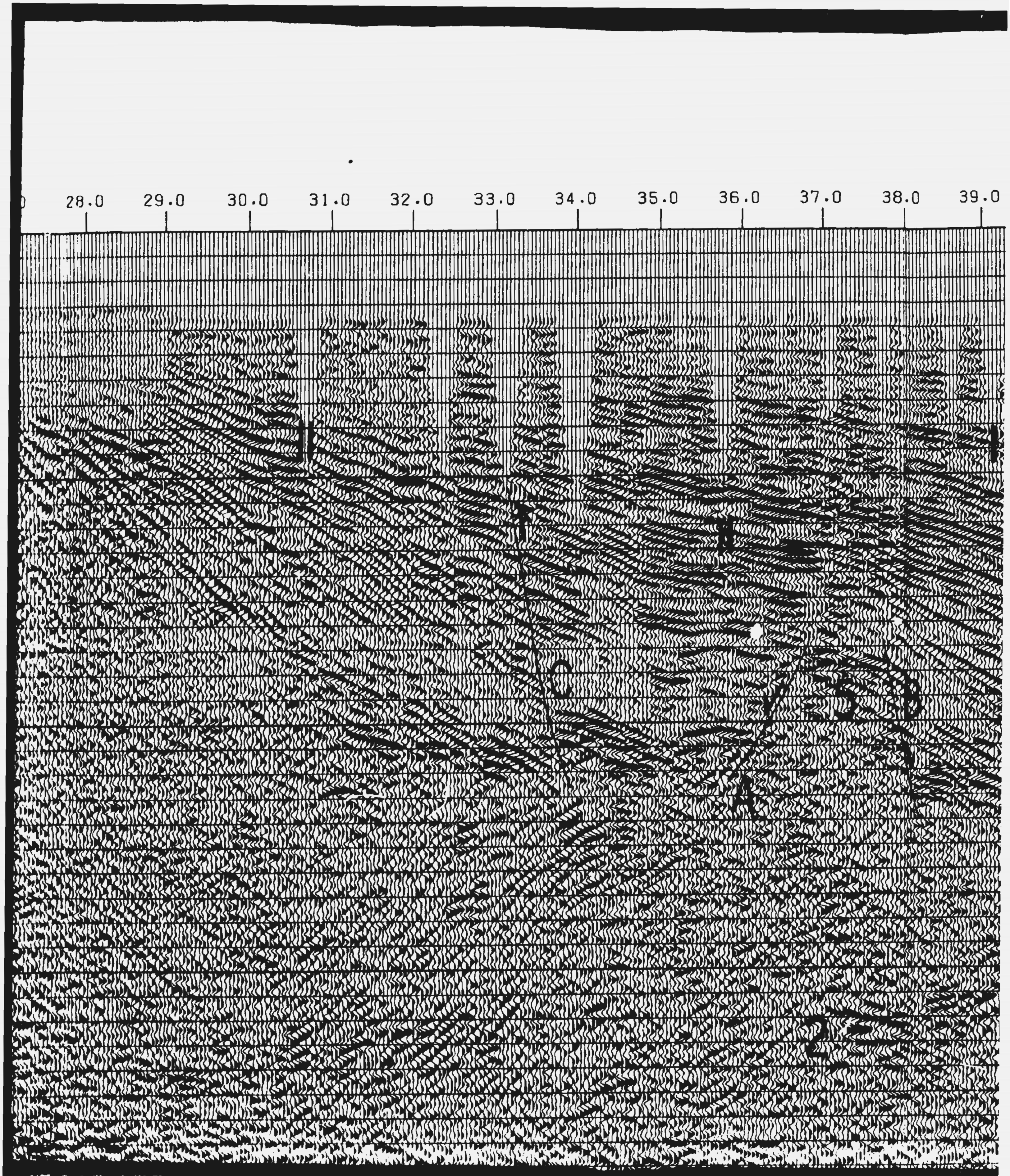
28.0
29.0
30.0
31.0
32.0
33.0
34.0
35.0
36.0
37.0
38.0
39.0

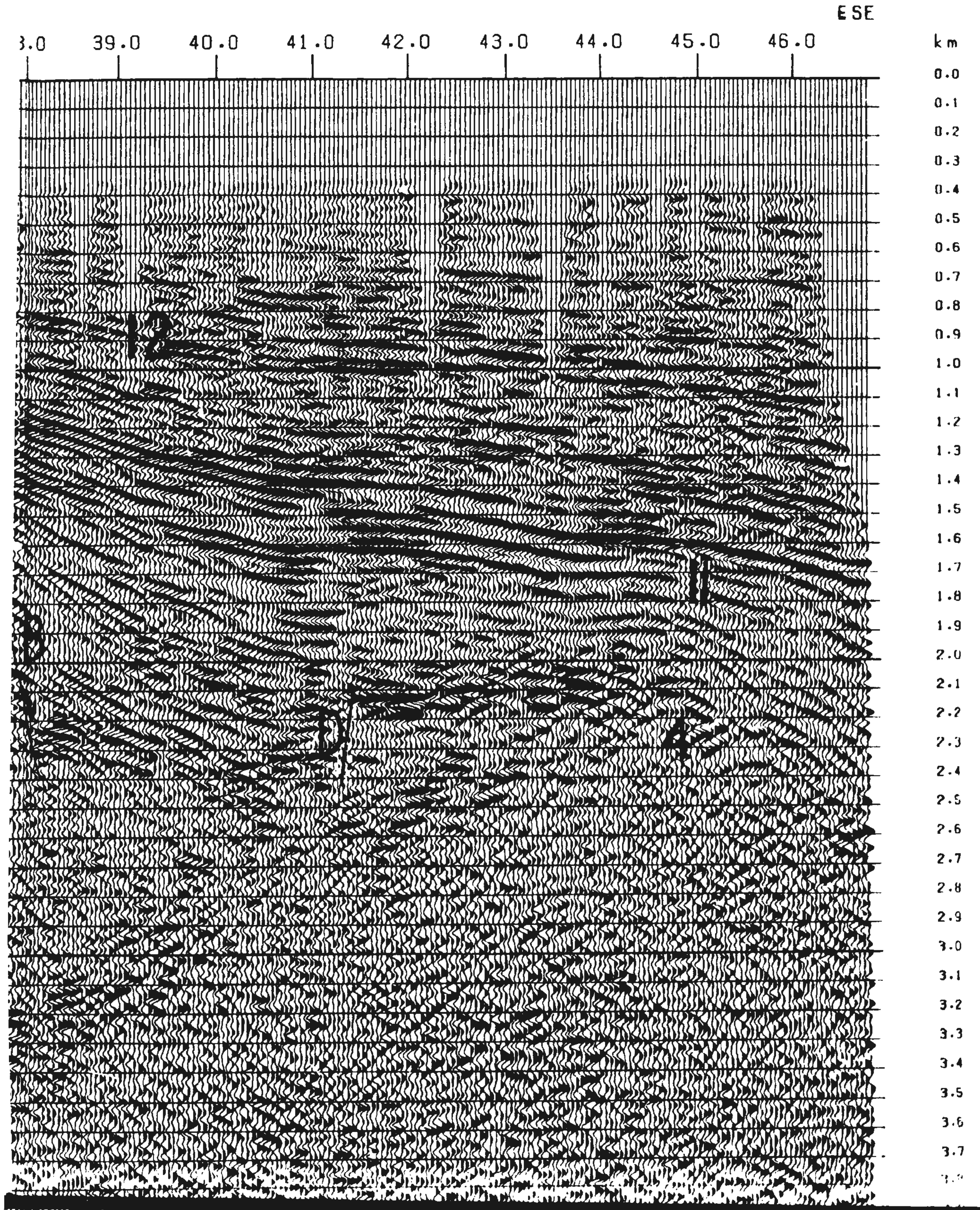
ESE
39.0
40.0
41.0
42.0
43.0
44.0
45.0
46.0
km
0.0
0.1
0.2
0.3
0.4
0.5
0.6
0.7
0.8
0.9
1.0
1.1
1.2
1.3
1.4
1.5
1.6
1.7
1.8
1.9
2.0
2.1
2.2
2.3
2.4
2.5
2.6
2.7
2.8
2.9
3.0
3.1
3.2
3.3
3.4
3.5
3.6
3.7
12
11
D

m/s 1:1 original section
on, bandpass filtering, trace summation

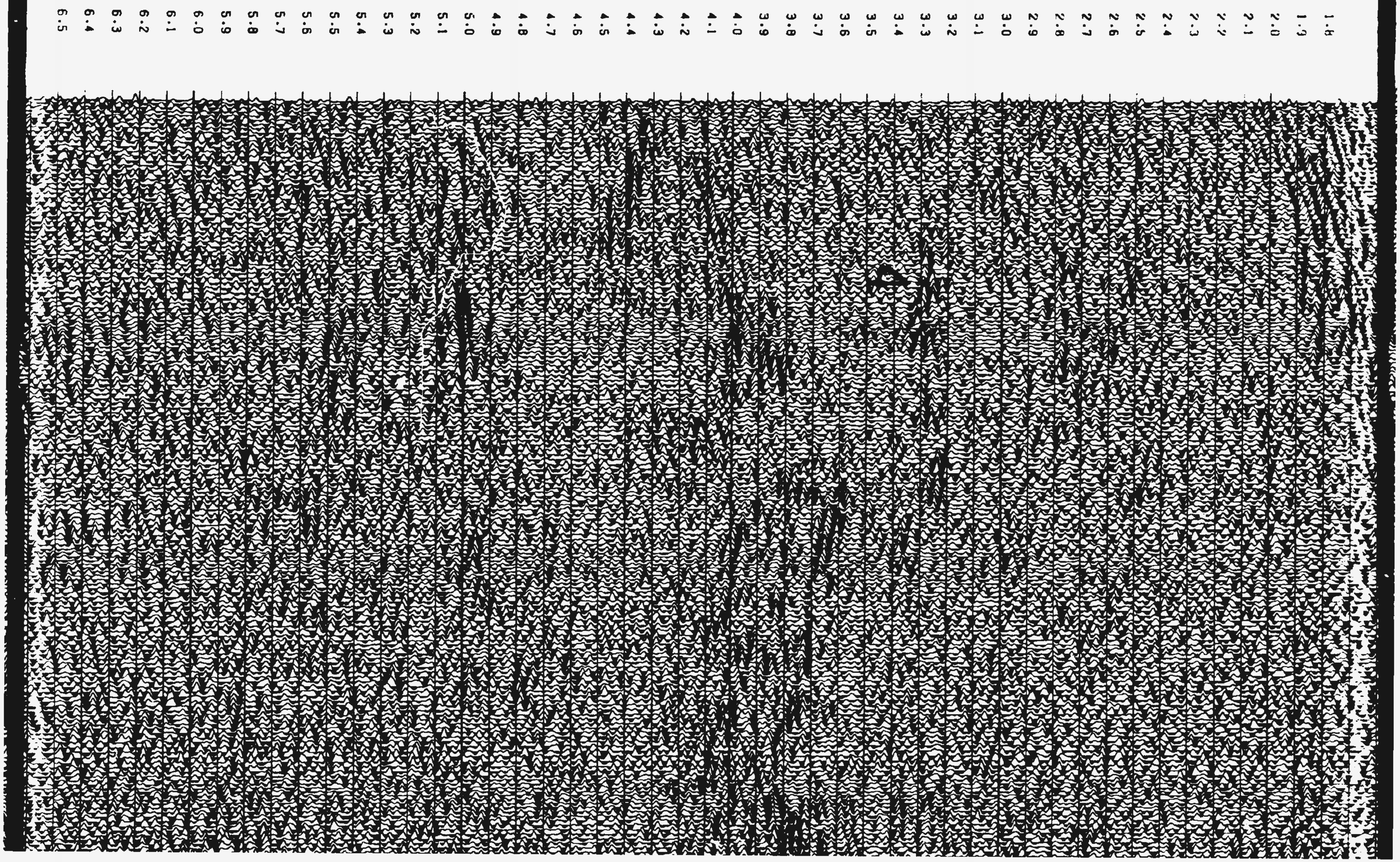

...7: Reprocessed section of line 689/87. Pre-stack processing by Geofyzika Brno. ...s 1 are thrust planes within the Modra massif of the Envelope nappe, though the ...ne left edge of the plate may be the base of the Modra massif. Events 2 are ...ents of the thrust plane between the Modra massif and overlying Bratislava massif. ...t 3 is a conjugated fault to event 2. Events 4 are shear zones.

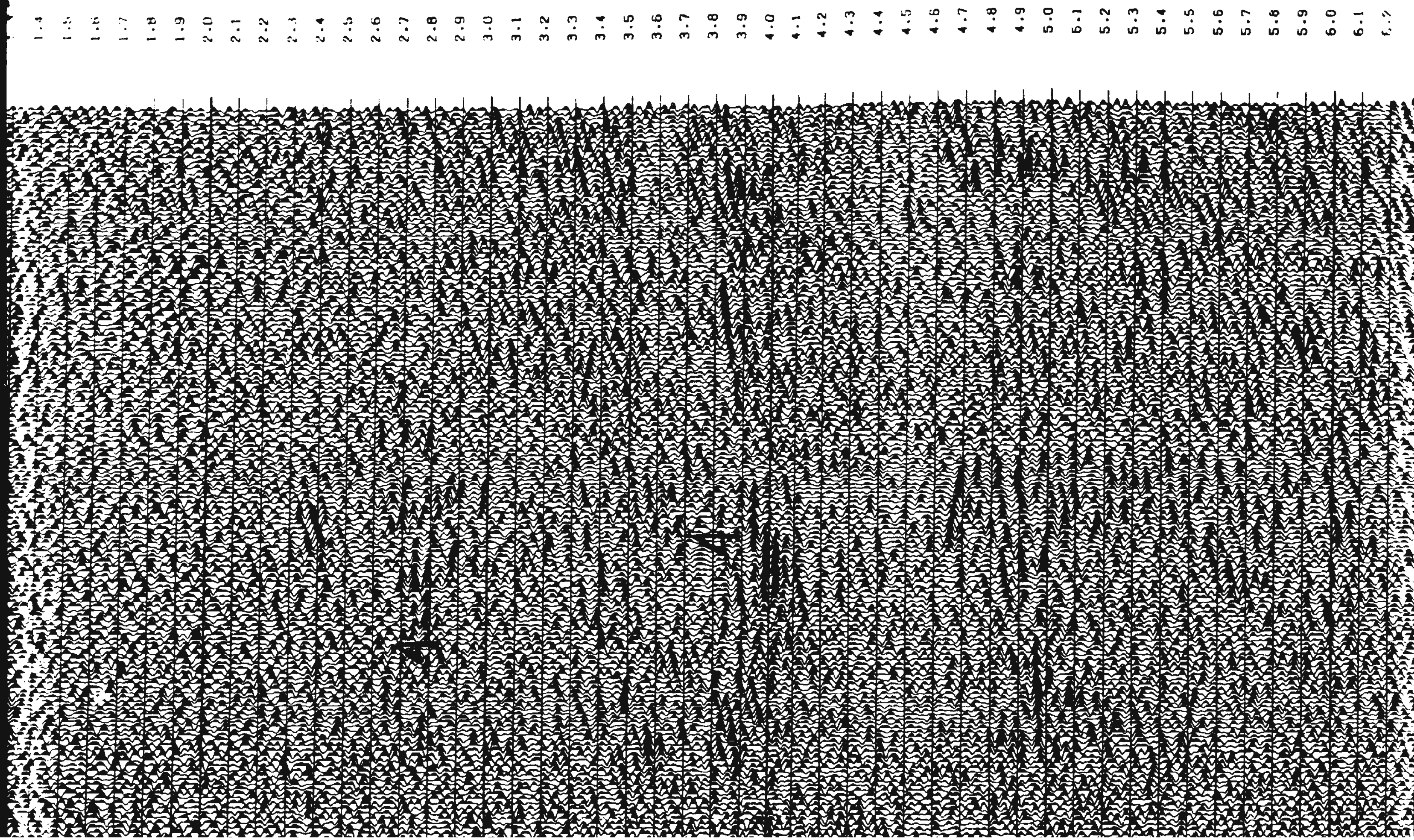

Carpathians and West Danube basin
vertical scale

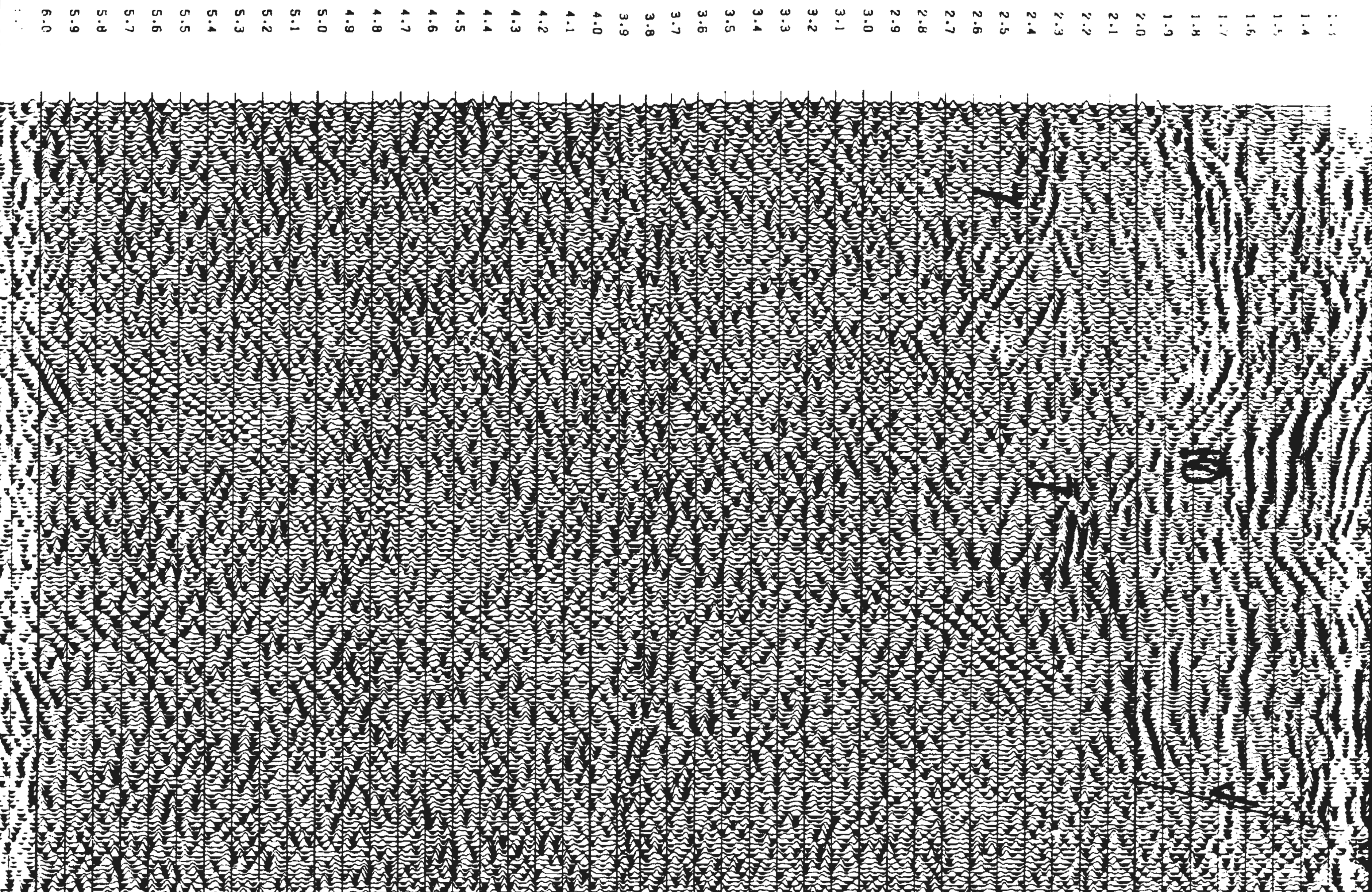

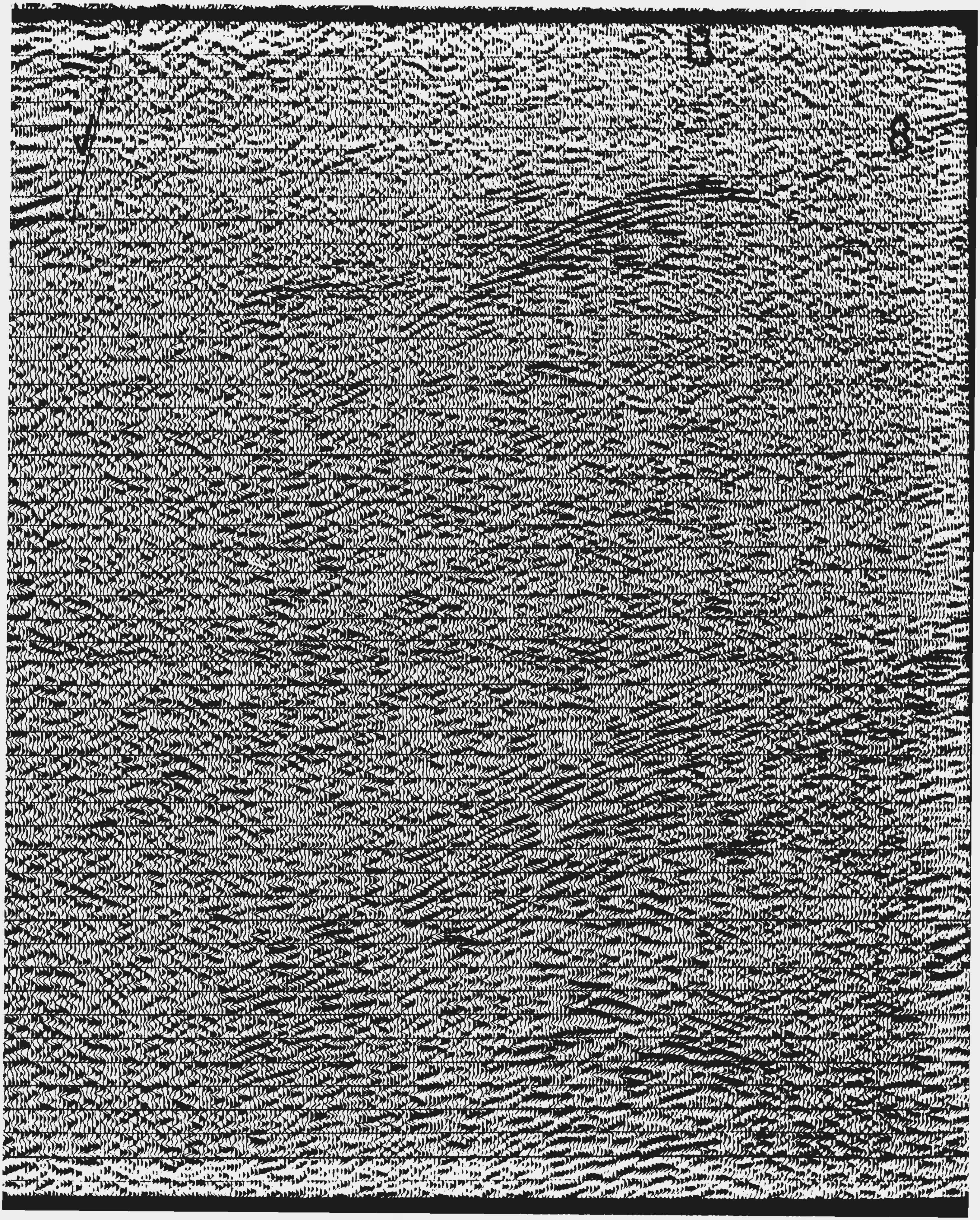

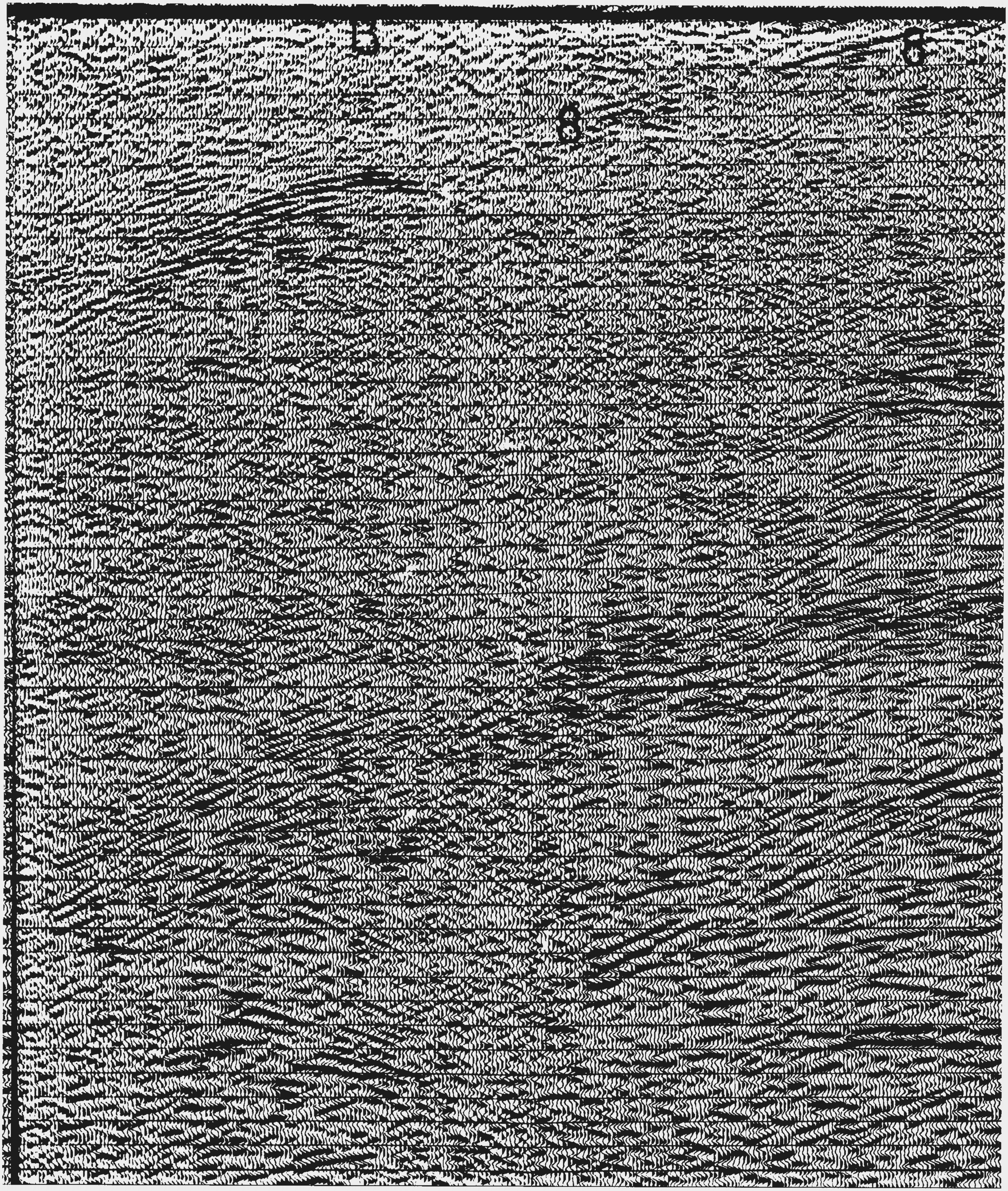

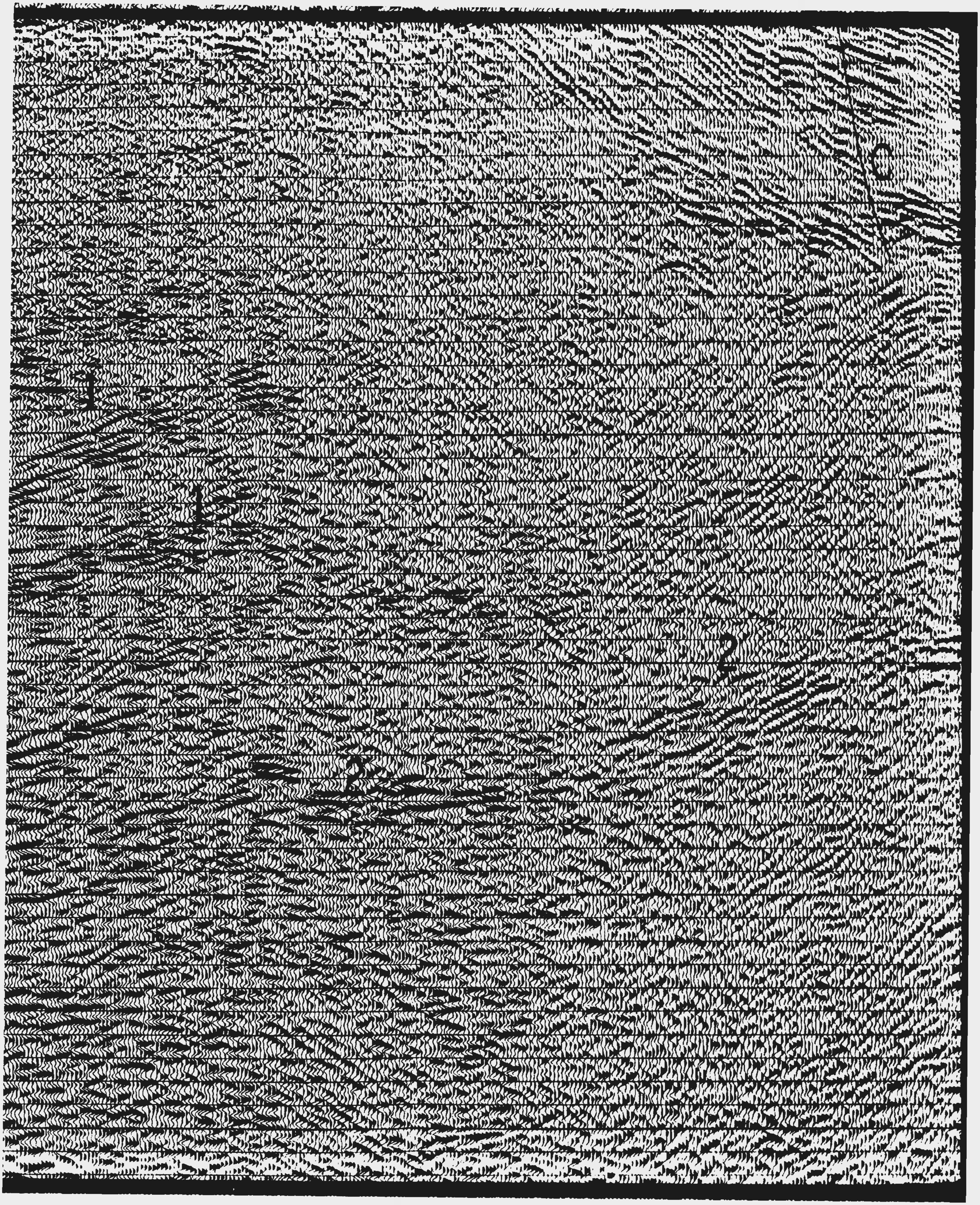

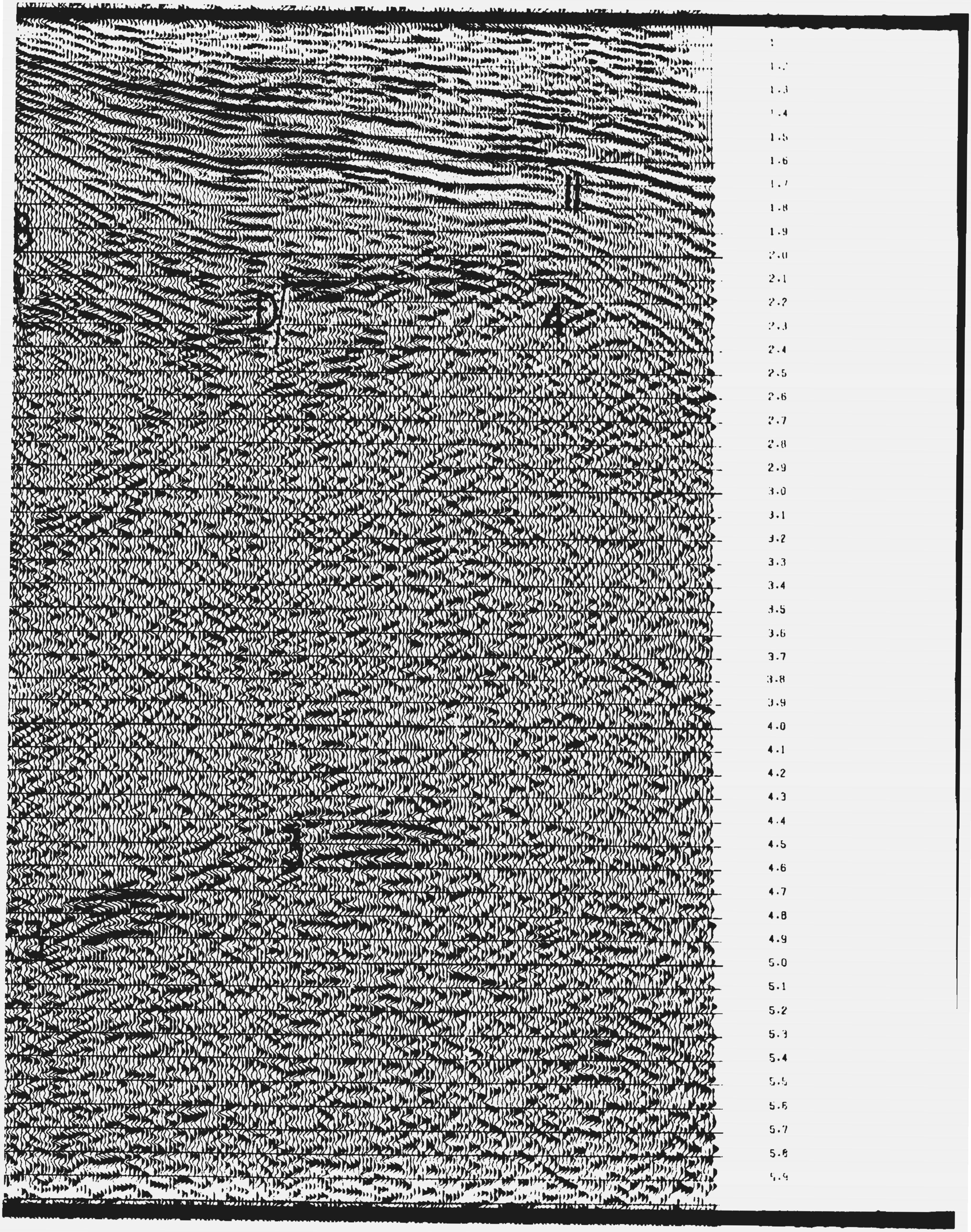
1.3
1.5
1.6
1.8
1.9
2.1
2.2
2.4
2.5
2.6
2.7
2.8
2.9
3.0
3.1
3.2
3.3
3.4
3.5
3.6
3.7
3.8
4.0
4.1
4.2
4.3
4.4
4.5
4.6
4.7
4.8
4.9
5.0
5.1
5.2
5.3
5.4
5.6
5.7
5.8
A

Line 689/87: 6 km/s 1:1 original section
Trace normalization, bandpass filtering, trace s

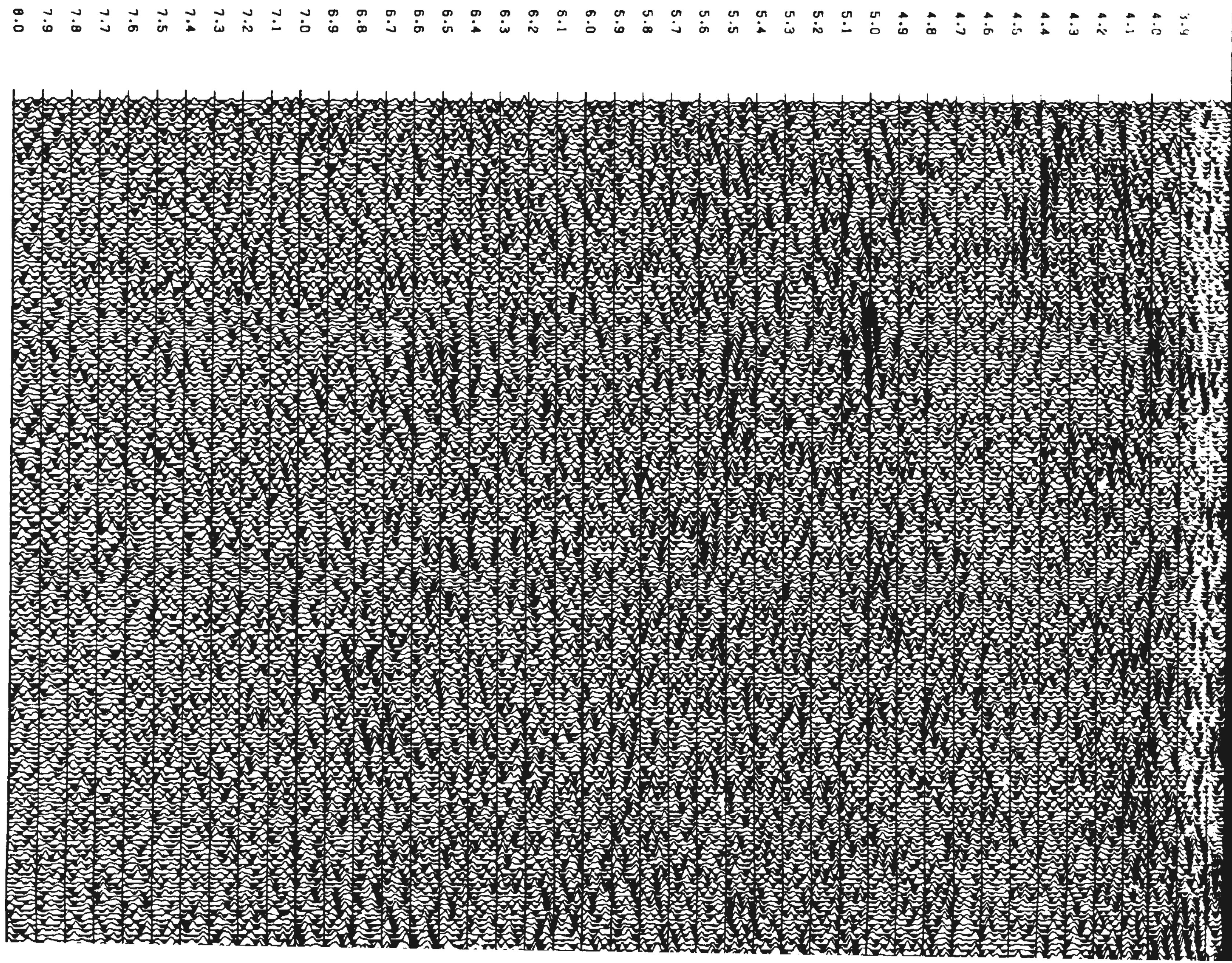

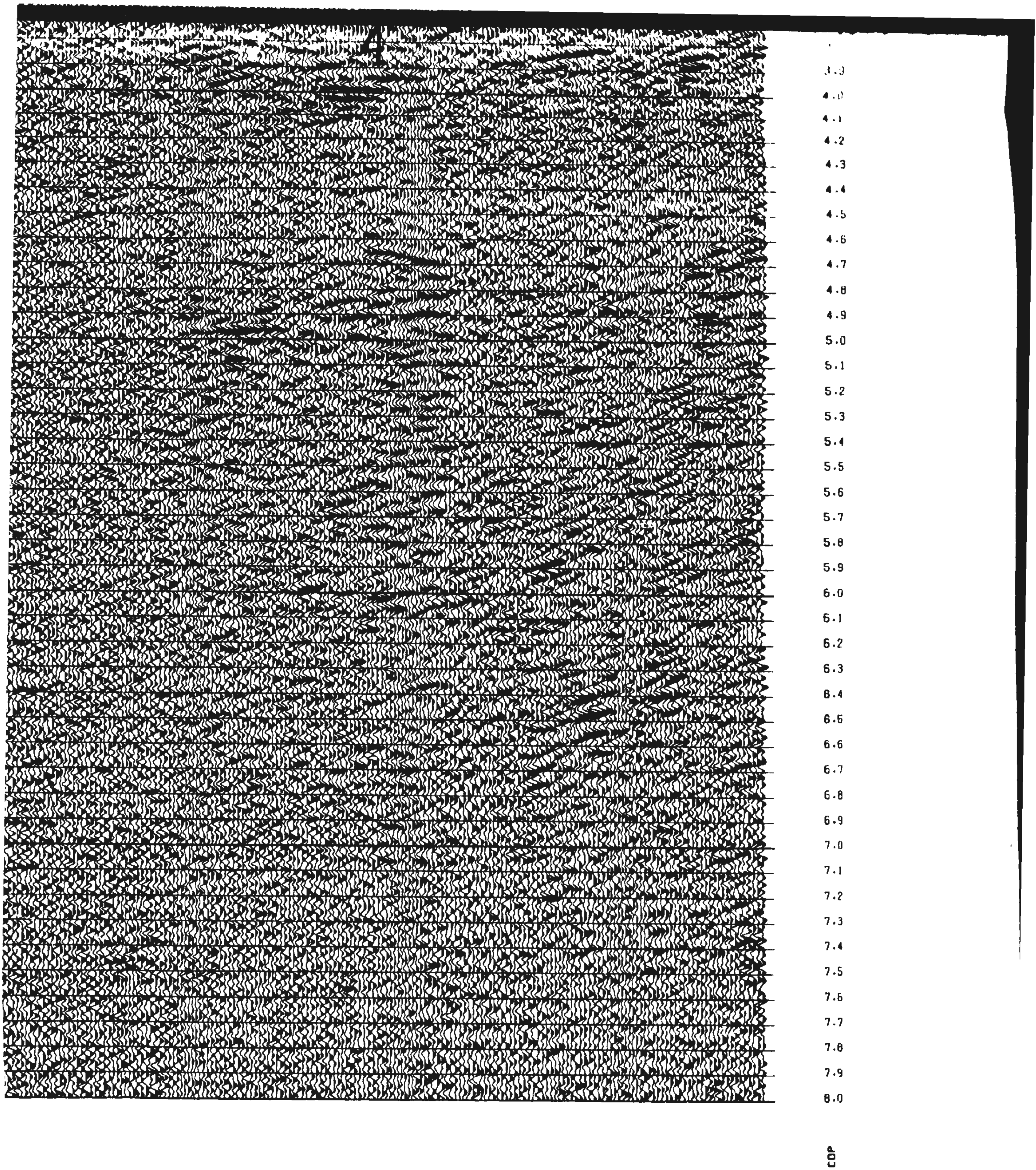
3.9
4.0
4.1
4.2
4.3
4.4
4.5
4.6
4.7
4.8
4.9
5.0
5.1
5.2
5.3
5.4
5.5
5.6
5.7
5.8
5.9
6.0
6.1
6.2
6.3
6.4
6.5
6.6
6.7
6.8
6.9
7.0
7.1
7.2
7.3
7.4
7.5
7.6
7.7
7.8
7.9
8.0

Line 3T
Vienna basin, Little Carpathians and West Danube
Final plot with 6 km/s vertical scale

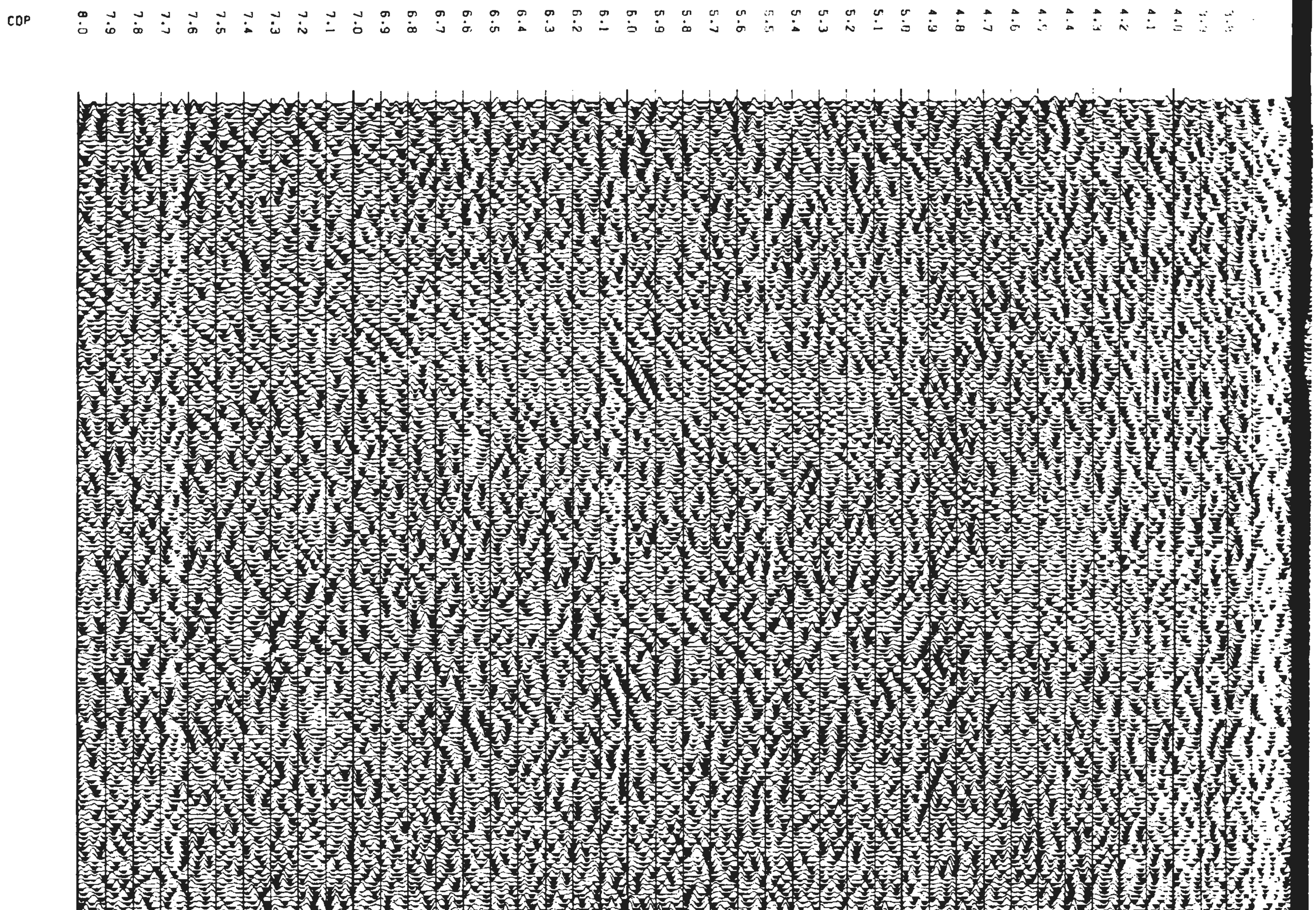

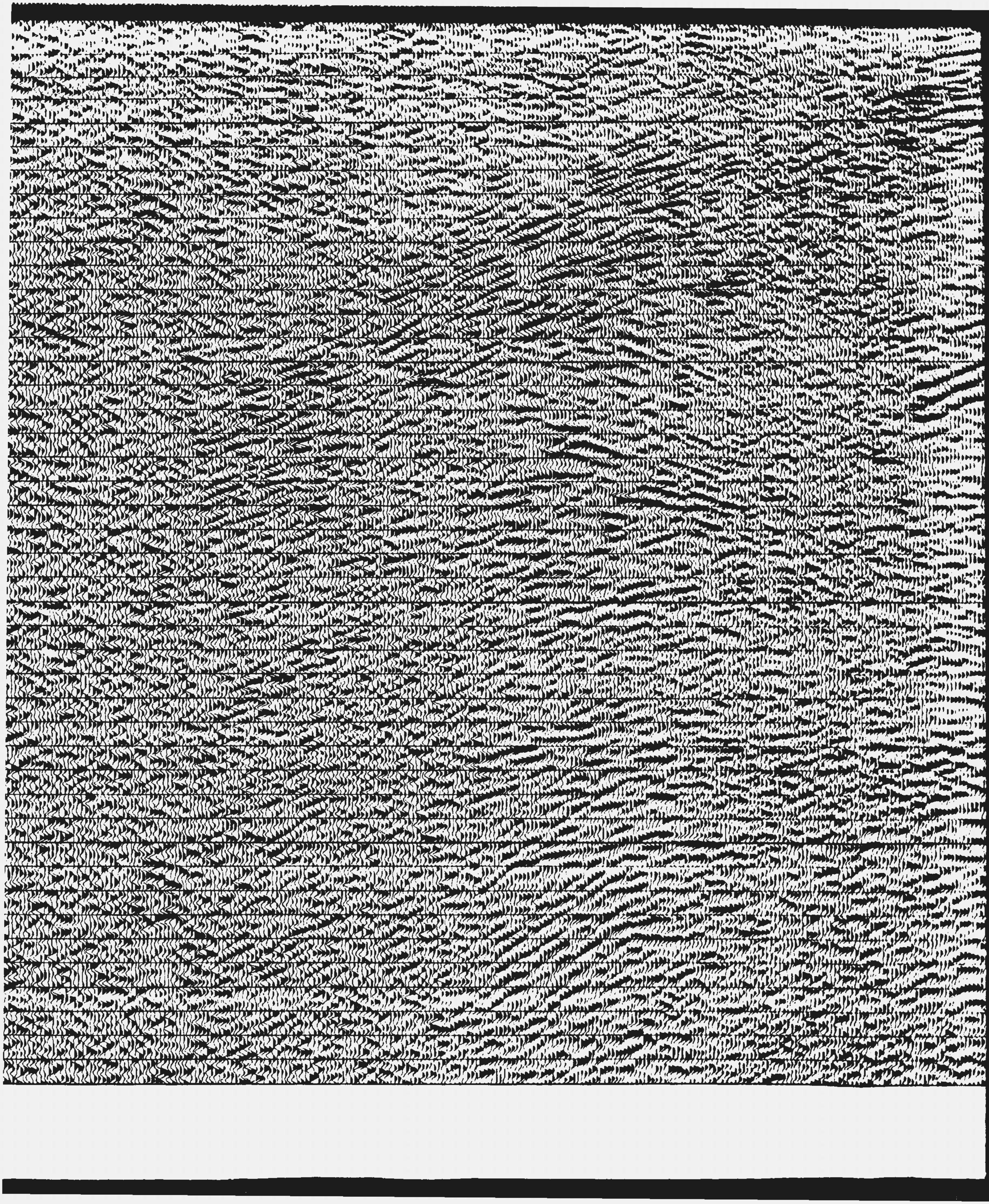

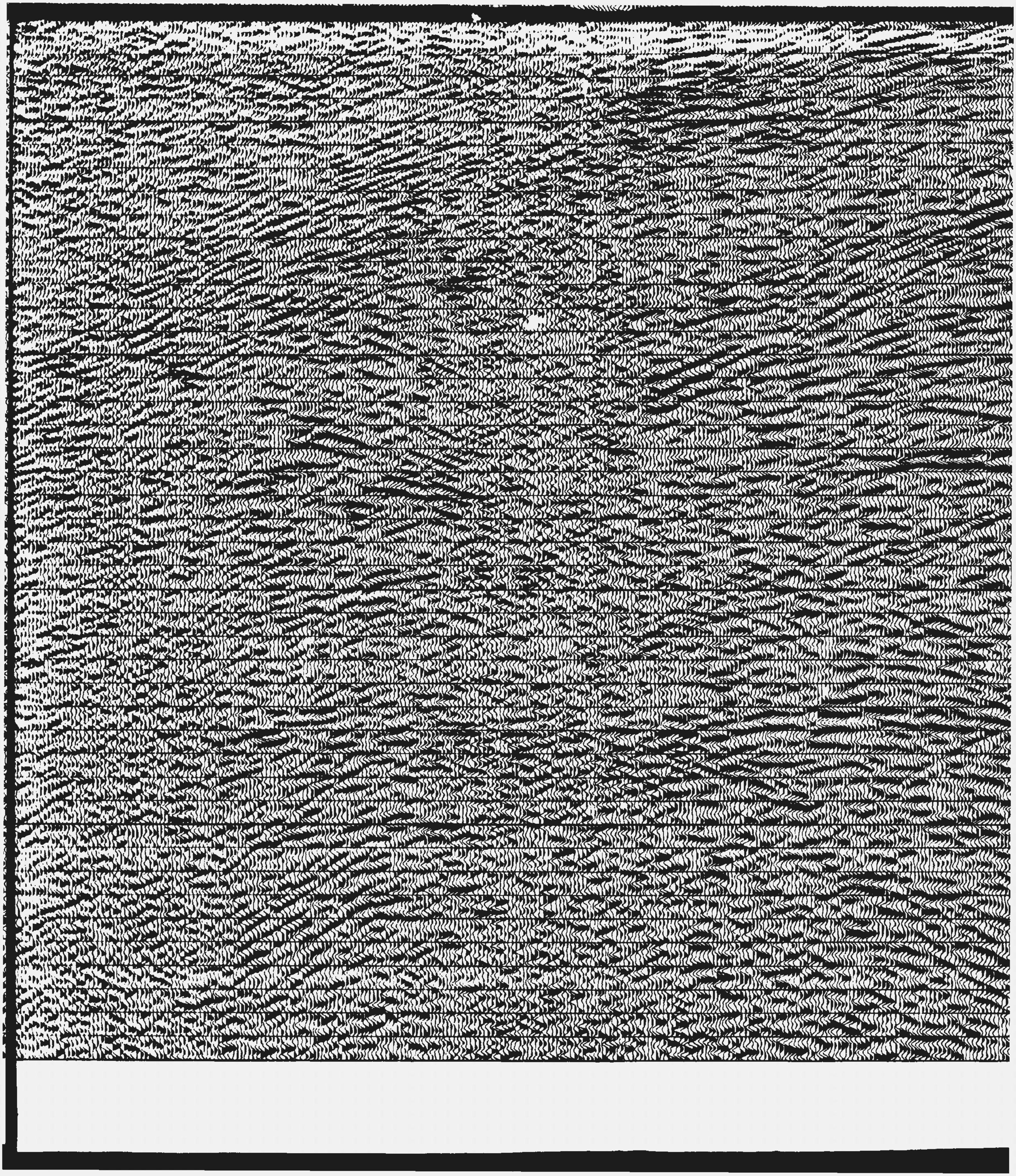

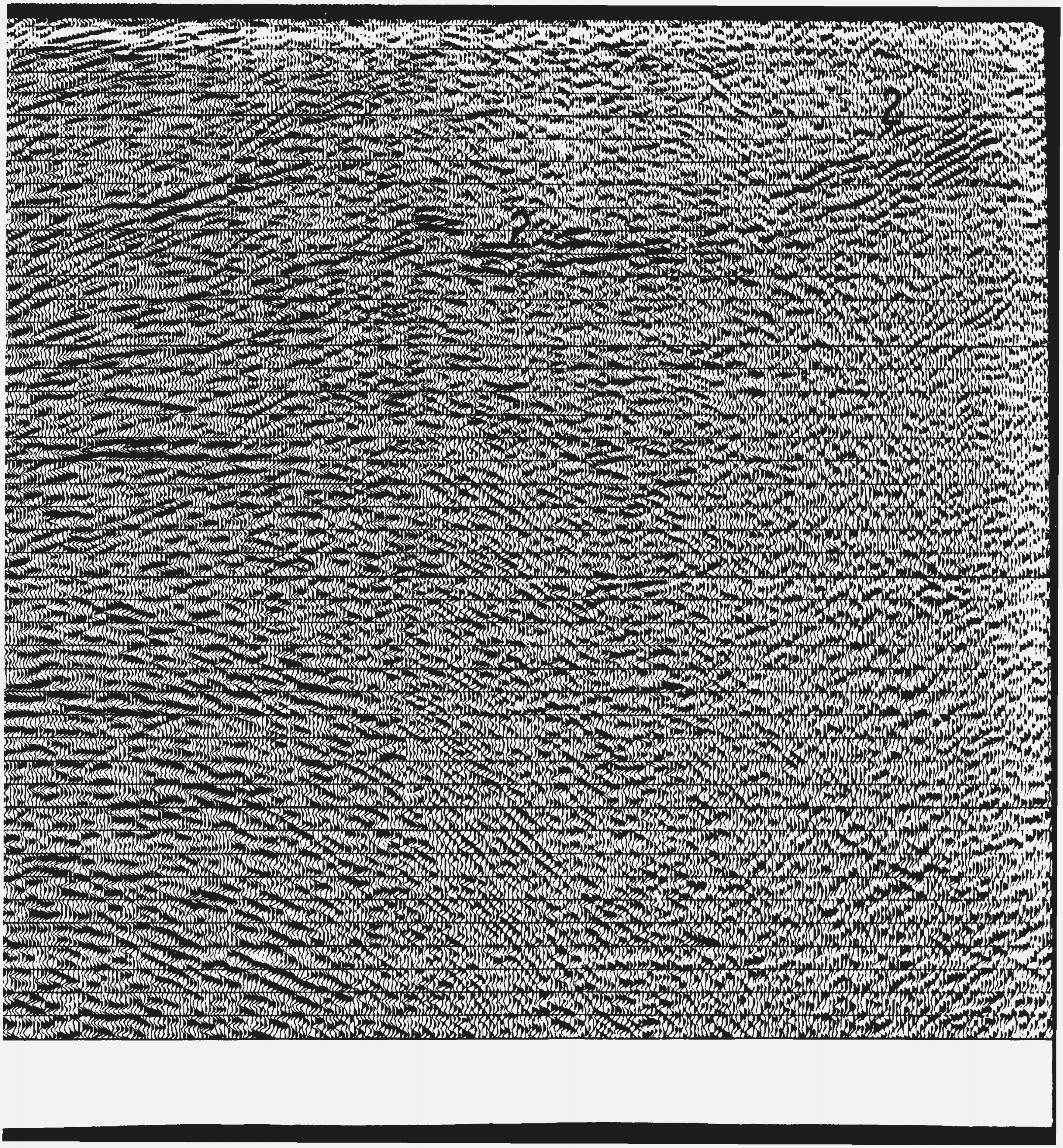

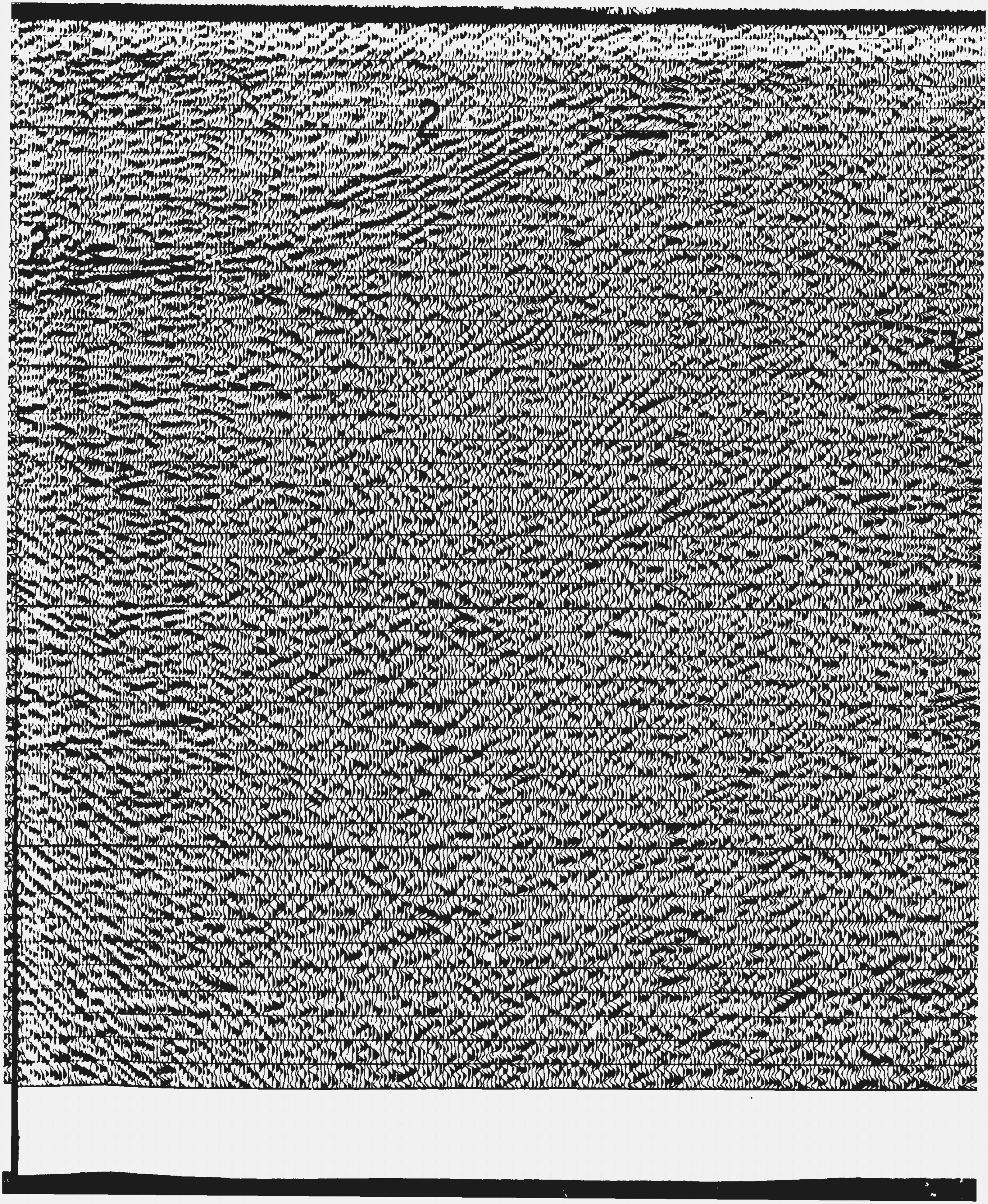
2
2
1

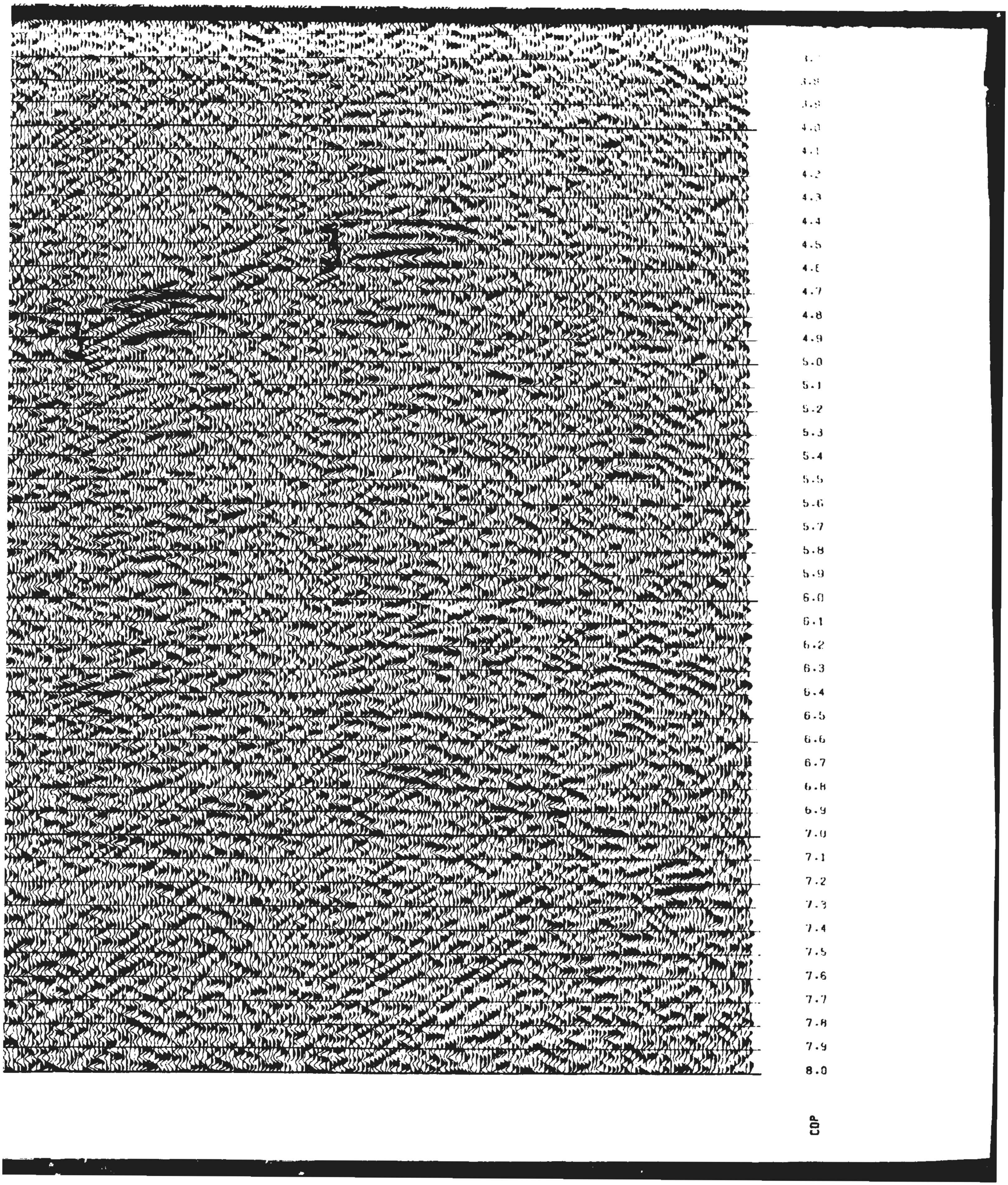
3.8
3.9
4.0
4.1
4.2
4.3
4.4
4.5
4.6
4.7
4.8
4.9
5.0
5.1
5.2
5.3
5.4
5.5
5.6
5.7
5.8
5.9
6.0
6.1
6.2
6.3
6.4
6.5
6.6
6.7
6.8
6.9
7.0
7.1
7.2
7.3
7.4
7.5
7.6
7.7
7.8
7.9
8.0
CDP

Plate 12: Dynamite source seismic line 8HR.

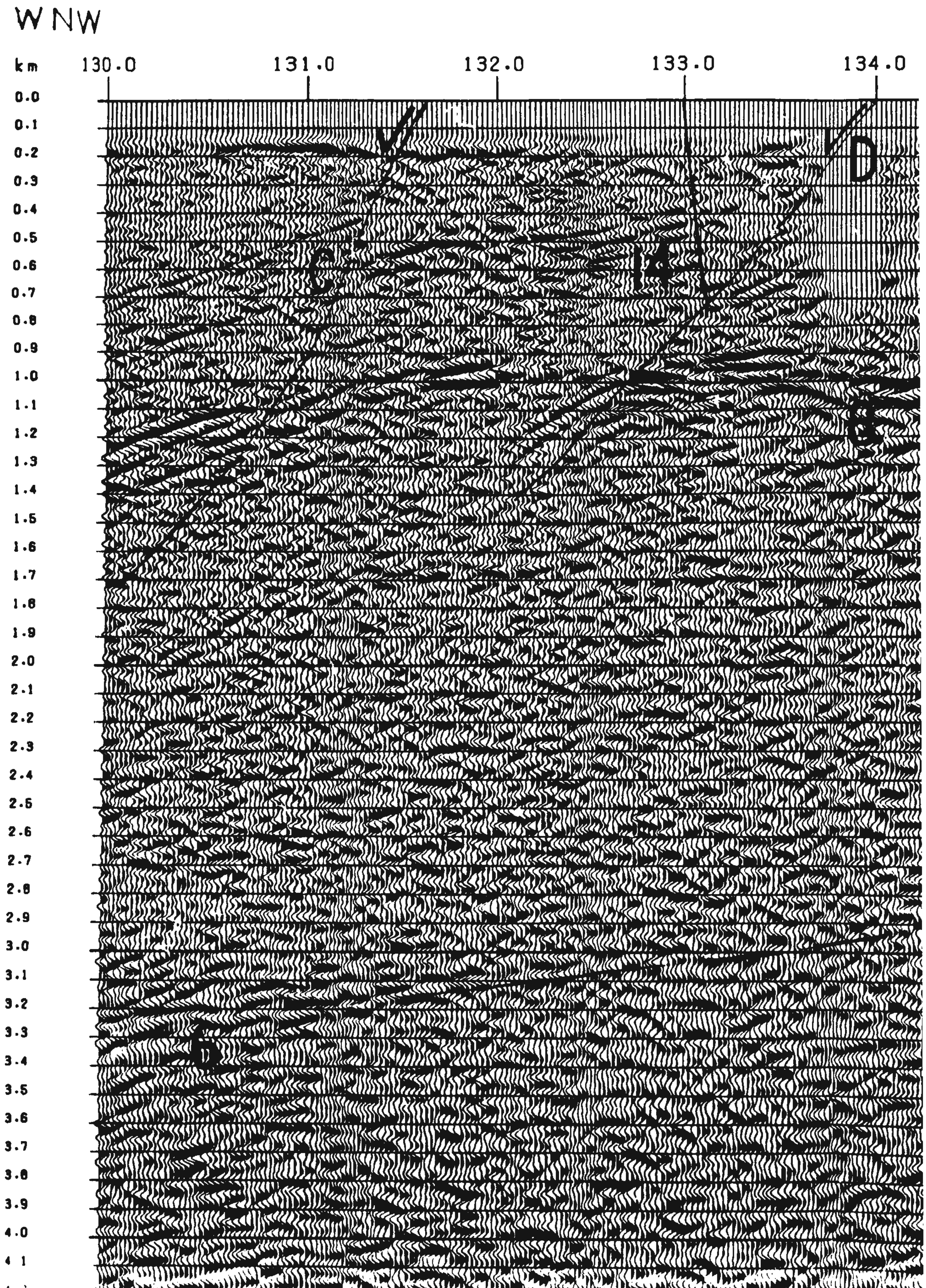

WNW
km
130.0
131.0
132.0
133.0
134.0
0.0
0.1
0.2
0.3
0.4
0.5
0.6
0.7
0.8
0.9
1.0
1.1
1.2
1.3
1.4
1.5
1.6
1.7
1.8
1.9
2.0
2.1
2.2
2.3
2.4
2.5
2.6
2.7
2.8
2.9
3.0
3.1
3.2
3.3
3.4
3.5
3.6
3.7
3.8
3.9
4.0
4.1

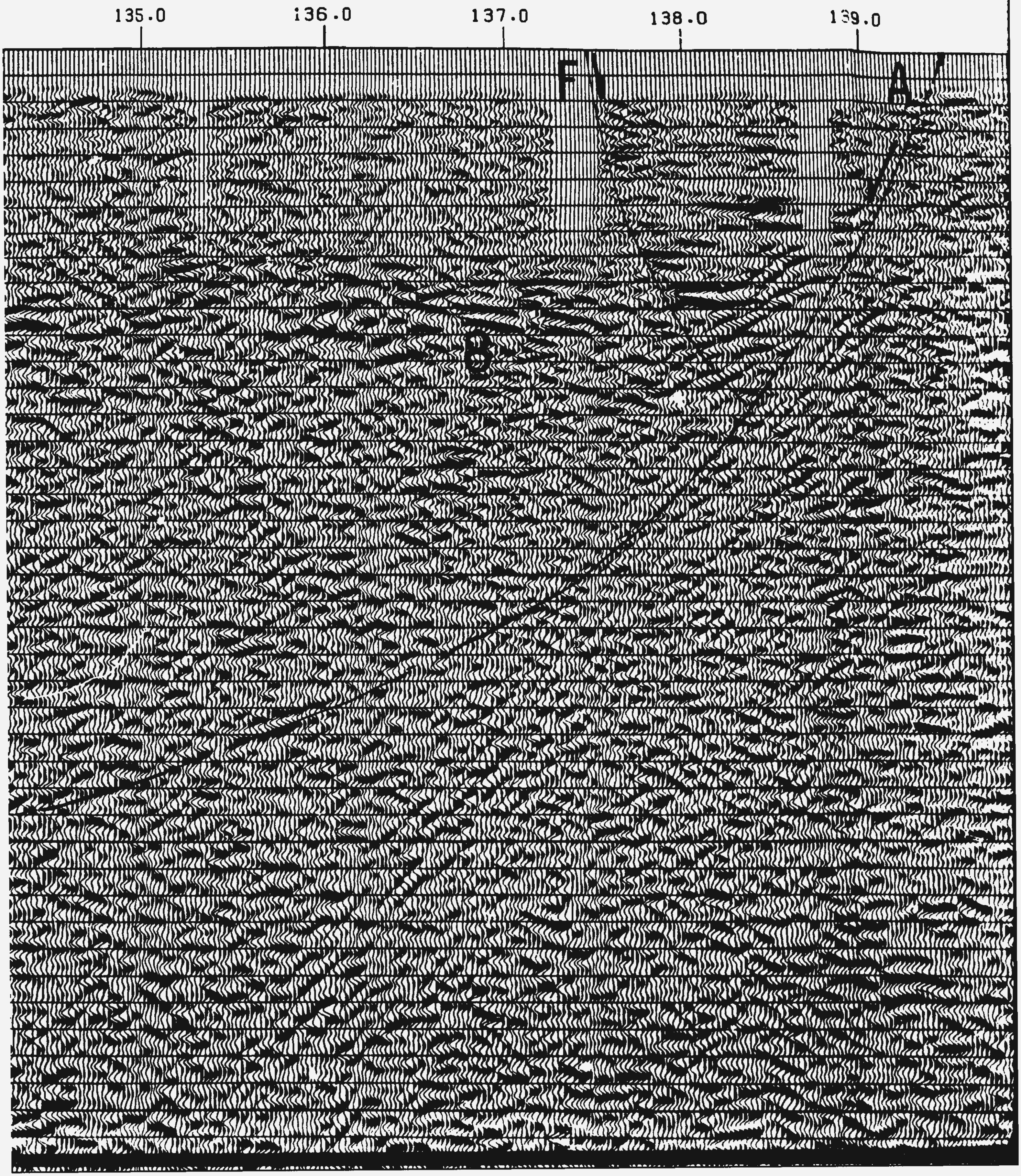

135.0
136.0
137.0
138.0
139.0
F
A
B

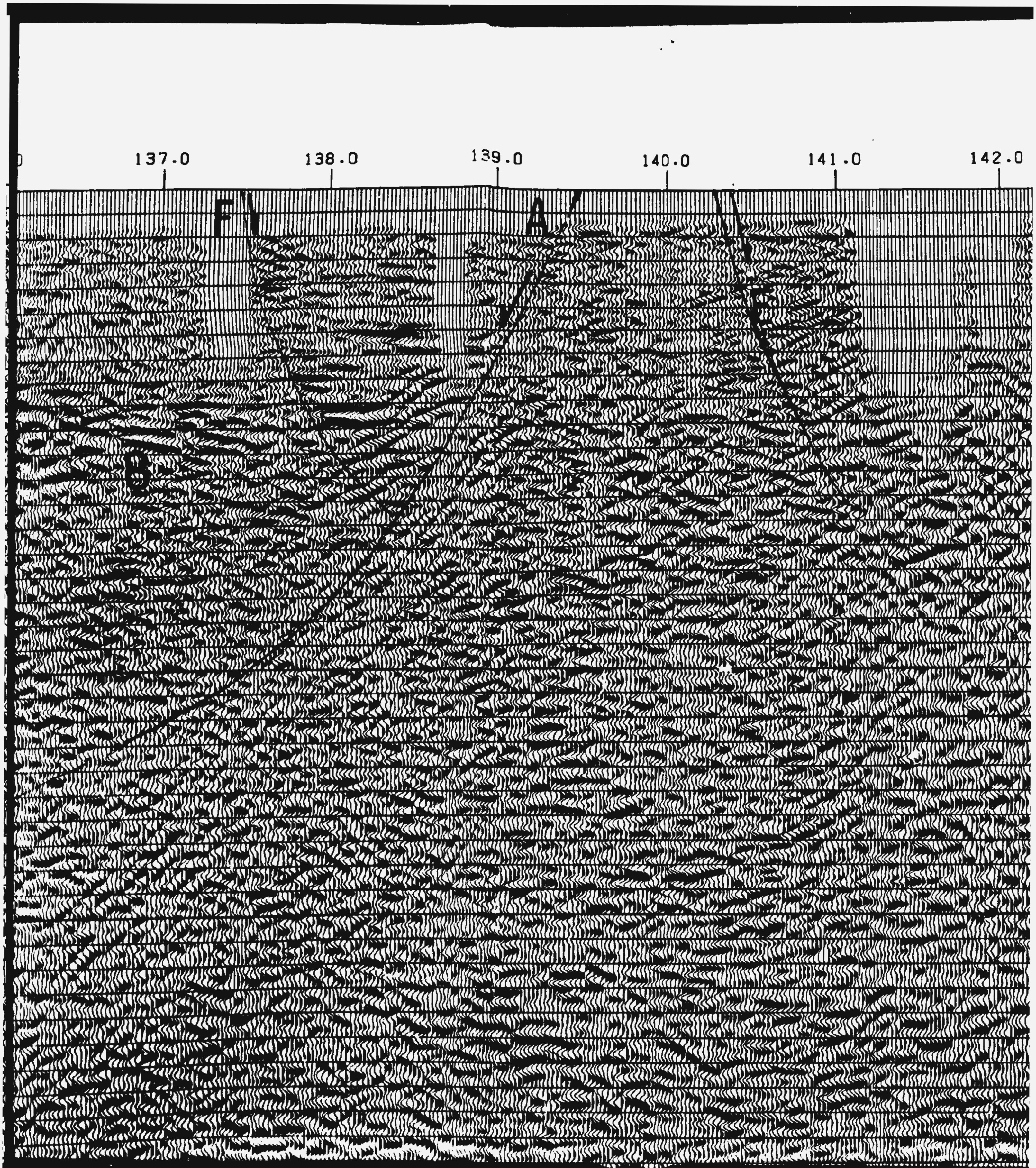

137.0
138.0
139.0
140.0
141.0
142.0
F
A
B

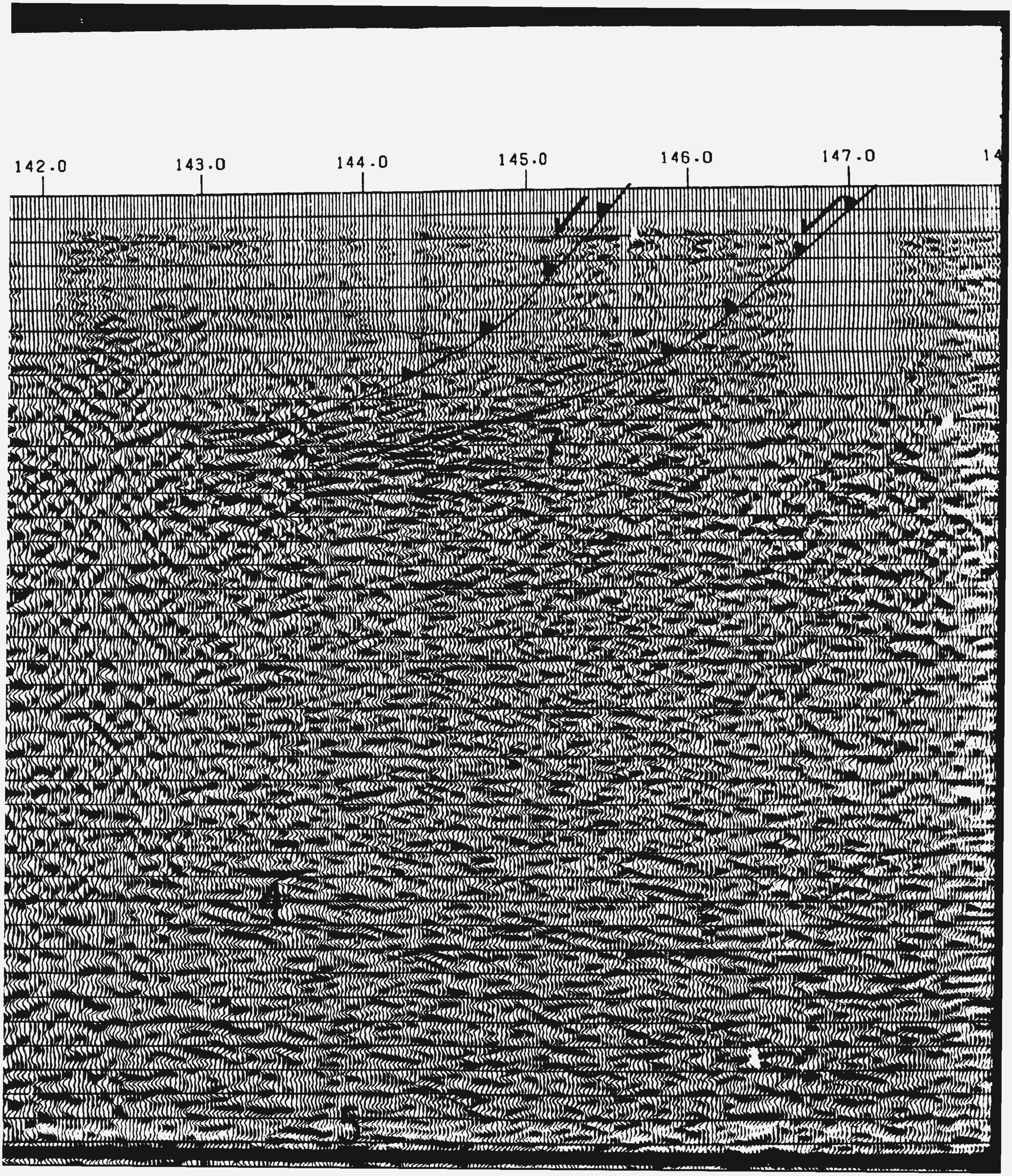
142.0
143.0
144.0
145.0
146.0
147.0

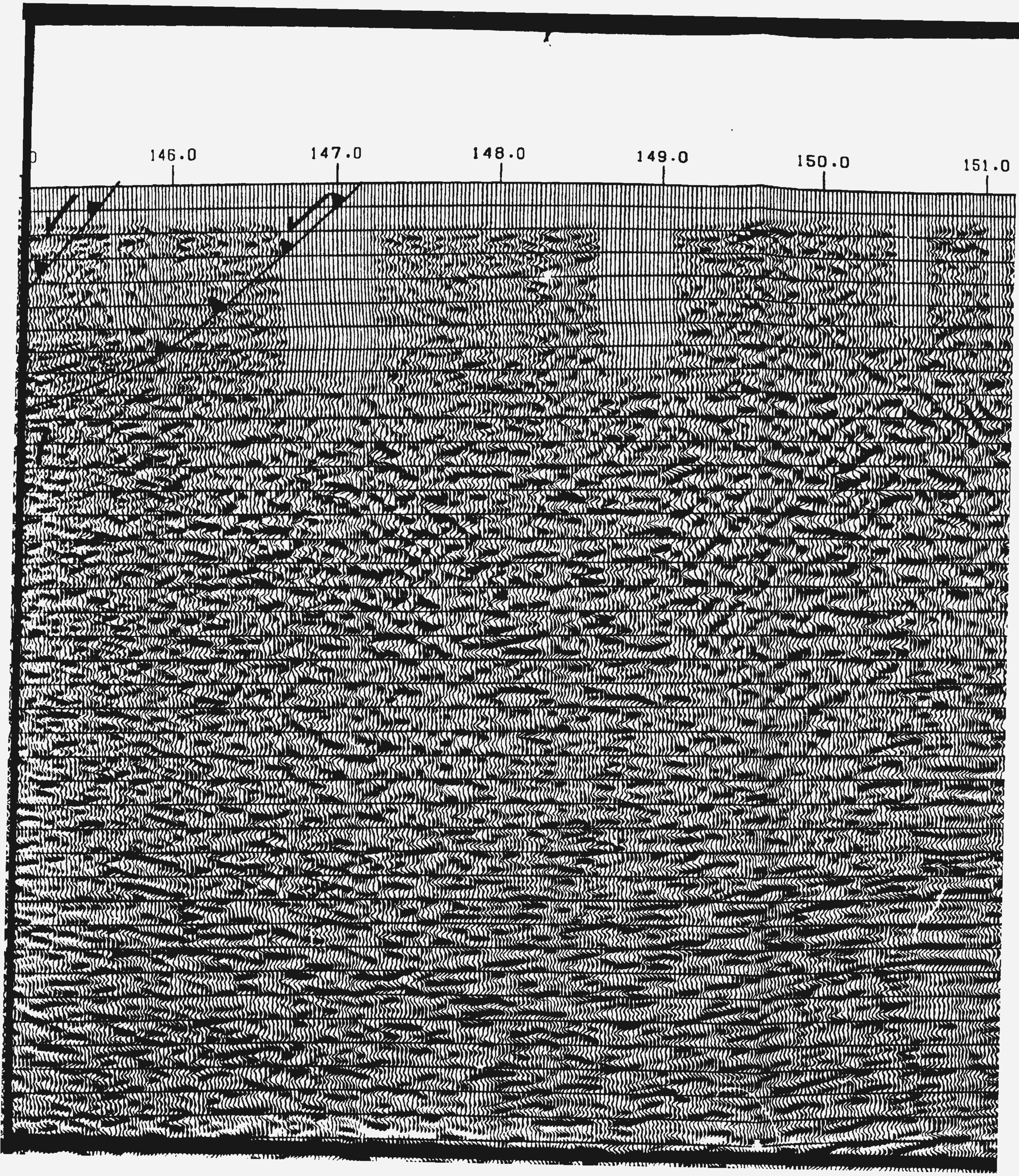

146.0
147.0
148.0
149.0
150.0
151.0

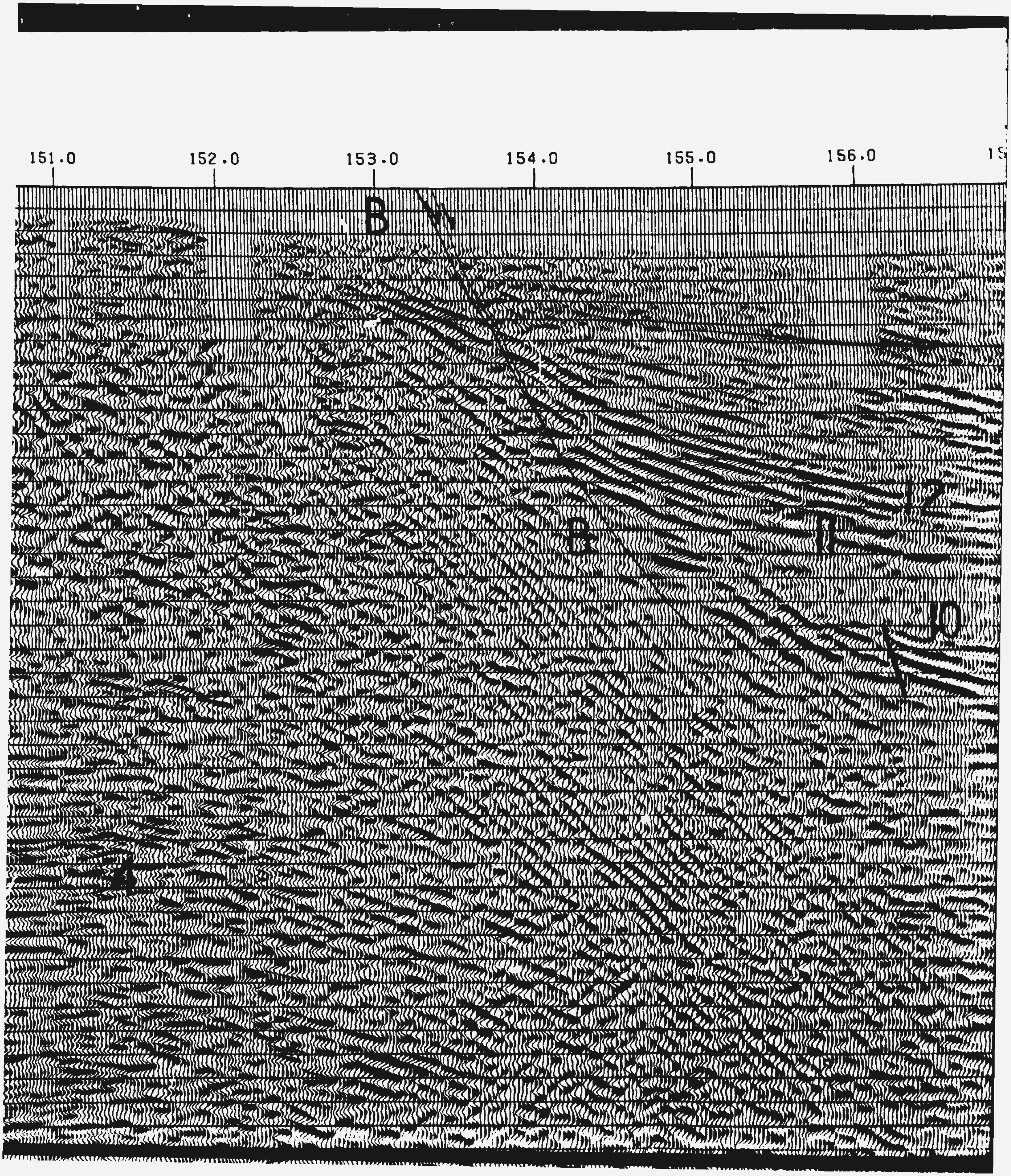
151.0
152.0
153.0
154.0
155.0
156.0
B
R

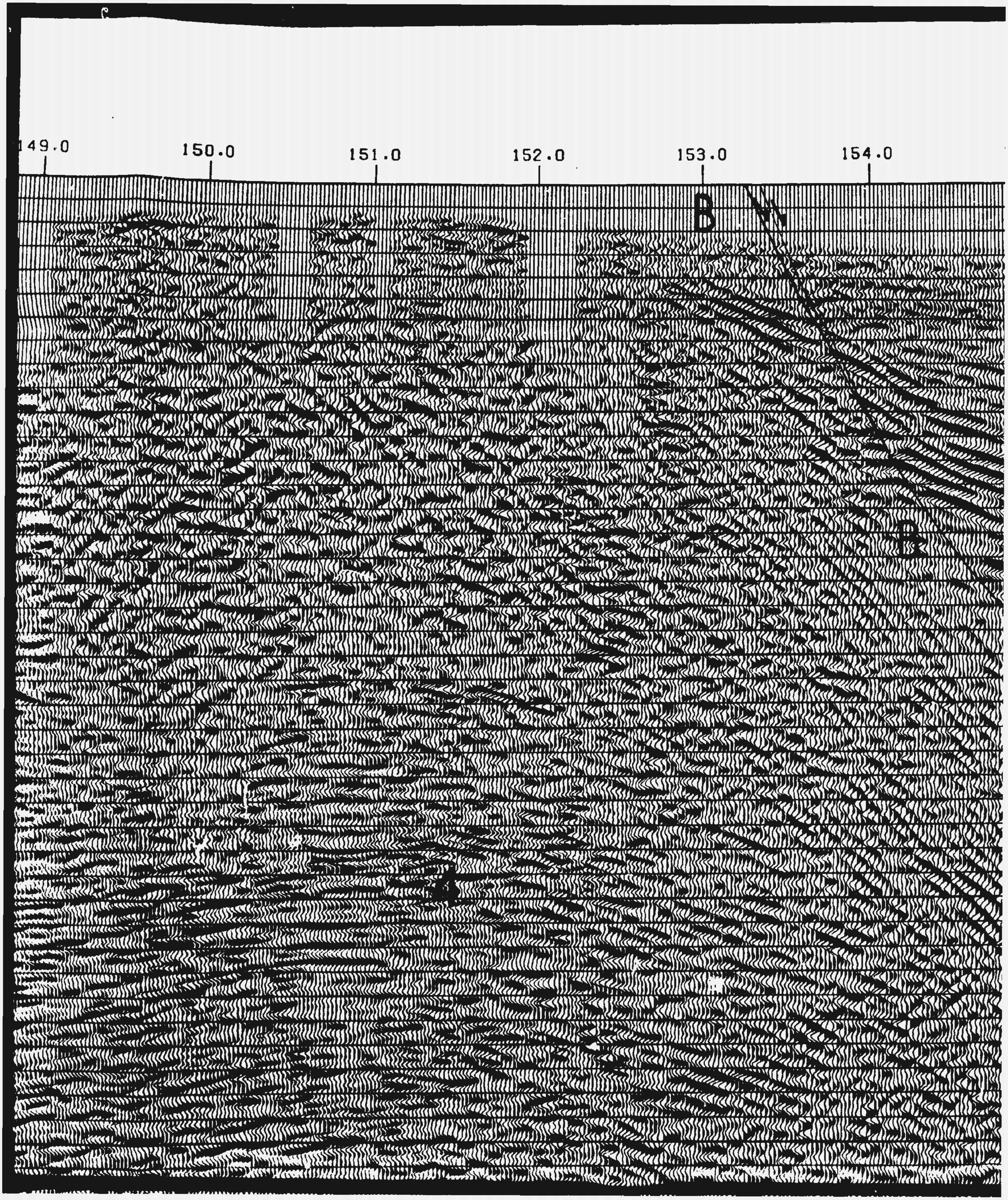
149.0
150.0
151.0
152.0
153.0
154.0
B

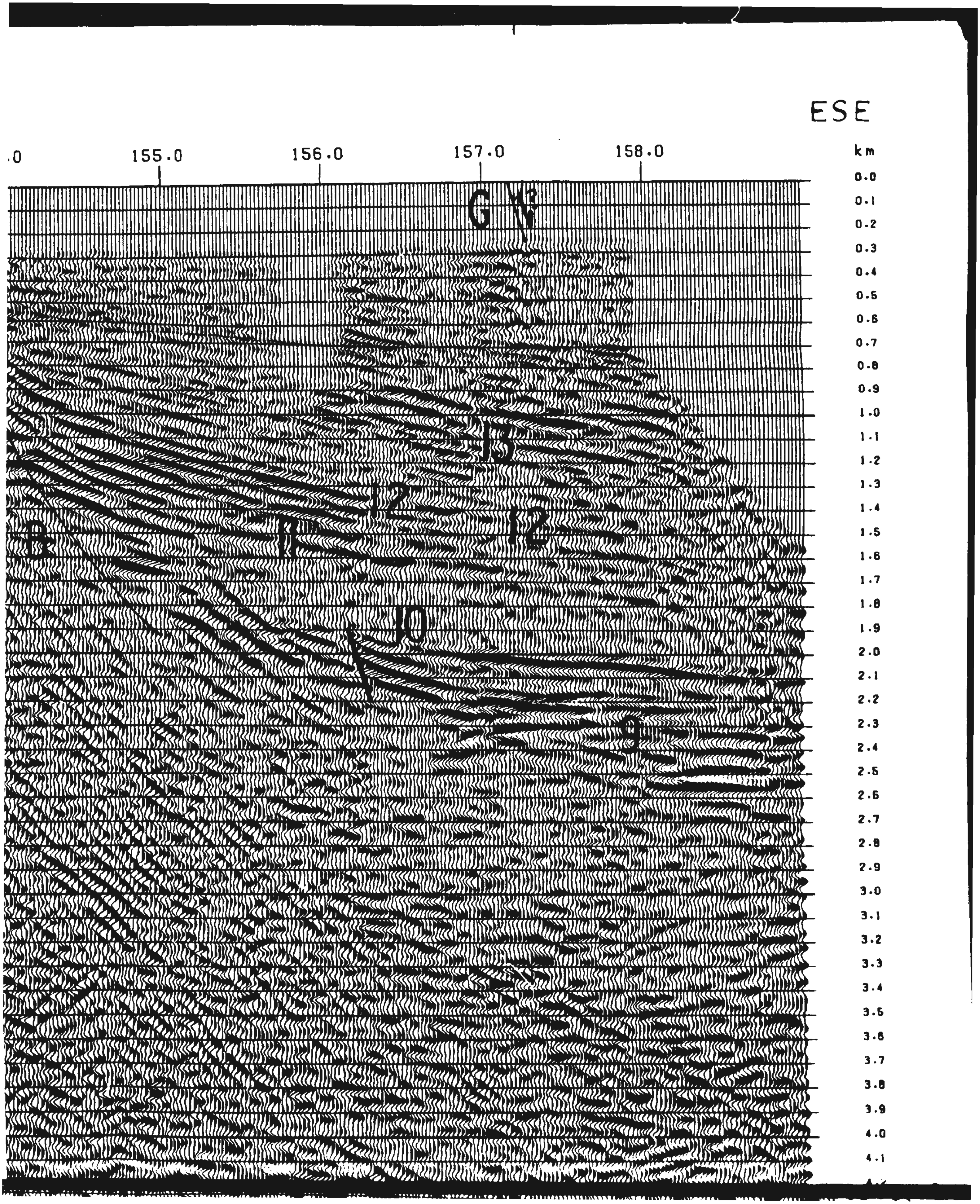
ESE
.0
155.0
156.0
157.0
158.0
km
0.0
0.1
0.2
0.3
0.4
0.5
0.6
0.7
0.8
0.9
1.0
1.1
1.2
1.3
1.4
1.5
1.6
1.7
1.8
1.9
2.0
2.1
2.2
2.3
2.4
2.5
2.6
2.7
2.8
2.9
3.0
3.1
3.2
3.3
3.4
3.5
3.6
3.7
3.8
3.9
4.0
4.1
G
13
12
12
11
10
9

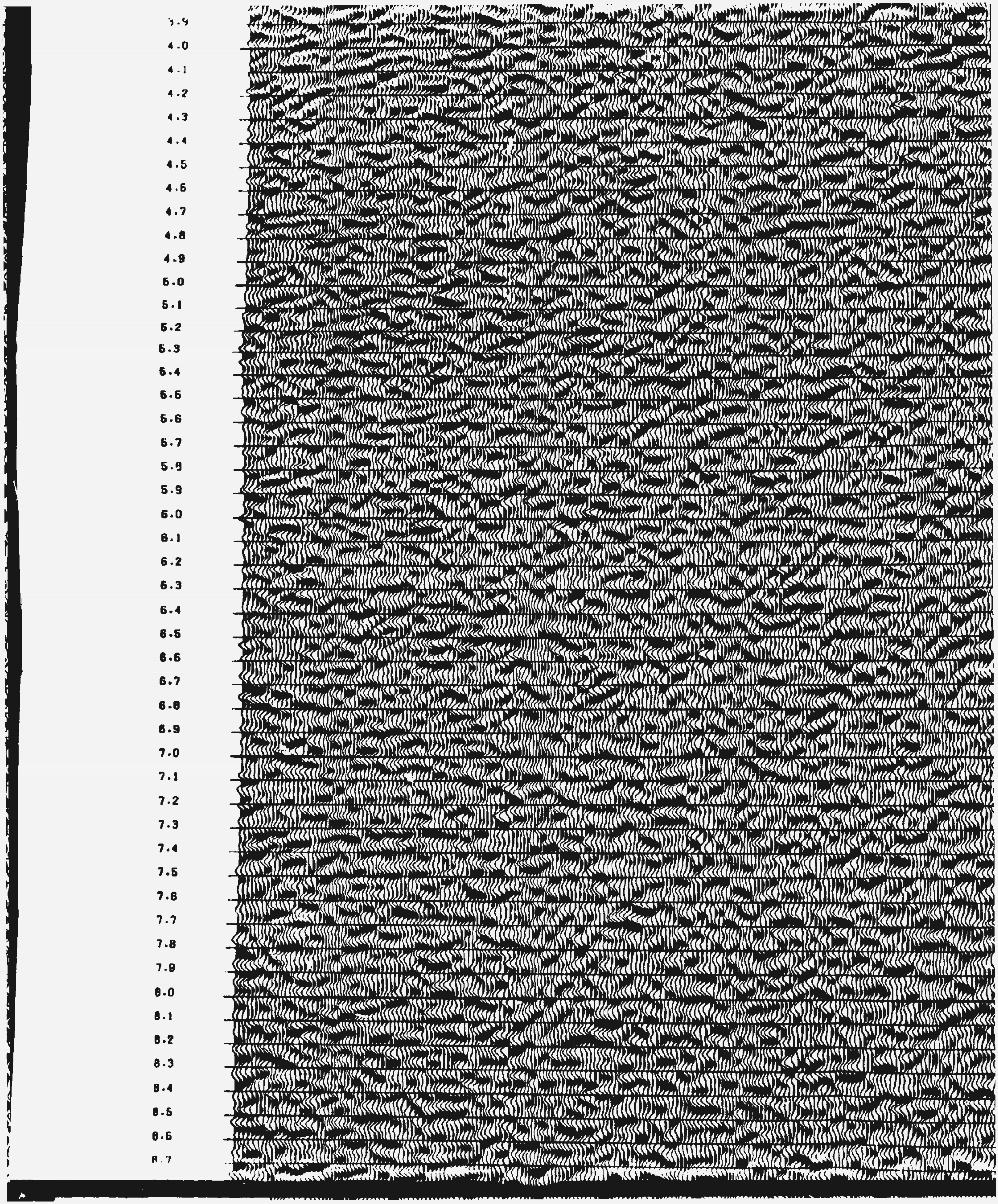
3.9
4.0
4.1
4.2
4.3
4.4
4.5
4.6
4.7
4.8
4.9
5.0
5.1
5.2
5.3
5.4
5.5
5.6
5.7
5.8
5.9
6.0
6.1
6.2
6.3
6.4
6.5
6.6
6.7
6.8
6.9
7.0
7.1
7.2
7.3
7.4
7.5
7.6
7.7
7.8
7.9
8.0
8.1
8.2
8.3
8.4
8.5
8.6
8.7

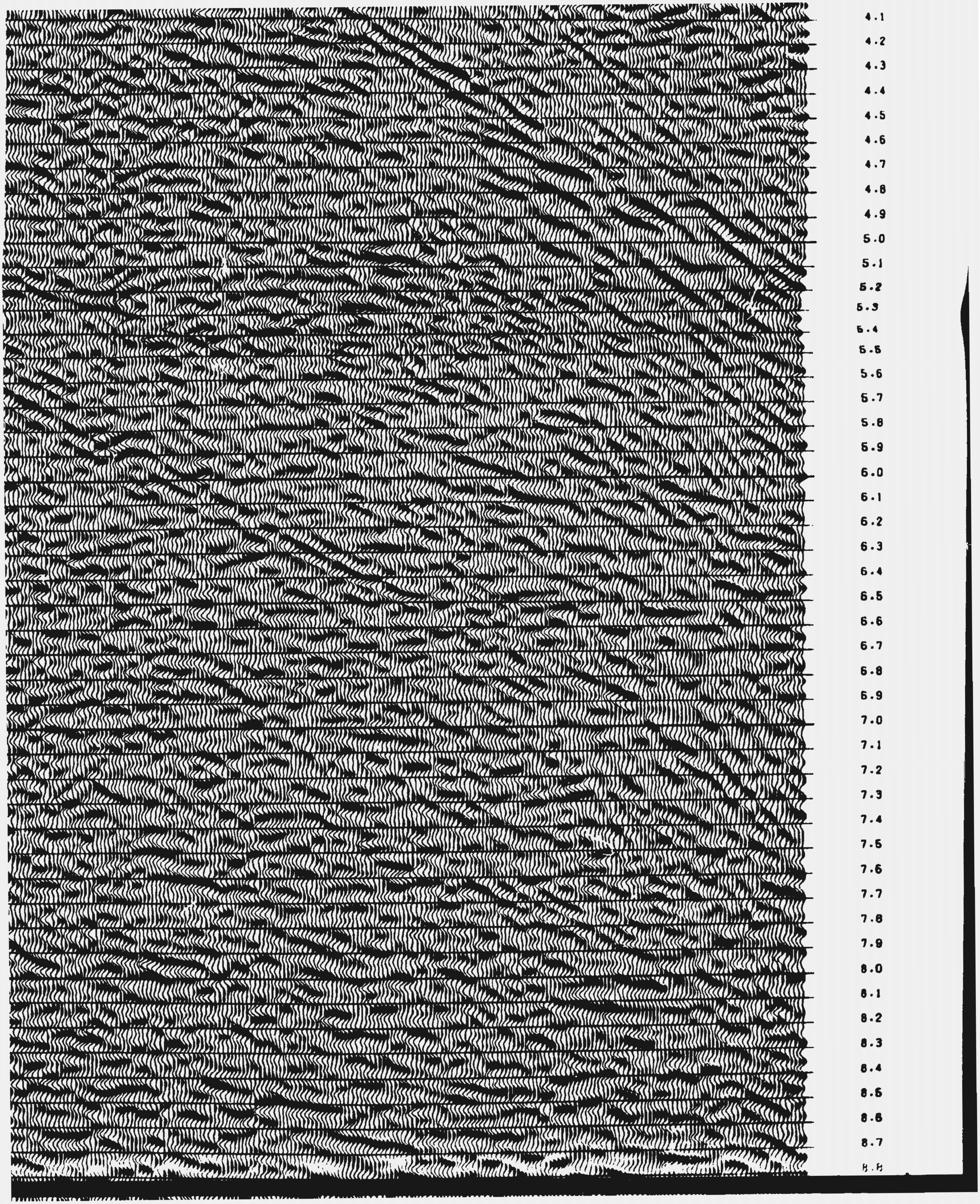
4.1
4.2
4.3
4.4
4.5
4.6
4.7
4.8
4.9
5.0
5.1
5.2
5.3
5.4
5.5
5.6
5.7
5.8
5.9
6.0
6.1
6.2
6.3
6.4
6.5
6.6
6.7
6.8
6.9
7.0
7.1
7.2
7.3
7.4
7.5
7.6
7.7
7.8
7.9
8.0
8.1
8.2
8.3
8.4
8.5
8.6
8.7
8.8

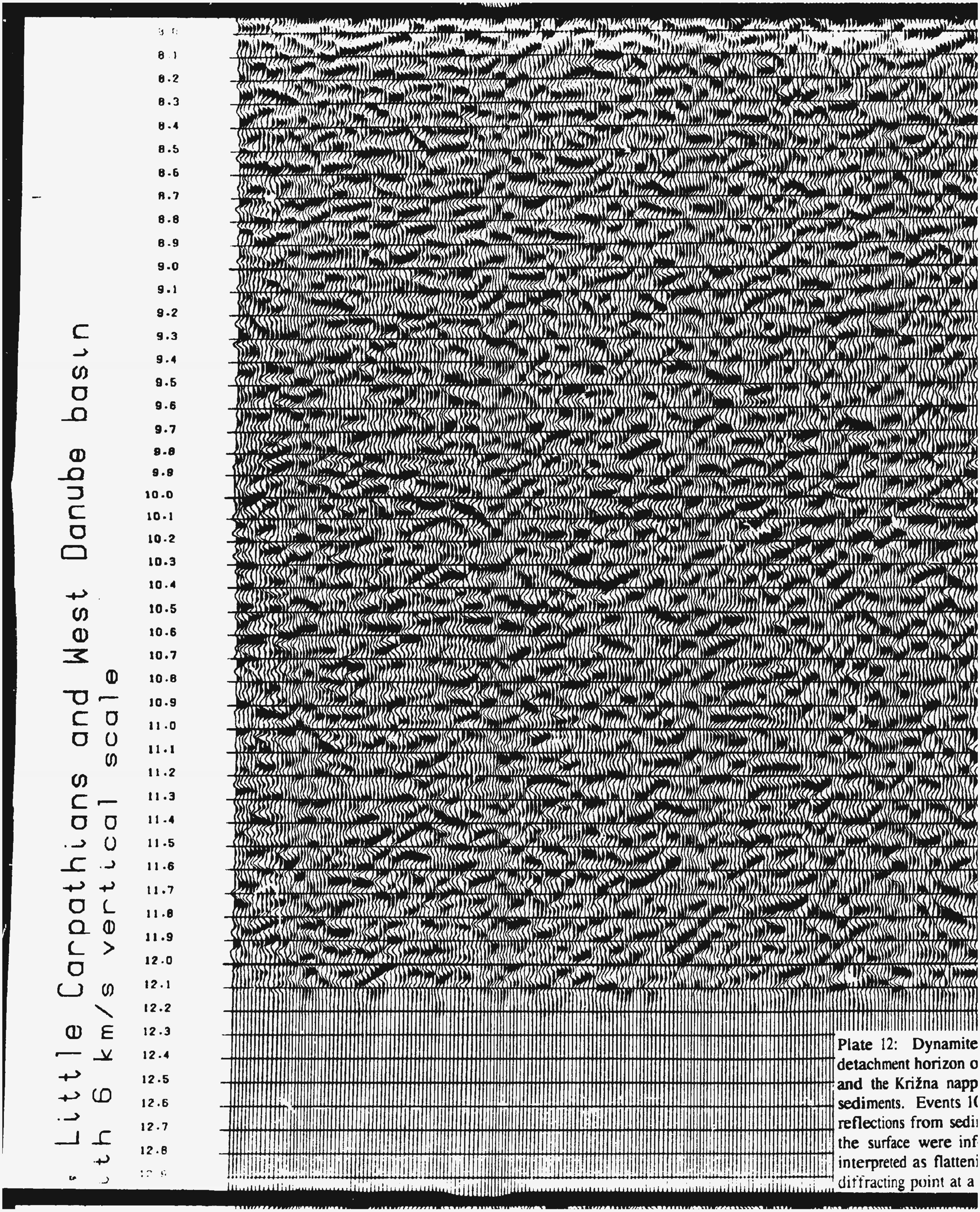

Plate 12: Dynamite
detachment horizon o
and the Križna napp
sediments. Events 1(
reflections from sedi
the surface were inf
interpreted as flatteni
diffracting point at a

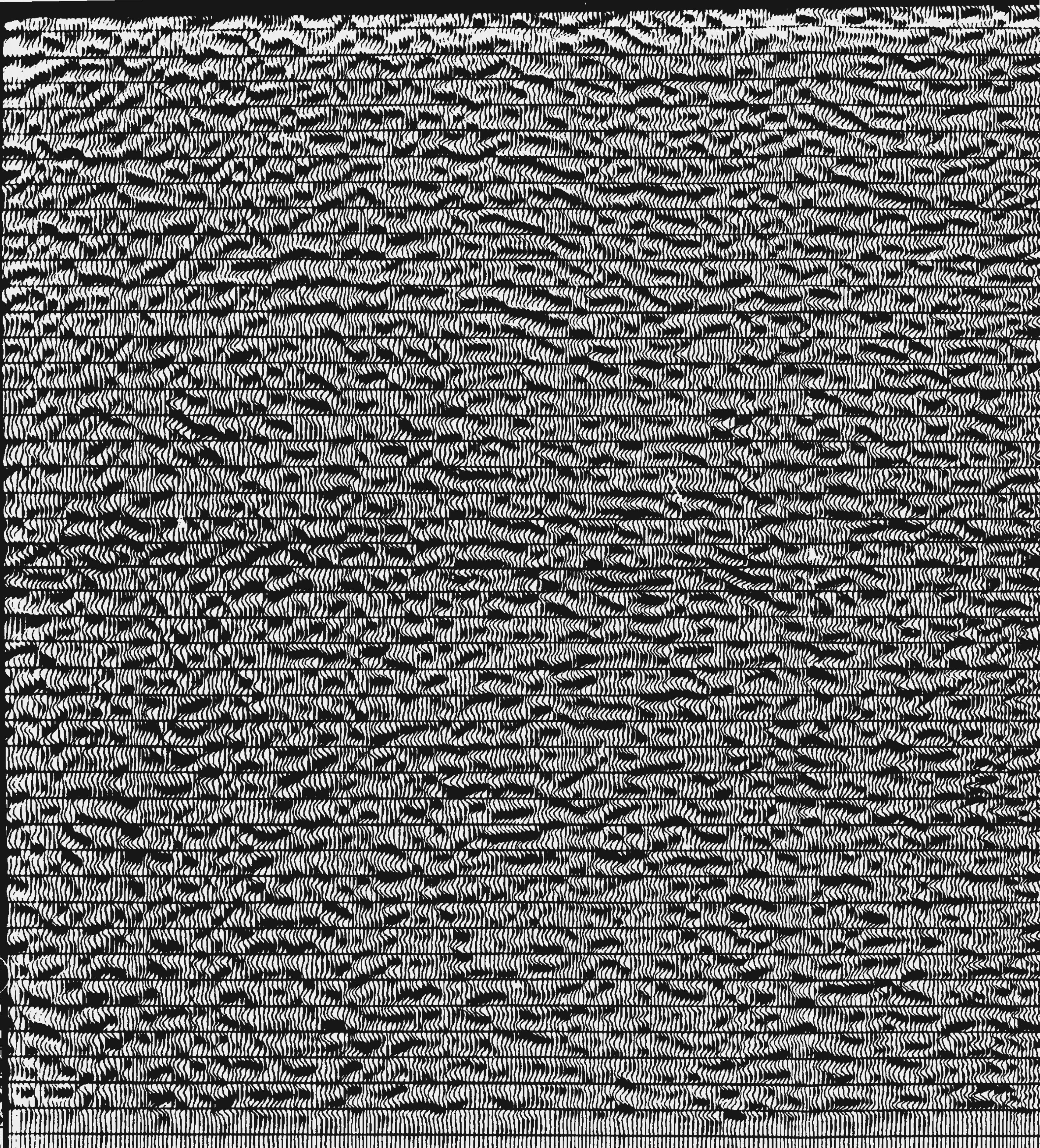

ynamite source seismic line 8HR with interpretation. Events 1 to 5 are shear zones. Event 6 is the
orizon of a dip-slip fault zone withi the Vienna basin. Event 7 is a thrust plane between the Envelope nappe
a nappe. Event 8 is the basement of the Vienna basin. Event 9 comes from deep beds of Neogene
vents 10 to 13 comes from sedimentary interfaces within the West Danube basin while events 14 to 16 are
om sedimetary interfaces within the Vienna basin. Faults A to G as well as non identified faults reaching
ere inferred from geologic map so their dip is uncertain (Plate 1). Fault A is of Neogene age and is
flattening into event 6. Fault B is the boundary of the West Danube basin. Fault D corresponds with a

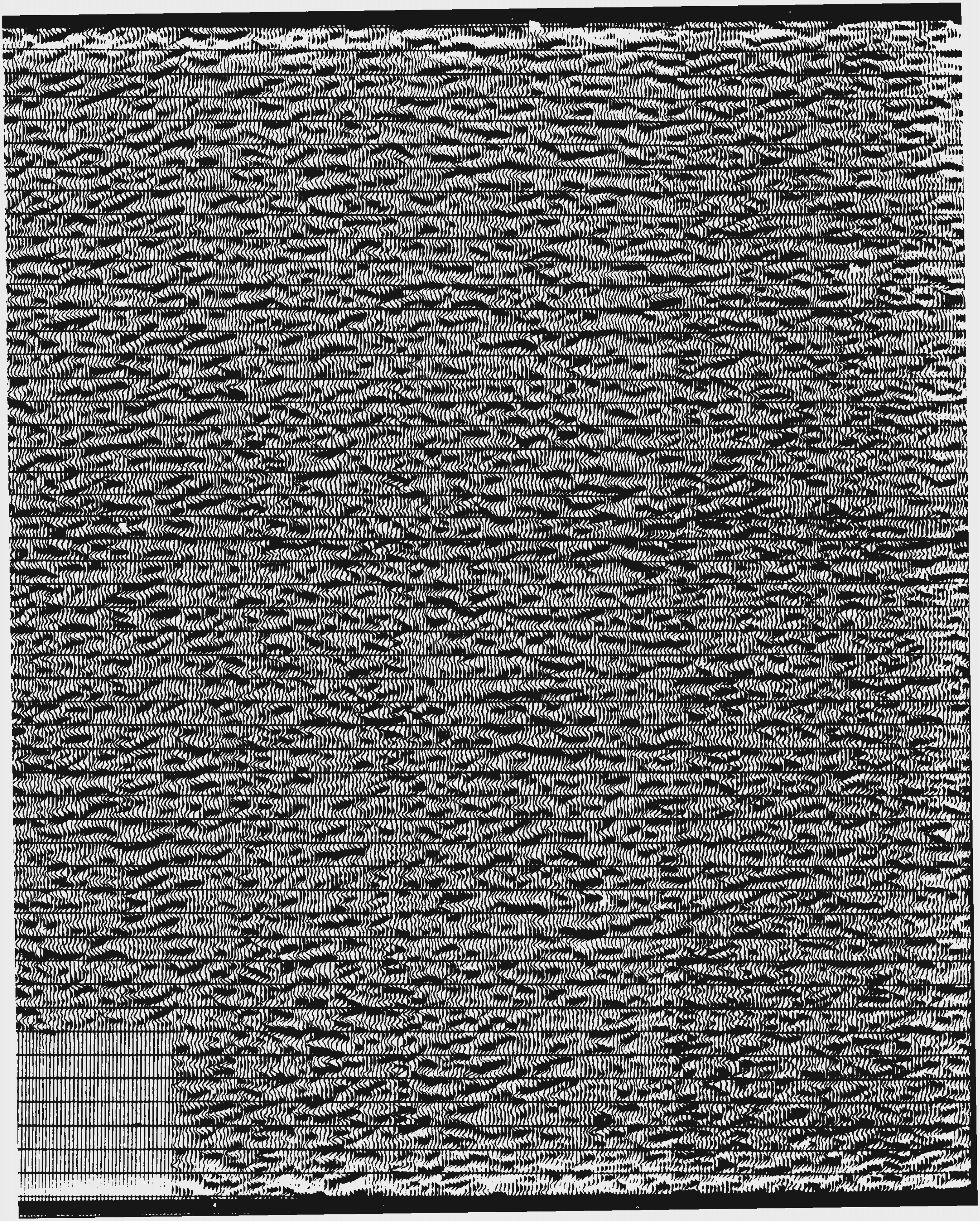

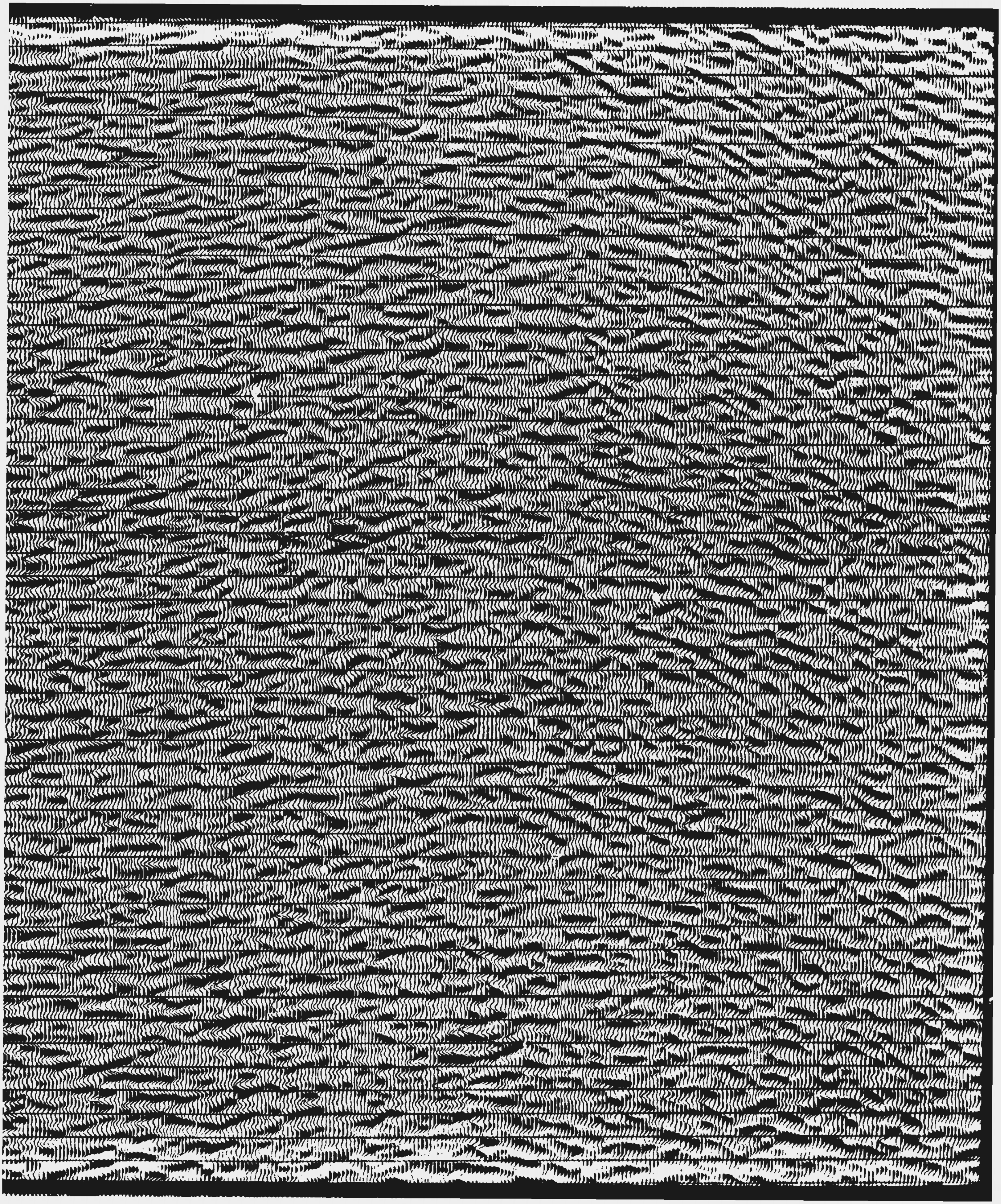

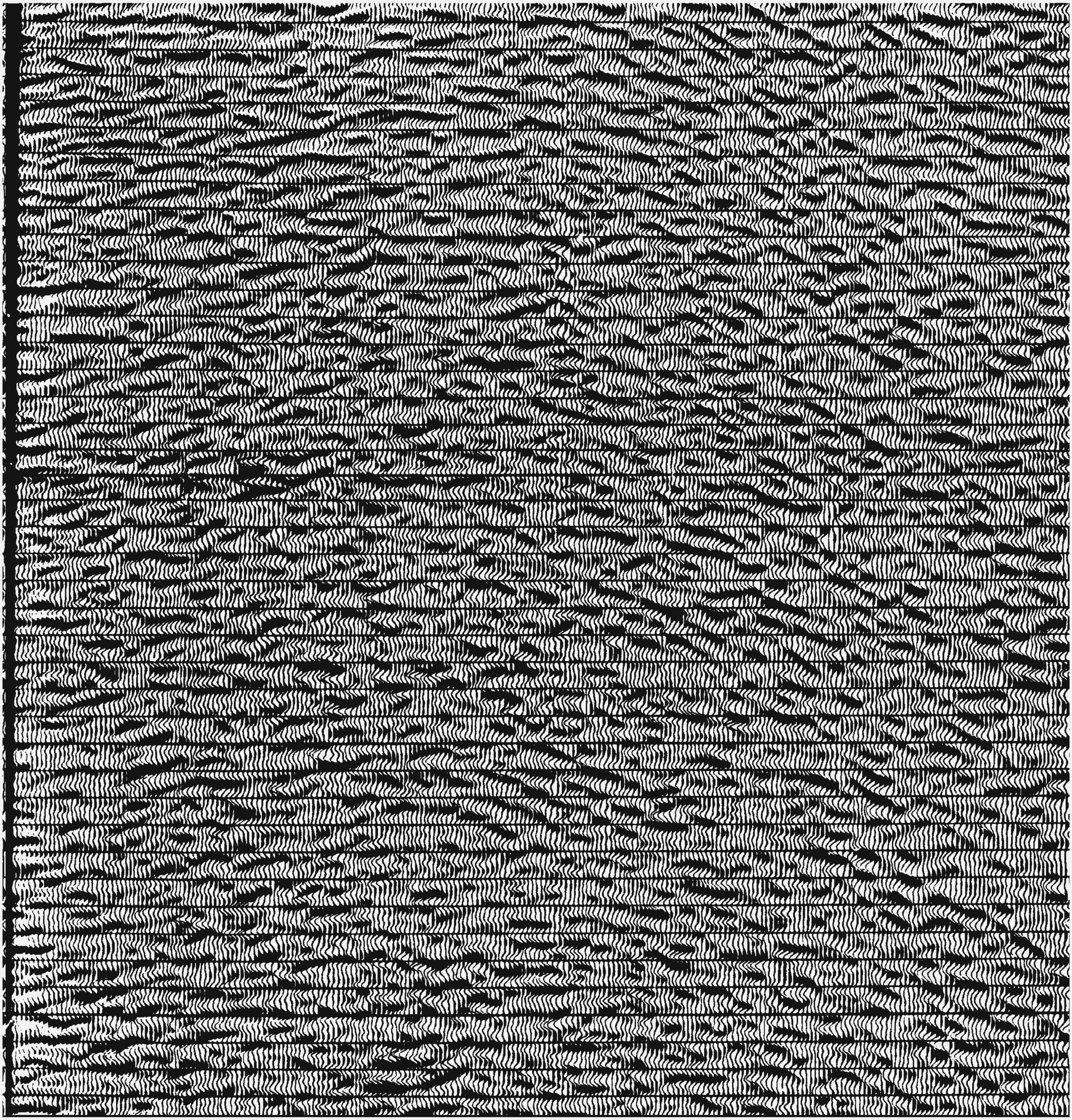

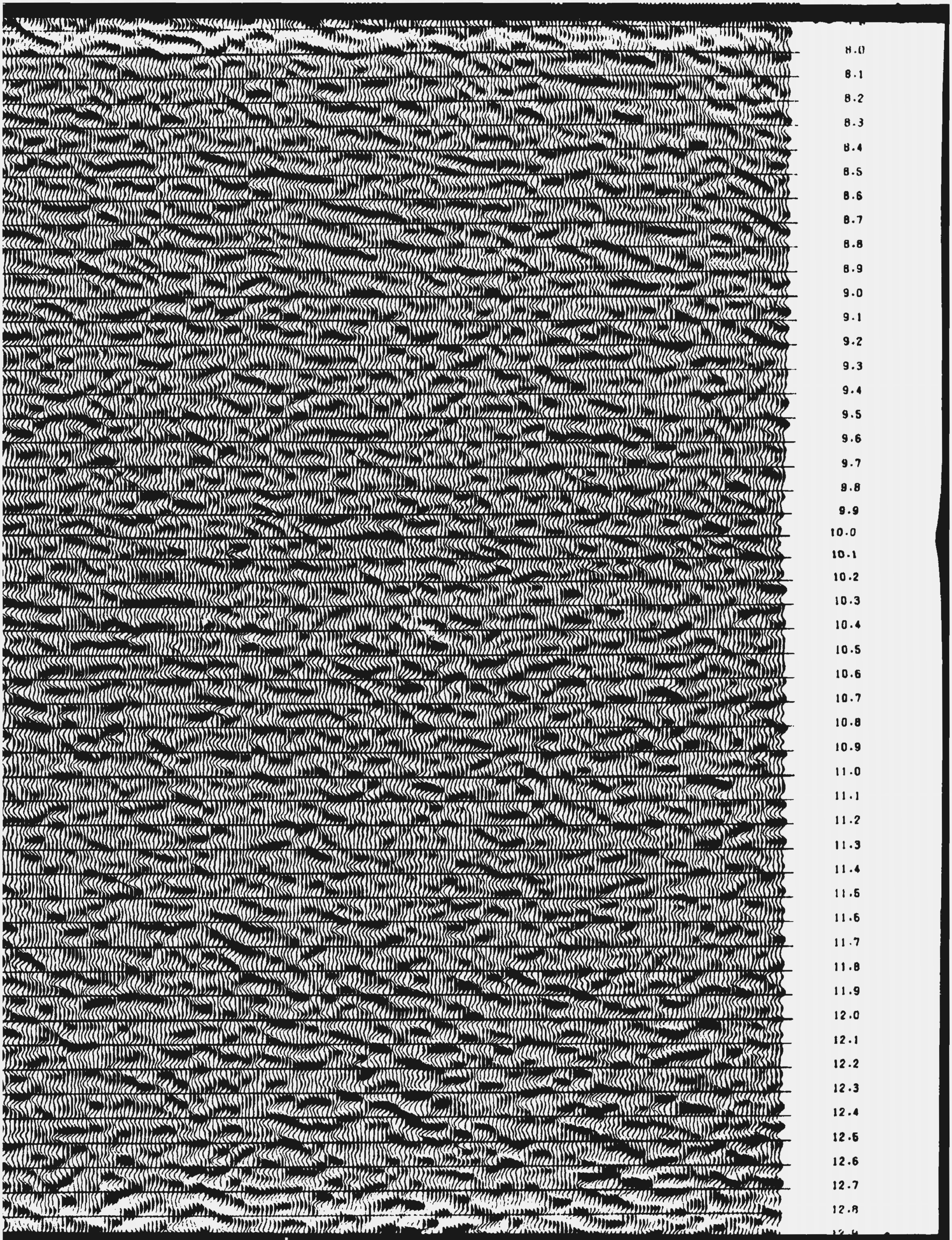
8.0
8.1
8.2
8.3
8.4
8.5
8.6
8.7
8.8
8.9
9.0
9.1
9.2
9.3
9.4
9.5
9.6
9.7
9.8
9.9
10.0
10.1
10.2
10.3
10.4
10.5
10.6
10.7
10.8
10.9
11.0
11.1
11.2
11.3
11.4
11.5
11.6
11.7
11.8
11.9
12.0
12.1
12.2
12.3
12.4
12.5
12.6
12.7
12.8

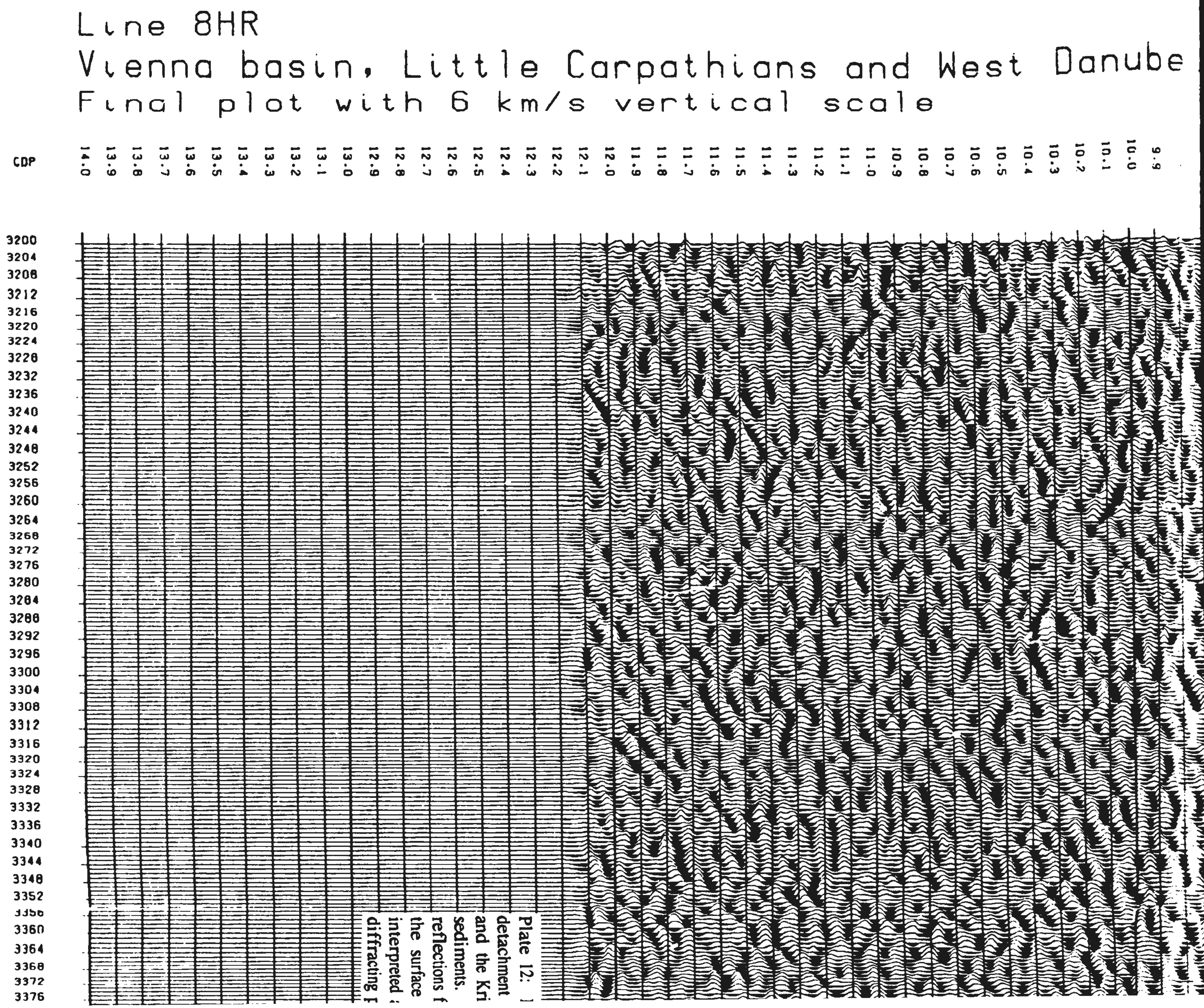

Plate 12: [illegible]
detachment
and the Kri
sediments.
reflections f
the surface
interpreted a
diffracting I

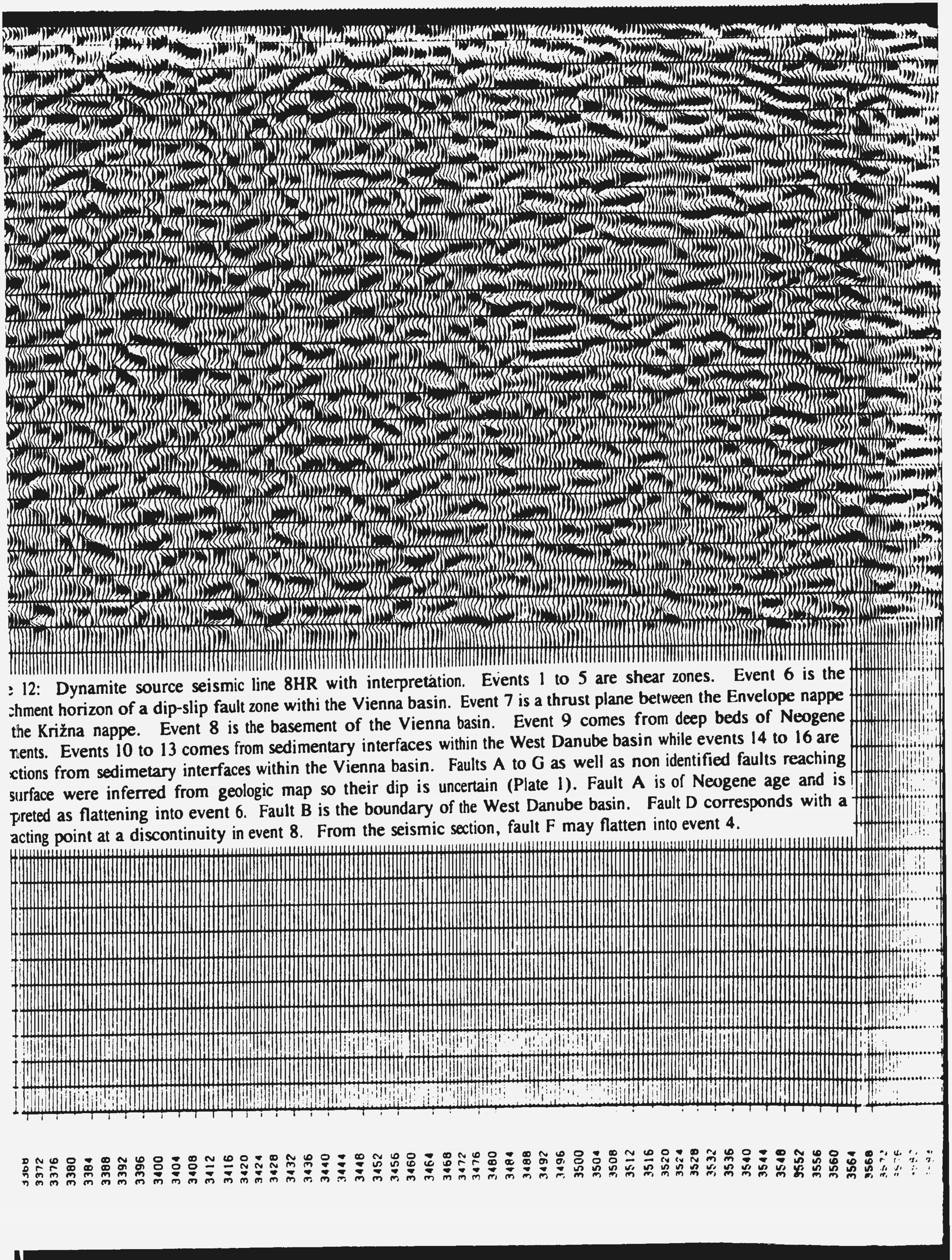

: 12: Dynamite source seismic line 8HR with interpretation. Events 1 to 5 are shear zones. Event 6 is the chment horizon of a dip-slip fault zone withi the Vienna basin. Event 7 is a thrust plane between the Envelope nappe the Križna nappe. Event 8 is the basement of the Vienna basin. Event 9 comes from deep beds of Neogene nents. Events 10 to 13 comes from sedimentary interfaces within the West Danube basin while events 14 to 16 are ctions from sedimetary interfaces within the Vienna basin. Faults A to G as well as non identified faults reaching surface were inferred from geologic map so their dip is uncertain (Plate 1). Fault A is of Neogene age and is preted as flattening into event 6. Fault B is the boundary of the West Danube basin. Fault D corresponds with a acting point at a discontinuity in event 8. From the seismic section, fault F may flatten into event 4.

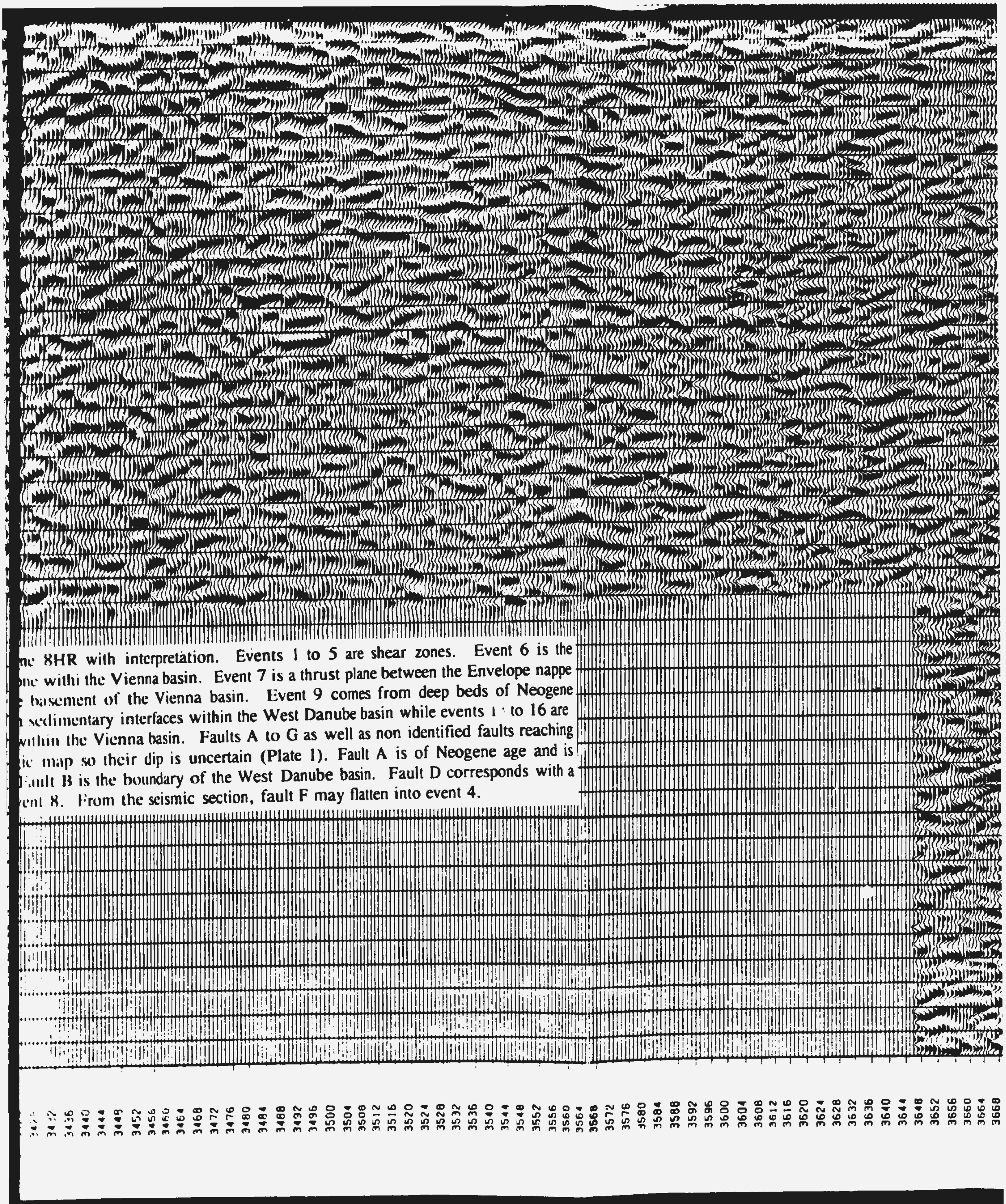

ne 8HR with interpretation. Events 1 to 5 are shear zones. Event 6 is the one withi the Vienna basin. Event 7 is a thrust plane between the Envelope nappe e basement of the Vienna basin. Event 9 comes from deep beds of Neogene n sedimentary interfaces within the West Danube basin while events 1[illegible] to 16 are within the Vienna basin. Faults A to G as well as non identified faults reaching ic map so their dip is uncertain (Plate 1). Fault A is of Neogene age and is Fault B is the boundary of the West Danube basin. Fault D corresponds with a vent 8. From the seismic section, fault F may flatten into event 4.

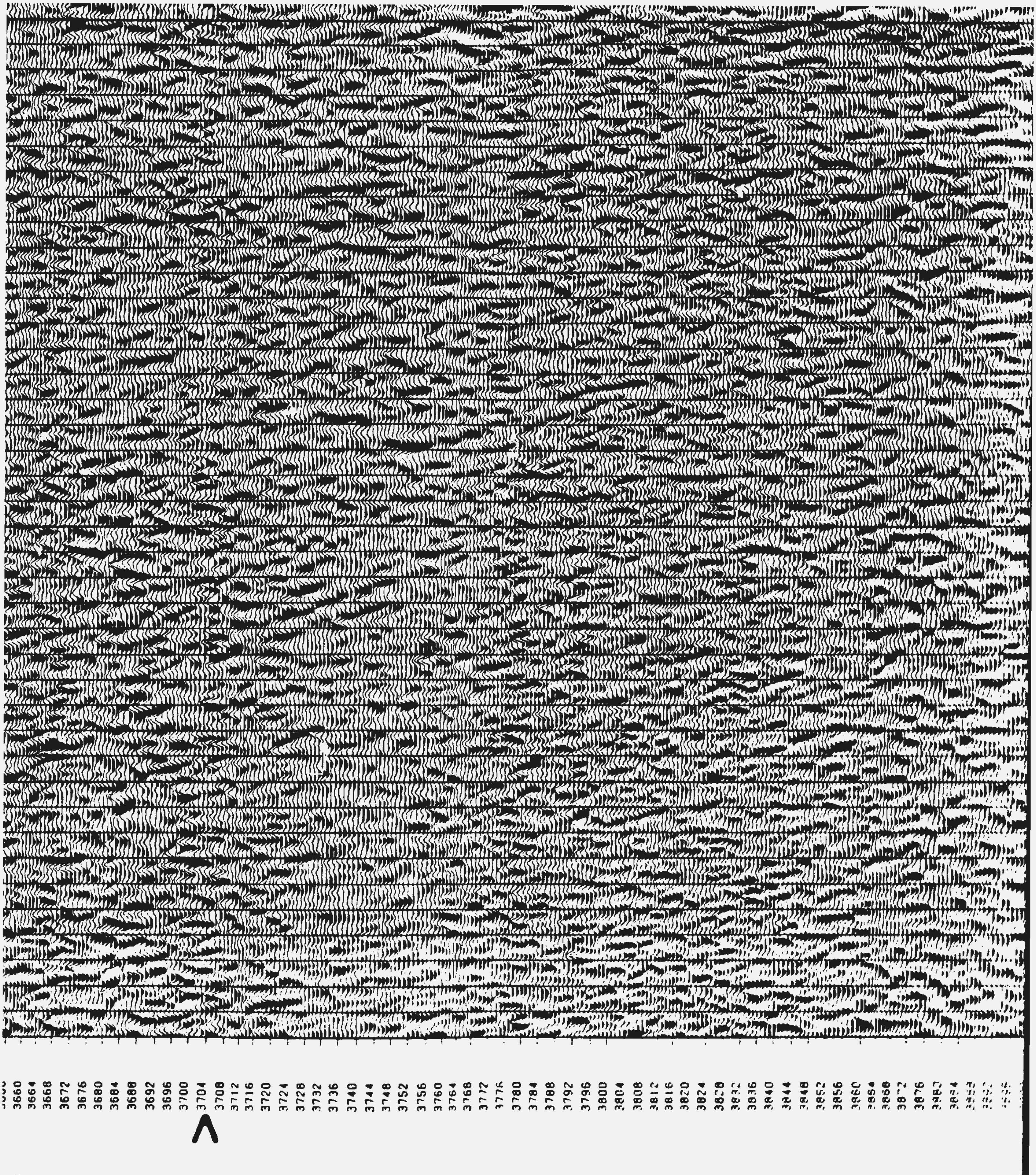
3660
3664
3668
3672
3676
3680
3684
3688
3692
3696
3700
3704
3708
3712
3716
3720
3724
3728
3732
3736
3740
3744
3748
3752
3756
3760
3764
3768
3780
3784
3788
3792
3796
3800
3804
3808
3816
3820
3824
3836
3840
3856
3876

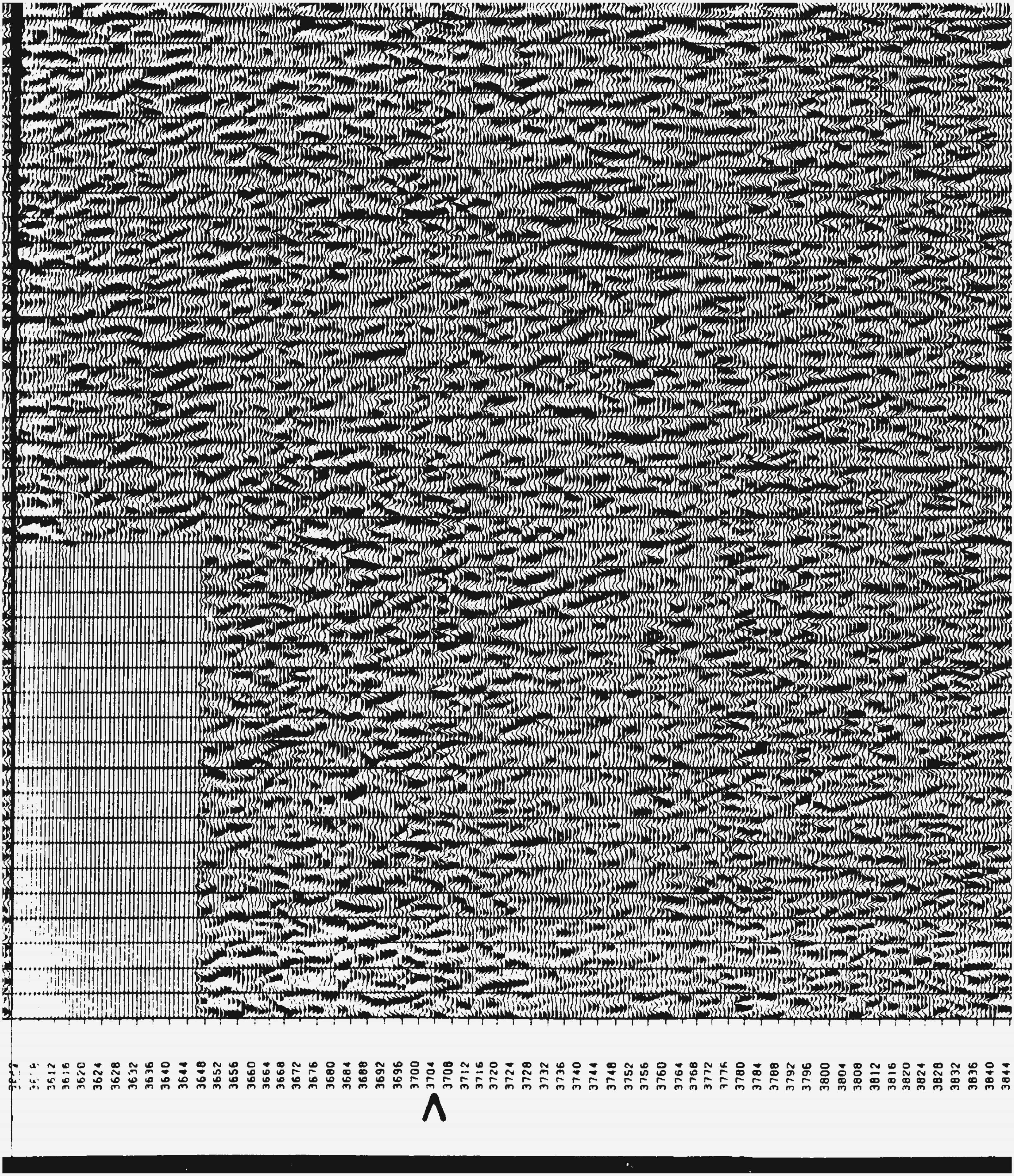
3616 3620 3624 3628 3632 3636 3640 3644 3648 3652 3656 3660 3664 3668 3672 3676 3680 3684 3688 3692 3696 3700 3704 3708 3712 3716 3720 3724 3728 3732 3736 3740 3744 3748 3752 3756 3760 3764 3768 3772 3776 3780 3784 3788 3792 3796 3800 3804 3808 3812 3816 3820 3824 3828 3832 3836 3840 3844

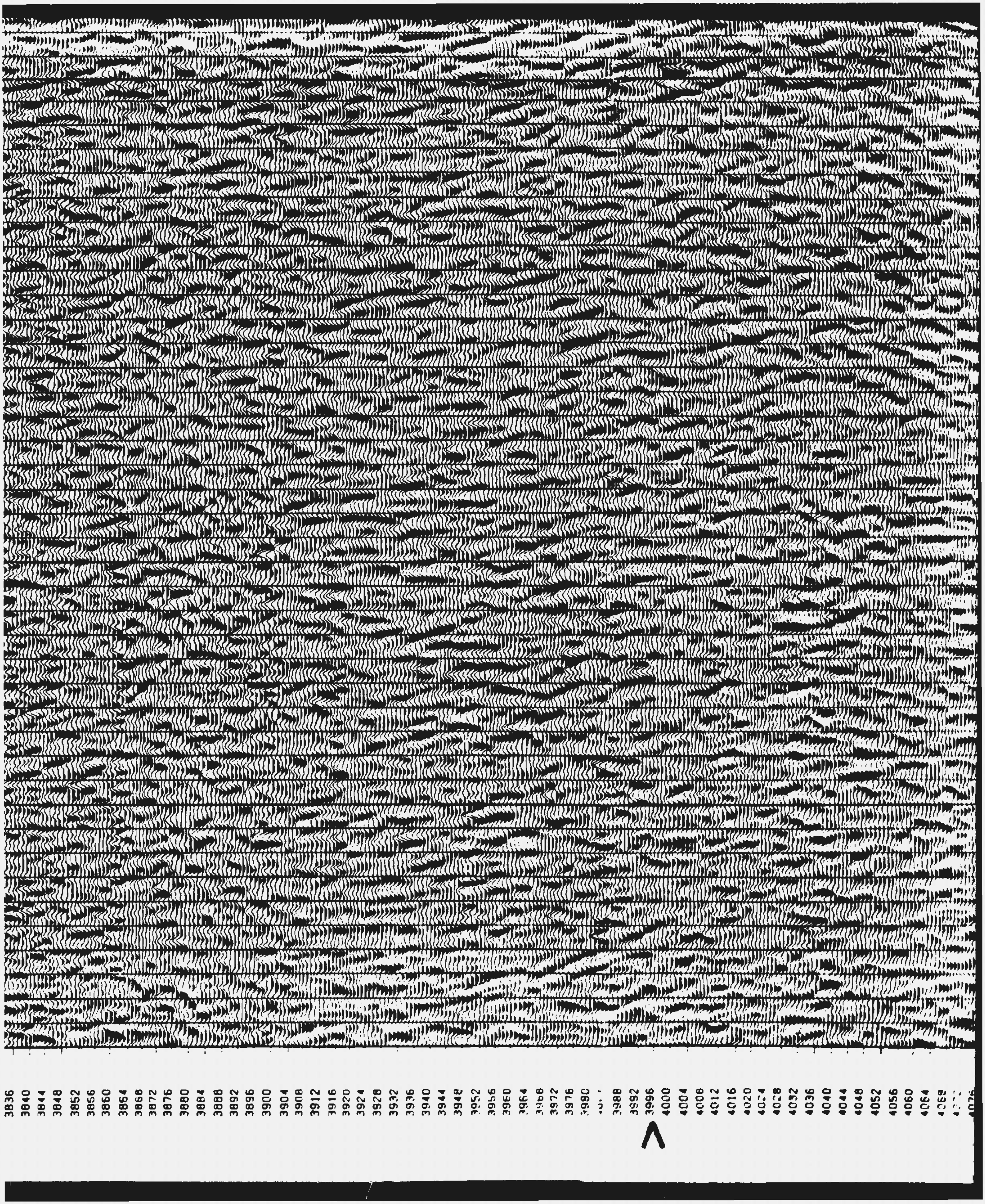
3836
3840
3844
3848
3852
3856
3860
3864
3868
3872
3876
3880
3884
3888
3892
3896
3900
3904
3908
3912
3916
3920
3924
3928
3932
3936
3940
3944
3948
3952
3956
3960
3964
3968
3972
3976
3980
3988
3992
3996
4000
4004
4008
4012
4016
4020
4024
4028
4032
4036
4040
4044
4048
4052
4056
4060
4064

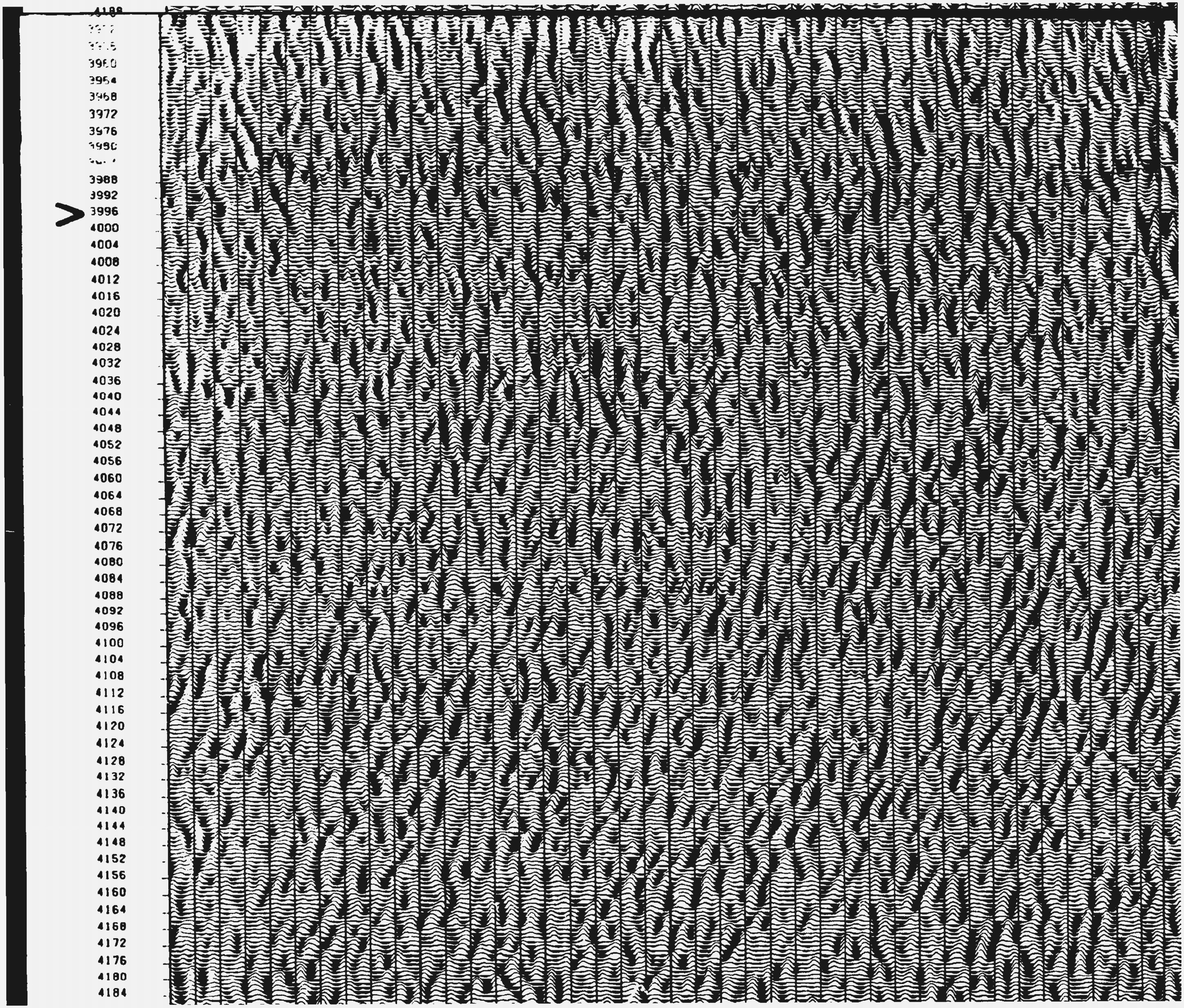
3968
3972
3976
3988
3992
3996
4000
4004
4008
4012
4016
4020
4024
4028
4032
4036
4040
4044
4048
4052
4056
4060
4064
4068
4072
4076
4080
4084
4088
4092
4096
4100
4104
4108
4112
4116
4120
4124
4128
4132
4136
4140
4144
4148
4152
4156
4160
4164
4168
4172
4176
4180
4184

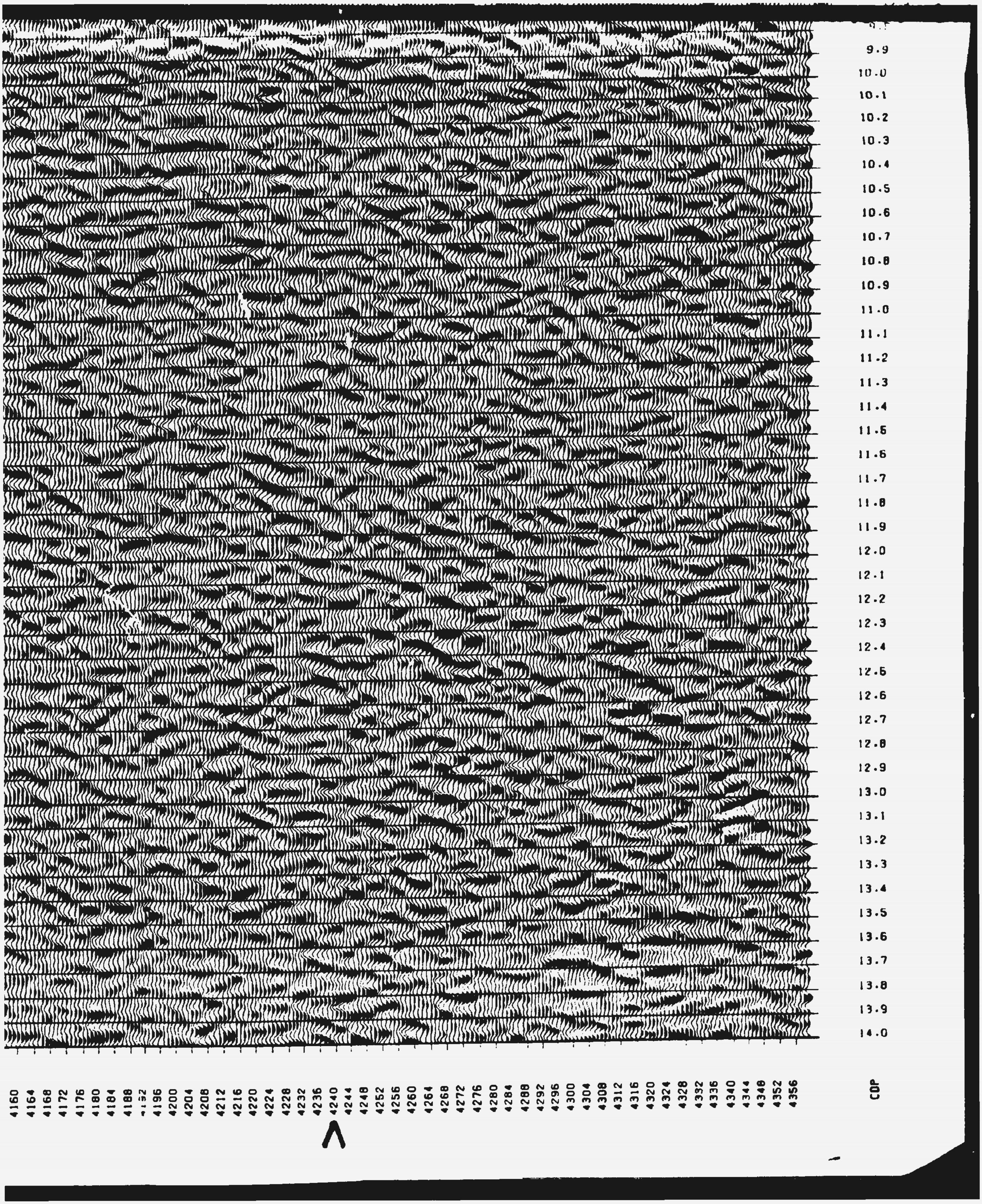

9.9
10.0
10.1
10.2
10.3
10.4
10.5
10.6
10.7
10.8
10.9
11.0
11.1
11.2
11.3
11.4
11.5
11.6
11.7
11.8
11.9
12.0
12.1
12.2
12.3
12.4
12.5
12.6
12.7
12.8
12.9
13.0
13.1
13.2
13.3
13.4
13.5
13.6
13.7
13.8
13.9
14.0
4160
4164
4168
4172
4176
4180
4184
4188
4196
4200
4204
4208
4212
4216
4220
4224
4228
4232
4236
4240
4244
4248
4252
4256
4260
4264
4268
4272
4276
4280
4284
4288
4292
4296
4300
4304
4308
4312
4316
4320
4324
4328
4332
4336
4340
4344
4348
4352
4356
CDP

Plate 8: Line drawing from line 671/87 with interpretation.

Legend:

TERTIARY

Pliocene

Nl: Pebbly clay to gravel.

Late Late Miocene (Pontian)

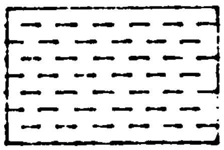

Npt: Variegated clays, subordinate gravel and sand (5.5-8.5 Ma).

Late Middle Miocene to Middle Late Miocene (Pannoniai

Np: Calcarous clay, gravel and sand (8.5 to

Late Middle Miocene (Sarmatian)

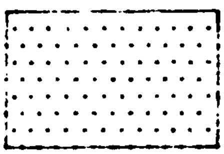

$_1$Ns: Calcarous clay to gravel, coquina, gravel to conglomerate (11.5 to 13.6 Ma).

Early Middle Miocene (Badenian)

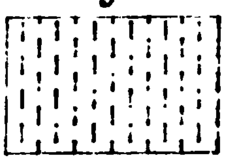

^{p}Nt^2: Calcarous clay to fine gravel (13.6

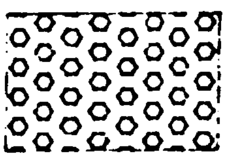

^{k}Nt^1: Middle Miocene (Lower Badenian, 15 conglomerate to sandstone alternating witl

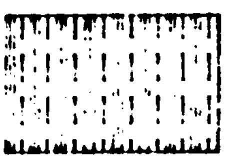

pNh^2: Early Middle miocene (Karpathian, flysch deposits such as calcareous clay, cl sand.

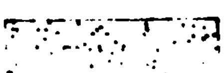

^{k}Nh^2: Early Miocene (pre-rift) conglomer

)

11.5 Ma).

o 15.5 Ma)

5–16.5 Ma)
clay.

17.5–16.5 Ma)
ay and

ite

Upper Triassic

Tnk: Norian–Carpathian keuper:
shales, sandstone and dolomite (2

Middle Triassic

^{v}T2: grey to dark–grey limestone.

^{d}T2: Grey dolomite.

^{v}T1: Ladinian light–grey limestone

Lower Triassic to Permian

^{q}T1: Lower Triassic quartzite from

Tm: Permian to Lower Triassic m
Variegated sandstone, shales and
some melaphyre clasts.

'T: Permian to Lower Triassic.
such as melaphyre, quartz porph

gravel.

ys, subordinate gravel
Ma).

Late Miocene (Pannonian)

gravel and sand (8.5 to 11.5 Ma).

n)

to gravel, coquina,
rate (11.5 to 13.6 Ma).

n)
ay to fine gravel (13.6 to 15.5 Ma)

ene (Lower Badenian, 15.5–16.5 Ma)
ndstone alternating with clay.

e miocene (Karpathian, 17.5–16.5 Ma)
h as calcareous clay, clay and

ne (pre-rift) conglomerate
19 Ma, see Fig. B.2)

Upper Triassic

Tnk: Norian-Ca
shales, sandsto

Middle Triassic

^{v}T2: grey to da

^{d}T2: Grey dolo

^{v}T1: Ladinian l

Lower Triassic to Permian

^{q}T1: Lower Tri

Tm: Permian t
Variegated san
some melaphyr

'T: Permian t
such as melap

ın–Carpathian keuper: Variegated
ndstone and dolomite (204–220 Ma).

to dark–grey limestone.

dolomite.

ıian light–grey limestone

mian

r Triassic quartzite frcm quartz conglomerate.

ian to Lower Triassic melaphyre formation.
ı sandstone, shales and arkose containing
aphyre clasts.

ian to Lower Triassic. Basic igneous rocks
nelaphyre, quartz porphyry, augitic porphyry etc.

Plate 8: Interp

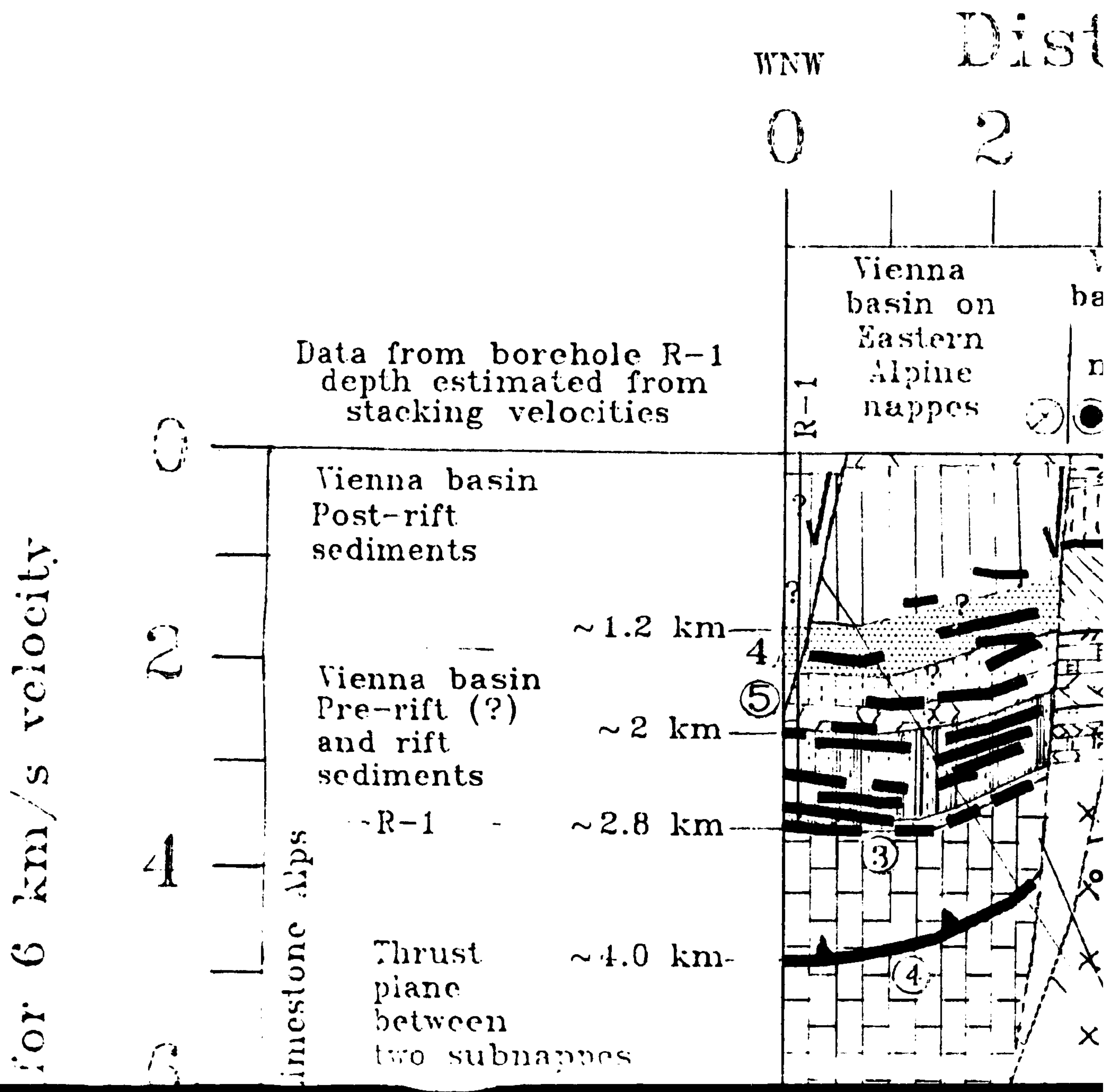

nterpretation of line 671/87.

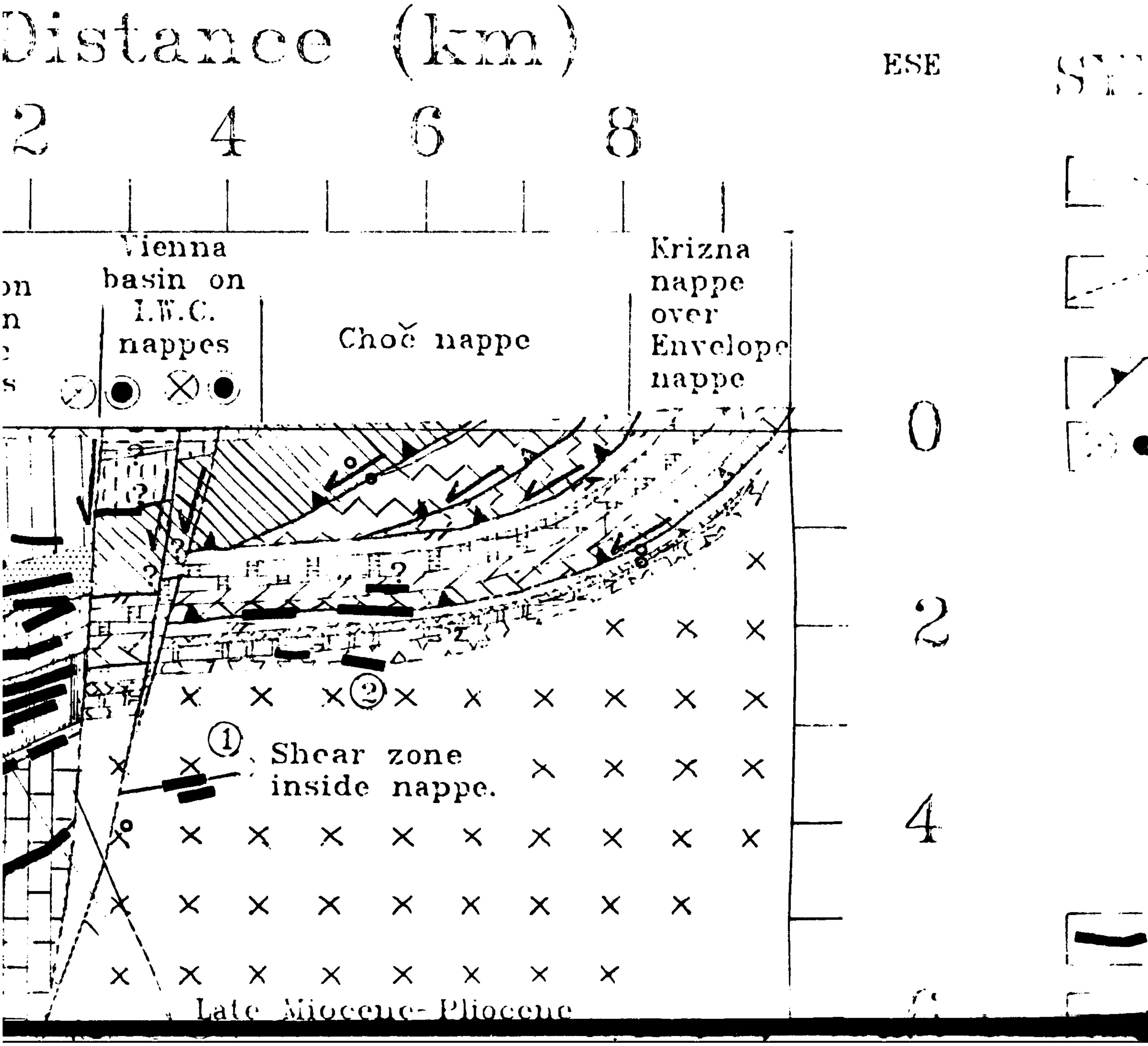

Plate 8: Interpretation of line 671/87.

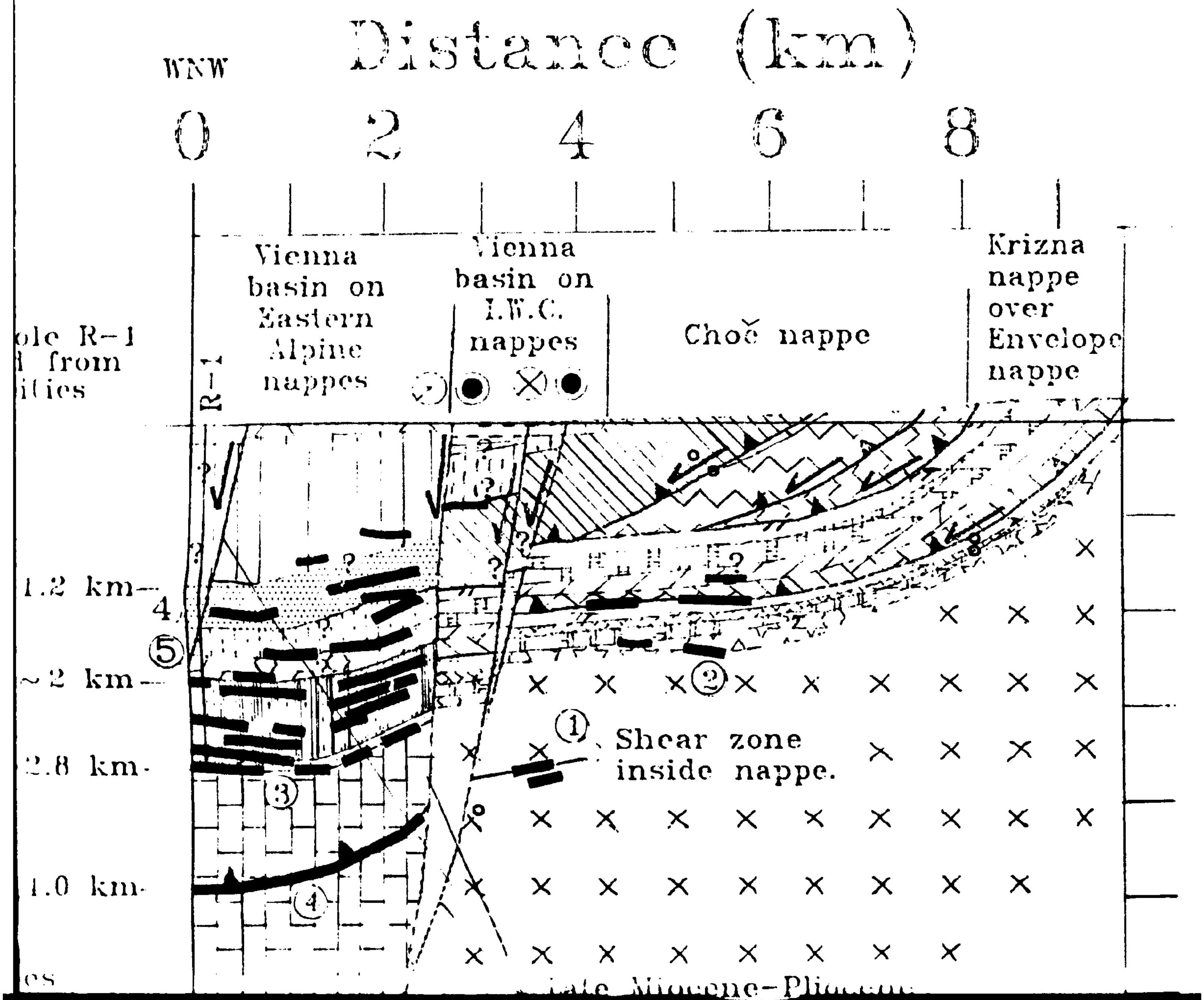

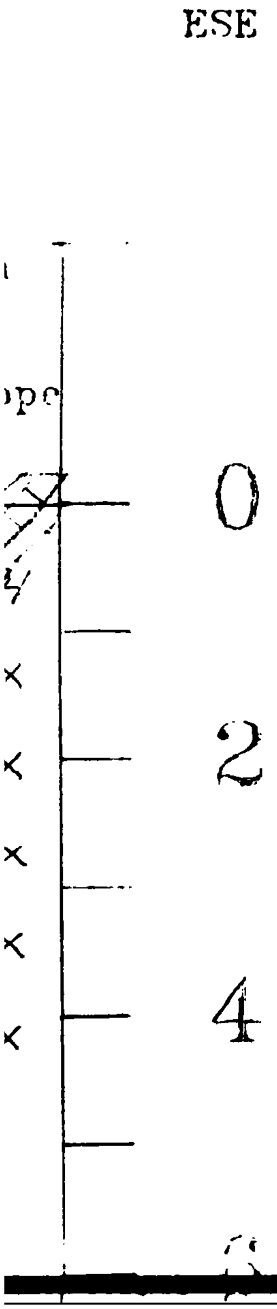

SYMBOLS:

Limit of geologic unit

Fault

Thrust fault

Right-slip movement. Right-slip in middle Middle Miocene (13.6-16.5 Ma), short period of left-slip in late Middle Miocene (11.5-ca 12 Ma) (Fodor et al., 1990). This strike-slip movement is simultaneous with normal movement as the total movement is dip-slip.

Reflector

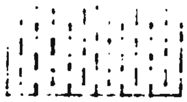

$^{p}Nt^{2}$. Calcarous clay to ... gravel (...Ma)

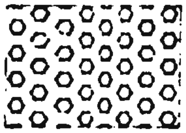

$^{k}Nt^{1}$: Middle Miocene (Lower Badenian, 15.5–16.5 Ma) conglomerate to sandstone alternating with clay.

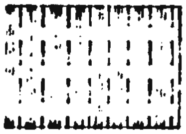

pNh^{2}: Early Middle miocene (Karpathian, 17.5–16.5 Ma flysch deposits such as calcareous clay, clay and sand.

$^{k}Nh^{2}$: Early Miocene (pre-rift) conglomerate (Eggenburgian, 23 to 19 Ma, see Fig. B.2).

CRETACEOUS

Lower to Middle Cretaceous

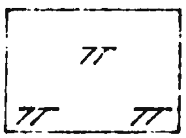

K2al–c: Marly shale, marlstone and calcarous sandstone (91–107 Ma).

Upper Jurassic to Lower Cretaceous

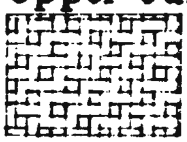

K1V: Marly and cherty limestone and marlstone of Vysoka group (107–130 Ma).

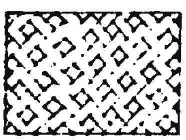

K1M: Grey cherty limestone or dark-grey limestone with chert of Little Carpathian group (107–130 Ma).

JURASSIC

Lower Jurassic

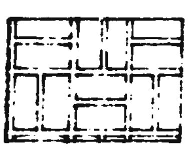

Marl, variegated limestones, sandstone with some dolomite and breccia (Little Carpathian group.

el (... M.)

:nian, 15.5–16.5 Ma)
ting with clay.

pathian, 17.5–16.5 Ma)
clay, clay and

onglomerate
.g. B.2).

calcarous

nd marlstone of

k–grey
athian group

one
ittle Carpathian

Lower Triassic to Permian

^{q}T1: Lower Triassic quartzite from

Tm: Permian to Lower Triassic mel
Variegated sandstone, shales and ar
some melaphyre clasts.

'T: Permian to Lower Triassic. Ba
such as melaphyre, quartz porphyr

PALEOZOIC

Late Carboniferous

Granodiorite intruded at the end of
orogen (302 Ma + 40 Ma, K/Ar). M
south of this section (Hrouda, 1988
The intrusive is likely overlain by P
to Paleozoic metasediments such as

Up to Devonian

Graywacke Zone of Eastern Alps.
Fossiliferous.

PROTEROZOIC TO PALEOZ

Devonian

Biotitic to biotitic–sericitic phyllite
deposited in late Late Proterozoic
and metamorphised into phyllite (
500 C isotherm, K/Ar) (Burchart e

Cambrian

Biotitic gneiss to paragneiss with g
Sedimentary sequences deposited 6
grade metamorphism during Cambr

?

)

ay to fine gravel (13.6 to 15.5 Ma)

ne (Lower Badenian, 15.5–16.5 Ma)
ndstone alternating with clay.

miocene (Karpathian, 17.5–16.5 Ma)
n as calcareous clay, clay and

ne (pre-rift) conglomerate
o 19 Ma, see Fig. B.2).

marlstone and calcarous
Ma).

eous

ty limestone and marlstone of
130 Ma).

nestone or dark-grey
t of Little Carpathian group

estones, sandstone
and breccia (Little Carpathian

Lower Triassic to Permian

qT1: Lower Triassic

Tm: Permian to Lo
Variegated sandsto
some melaphyre cl

'T: Permian to Lo
such as melaphyre

PALEOZOIC

Late Carboniferous

Granodiorite intrud
orogen (302 Ma + 4
south of this sectio
The intrusive is lik
to Paleozoic metase

Up to Devonian

Graywacke Zone of
Fossiliferous.

PROTEROZOIC TO

Devonian

Biotitic to biotitic–
deposited in late L
and metamorphised
500 C isotherm, K/

Cambrian

Biotitic gneiss to p
Sedimentary sequen
grade metamorphis

Permian

Lower Triassic quartzite from quartz conglomerate.

Permian to Lower Triassic melaphyre formation.
gated sandstone, shales and arkose containing
melaphyre clasts.

Permian to Lower Triassic. Basic igneous rocks
as melaphyre, quartz porphyry, augitic porphyry etc.

C

is

diorite intruded at the end of the Hercynian
n (302 Ma + 40 Ma, K/Ar). Mylonitized to the
of this section (Hrouda, 1988).
ntrusive is likely overlain by Proterozoic
leozoic metasediments such as below.

acke Zone of Eastern Alps.
iferous.

ZOIC TO PALEOZOIC

ic to biotitic-sericitic phyllite. Sediments
ited in late Late Proterozoic (after 800 Ma), buried
metamorphised into phyllite (394 + 20 Ma for the
isotherm, K/Ar) (Burchart et al., 1987).

c gneiss to paragneiss with garnet and staurolite.
entary sequences deposited 600-800 Ma. Medium
metamorphism during Cambrian (Rudaskov, 1985).

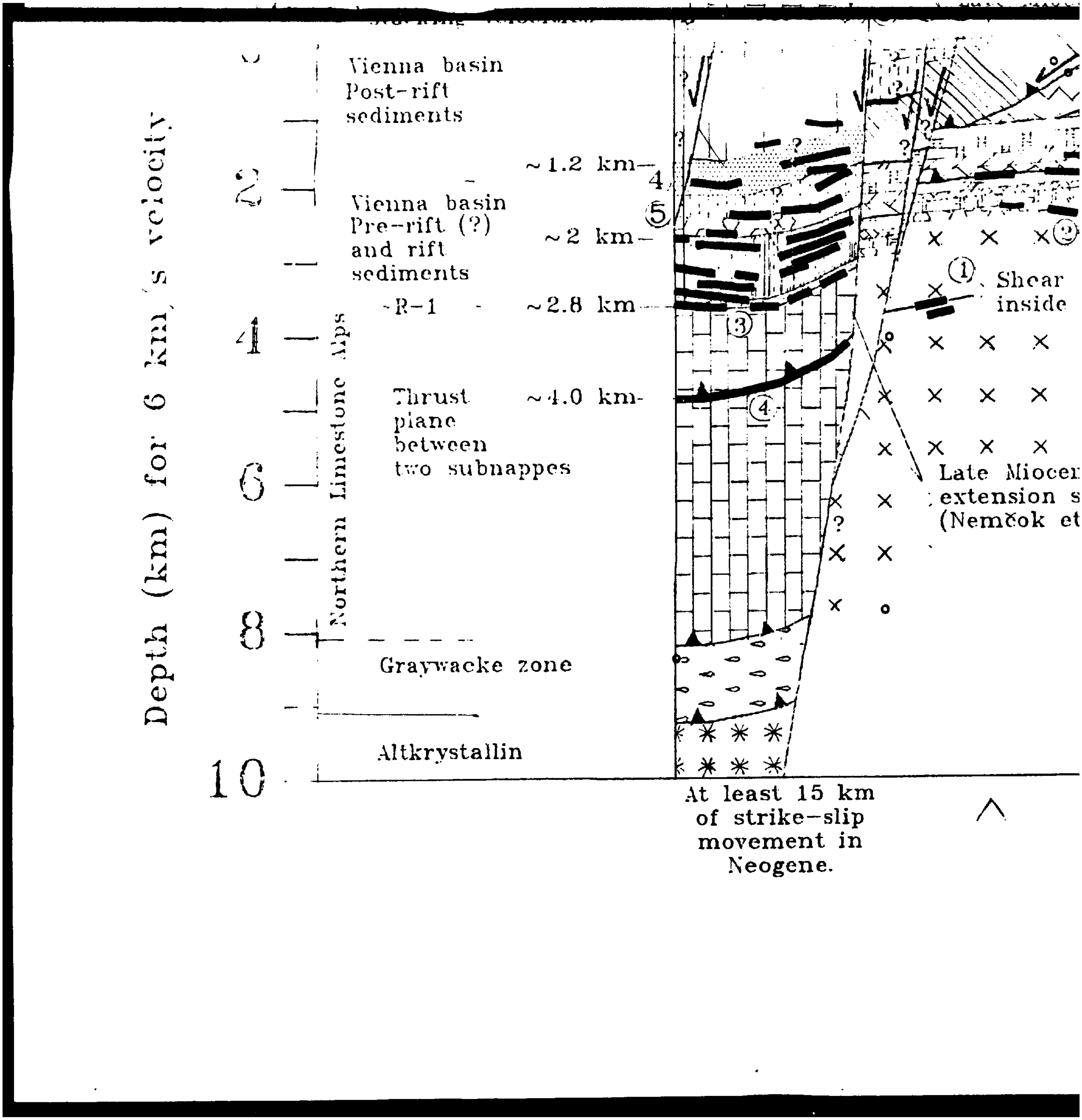
Depth (km) for 6 km/s velocity
2
4
6
8
10
Vienna basin
Post-rift
sediments
~1.2 km
Vienna basin
Pre-rift (?)
and rift
sediments
~2 km
-R-1
~2.8 km
Northern Limestone Alps
Thrust
plane
between
two subnappes
~4.0 km
Graywacke zone
Altkrystallin
At least 15 km
of strike-slip
movement in
Neogene.
Shear
inside
Late Miocen
extension s
(Nemčok et

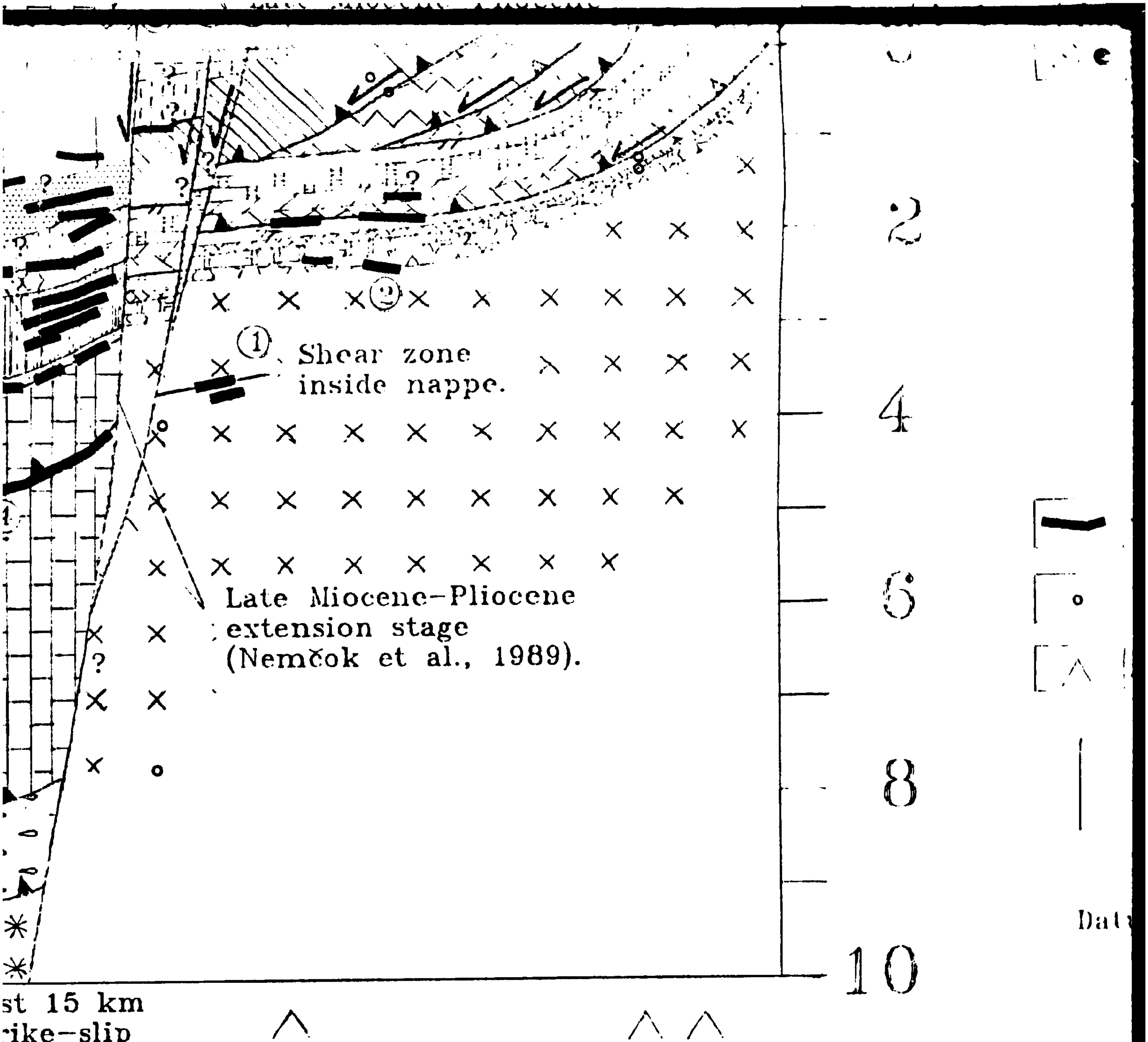

st 15 km
rike-slip
ment in
ogene.

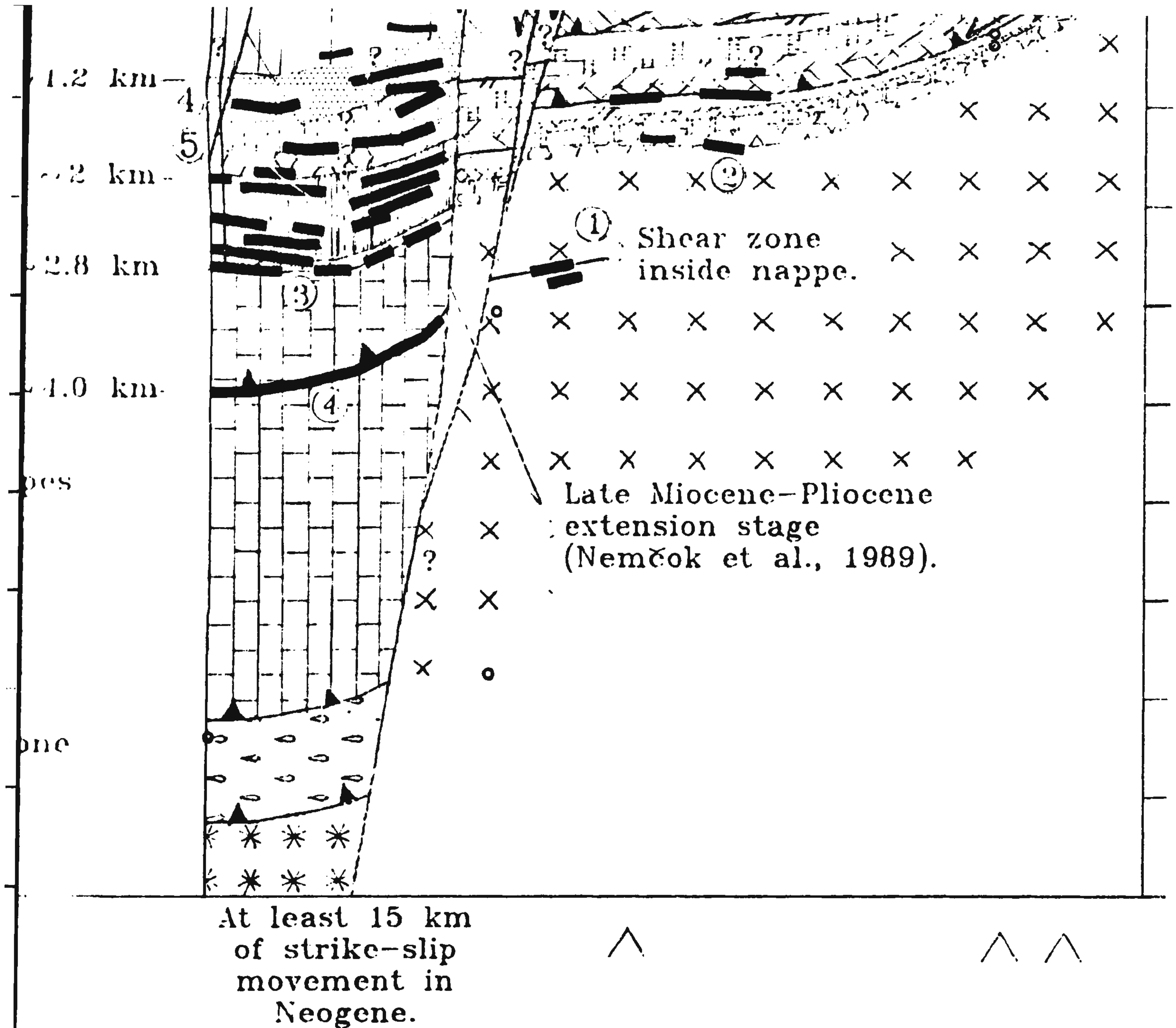
1.2 km
2 km
2.8 km
4.0 km
Shear zone inside nappe.
Late Miocene–Pliocene extension stage (Nemčok et al., 1989).
At least 15 km of strike-slip movement in Neogene.

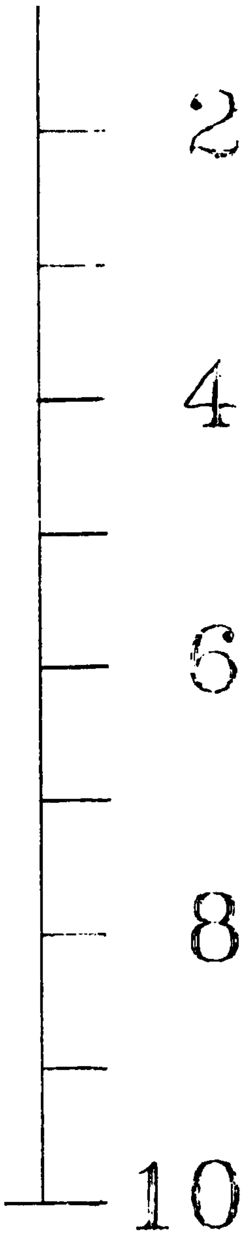

[illegible]
short period of left-slip in late Middle Miocene (11.5–ca 12 Ma) (Fodor et al., 1990). This strike-slip movement is simultaneous with normal movement as the total movement is dip-slip.

Reflector

Diffracting point

Change of direction of binning line.

Borehole R-1 (location on Fig. A.1).

Datum level - 200 m amsl.

CRETACEOUS

Lower to Middle Cretaceous

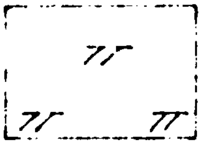

K2al–c: Marly shale, marlstone and calcarous sandstone (91–107 Ma).

Upper Jurassic to Lower Cretaceous

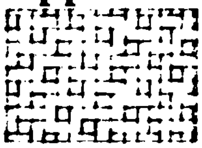

K1V: Marly and cherty limestone and marlstone Vysoka group (107–130 Ma).

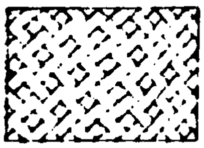

K1M: Grey cherty limestone or dark–grey limestone with chert of Little Carpathian group (107–130 Ma).

JURASSIC

Lower Jurassic

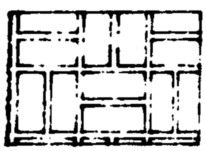

Marl, variegated limestones, sandstone with some dolomite and breccia (Little Carpathia group.

TRIASSIC

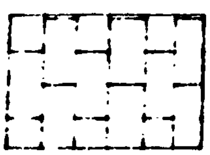

Northern Limestone Alps.

lcarous

marlstone of

rey
ian group

e Carpathian

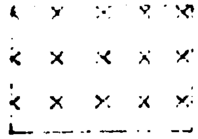

Granodiorite intruded at the end of (
orogen (302 Ma + 40 Ma, K/Ar). Myl
south of this section (Hrouda, 1988).
The intrusive is like'y overlain by Pro
to Paleozoic metasediments such as b

Up to Devonian

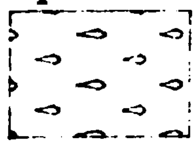

Graywacke Zone of Eastern Alps. Fossiliferous.

PROTEROZOIC TO PALEOZO

Devonian

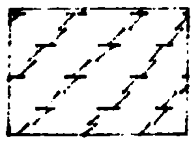

Biotitic to biotitic–sericitic phyllite.
deposited in late Late Proterozoic (af
and metamorphised into phyllite (394
500 C isotherm, K/Ar) (Burchart et a

Cambrian

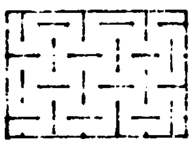

Biotitic gneiss to paragneiss with garn
Sedimentary sequences deposited 600-
grade metamorphism during Cambrian

?

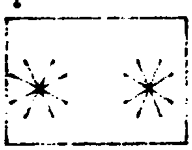

Altkrystallin of the Eastern Alps. It i
the crystalline complex formed by th
metasediments and intrusives of the

References: Fodor et al. (1990); Mahel' et al. (19
(1989); Tomek, personal communication (1992).

e, marlstone and calcarous
Ma).

ceous

erty limestone and marlstone of
-130 Ma).

imestone or dark-grey
rt of Little Carpathian group

nestones, sandstone
e and breccia (Little Carpathian

Alps.

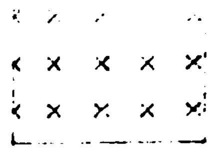

Granodiorite
orogen (302 M
south of this
The intrusive
to Paleozoic

Up to Devonian

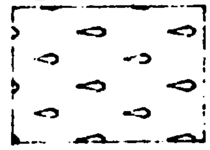

Graywacke Zo
Fossiliferous.

PROTEROZOIC

Devonian

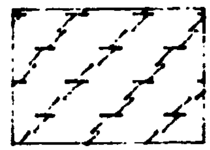

Biotitic to bi
deposited in
and metamor
500 C isother

Cambrian

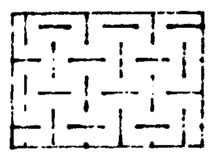

Biotitic gneis
Sedimentary
grade metam

?

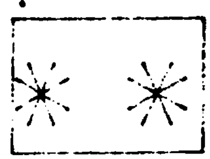

Altkrystallin
the crystallin
metasediment

References: Fodor et al.
(1989); Tomek, personal

ie intruded at the end of the Hercynian
)2 Ma + 40 Ma, K/Ar). Mylonitized to the
:his section (Hrouda, 1988).
ive is likely overlain by Proterozoic
ic metasediments such as below.

Zone of Eastern Alps.
us.

[C TO PALEOZOIC

biotitic-sericitic phyllite. Sediments
in late Late Proterozoic (after 800 Ma), buried
norphised into phyllite (394 + 20 Ma for the
:herm, K/Ar) (Burchart et al., 1987).

ieiss to paragneiss with garnet and staurolite.
ry sequences deposited 600-800 Ma. Medium
amorphism during Cambrian (Rudaskov, 1985).

in of the Eastern Alps. It is equivalent to
lline complex formed by the Pre-Triassic
.ents and intrusives of the Envelope nappe.

al. (1990); Mahel' et al. (1974); Nemčok et al.
al communication (1992).

Plate 9: Line drawing from line 671A/87 with interpretation.

Legend:

TERTIARY

Miocene

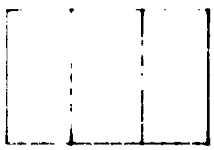

Np: Calcarous clay and clay, sand, grave
(8.5–11.5 Ma).

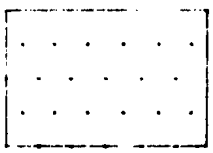

$_1$Ns: Calcarous clay and sand, sandstone
gravel and conglomerate. Locally some
material (11.5–13.5 Ma).

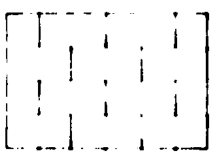

^{P}Nt^{2}: Calcarous fine sandy clay with sul
sandstone (13.5–15 Ma).

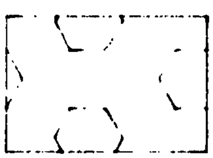

^{k}Nt^{1}: Middle Miocene conglomerate and
(15–16.5 Ma).

CRETACEOUS

Lower to Middle Cretaceous

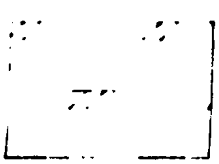

K2al–c: Marly shale, marlstone and calc
sandstone (91–107 Ma).

Upper Jurassic to Lower Cretaceous

ıd, gravel

andstone, coquina
ly some volcanic

with subordinate

ate and gravel

ınd calcarous

TRIASSIC

Upper Triassic

Tnk: Norian–Carpathian keu
shales, sandstone and dolom

Middle Triassic

^{v}T2: grey to dark–grey lime

^{d}T2: Grey dolomite.

Lower Triassic

^{q}T1: Quartzite from quartz

PALEOZOIC

Late Carboniferous

Granodiorite intruded at th
orogen (302 Ma + 40 Ma, K
south of this section (Hrov

Silurian–Devonian

lay and clay, sand, gravel

clay and sand, sandstone, coquina
lomerate. Locally some volcanic
3.5 Ma).

fine sandy clay with subordinate
-15 Ma).

ocene conglomerate and gravel

hale, marlstone and calcarous
07 Ma).

taceous

TRIASSIC

Upper Triassic

Tnk: Noria
shales, sar

Middle Triassic

^{v}T2: grey

^{d}T2: Grey

Lower Triassic

^{q}T1: Quart

PALEOZOIC

Late Carboniferous

Granodiori
orogen (30
south of t

Silurian–Devonian

'orian–Carpathian keuper: Variegated
, sandstone and dolomite (204–220 Ma).

rey to dark–grey limestone.

rey dolomite.

uartzite from quartz conglomerate.

s

liorite intruded at the end of the Hercynian
(302 Ma + 40 Ma, K/Ar). Mylonitized to the
of this section (Hrouda, 1988).

Plate 9: Interpretatio

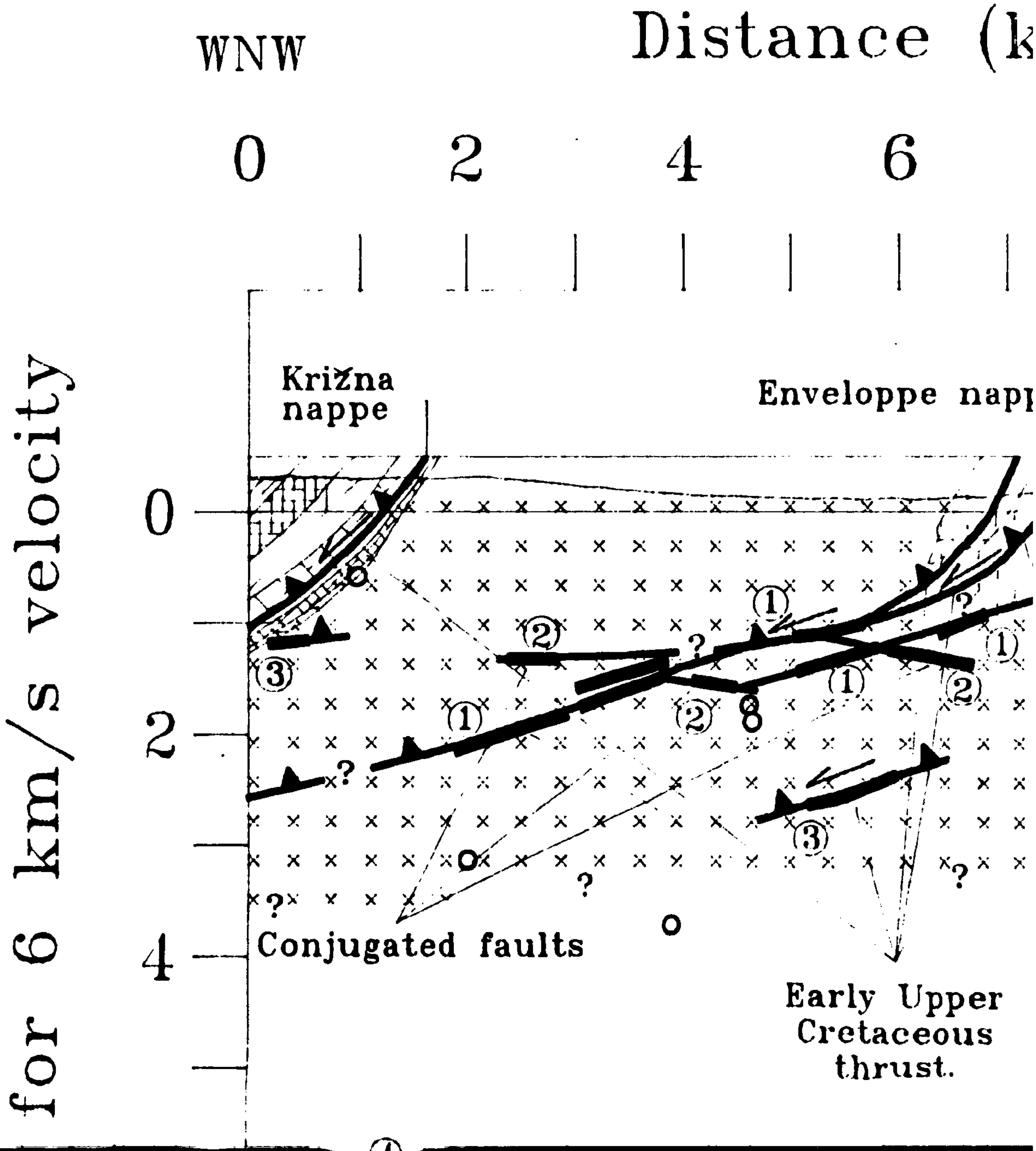

erpretation of line 671A/87.

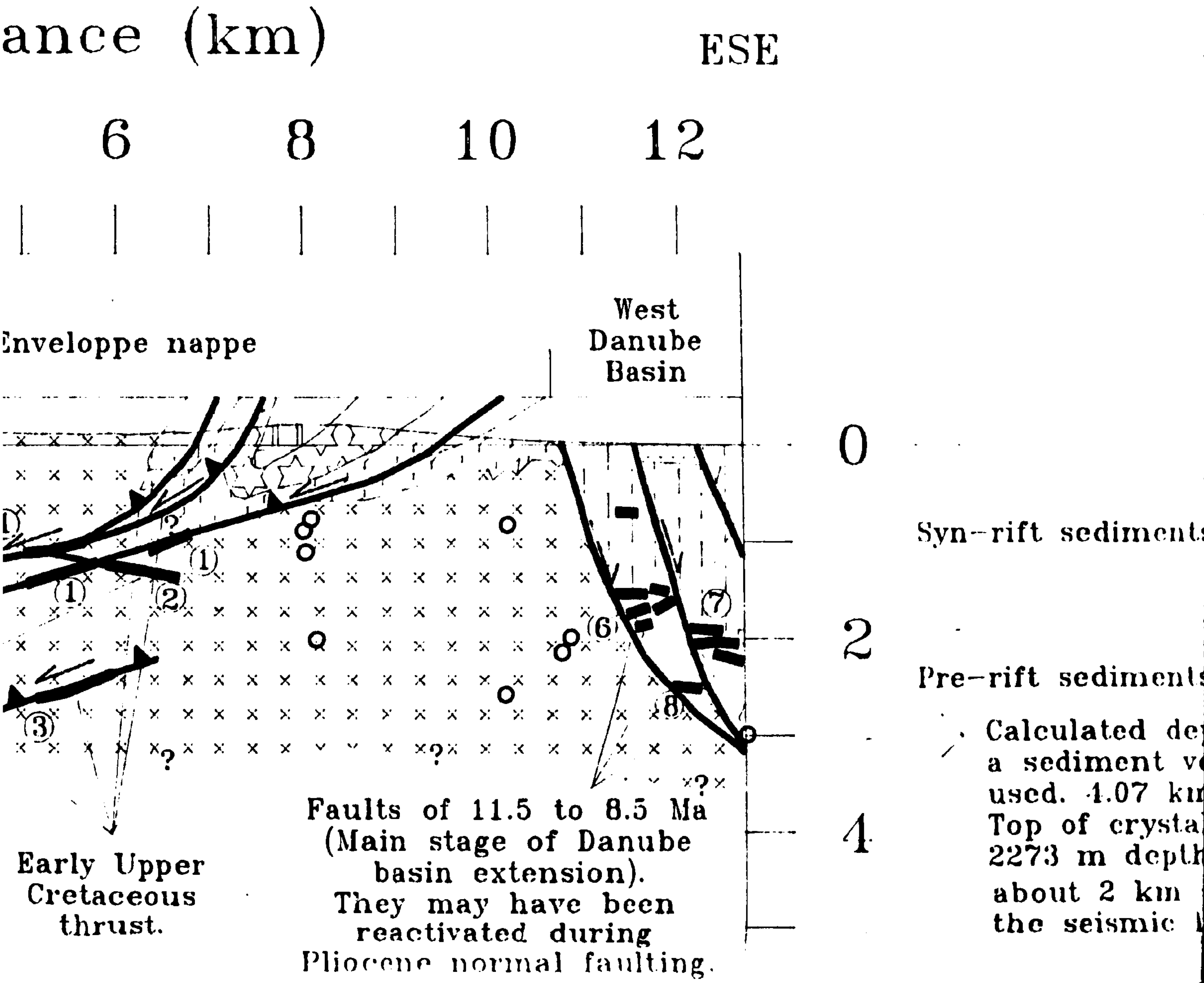

Plate 9: Interpretation of line 671A/87.

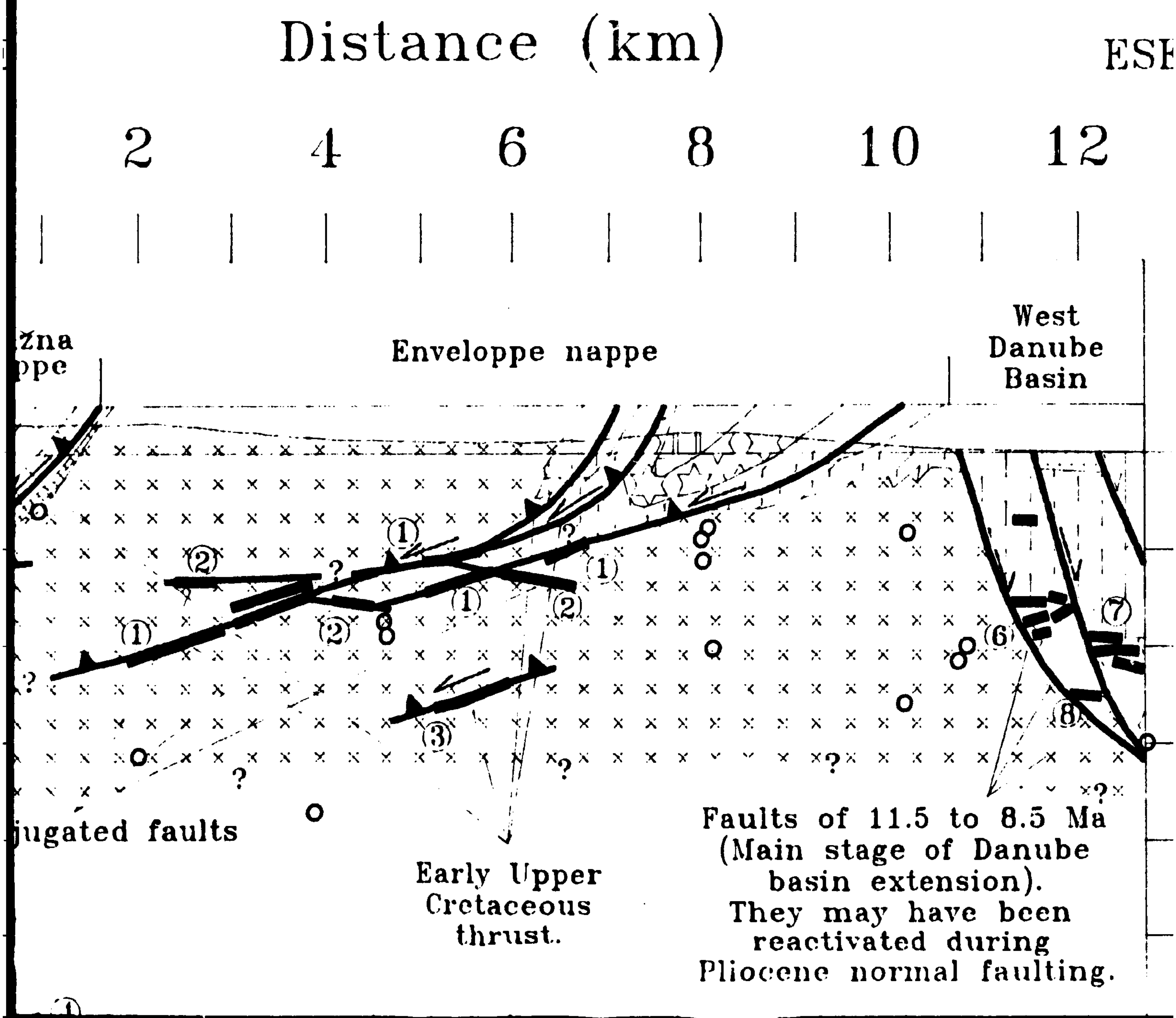

7.

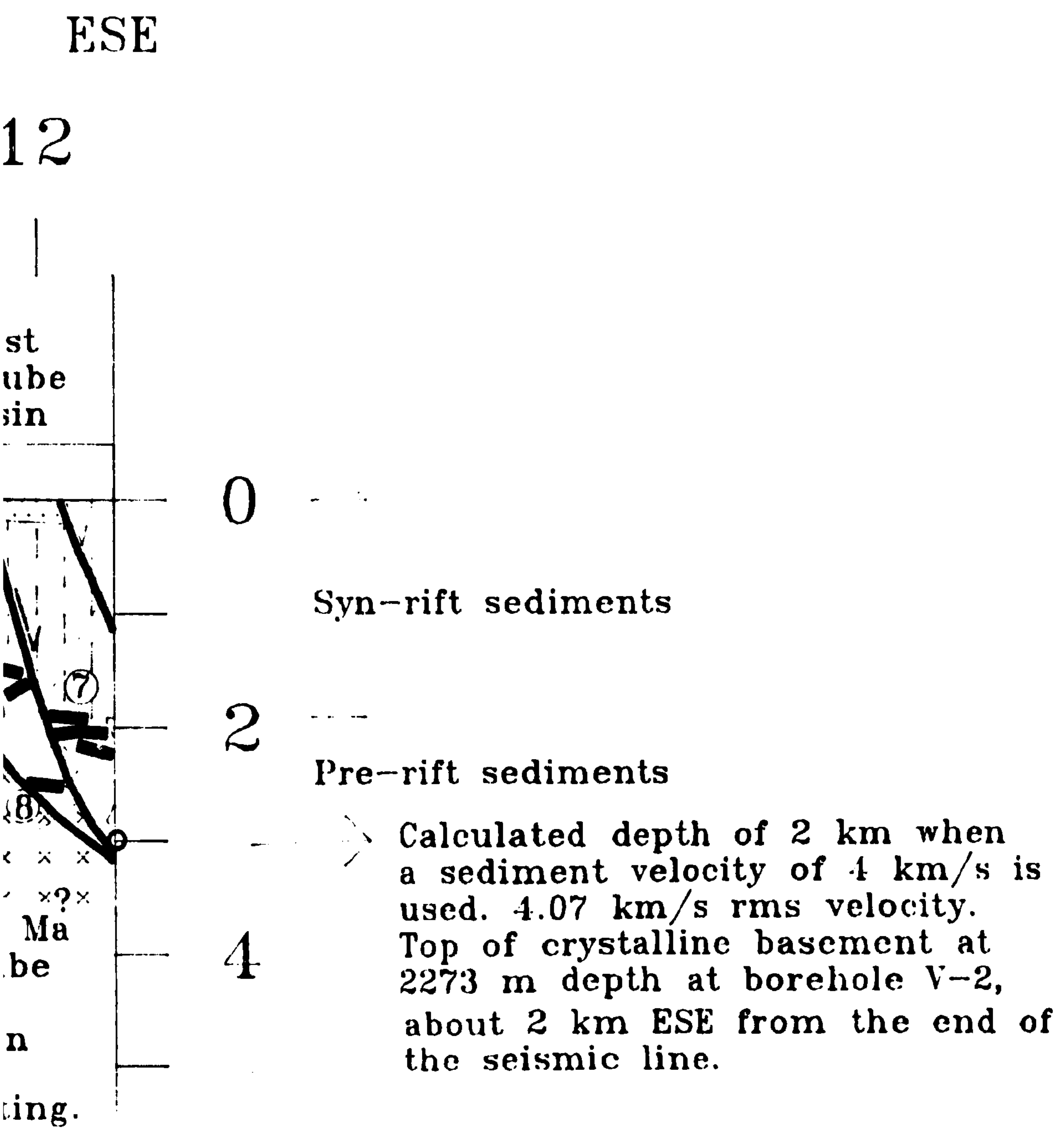

ESE
12
st
ube
sin
(7)
8
Ma
be
n
ing.
0
2
4
Syn–rift sediments
Pre–rift sediments
Calculated depth of 2 km when a sediment velocity of 4 km/s is used. 4.07 km/s rms velocity. Top of crystalline basement at 2273 m depth at borehole V–2, about 2 km ESE from the end of the seismic line.

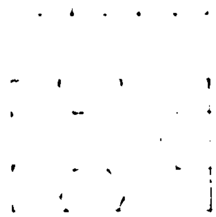

k_{Nt}^{1}: Middle Miocene conglomerate and g
(15–16.5 Ma).

CRETACEOUS

Lower to Middle Cretaceous

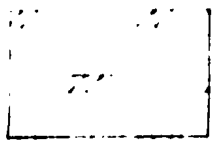

K2al–c: Marly shale, marlstone and calca
sandstone (91–107 Ma).

Upper Jurassic to Lower Cretaceous

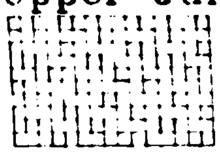

K1V: Marly and cherty limestone and ma
Vysoka group (107–130 Ma).

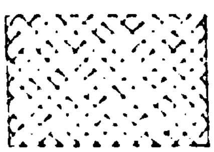

K1M: Grey cherty limestone or dark-grey
limestone with chert of Little Carpathian
(107–130 Ma).

JURASSIC

Lower Jurassic

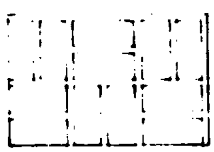

Marl, variegated limestones, sandstone
with some dolomite and breccia (Little (
group).

References: Mahel'et al. (1974); Nemcok et al. (1989 ate and gravel

and calcarous

e and marlstone of

dark-grey
Carpathian group

ndstone
a (Little Carpathian

al. (1989); Tomek, personal communication (1992).

Lower Triassic

qT1: Quartzite from quartz

PALEOZOIC

Late Carboniferous

Granodiorite intruded at the
orogen (302 Ma + 40 Ma, K
south of this section (Hrou

Silurian-Devonian

Harmonia series. Sediments
earlier in Paleozoic. Metam
sericitic-chloritic phyllite, g
phyllite, biotitic chert, schis
Some occurrences of crystal
chert and pyroclastics.

PROTEROZOIC TO PAL

Cambrian

Biotitic gneiss to paragneiss
Sedimentary sequences depo
grade metamorphism during

taceous

15 Ma).

ocene conglomerate and gravel

hale, marlstone and calcarous
07 Ma).

etaceous

cherty limestone and marlstone of
107–130 Ma).

y limestone or dark-grey
chert of Little Carpathian group

limestones, sandstone
mite and breccia (Little Carpathian

Lower Triassic

q_{T1}: Quartzite fı

PALEOZOIC

Late Carboniferous

Granodiorite int
orogen (302 Ma
south of this se

Silurian–Devonian

Harmonia series
earlier in Paleo
sericitic–chlorit
phyllite, biotitic
Some occurrenc
chert and pyroc

PROTEROZOIC

Cambrian

Biotitic gneiss
Sedimentary se
grade metamor

71); Nemcok et al. (1989); Tomek, personal communication (1992).

·tzite from quartz conglomerate.

rite intruded at the end of the Hercynian
302 Ma + 40 Ma, K/Ar). Mylonitized to the
this section (Hrouda, 1988).

ı series. Sediments deposited in Silurian or
ı Paleozoic. Metamorphosed in Devonian into
·chloritic phyllite, graphitic to cherty biotitic
biotitic chert, schist.
:urrences of crystalline limestones to limy–silicitic
d pyroclastics.

ıIC TO PALEOZOIC

gneiss to paragneiss with garnet and staurolite.
tary sequences deposited 600–800 Ma. Medium
etamorphism during Cambrian (Rudaskov, 1985).

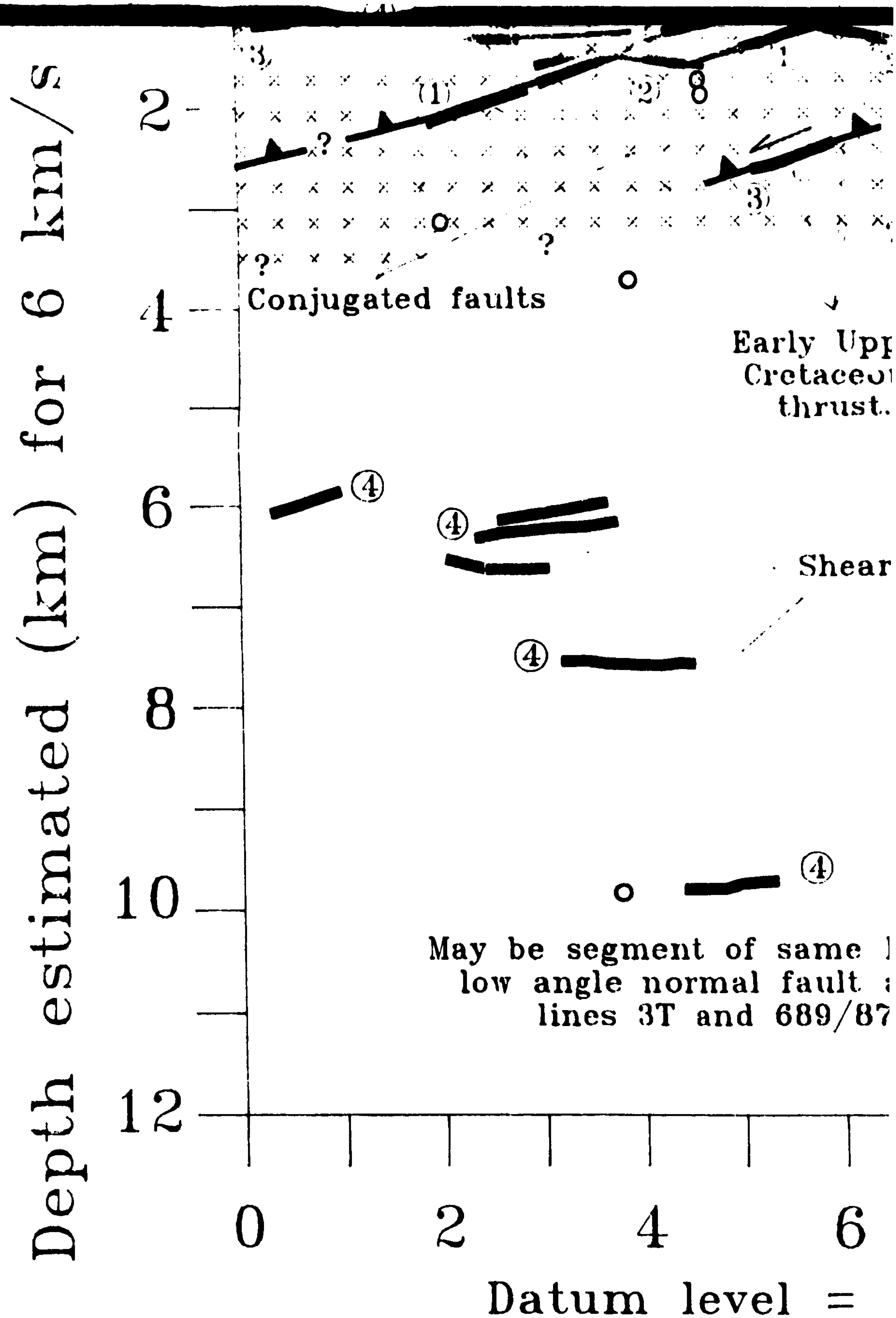

Depth estimated (km) for 6 km/s
2
4
6
8
10
12
(1)
(2)
(3)
8
?
Conjugated faults
Early Upp
Cretaceou
thrust.
④
Shear
May be segment of same
low angle normal fault
lines 3T and 689/87
0
2
4
6
Datum level =

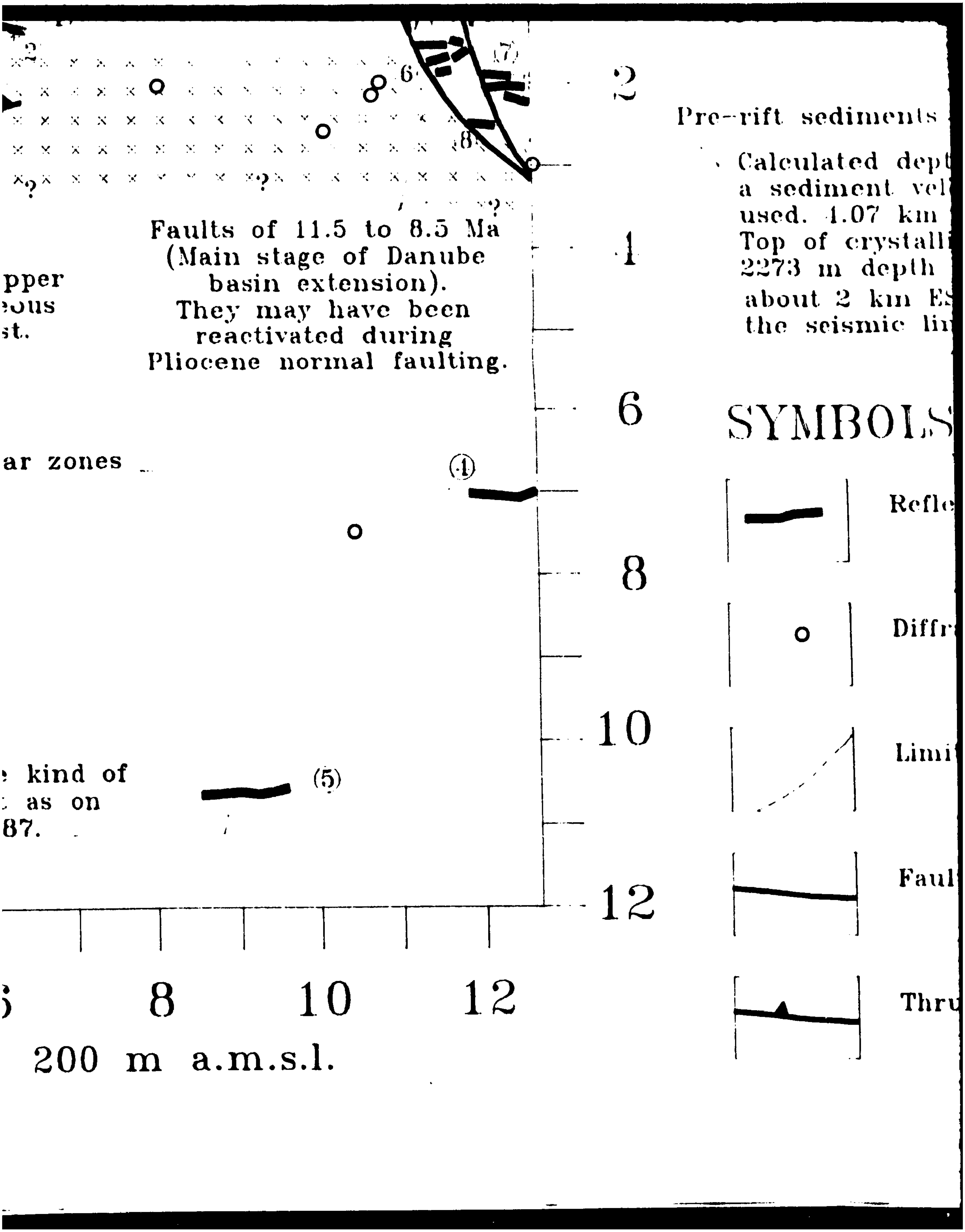

2
6
(7)
8
Faults of 11.5 to 8.5 Ma
(Main stage of Danube
basin extension).
They may have been
reactivated during
Pliocene normal faulting.
pper
ous
st.
ar zones
(4)
kind of
as on
87.
(5)
2
4
6
8
10
12
8
10
12
200 m a.m.s.l.
Pre-rift sediments
Calculated dept
a sediment vel
used. 4.07 km
Top of crystalli
2273 m depth
about 2 km ES
the seismic lin
SYMBOLS
Refle
Diffr
Limi
Faul
Thru

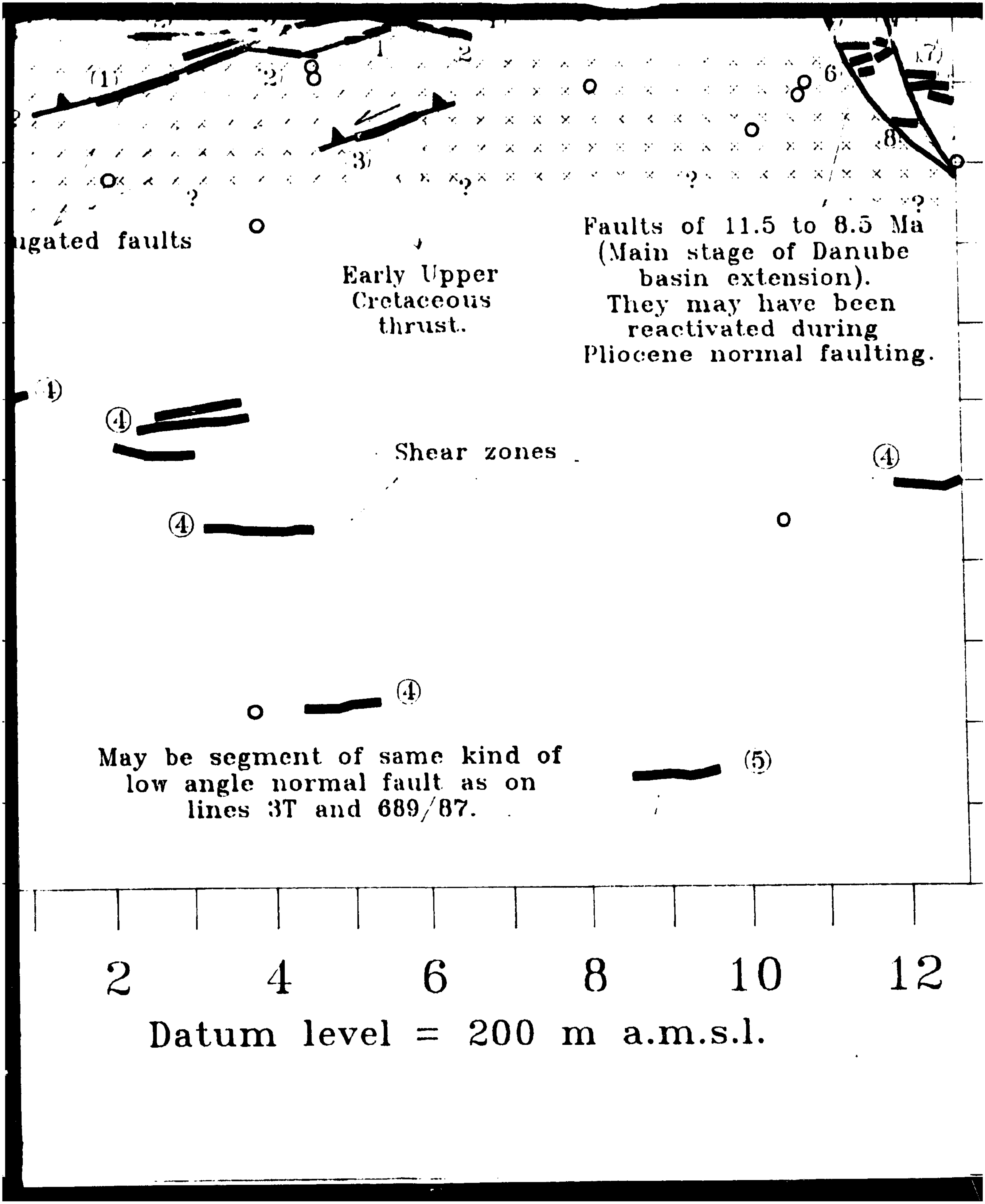

ugated faults
Early Upper Cretaceous thrust.
Faults of 11.5 to 8.5 Ma (Main stage of Danube basin extension). They may have been reactivated during Pliocene normal faulting.
Shear zones
May be segment of same kind of low angle normal fault as on lines 3T and 689/87.
(1)
(2)
(3)
(4)
(5)
(6)
(7)
(8)
2
4
6
8
10
12
Datum level = 200 m a.m.s.l.

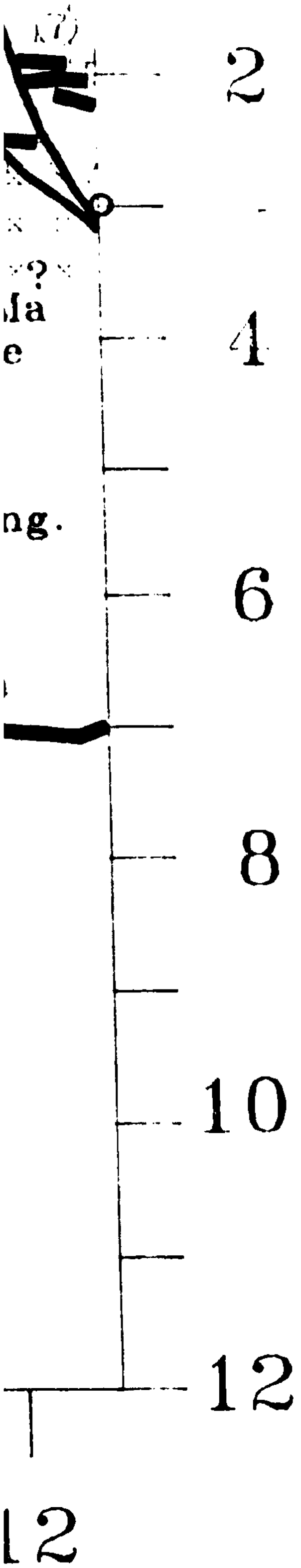

Pre-rift sediments

- Calculated depth of 2 km when a sediment velocity of 4 km/s is used. 4.07 km/s rms velocity. Top of crystalline basement at 2273 m depth at borehole V-2, about 2 km ESE from the end of the seismic line.

SYMBOLS

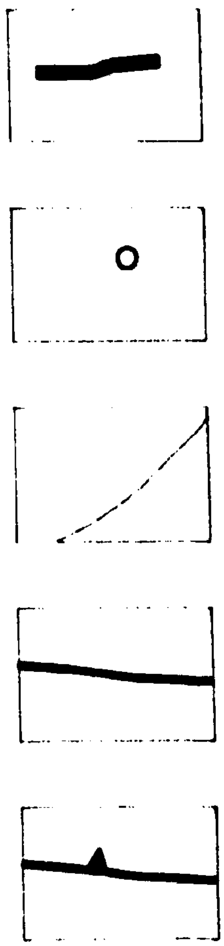

Reflectors

Diffracting points

Limit of unit

Fault

Thrust fault

Plate 10: Line drawing from line 689/87 with interpretation.

Legend:

MESOZOIC
CRETACEOUS

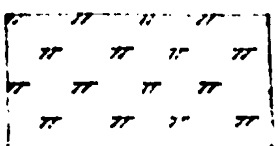

K2al-c: Middle Creta
Cenomanian) shaly n
calcareous sandstone

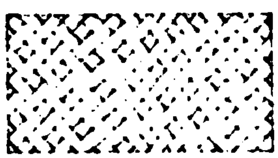

K1M: Lower-Middle C
cherty limestone, lin
Little Carpathian gro

JURASSIC

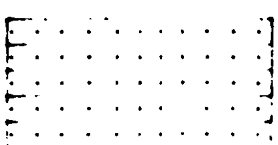

J: Jurassic shale of
with marlstone, lime

eous (Albian to
arlstone and
.

etaceous (Tithonian–Aptian)
estone and chert of the
up.

the Little Carpathian group
stone and silicite.

PALEOZO

Late Carbo

PROTER

Cretaceous (Albian to
shaly marlstone and
dstone.

ddle Cretaceous (Tithonian–Aptian)
ne, limestone and chert of the
an group.

le of the Little Carpathian group
, limestone and silicite.

PALE

Late C

PROT

.EOZOIC

Carboniferous, end of Hercynian orogen.

Bratislava massif granodiorite intrusive.
on the SE side. Mylonitized on the NW

Modra massif granodiorite intrusive (302
Less acidic than Bratislava intrusive.
Mylonitized south of this section.

)TEROZOIC TO PALEOZOIC (Pezinok–P

fb^x: Devonian (394 ± 24 Ma K/Ar age) bi
biotitic–sericitic phyllite from Late Prote
(after 800 Ma) (Burchart et al., 1987).

ZOIC

rboniferous, end of Hercynian orogen.

Bratislava massif granodiorite intrusive. Peg
on the SE side. Mylonitized on the NW edge

Modra massif granodiorite intrusive (302±40
Less acidic than Bratislava intrusive.
Mylonitized south of this section.

ROZOIC TO PALEOZOIC (Pezinok–Per

fb^x: Devonian (394 ± 24 Ma K/Ar age) bioti
biotitic–sericitic phyllite from Late Proteroz
(after 800 Ma) (Burchart et al., 1987).

Pegmatite veins
edge.

±40 Ma K/Ar age).

ᴾernek group)

ıiotitic to
erozoic sediments

[illegible]
calcarcous sandstone.

K1M: Lower–Middle Cret
cherty limestone, limes
Little Carpathian group

JURASSIC

J: Jurassic shale of the
with marlstone, limestc

JM: Middle to Upper Ju
of Little Carpathian grc

TRIASSIC

$^{d}T_{2-3}$: Middle to Late T

$^{v}T_{2}$: Middle Triassic gre

$^{q}T_{1}$: Lower Triassic qua
conglomerate with som

SYMBOLS

...ne and
ne.

Cretaceous (Tithonian--Aptian) limestone and chert of the group.

PROTER

f the Little Carpathian group nestone and silicite.

er Jurassic limestone n group.

ate Triassic dolomite.

c grey to dark grey limestone.

quartzite and quartz some schist.

ndstone.

ddle Cretaceous (Tithonian--Aptian)
ne, limestone and chert of the
an group.

PROT

ale of the Little Carpathian group
e, limestone and silicite.

Upper Jurassic limestone
athian group.

to Late Triassic dolomite.

riassic grey to dark grey limestone.

iassic quartzite and quartz
with some schist.

Limit of

Modra massif granodiorite intrusive (302
Less acidic than Bratislava intrusive.
Mylonitized south of this section.

)TEROZOIC TO PALEOZOIC (Pezinok--P

fb^{x}: Devonian (394 ± 24 Ma K/Ar age) bi
biotitic–sericitic phyllite from Late Prote
(after 800 Ma) (Burchart et al., 1987).

mg^{x}: Biotitic gneiss to paragneiss with
Sedimentary sequences deposition age of
Metamorphosed during Cambrian (Rudako

fgf^{x}: Cambrian to Devonian pyritic, gra
tuffitic schist.

Amphibolite.
394 ± 24 Ma K/Ar age (Hrouda, 1988).

of geological unit

on the SE side. Mylonitized on the NW edg

Modra massif granodiorite intrusive (302±4(
Less acidic than Bratislava intrusive.
Mylonitized south of this section.

ROZOIC TO PALEOZOIC (Pezinok--Per

fb^x: Devonian (394 ± 24 Ma K/Ar age) biot
biotitic-sericitic phyllite from Late Proteroz
(after 800 Ma) (Burchart et al., 1987).

mg^x: Biotitic gneiss to paragneiss with ga
Sedimentary sequences deposition age of 6(
Metamorphosed during Cambrian (Rudakov,

fgf^x: Cambrian to Devonian pyritic, graphi
tuffitic schist.

Amphibolite.
394 ± 24 Ma K/Ar age (Hrouda, 1988).

age.

40 Ma K/Ar age).

ernek group)

otitic to
rozoic sediments

garnet and staurolite.
600 to 800 Ma.
v, 1985).

hitic phyllite with

TRIASSIC

$^{d}T_{2-3}$: Middle to Late Tri

$^{v}T_{2}$: Middle Triassic grey

$^{q}T_{1}$: Lower Triassic quart
conglomerate with some

SYMBOLS

Reflection

Diffracting point

Change in binning line

ıte Triassic dolomite.

f
l

grey to dark grey limestone.

A
3

quartzite and quartz
some schist.

Limit of geo

Fault

g line direction.

Thrust fault

o Late Triassic dolomite.

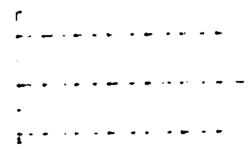

assic grey to dark grey limestone.

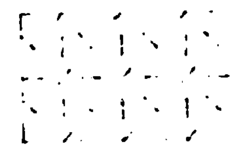

assic quartzite and quartz
vith some schist.

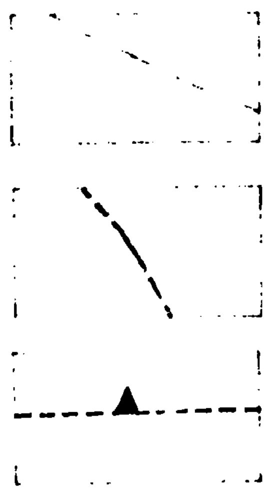

Limit of

oint

Fault

nning line direction.

Thrust f

fgf^{X}: Cambrian to Devonian pyritic, grap
tuffitic schist.

Amphibolite.
394 ± 24 Ma K/Ar age (Hrouda, 1988).

of geological unit

⊗ ◉ Righ

t fault

Reference: Maho
Nemčok et al. (1
personal commu

fgf^{x}: Cambrian to Devonian pyritic, graphi
tuffitic schist.

Amphibolite.
394 ± 24 Ma K/Ar age (Hrouda, 1988).

geological unit

⊗◉

Right-

Reference: Mahel'
Nemčok et al. (19
personal communi

ault

hitic phyllite with

t-slip

el' et al. (1972);
1989); Tomek,
nication, 1992.

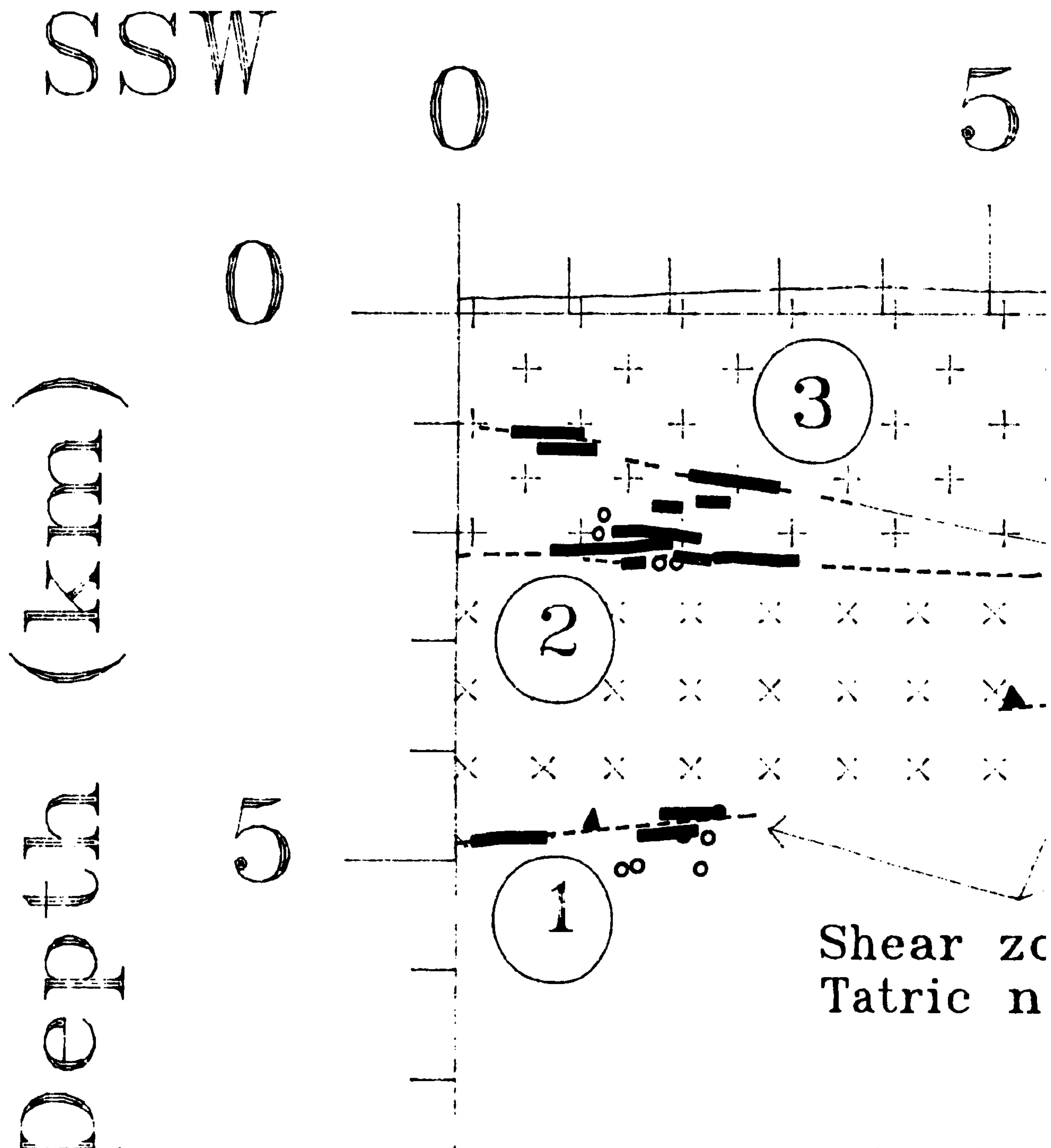
SSW
0
5
0
5
Depth (km)
3
2
1
Shear zc
Tatric n

Plate 10: Interpretation o

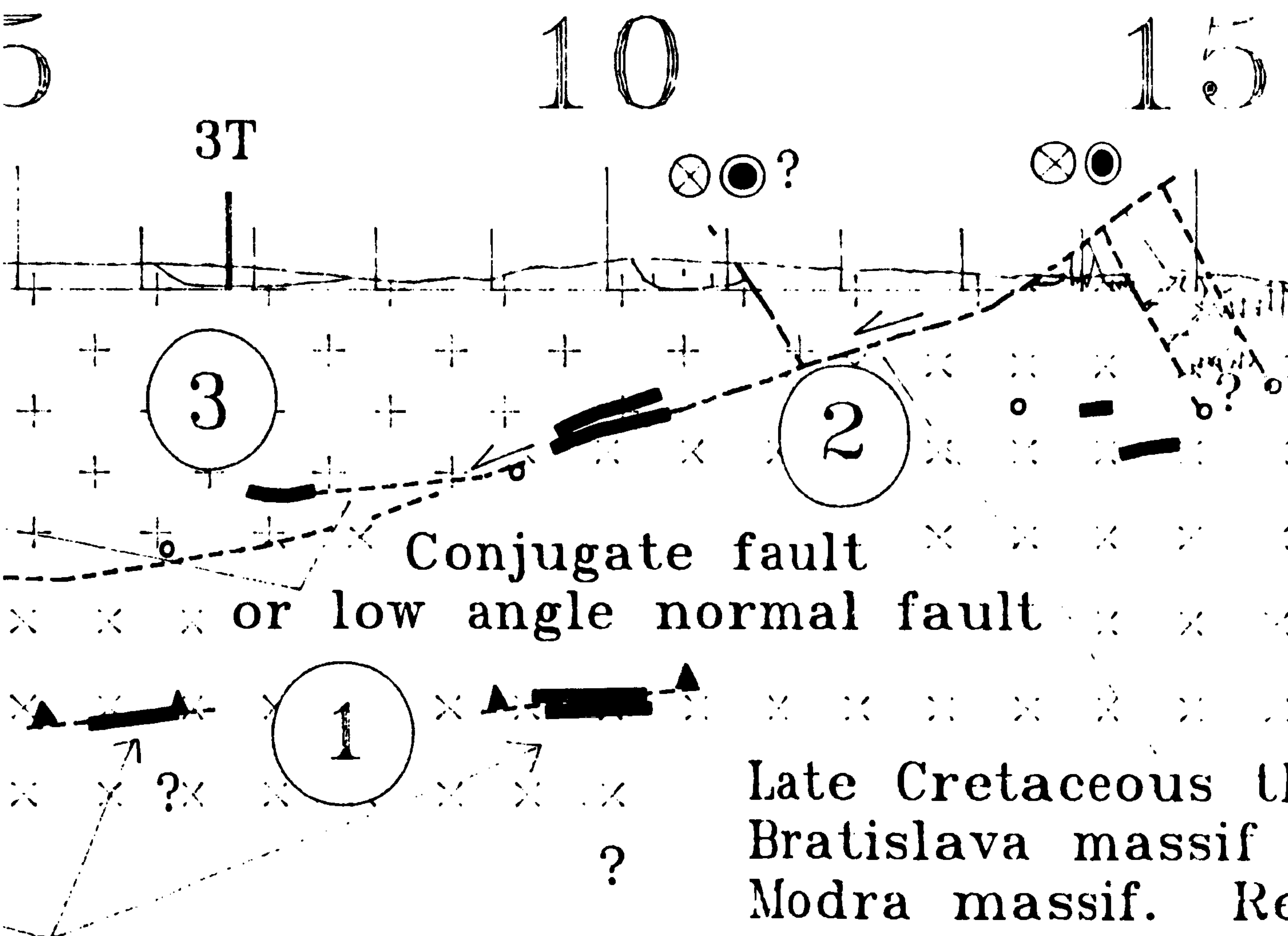

zone in
nappes.

Late Cretaceous t
Bratislava massif
Modra massif. Re
as an Early Mioce
fault related to n
slip of Modra mas
faults. Right-slip

Plate 10: Interpretati

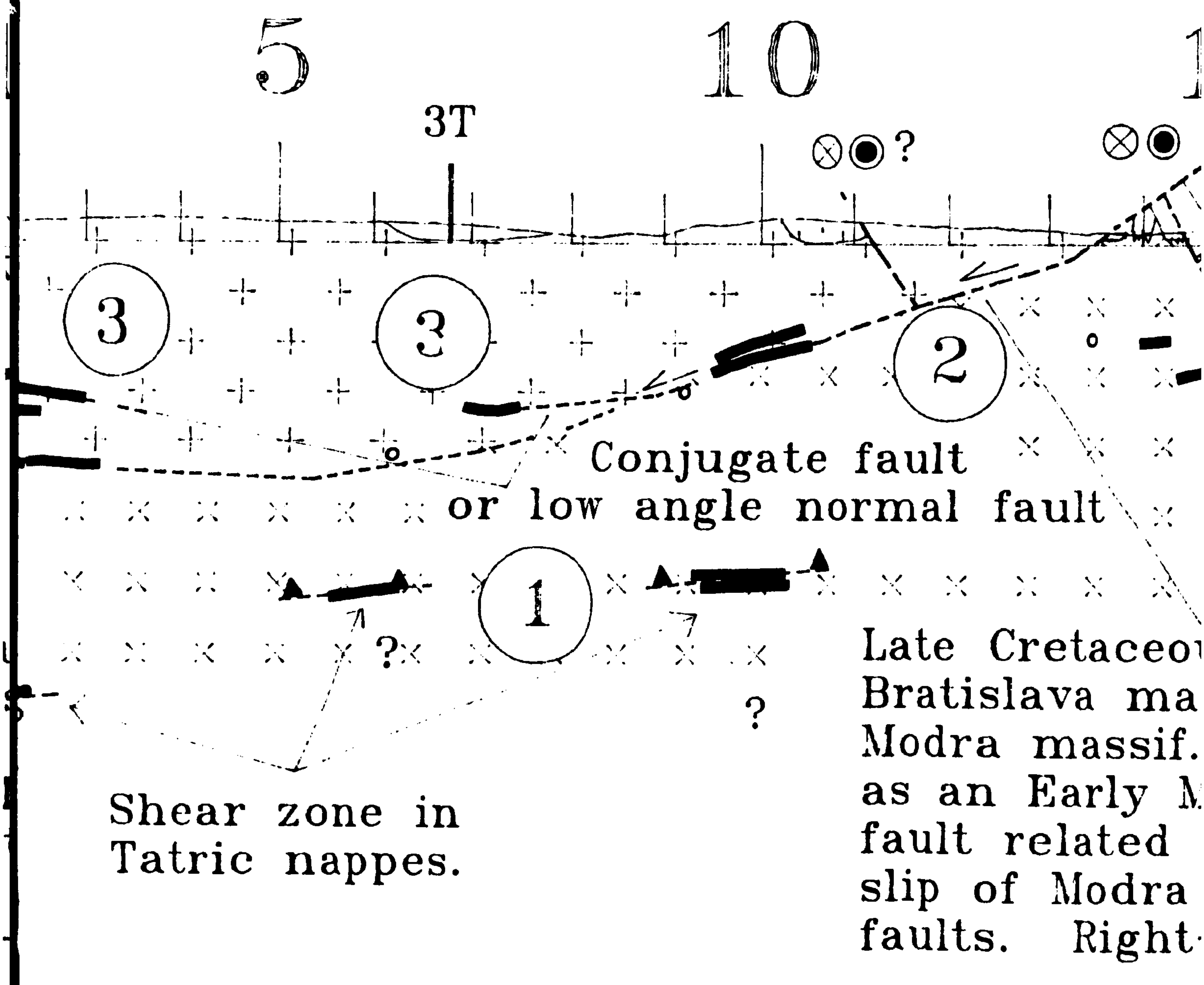

ation of line 689/87.

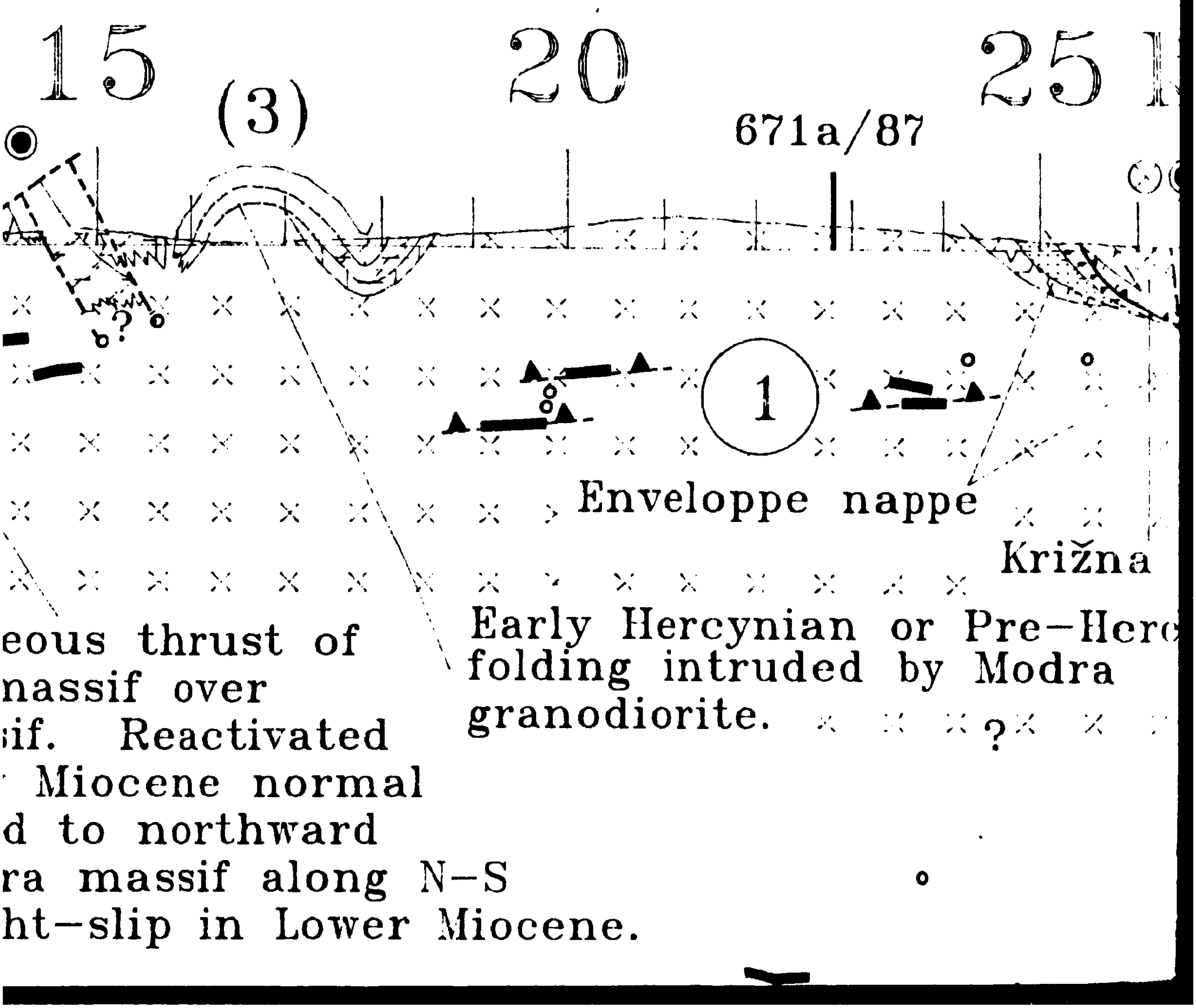

erpretation of line 689/87.

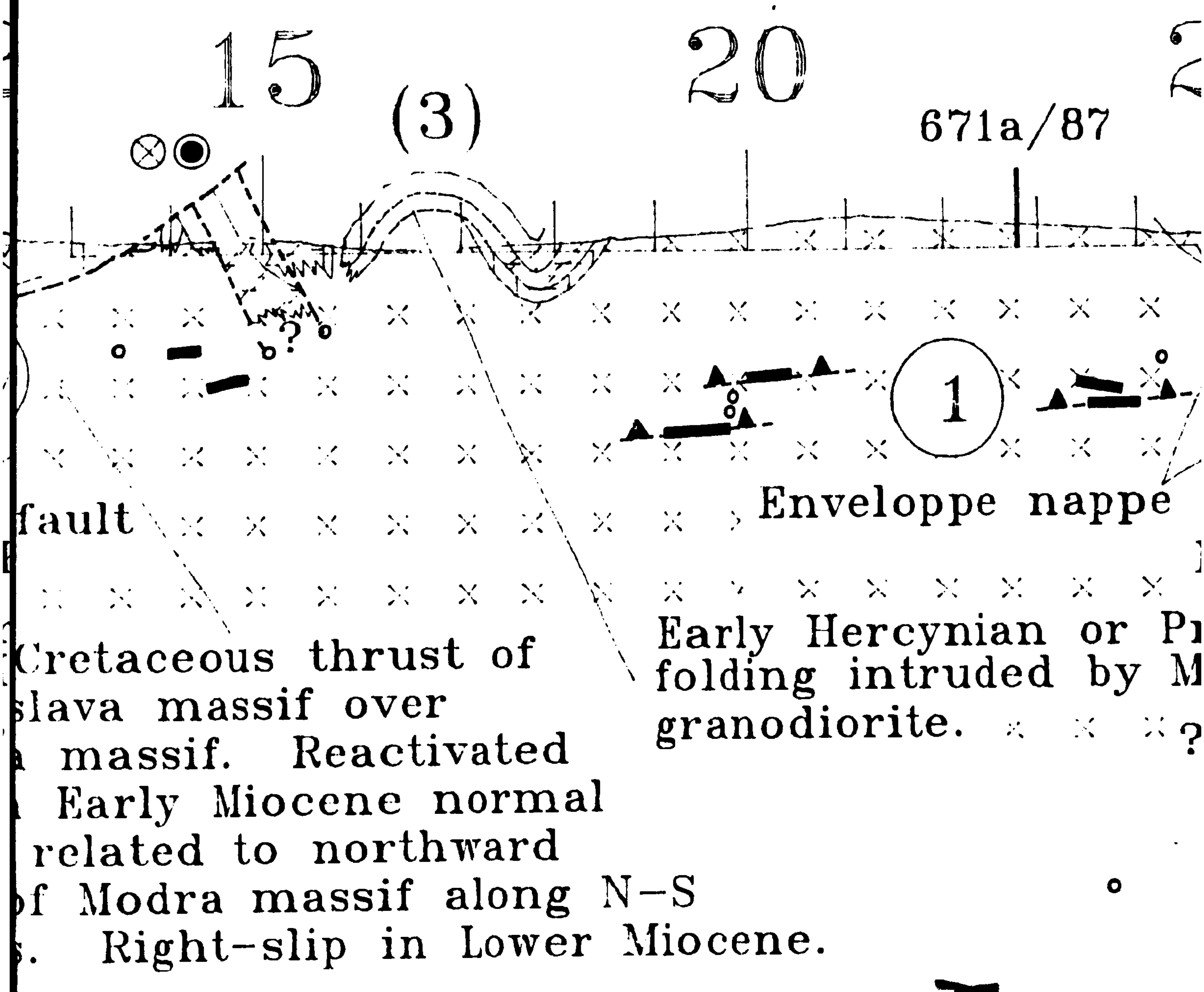

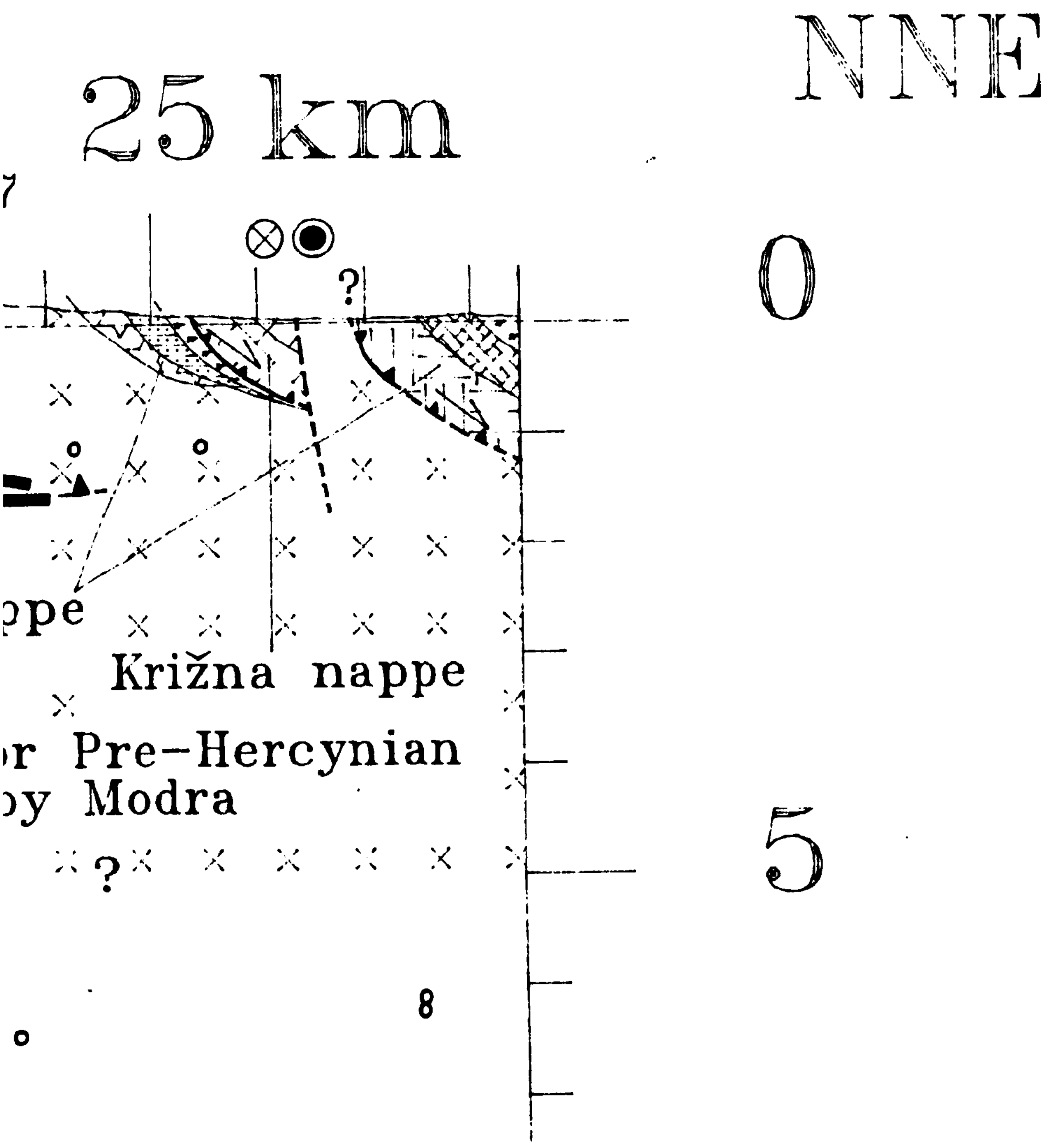
25 km
NNE
0
5
?
ppe
Križna nappe
r Pre-Hercynian
by Modra
?
8

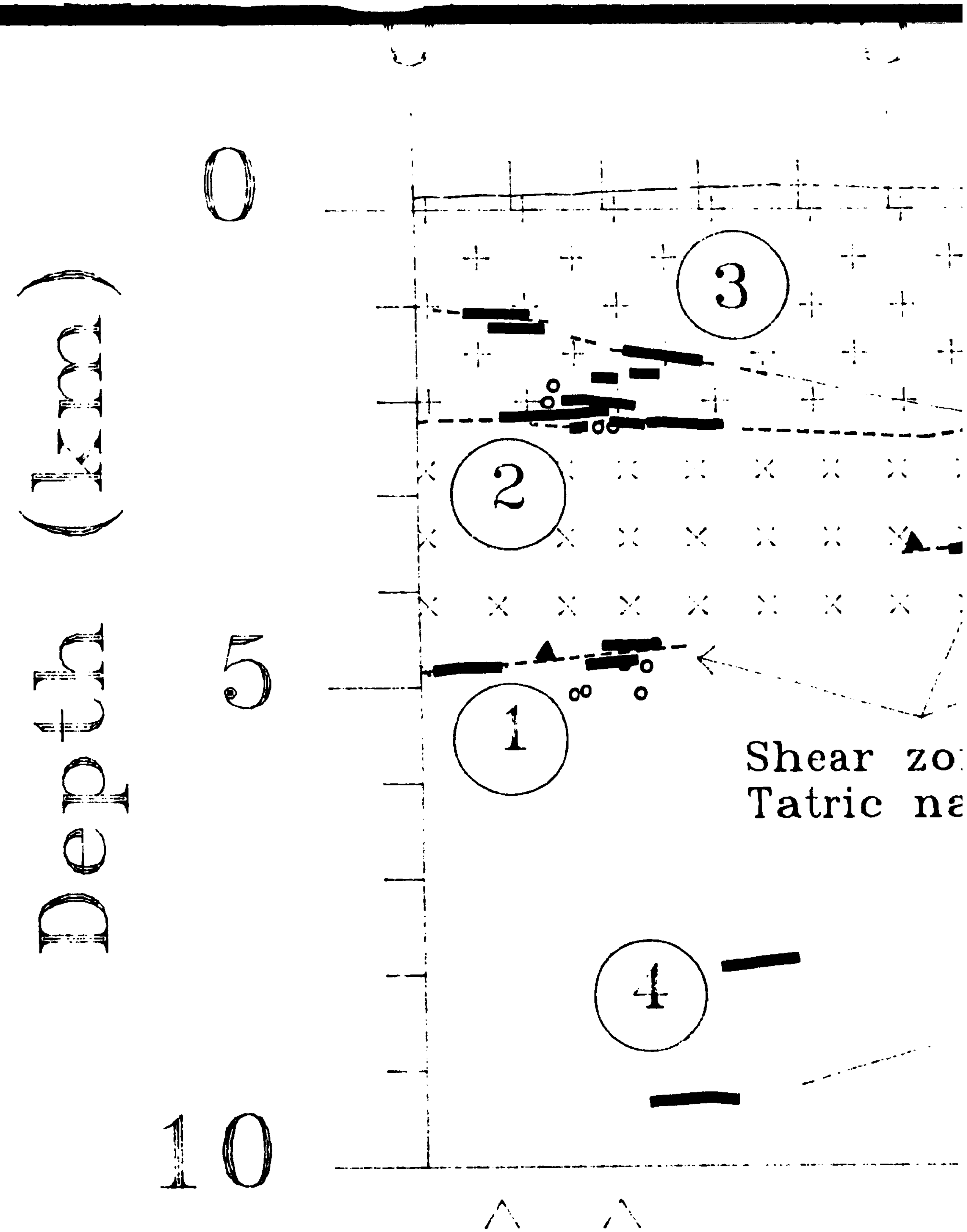

Depth (km)
0
5
10
3
2
1
4
Shear zo
Tatric na

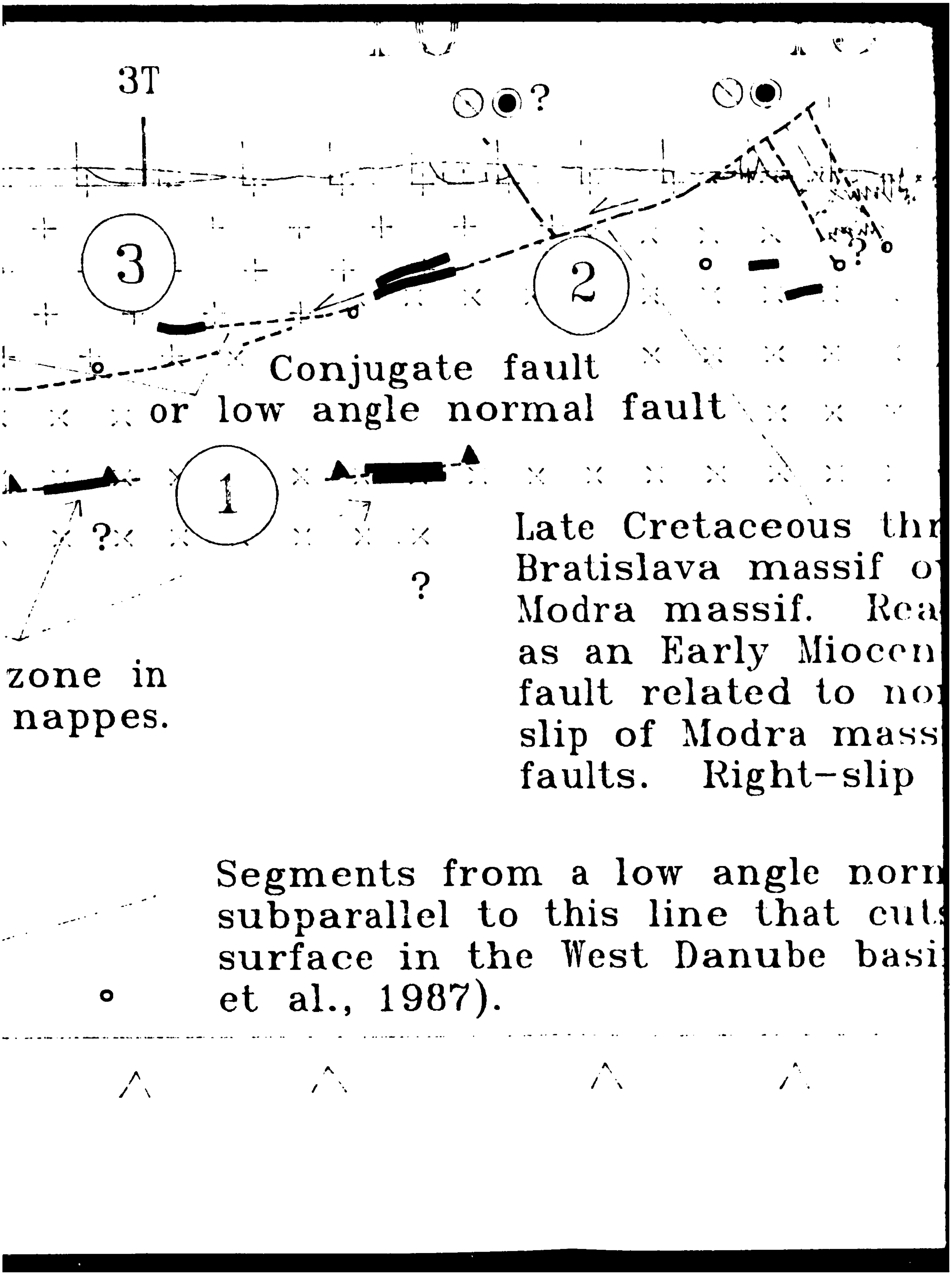

3T
3
2
1
?
Conjugate fault
or low angle normal fault
zone in
nappes.
Late Cretaceous th
Bratislava massif o
Modra massif. Rea
as an Early Miocen
fault related to no
slip of Modra mass
faults. Right-slip
Segments from a low angle norn
subparallel to this line that cut
surface in the West Danube basi
et al., 1987).

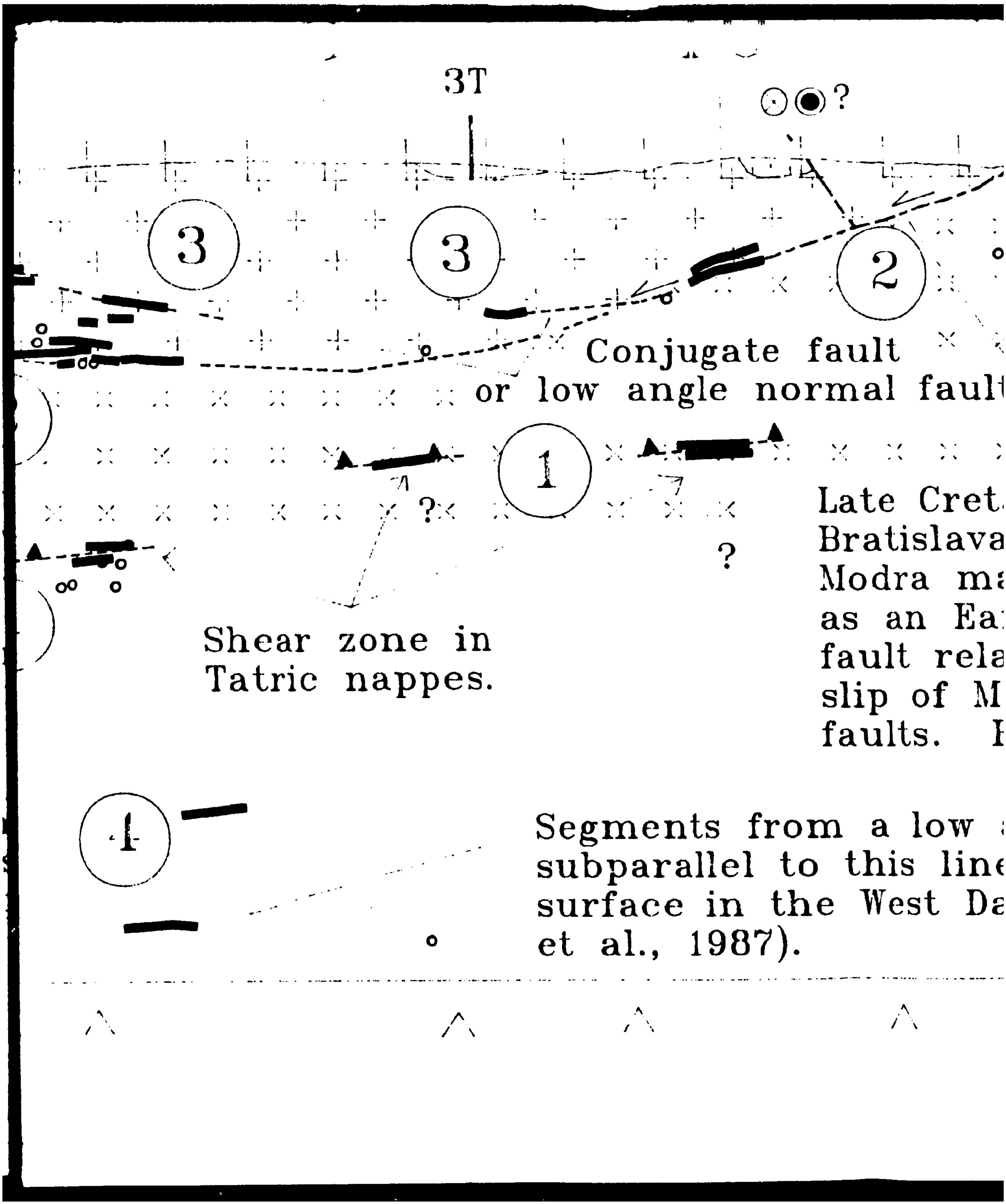
3T
?
3
3
2
Conjugate fault
or low angle normal faul
1
?
?
Late Cret
Bratislava
Modra m
as an Ea
fault rela
slip of M
faults.
Shear zone in
Tatric nappes.
4
Segments from a low
subparallel to this line
surface in the West Da
et al., 1987).

(3) 671a/87

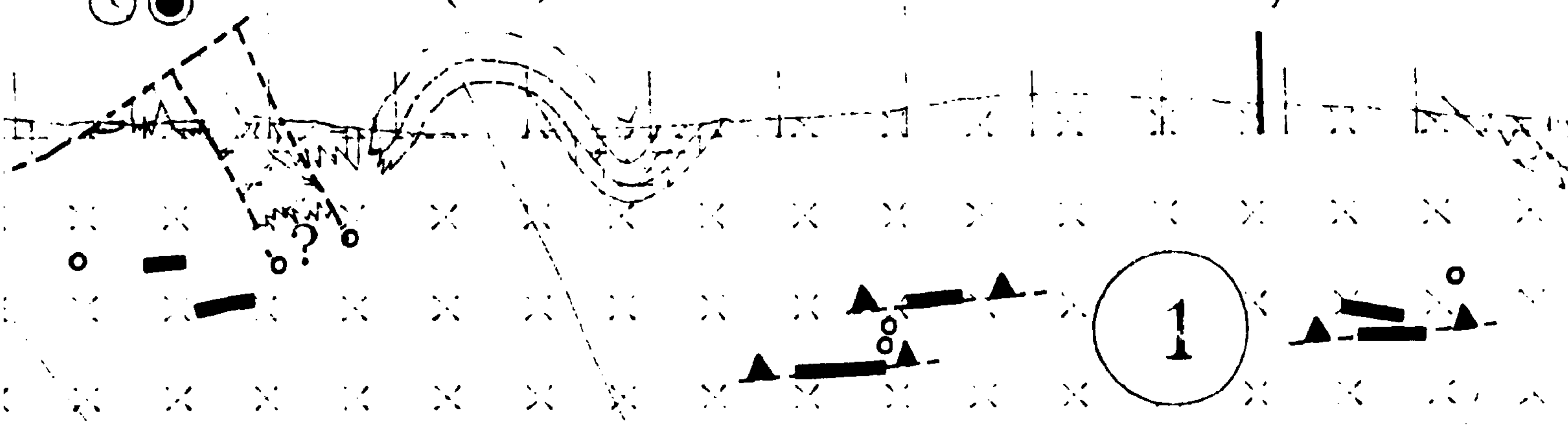

ult

Enveloppe nappe

Kr

retaceous thrust of
ava massif over
massif. Reactivated
Early Miocene normal
elated to northward
Modra massif along N–S
Right-slip in Lower Miocene.

Early Hercynian or Pre-
folding intruded by Mod
granodiorite. ?

w angle normal fault
ine that cuts the
Danube basin (Tomek

4

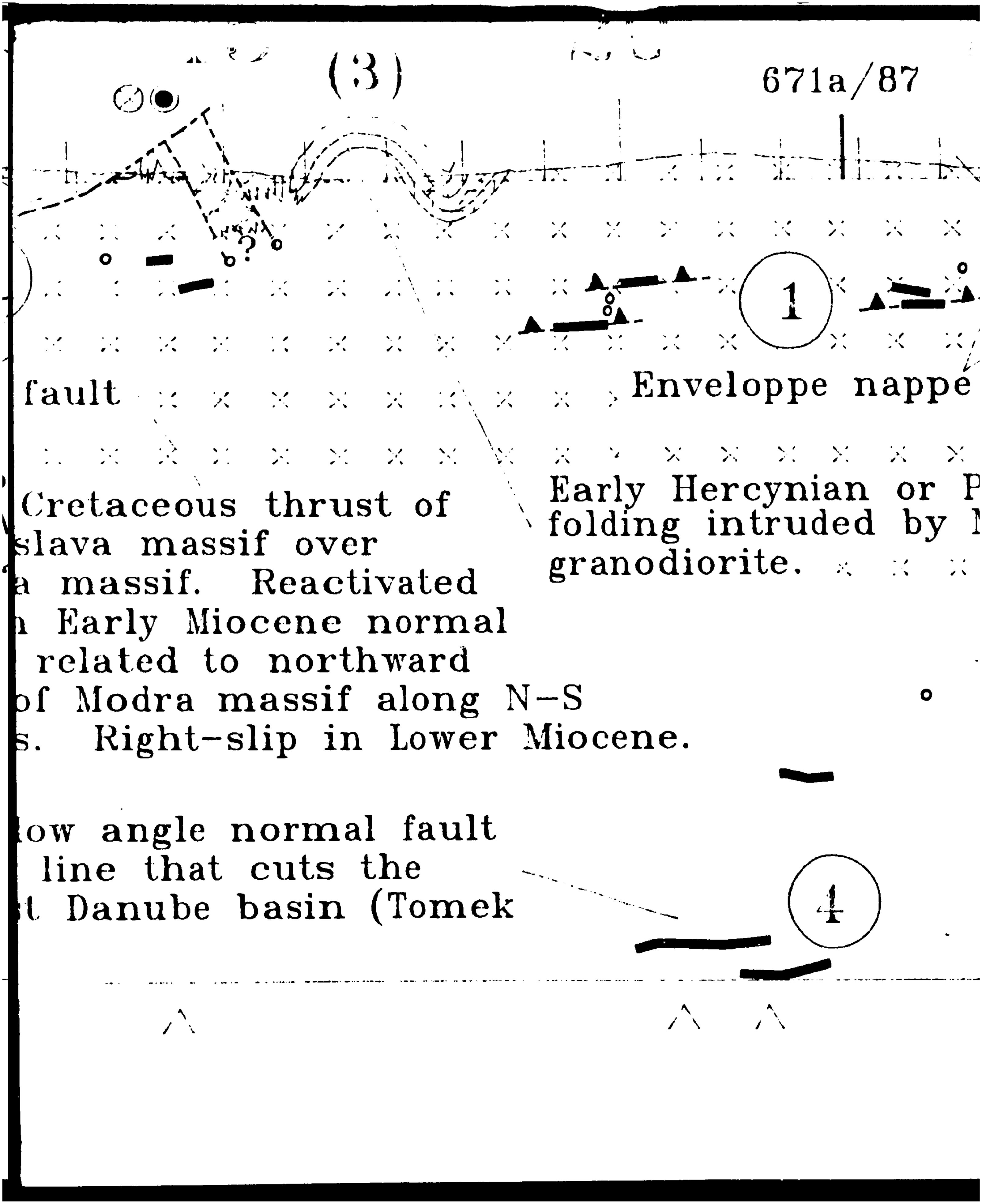
(3)
671a/87
1
fault
Enveloppe nappe
Cretaceous thrust of
slava massif over
a massif. Reactivated
n Early Miocene normal
related to northward
of Modra massif along N–S
s. Right–slip in Lower Miocene.
Early Hercynian or P
folding intruded by I
granodiorite.
ow angle normal fault
line that cuts the
t Danube basin (Tomek
4

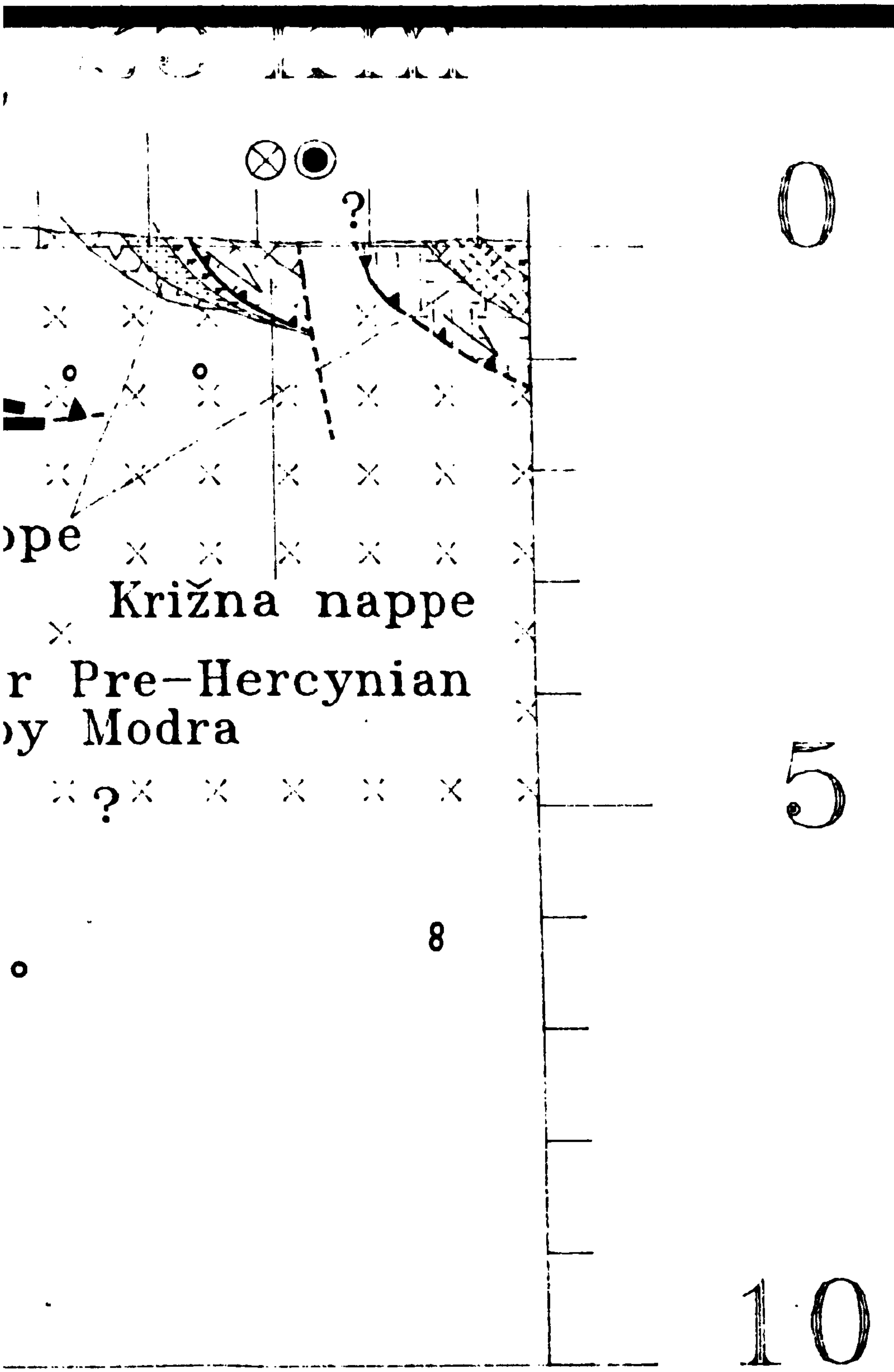
0
?
pe
Križna nappe
r Pre–Hercynian
y Modra
5
?
8
10